

**Metal-Based Turn-On Fluorescent Probes
for Nitric Oxide Sensing**

by

Mi Hee Lim

M.Sc., Chemistry

Ewha Womans University, 2001

SUBMITTED TO THE DEPARTMENT OF CHEMISTRY IN PARTIAL FULFILLMENT
OF THE REQUIREMENTS FOR THE DEGREE OF

DOCTOR OF PHILOSOPHY IN INORGANIC CHEMISTRY
AT THE
MASSACHUSETTS INSTITUTE OF TECHNOLOGY

May 2006
[June 2006]

© Massachusetts Institute of Technology, 2006

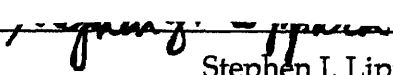
All rights reserved

Signature of Author: _____

Department of Chemistry

May 10, 2006

Certified By: _____


Stephen J. Lippard

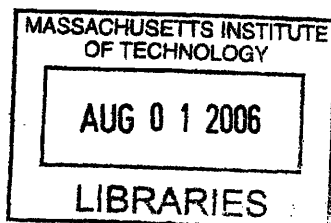
Arthur Amos Noyes Professor of Chemistry

Thesis Supervisor

Accepted by: _____

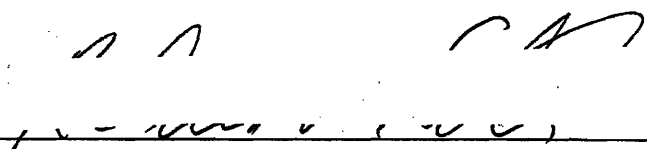
Robert W. Field

Chairman, Departmental Committee on Graduate Studies



ARCHIVES

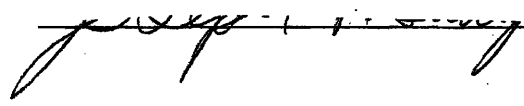
This doctoral thesis has been examined by a committee of the Department of Chemistry as follows:



Richard R. Schrock
Frederick G. Keyes Professor of Chemistry
Committee Chairman



Stephen J. Lippard
Arthur Amos Noyes Professor of Chemistry
Thesis Supervisor



Joseph P. Sadighi
Professor of Chemistry

Metal-Based Turn-On Fluorescent Probes for Nitric Oxide Sensing

by
Mi Hee Lim

Submitted to the Department of Chemistry on May 10, 2006, in partial fulfillment
of the requirements for the degree of Doctor of Philosophy.

Abstract

Chapter 1. Metal-Based Turn-On Fluorescent Probes for Sensing Nitric Oxide

Nitric oxide, a reactive free radical, regulates a variety of biological processes. The absence of tools to detect NO directly, rapidly, specifically and selectively motivated us to develop metal-based fluorescent probes to visualize the presence of NO. We have prepared and investigated Co(II), Fe(II), Ru(II), Rh(II), and Cu(II) complexes as turn-on fluorescent NO sensors. Our exploration has provided insight into how the interaction of transition metal centers with nitric oxide can be utilized for NO sensing.

Chapter 2. Fluorescence-Based Nitric Oxide Detection by Ruthenium Porphyrin Fluorophore Complexes

The ruthenium(II) porphyrin fluorophore complexes [Ru(TPP)(CO)(Ds-R)] (TPP = tetraphenylporphinato dianion; Ds = dansyl; R = imidazole (im), **1**, or thiomorpholine (tm), **2**) were synthesized and investigated for their ability to detect nitric oxide (NO) based on fluorescence. The X-ray crystal structures of **1** and **2** were determined. The Ds-im or Ds-tm ligand coordinates to an axial site of the ruthenium(II) center through a

nitrogen or sulfur atom, respectively. Both exhibit quenched fluorescence when excited at 368 or 345 nm. Displacement of the metal-coordinated fluorophore by NO restores fluorescence within minutes. These observations demonstrate fluorescence-based NO detection using ruthenium porphyrin fluorophore conjugates.

Chapter 3. Nitric Oxide-Induced Fluorescence Enhancement by Displacement of Dansylated Ligands from Cobalt

The cobalt complexes, $[\text{Co}(\text{Ds-AMP})_2]$ (**1**) and $[\text{Co}(\text{Ds-AQ})_2]$ (**2**), where Ds-AMP and Ds-AQ are the conjugate bases of dansyl aminomethylpyridine, Ds-HAMP, and dansyl aminoquinoline, Ds-HAQ, respectively, were synthesized in two steps as fluorescence-based nitric oxide (NO) sensors and characterized by X-ray crystallography. The fluorescence of both complexes was significantly quenched in CH_3CN or CH_3OH compared to that of the free Ds-HAMP or Ds-HAQ ligands. Addition of NO to a CH_3CN solution of **1** or **2** enhanced the integrated fluorescence emission by factors of $2.1(\pm 0.3)$ or $3.6(\pm 0.4)$ within 35 or 20 min, respectively. Introduction of NO to methanolic solutions similarly increased the fluorescence by $1.4(\pm 0.1)$ for **1** or $6.5(\pm 1.4)$ for **2** within 1 h. These studies demonstrate that **1** and **2** can monitor the presence of NO with turn-on emission, and that their fluorescence responses are more rapid than those of previously reported cobalt systems in coordinating solvents such as CH_3CN and CH_3OH . ^1H NMR and IR spectroscopic data revealed the formation of a $\{\text{Co}(\text{NO})_2\}^{10}$ cobalt dinitrosyl adduct with concomitant dissociation of one ligand from the cobalt center as the metal-containing product of the NO reactions, indicating NO-induced ligand release to be the cause of the fluorescence increase.

Chapter 4. Fluorescent Nitric Oxide Detection by Copper Complexes Bearing Anthracenyl and Dansyl Fluorophore Ligands

Anthracenyl and dansyl fluorophore ligands (AnCH₂pipCS₂K (1), Ds-Hen (2), Ds-HAMP (3), Ds-HAQ (4), and Ds-HAPP (5)) were prepared for copper(II). Five copper complexes, [Cu(AnCH₂pipCS₂)₂] (6), [Cu(Ds-en)₂] (7), [Cu(Ds-AMP)₂] (8), [Cu(Ds-AQ)₂] (9), and [Cu(Ds-APP)(OTf)] (10), were synthesized for fluorescent nitric oxide (NO) detection and were characterized by X-ray crystallography. A decrease in fluorescence of free ligands (1 – 5) coordinated to the Cu(II) center was observed in all Cu(II) complexes (6 – 10). The fluorescence of fluorophore ligands in Cu(II) complexes was restored in the presence of NO in a CH₃OH/CH₂Cl₂ solvent. Furthermore, compounds 7, 8, and 10, exhibited fluorescence response to NO in aqueous pH 7.0 or 9.0 buffered solutions. Fluorescence enhancement of these Cu(II) complexes occurs by NO-induced reduction from Cu(II) to Cu(I), as demonstrated spectroscopically. The present work suggest that a copper(II) complex would be effective as a fluorescent probe for sensing NO in both organic and aqueous settings.

Chapter 5. Direct Nitric Oxide Detection In Aqueous Solution by Copper(II) Fluorescein Complexes

Fluorescein-based ligands (FL_n, n = 1 – 5) for Cu(II) were synthesized and their photophysical properties were determined. Introduction of nitric oxide (NO) to a pH 7.0 buffered solution of Cu(FL_n) (1 μM CuCl₂ and 1 μM FL_n) induces an increase in fluorescence at 37 °C. The fluorescence response of Cu(FL_n) is direct and specific, which is a significant improvement of commercially available small molecule-based probes that are capable only of indirect NO detection. NO-triggered fluorescence increase of

$\text{Cu}(\text{FL}_n)$ occurs by reduction of $\text{Cu}(\text{II})$ to $\text{Cu}(\text{I})$ with concomitant dissociation of the *N*-nitrosated fluorophore ligand from copper. Spectroscopic and product analyses of the reaction of the copper fluorescein complex with NO suggest that the *N*-nitrosated fluorescein ligand ($\text{FL}_n\text{-NO}$) is the species for fluorescence turn-on. Density functional theory (DFT) calculations of FL_5 versus $\text{FL}_5\text{-NO}$ reveal how *N*-nitrosation of the fluorophore ligand causes the fluorescence increase. The investigation of copper-based probes described in the present work is the basis for developing a metal complex for fluorescent NO detection.

Chapter 6. Visualization of Nitric Oxide in Living Cells by a Copper-Based Fluorescent Probe

Nitric oxide (NO) is a highly reactive gaseous free radical that serves as a messenger for cellular signaling. To visualize NO in living cells, a turn-on fluorescent probe was designed and synthesized for use in combination with microscopy. Unlike existing fluorescent sensors, the construct, a $\text{Cu}(\text{II})$ complex of a fluorescein modified with an appended metal-chelating ligand (FL), directly and immediately images NO rather than a derivative reactive nitrogen species (RNS). Nitric oxide produced by both constitutive (cNOS) and inducible (iNOS) NO synthases in live neurons and macrophages is detected by the $\text{Cu}(\text{II})$ -based imaging agent in a concentration- and time-dependent manner. The sensitivity to nM levels of NO and the spatiotemporal information provided by this complex demonstrate its value for numerous biological applications.

Appendix. Fluorescent Detection of Nitric Oxide by a Rhodium Fluorophore Embedded in a Silastic Polymer Using Two-Photon Microscopy

A Silastic membrane embedded with a dirhodium fluorophore conjugate, $[\text{Rh}_2(\mu\text{-O}_2\text{CPr})_4(\text{Ds-pip})]$ (Ds-pip = dansyl-piperzine), was prepared. Nitric oxide (NO) in aqueous media replaces the Ds-pip bound to the dirhodium core in the solid state, inducing the fluorescence increase observed by two-photon spectroscopy. This observation is the first effort for NO detection using two-photon microscopy and represents an initial step toward fiber-optic-based NO sensing in aqueous media using this dirhodium-containing polymer.

Thesis Supervisor: Stephen J. Lippard

Title: Arthur Amos Noyes Professor of Chemistry

To my parents, my sisters, and Jan-Uwe

Acknowledgements

“Building 18 Room 444”

The last four years was like a difficult and long test, which directed me to look over my scientific ability. While taking it, I fought with myself not to give it up several times. Now I did finish it with invaluable answers that were provided by people who I want to acknowledge.

First and foremost, I wish to thank my advisor, an outstanding scientist, Steve Lippard for his guidance for four years and the opportunity to perform a very challenging project, *nitric oxide sensing*. I also appreciate his encouragement and confidence in me. His insightful scientific knowledge has inspired me to exert myself to become a genuine scientist. I am grateful for the advice and the training that he provides for me to be prepared for anything in my future endeavors and I am greatly proud of being a member of his group. I also thank the other Inorganic Chemistry faculty members, especially Professor Dick Schrock, Professor Joseph Sadighi and Professor Dan Nocera, for their helpful suggestions and encouragement. I also give my gratitude to my former advisor, Professor Wonwoo Nam who inspired and encouraged me to go into a Ph.D. program in USA. His great support and guidance have been continuing since I was an undergraduate student at Ewha Womans University.

When I joined the lab in the fall of 2002, Scott Hilderbrand shared his bench with me and helped me settle down in the lab. He taught a fantastic skill for dealing with a gas molecule, nitric oxide. He also gave me many useful insights on the project. I am also indebted to Chris Chang and Matt Clark for teaching me about organic synthesis as well as their advice and suggestions on my project. I also thank Carolyn Woodroffe and Ben Davis for their encouragement. I am greatly grateful to Liz Nolan who has supported me from the beginning to the end of my graduate studies. Sungho Yoon was like my Korean brother, helped me set up in the lab and taught me about X-ray crystal structures. I also enjoyed our conversations about science.

I thank Katie Barnes and Emily Carson who were like my older sisters for their practical suggestions and direction of my graduate studies. They also relieved my

homesickness. I also thank Yongwon Jung and Yoon Jin Kim for their encouragement. My best friend, Viviana Izzo showed me how to go through hard times. I have had terrific time with her (eating together and learning European culture and science) for two years. I really appreciate her incredible support in my graduate course and I will miss you! I have had the pleasure of knowing my classmates Lesile Murry and Amy Kelley. Lesile Murry was a very friendly and supportive friend. I am grateful to Sumi Mukhopadhyady, Datong Song and Rodney Feazell for teaching me about X-ray crystal structures. My teachers of organic synthesis, Jeremy Kodanko and Rayane Moreira provided useful suggestions on my projects. I have enjoyed discussions with Todd Harrop on my project and other bioinorganic chemistry. I really thank him for his huge encouragement. I appreciate the friendship and collaboration offered by Brian Wong. Dong Xu was like my older brother. I was fortunate to have him as a great bio-teacher and coworker on my bio-project. I thank Rhett Smith, Andy Tennyson (funny and helpful), Xiao-An Zhang, Lindsey McQuade, and Chris Goldsmith as metalloneurochemistry subgroup members. I have had great time with other lab members, Evan Guggenheim (my coffee friend, very kind for everything), Mike McCormick (great computer designer), Min Zhao (like my older sister), Erik Dill, Laurance Beauvais, Kate Lovejoy, Simone Friedle, and Erwin Reisner. I enjoyed teaching my wonderful UROPs, Charlie Chuang, Jacque Tio, and Deepa Mokshagundam. Out of the lab, I am greatly grateful to my best friend, Junghyun Chae for her encouragement and helpful suggestions about organic synthesis. I apologize to those people who I fail to mention by name.

This thesis is dedicated to my family. My success in graduate school wouldn't exist without the incredible love and encouragement. Mom and Dad have always supported me to do my best in any position. I consider myself exceptionally fortunate to have my older sister Mi Sook and younger sister Mi Sun whose confidence made this thesis and my Ph.D. degree. I love my family so much and pray for their health everyday. Jan-Uwe Rohde, I love you and thank you for all of your support for four years. You are the person who strengthened me and made me finish my Ph.D. in USA without my family. I am also grateful for your understanding of my crazy lab work.

Table of Contents

Abstract.....	3
Dedication.....	8
Acknowledgements	9
Table of Contents	11
List of Tables.....	16
List of Schemes.....	17
List of Figures.....	19
Chapter 1. Metal-Based Turn-On Fluorescent Probes for Sensing Nitric Oxide.....	25
Introduction.....	26
Strategies for Metal-Based Fluorescent Nitric Oxide Sensing.....	27
Fluorophore Displacement without Metal Reduction.	27
Metal Reduction without Fluorophore Displacement	28
Metal Reduction with Fluorophore Displacement.....	28
Cobalt(II) Complexes.....	29
Co-DATI Systems	29
Dicobalt(II) Tetracarboxylate Complex	30
Other Cobalt Dansyl Complexes.....	31
Co-FATI Systems.....	32
Iron(II) Complexes.....	33
Iron(II) Mmc-cyclam.....	33
Diiron(II) Tetracarboxylate Complex.....	34
Ruthenium(II) Tetraphenylporphyrins.....	34
Dirhodium(II) Tetracarboxylates.....	35
Copper(II) Complexes.....	37
Copper(II) Dansyl Complexes.....	37
Copper(II) Conjugated Polymer.....	39
Copper(II) Anthracenyl-Cyclam.....	39
Copper(II) Fluorescein Complex.....	40
Summary.....	41
References	42
Chapter 2. Fluorescence-Based Nitric Oxide Detection by Ruthenium Porphyrin	
Fluorophore Complexes	70

Introduction.....	71
Experimental	72
General Considerations	72
X-ray Crystallographic Studies.....	72
Dansyl-thiomorpholine (Ds-tm)	73
[Ru(TPP)(CO)(Ds-im)] (1).....	74
[Ru(TPP)(CO)(Ds-tm)] (2).....	74
Results and Discussion.....	75
Syntheses of Fluorophore-Derived Ruthenium Porphyrin Complexes.	75
X-ray Crystal Structure Determinations of [Ru(TPP)(CO)(Ds-im)] (1) and [Ru(TPP)(CO)(Ds-tm)] (2).....	76
Fluorescence Properties.....	76
Nature of the Reaction of [Ru(TPP)(CO)(Ds-im)] (1) with Nitric Oxide	77
Conclusions	78
References.....	78
Chapter 3. Nitric Oxide-Induced Fluorescence Enhancement by Displacement of Dansylated Ligands from Cobalt.....	92
Introduction.....	93
Experimental.....	94
Materials and Procedures.....	94
X-ray Crystallographic Studies	95
[Co(Ds-AMP) ₂] (1).....	95
5-Dimethylamino-N-(8-quinolinyl)-1-naphthalenesulfonamide, (Ds-HAQ).....	96
[Co(Ds-AQ) ₂] (2)	97
Results and Discussion.....	98
Syntheses and Structural Characterization of Cobalt Complexes.....	98
Fluorescence Spectroscopic Measurements	99
Investigation of the Chemistry of the Cobalt Complexes with Nitric Oxide	100
Conclusions	101
References.....	102
Chapter 4. Fluorescent Nitric Oxide Detection by Copper Complexes Bearing Anthracenyl and Dansyl Fluorophore Ligands.	120
Introduction.....	121

Experimental	122
Materials and Procedures.....	122
X-ray Crystallography	123
Electrochemistry.....	123
Spectroelectrochemistry.....	124
EPR Spectroscopy.....	124
Syntheses.....	124
Potassium 4-(Anthracen-9-ylmethyl)piperazine-1-dithiocarbamate (An- CH ₂ pipCS ₂ K, 1).....	125
5-Dimethylamino- <i>N</i> -(2-pyridylmethyl)-1-naphthalenesulfonamide (Ds-HAMP, 3)	125
5-Dimethylamino-{3-[4-(3-amino-propyl)-piperazin-1-yl]-propyl}-1 naphthal- enesulfonamide (Ds-HAPP, 5)	126
[Cu(AnCH ₂ pipCS ₂) ₂] (6).....	127
[Cu(Ds-AMP) ₂] (8).....	127
[Cu(Ds-AQ) ₂] (9)	128
[Cu(Ds-APP)(OTf)] (10)	129
Results.....	129
Syntheses of Ligands.....	129
Synthesis and Structural Characterization of Copper Complexes.....	130
Electrochemistry of Copper Complexes.....	132
Fluorescence Studies	132
NO Reactivity of Copper Anthracenyl Complex 6	134
NO Reactivity of Copper Dansyl Complex 8.....	136
Discussion.....	137
Summary.....	139
References.....	139
Chapter 5. Direct Nitric Oxide Detection In Aqueous Solution by Copper(II)	
Fluorescein Complexes.....	169
Introduction.....	170
Experimental	172
Materials and Procedures	172
EPR Spectroscopy.....	173

X-ray Crystallographic Studies.....	173
Calculation Methods	174
Syntheses.....	174
8-Nitro-2-quinolinecarboxylic acid methyl ester (1)	175
8-Amino-2-quinolinecarboxylic acid methyl ester (2).....	175
(8-Amino-2-quinolinyl)-methanol (3).....	175
2-[2-Chloro-6-hydroxy-5-[(2-(methylcarboxy)quinolin-8-ylamino)methyl]-3-oxo-3H-xanthen-9-yl]benzoic acid (FL ₁)	176
2-[2-Chloro-6-hydroxy-5-[(2-(carboxy)quinolin-8-ylamino)methyl]-3-oxo-3H-xanthen-9-yl]benzoic acid (FL ₂).....	177
2-[2-Chloro-6-hydroxy-5-[(2-hydroxymethyl-quinolin-8-ylamino)-methyl]-3-oxo-3H-xanthen-9-yl]benzoic acid (FL ₃)	177
2-[2-Chloro-6-hydroxy-5-[(2-methyl-quinolin-8-ylamino)-methyl]-3-oxo-3H-xanthen-9-yl]benzoic acid (FL ₅).....	178
2-[2-Chloro-6-hydroxy-5-[(2-methylquinolin-8-yl)(nitroso)amino)methyl]-3-oxo-3H-xanthen-9-yl]benzoic acid (FL ₅ -NO).....	179
[Cu ₂ (modL') ₂ (CH ₃ OH)](BF ₄) ₂ ·CH ₃ OH and [Cu(modL) ₂](BF ₄) ₂ ·2CH ₃ OH.....	180
Results and Discussion.....	181
Design Considerations for Cu(II)-Based NO Sensors	181
Synthesis of Fluorescein-Based Ligands (FL _n)	182
Preparation and Fluorescence Studies of Copper Fluorescein Compounds.....	183
Mechanism of Fluorescence Detection of NO by Cu(FL _n)	185
DFT Calculation of FL ₅ versus FL ₅ -NO	191
Summary.....	193
References.....	193
Chapter 6. Visualization of Nitric Oxide in Living Cells by a Copper-Based Fluorescent Probe	224
Introduction.....	225
Experimental	226
Cell Culture and Materials	226
MTT Cytotoxicity Assay	227
Silencing of iNOS in Raw 264.7 Cells by Short Hairpin RNA-Induced RNA Interference	227

Western Blot Analysis on iNOS Expression in Raw 264.7 Cells	228
Results.....	228
CuFL Detection of NO Produced by cNOS.....	228
CuFL Detection of NO Produced by iNOS	230
NO Imaging in a Raw 264.7 and SK-N-SH Co-culture	231
Discussion.....	232
Summary.....	234
References.....	234
Appendix. Fluorescent Detection of Nitric Oxide by a Rhodium Fluorophore	
Embedded in a Silastic Polymer Using Two-Photon Microscopy.....	257
Introduction.....	258
Experimental	259
Materials and Procedures....	259
Preparation of a Silastic Membrane with the Dirhodium Complex and Ds-pip.....	259
Study of a Dirhodium-Containing Silastic Membrane with NO	259
Two-Photon Measurements	260
Results and Discussion.....	260
Preparation and Nitric Oxide Reactivity of the Dirhodium-Containing Silastic	
Membrane	261
Two-Photon Experiment.....	261
Summary.....	262
References.....	262
Biographic Note	273

List of Tables**Chapter 2**

Table 2.1.	Summary of X-ray Crystallographic Data	82
Table 2.2.	Selected Bond Distances (Å) and Angles (deg)	83

Chapter 3

Table 3.1.	Summary of X-ray Crystallographic Data	105
Table 3.2.	Selected Bond Distances (Å) and Angles (deg)	106
Table 3.3.	NO Detection Times of Cobalt Complexes	107

Chapter 4

Table 4.1.	Summary of X-ray Crystallographic Data	143
Table 4.2.	Selected Bond Distances (Å) and Angles (deg)	144

Chapter 5

Table 5.1.	Spectroscopic Results	197
Table 5.2.	Summary of X-ray Crystallographic Data	198
Table 5.3.	Selected Bond Distances (Å) and Angles (deg)	199

List of Schemes

Chapter 1

Scheme 1.1. Strategies for Metal-Based Nitric Oxide Sensing	46
Scheme 1.2. NO Reactivity of Co-DATI Complexes.....	47
Scheme 1.3. Nitric Oxide Reactivity of 5 and 6	48
Scheme 1.4. Nitric Oxide Detection by 11	49
Scheme 1.5. Nitric Oxide Sensing by 21	50

Chapter 2

Scheme 2.1. Nitric Oxide Chemistry of 1	84
--	----

Chapter 3

Scheme 3.1. Fluorophore Displacement Strategy	108
Scheme 3.2. Nitric Oxide Detection of 1	109

Chapter 4

Scheme 4.1. Strategies of Nitric Oxide Detection Using Transition Metal Complexes	145
Scheme 4.2. One-Electron Oxidation/Reduction of 6	146
Scheme 4.3. NO Reactivity of Cu(II) Complexes	147
Scheme 4.4. Proposed Reaction Pathways of Cu(II) Complexes with NO	148

Chapter 5

Scheme 5.1. Strategies for Nitric Oxide Detection	200
Scheme 5.2. Syntheses of Compounds 1 , 2 , and 3	201
Scheme 5.3. Syntheses of FL _n Ligands (n = 1 – 5, FL ₄ ³¹).....	202
Scheme 5.4. NO Reactivity of Cu(FL _n).....	203
Scheme 5.5. Plausible Pathways of the Reaction of Cu(FL _n) with NO.....	204

Chapter 6

Scheme 6.1. DNA Inserts for Silencing Inducible Nitric Oxide Synthase (iNOS) in Mouse Raw 264.7 Cells.....	237
---	-----

Appendix

Scheme A.1. Nitric Oxide Detection of Dirhodium Dansyl Complexes265

List of Figures

Chapter 1

Figure 1.1.	Schematic drawings of DAN and DAFs	51
Figure 1.2.	Schematic drawings of H ^R DATI and H ₂ DATI-4.....	52
Figure 1.3.	ORTEP diagrams of [Co(^{iPr} DATI) ₂] (1), [Co(^{tBu} DATI) ₂] (2), [Co(^{Bz} DATI) ₂] (3), and [Co(DATI-4)] (4) showing 50% probability thermal ellipsoids.	53
Figure 1.4.	Fluorescence responses of H ^{iPr} DATI, [Co(^{iPr} DATI) ₂] (1), and 1 upon addition of excess NO, excited at 350 nm.	54
Figure 1.5.	ORTEP diagrams of windmill [Co ₂ (μ-O ₂ CAR ^{Tol}) ₂ (O ₂ CAR ^{Tol}) ₂ (Ds-pip) ₂] (5) and paddlewheel [Co ₂ (μ-O ₂ CAR ^{Tol}) ₄ (Ds-pip) ₂] (6) showing 50% probability thermal ellipsoids.....	55
Figure 1.6.	ORTEP diagrams of [Co(Ds-AMP) ₂] (7) and [Co(Ds-AQ) ₂] (8) showing 50% probability thermal ellipsoids.....	56
Figure 1.7.	Schematic drawings of [Co(^{iPr} FATI-3)] (9) and [Co(^{iPr} FATI-4)] (10).....	57
Figure 1.8.	ORTEP diagram of [Co ₂ (^{iPr} SATI-4) ₂] showing 50% probability thermal ellipsoids and schematic drawing of H ₂ ^{iPr} SATI.....	58
Figure 1.9.	ORTEP diagram of [Fe ₂ (μ-O ₂ CAR ^{Tol}) ₄ (Ds-pip) ₂] (12) showing 50% probability thermal ellipsoids.....	59
Figure 1.10.	ORTEP diagrams of [Ru(TPP)(CO)(Ds-im)] (13) and [Ru(TPP)(CO)(Ds-tm)] (14) showing 50% probability thermal ellipsoids.....	60
Figure 1.11.	Schematic drawings of [Rh ₂ (μ-O ₂ CMe) ₄ (Ds-pip)] (15) and [Rh ₂ (μ-O ₂ CMe) ₄ (Ds-im)] (16).....	61
Figure 1.12.	ORTEP diagram of [Rh ₂ (μ-O ₂ CMe) ₄ (NO) ₂] showing 50% probability thermal ellipsoids.....	62
Figure 1.13.	Fluorescence response of Silastic membrane- embedded [Rh ₂ (μ-O ₂ CPr) ₄ (Ds-pip)] to NO in water	63
Figure 1.14.	ORTEP diagrams of [Cu(Ds-en) ₂] (17) and [Cu(Ds-AMP) ₂] (18) showing 50% probability thermal ellipsoids.....	64
Figure 1.15.	Schematic drawing of CP1a	65
Figure 1.16.	Schematic drawing of [Cu(DAC)] ²⁺ (20)	66
Figure 1.17.	Schematic drawing of CuFL (21)	67

Figure 1.18.	Detection by 21 of NO produced in Raw 264.7 cells.....	68
Figure 1.19.	Detection by 21 of NO produced in SK-N-SH cells	69
Chapter 2		
Figure 2.1.	ORTEP diagrams of [Ru(TPP)(CO)(Ds-im)] (1) and [Ru(TPP)(CO)(Ds-tm)] (2) showing 50% probability thermal ellipsoids.....	85
Figure 2.2.	Fluorescence emission spectra of 1 , Ds-im, 2 , and Ds-tm in CH ₂ Cl ₂	86
Figure 2.3.	Fluorescence response of [Ru(TPP)(CO)(Ds-im)] (1) and [Ru(TPP)(CO)(Ds-tm)] (2) to NO	87
Figure 2.4.	IR spectra (in KBr) of [Ru(TPP)(CO)(Ds-im)] (1) and [Ru(TPP)(NO)(ONO)]	88
Figure 2.5.	UV-vis spectrum of the isolated NO reaction product in CH ₂ Cl ₂	89
Figure 2.6.	ORTEP diagram of [Ru(TPP)(NO)(ONO)] showing 20% probability thermal ellipsoid	90
Figure 2.7.	Expanded ¹ H NMR spectra (6.0 ppm – 8.8 ppm) of CD ₂ Cl ₂ solutions of Ds-im, 1 , and 1 upon addition of NO (g).....	91
Chapter 3		
Figure 3.1.	Schematic drawings of H ^R DATI and H ₂ DATI-4.....	110
Figure 3.2.	Schematic drawings of Ds-HAMP and Ds-HAQ.....	111
Figure 3.3.	ORTEP diagrams of [Co(Ds-AMP) ₂] (1) and [Co(Ds-AQ) ₂] (2) showing 50% probability thermal ellipsoids.....	112
Figure 3.4.	Fluorescence emission spectra of 1 , Ds-HAMP, 2 , and Ds-HAQ in CH ₃ CN	113
Figure 3.5.	Fluorescence responses of a CH ₃ CN solution of 1 or 2 upon addition of NO	114
Figure 3.6.	Fluorescence emission spectra of 1 , Ds-HAMP, 2 , and Ds-HAQ in CH ₃ OH	115
Figure 3.7.	Fluorescence responses of a CH ₃ CN solution of 1 or 2 upon addition of NO	116
Figure 3.8.	Solution IR spectra of the reaction of 1 with NO in CH ₃ CN	117
Figure 3.9.	¹ H NMR spectrum taken 2 h after the reaction of 1 with NO in CD ₃ CN	118

Figure 3.10. Fluorescence emission spectra of 1, Ds-HAMP, 1 with NO in CH₃CN.... 119

Chapter 4

- Figure 4.1. Schematic drawings of DAN and DAFs 149
- Figure 4.2. Schematic drawings of AnCH₂pipCS₂K (1), Ds-HAQ (2), Ds-HAMP (3), Ds-Hen (4), and Ds-HAPP (5)..... 150
- Figure 4.3. ORTEP diagrams of 6, 8, 9, and 10 showing 50% probability thermal ellipsoids 151
- Figure 4.4. Cyclic voltammogram of 6 in CH₂Cl₂ with 0.5 M (Bu₄N)(PF₆) as supporting electrolyte and a scan rate of 50 mV/s 153
- Figure 4.5. Cyclic voltammograms of 7, 8, 9, and 10 in CH₃CN 154
- Figure 4.6. Fluorescence emission spectra of 1, 6, and 6 upon addition of NO..... 156
- Figure 4.7. Fluorescence emission spectra of 2, 3, 4, 7, 8, and 9 in CH₃OH/CH₂Cl₂ (4:1) at 25 °C. Fluorescence response of 7, 8, or 9 to NO (g)..... 157
- Figure 4.8. Fluorescence response to of 7 or 8 to NO (g) in pH 9.0 CHES buffered solution at 37 °C 158
- Figure 4.9. Fluorescence emission spectra of 5 and 10 in CH₃OH or at pH 7.0 (50 mM PIPES, 100 mM KCl). Fluorescence response of 10 (10 μM, dashed line) to NO (g) in CH₃OH or at pH 7.0..... 159
- Figure 4.10. Optical spectra from the reaction of 6 with NO in CH₂Cl₂/CH₃OH (1/1) and spectra of a solution of 6 during oxidation and reduction..... 160
- Figure 4.11. Fluorescence spectra of a 1:1 CH₃OH:CH₂Cl₂ solution of 6 and 1 with [Cu(CH₃CN)₄](BF₄)..... 161
- Figure 4.12. Fluorescence response of a solution of 6 in CH₂Cl₂ upon addition of NO 162
- Figure 4.13. EPR spectra of a solution of 8 in 4:1 CH₃OH:CH₂Cl₂ after addition of NO 163
- Figure 4.14. Fluorescence spectra of a 4:1 CH₃OH:CH₂Cl₂ solution of 3 without and with [Cu(CH₃CN)₄](BF₄) in the presence of triethylamine 164
- Figure 4.15. Fluorescence response of a solution of 8 in CH₂Cl₂ upon addition of NO 165
- Figure 4.16. IR spectra of 8, 8 with NO, and 8 with NOBF₄ in KBr 166

Figure 4.17.	^1H NMR spectra (6.6 – 9.0 ppm) of Ds-HAMP, a reaction solution of 2 with 10 equiv of NO, and the latter solution to which was added Ds-HAMP	167
Figure 4.18.	Fluorescence spectra of 4:1 $\text{CH}_3\text{OH}:\text{CH}_2\text{Cl}_2$ solution of 8 , 8 with NOBF_4 , and 2 with NO.....	168
Chapter 5		
Figure 5.1.	Schematic drawings of FL_n ($n = 1 - 5$).....	205
Figure 5.2.	Job's plot for the formation of the $\text{FL}_n:\text{Cu}(\text{II})$ complex ($n = 1 - 5$).....	206
Figure 5.3.	ORTEP diagrams of $[\text{Cu}(\text{modL})](\text{BF}_4)_2$ and $[\text{Cu}_2(\text{modL}')_2(\text{CH}_3\text{OH})](\text{BF}_4)_2$ showing 50% probability thermal ellipsoids.....	207
Figure 5.4.	Fluorescence emission spectra of a solution of $\text{Cu}(\text{FL}_n)$ ($1 \mu\text{M}$ FL_n and $1 \mu\text{M}$ CuCl_2) in deoxygenated buffered solution (50 mM PIPES, pH 7.0, 100 mM KCl) before and after admission of NO (g) at 37 °C.....	208
Figure 5.5.	Specificity of $\text{Cu}(\text{FL}_5)$ for NO in buffered aqueous solution (50 mM PIPES, pH 7.0, 100 mM KCl).....	209
Figure 5.6.	Fluorescence emission spectra of a solution of $\text{Cu}(\text{FL}_5)$ upon addition of excess NO.....	210
Figure 5.7.	Fluorescence response of DAF-2 to NO.....	211
Figure 5.8.	Measurement of the dissociation constant (K_d) of $\text{Cu}(\text{FL}_1)$ or $\text{Cu}(\text{FL}_5)$	212
Figure 5.9.	Fluorescence response of FL_5 and $\text{Cu}(\text{FL}_5)$ to NO.....	213
Figure 5.10.	EPR spectra of $\text{Cu}(\text{FL}_5)$ and $\text{Cu}(\text{FL}_5)$ with NO in DMF.....	214
Figure 5.11.	Fluorescence spectra of a mixture of FL_5 and $\text{Cu}(\text{I})$ in the absence and presence of NO.....	215
Figure 5.12.	UV-vis spectra of FL_5 , $\text{Cu}(\text{FL}_5)$, $\text{Cu}(\text{FL}_5)$ treated with NO (g), and FL_5 with the addition of $[\text{Cu}(\text{CH}_3\text{CN}_4)](\text{BF}_4)$ in aqueous solution (50 mM PIPES, pH 7.0, 100 mM KCl).....	216
Figure 5.13.	ESI(-)MS spectrum of the $\text{Cu}(\text{FL}_5)$ species.....	217
Figure 5.14.	LC-MS analyses of $\text{FL}_5\text{-NO}$	218
Figure 5.15.	MS/MS analyses of $\text{FL}_5\text{-NO}$	219
Figure 5.16.	UV-vis spectra of FL_5 and NO reaction solutions at different pHs.....	220
Figure 5.17.	Isosurface plots (isodensity value = 0.5 a.u.) of the key molecular orbitals in the $\text{FL}_5/\text{FL}_5\text{-NO}$ system.....	221

Figure 5.18.	Molecular orbital diagram for the ground, excited, and charge-transfer states of FL ₅	222
Figure 5.19.	Relative energy spacings of the molecular orbitals for the ground states of FL ₅ and FL ₅ -NO.....	223
Chapter 6		
Figure 6.1.	Schematic drawings of FL and CuFL.....	238
Figure 6.2.	NO detection in SK-N-SH cells by CuFL.....	239
Figure 6.3.	Fluorescence response of fluo-4 AM and CuFL in SK-N-SH cells.....	240
Figure 6.4.	NO production with or without L-NNA	241
Figure 6.5.	Fluorescence response of FL in SK-N-SH cells.....	242
Figure 6.6.	Fluorescence response of CuFL in HeLa cells with or without 17β-estradiol	243
Figure 6.7.	MTT assay of SK-N-SH cells treated with CuFL.....	244
Figure 6.8.	NO detection in Raw 264.7 macrophage cells by CuFL	245
Figure 6.9.	A comparison of the time dependence of NO detection by CuFL and with the Griess assay	246
Figure 6.10.	NO detection by CuFL in Raw 264.7 cells with iNOS silenced by RNAi	247
Figure 6.11.	Fluorescence response of CuFL in Raw 264.7 cells stimulated with LPS and IFN-γ in the absence and presence of L-NMA	248
Figure 6.12.	Fluorescence response of FL in Raw 264.7 cells	249
Figure 6.13.	HeLa cells co-treated with CuFL, LPS and IFN-γ.....	250
Figure 6.14.	MTT assay on Raw 264.7 cells treated with CuFL	251
Figure 6.15.	Western blot analysis of cytosolic and nuclear extracts of Raw 264.7 cells	252
Figure 6.16.	NO detection in SK-N-SH and Raw 264.7 cells by CuFL	253
Figure 6.17.	Fluorescence response of CuFL and DAF-2 DA to nitric oxide generation in SK-N-SH cells.....	254
Figure 6.18.	MTT assay of SK-N-SH cells treated with FL-NO	255
Figure 6.19.	Fluorescence response of Cu(I)FL and Cu(II)FL to SNAP	256

Appendix

Figure A.1.	Schematic diagram of two-photon microscope	266
Figure A.2.	Fluorescence response of Silastic membranes of Ds-pip and $[\text{Rh}_2(\mu\text{-O}_2\text{CPr})_4(\text{Ds-pip})]$	267
Figure A.3.	Fluorescence response in the reaction of the Silastic membrane containing $[\text{Rh}_2(\mu\text{-O}_2\text{CPr})_4(\text{Ds-pip})]$ with NO	268
Figure A.4.	Fluorescence response in the reaction of the Silastic membrane containing $[\text{Rh}_2(\mu\text{-O}_2\text{CPr})_4(\text{Ds-pip})]$ with NO (1.9 mM, 0.63 mM, and 0.38 mM)	269
Figure A.5.	Images of the membrane of Ds-pip, $[\text{Rh}_2(\mu\text{-O}_2\text{CPr})_4(\text{Ds-pip})]$, and $[\text{Rh}_2(\mu\text{-O}_2\text{CPr})_4(\text{Ds-pip})]$ with NO by two photon microscopy	270
Figure A.6.	Images of the membrane of $[\text{Rh}_2(\mu\text{-O}_2\text{CPr})_4(\text{Ds-pip})]$ with 0.38, 0.63 and 1.9 mM NO (aq) by two photon microscopy.....	271
Figure A.7.	Stability of the signal of the membrane of $[\text{Rh}_2(\mu\text{-O}_2\text{CPr})_4(\text{Ds-pip})]$ with 1.9 mM NO (aq) over 1 h.....	272

Chapter 1

Metal-Based Turn-On Fluorescent Probes for Sensing Nitric Oxide

Introduction

Nitric oxide (NO) is produced by inducible and constitutive nitric oxide synthases (iNOS and cNOS) resulting in a wide range of concentrations in biological systems.¹⁻⁷ Depending on its concentrations in an organism, NO has diverse biological functions. At the low concentrations generated by cNOS, having both endothelial and neuronal isoforms (eNOS and nNOS), NO can regulate vasodilation, defend against pathogens, and effect long term potentiation.¹⁻⁶ In contrast, the micromolar concentrations of NO produced by iNOS stimulate the formation of reactive nitrogen species (RNS), which affects carcinogenesis and neurodegenerative disorders.^{4,6,8-10}

Since NO is a reactive free radical that rapidly diffuses through most cells and tissues,^{11,12} it is critical to have a method to follow NO immediately upon production. Such a method can enhance an understanding of nitric oxide activity *in vivo*. Fluorescence detection allows imaging of intracellular and extracellular NO when combined with microscopy, providing high spatiotemporal resolution^{13,14} compared to other methods such as chemiluminescence,¹⁵ EPR spectroscopy,¹³ and amperometry.¹⁶ For bioimaging of NO, the commercial organic molecule-based sensors, *o*-diaminonaphthalene (DAN) and *o*-diaminofluoresceins (DAFs) (Figure 1.1), are commonly used.^{13,17} Their fluorescent response, however, arises upon formation of a triazole species by oxidized NO products such as N₂O₃. They are therefore unable to monitor NO itself, which means that NO-related bio-events would not be evaluated in a real-time manner.

There are several requirements for fluorescent nitric oxide sensors to be useful in biology. Probes should be non-toxic and afford direct, fast, reversible, specific, and selective NO detection. It is preferable that they contain fluorophores that excite and emit in the visible or near-infrared region, which is relatively impervious to interference

from cellular damage by UV light. Real-time imaging with spatial information is desirable.

To address the lack of suitable NO sensors, we have investigated the reactions between nitric oxide and transition metal complexes to devise metal-based fluorescent sensors that satisfy the aforementioned criteria. This chapter describes the possible strategies of nitric oxide sensing utilizing redox active transition metal centers. The evolution of transition metal-based probes to achieve a viable biosensor are also described, accompanied by detailed mechanistic studies by our and other research groups.

Strategies for Metal-Based Fluorescent Nitric Oxide Sensing

The first metal-based fluorescent nitric oxide sensor, an iron cyclam complex, exhibited diminished emission intensity upon NO binding to the iron center.¹⁸ An iron dithiocarbamate complex with an acridine-TEMPO ligand also displayed a decrease in fluorescence after NO binding.¹⁹ Fluorescence enhancement is generally preferred over fluorescence quenching when monitoring an analyte in biological systems. When we embarked on our research, no examples of metal-based turn-on fluorescent nitric oxide sensors existed. Our strategies to design transition metal-based fluorescent probes with an increase in fluorescence upon introduction of NO are described herein.

Fluorophore Displacement without Metal Reduction. This approach relies upon the formation of a metal-nitrosyl adduct, releasing a fluorophore that was initially quenched by coordination to a paramagnetic transition metal center by electron or energy transfer (Scheme 1.1a).²⁰ Fluorophores can bind the metal center as axial ligands. Introduction of nitric oxide causes their release from the metal center with concomitant

fluorescence turn-on. This strategy has been applied in an iron cyclam complex,²¹ ruthenium porphyrins²² and dirhodium tetracarboxylate complexes.²³

Metal Reduction without Fluorophore Displacement. Nitric oxide reduces Cu(II) to Cu(I) in the presence of an alcohol or water (ROH), forming RONO and H⁺ (R = Me or H), without loss of the ligand from the metal center (Scheme 1.1b).²⁴ Detailed mechanistic studies of the reduction of Cu(II) to Cu(I) by NO suggested to us that their Cu(II)-based nitric oxide chemistry might form the sensors. Specifically, fluorophore fluorescence, quenched by a paramagnetic Cu(II) environment, is restored upon NO-induced reduction to a diamagnetic Cu(I) species having fluorophore ligands (Scheme 1.1b). We devised three Cu(II) complexes utilizing this strategy.^{25,26}

Metal Reduction with Fluorophore Displacement. Reductive nitrosylation has been reported in the reactions of NO with complexes of metals, including Co and Fe.^{24,27-29} In the cobalt and iron systems, the ligand can also be displaced by NO via reductive nitrosylation.^{24,27-29} In this reaction, fluorophore ligands initially coordinated to the metal are dissociated with a concomitant fluorescence increase upon exposure to NO. The displacement of fluorophore ligands by NO allowed us to design our first fluorescent NO sensors, cobalt-DATI (DATI = dansyl-aminotroponimine, Figure 1.2) and other cobalt compounds, which are described below (Scheme 1.1c.i).^{27,28}

During the metal reduction by NO, the nitrosonium ion, NO⁺, is formed as shown in Scheme 1.1b. It can then react with an amine functionality to produce an *N*-nitrosamine.³⁰ Upon addition of NO, a fluorophore containing an amine motif coordinated to the metal center is readily *N*-nitrosated via an intramolecular pathway, followed by its dissociation and consequent fluorescence enhancement (Scheme 1.1c.ii). Increased fluorescence was observed in the NO reaction of a copper anthracenyl-cyclam complex prepared via the *N*-nitrosation of a cyclam ligand.³¹ Utilizing this fluorophore-

displacement strategy via *N*-nitrosation of the ligand, new metal-based nitric oxide sensors were developed. We constructed a dicobalt(II) tetracarboxylate scaffold and a copper(II) fluorescein complex based on this approach for nitric oxide sensing by turn-on fluorescence.^{32,33}

Cobalt(II) Complexes

Co-DATI Systems. The reaction of air-stable cobalt(II) tropocoronand complexes with NO were previously studied in our laboratory.³⁴ Their NO reactivity suggested that Co(II)-DATI systems of the dansyl-containing aminotroponimine ligands, H^RDATI and H₂DATI-4 (Figure 1.2), may be suitable targets for fluorescent NO sensors. We prepared four Co(II) complexes: [Co(^{iPr}DATI)₂] (1), [Co(^{tBu}DATI)₂] (2), [Co(^{Bz}DATI)₂] (3), and [Co(DATI-4)] (4) (Figure 1.3).^{27,28} These Co(II) complexes all have a pseudo-tetrahedral geometry with dihedral angles between the 5-membered chelate rings in 1, 2, 3, and 4, of 76.1°, 81.4°, 73.8°, and 62.2°, respectively.²⁸ These various values reflect the different steric requirements of the R substituents. The dansyl groups in 3 and 4 align in a parallel-planar fashion, with an average distance between the ring planes of 3.5(1) Å and 3.63(9) Å, respectively. These distances are within the range for π - π stacking interactions,³⁵ which could possibly quench the fluorescence of the dansyl groups.

The fluorescence of the cobalt complexes (40 μ M) is significantly quenched to only 5 – 6% of the intensity of the free ligands in CH₂Cl₂ (Figure 1.4).²⁸ Quenching of fluorescence is hypothesized to result from the interaction between the excited fluorophore and the empty or filled d orbitals on the transition metal via electron or energy transfer.²⁰ Upon addition of NO to the CH₂Cl₂ solution of 1, a slow and steady 8-fold fluorescence increase relative to the starting complex 1 was noted over 6 h (Figure

1.4).²⁸ The initial fluorescent NO response of **4**, however, is faster than that of **1**. A two-fold fluorescence increase caused by the reaction of **4** with NO occurred within 3 min in CH₂Cl₂ and continued to rise over 6 h to a final 4-fold increase.²⁸ The NO detection limit of **4** is 50 – 100 μM. The tetramethylene linker chain of **4** (Figure 1.3) effects greater distortion at the Co(II) center than occurs in **1**, **2**, and **3**, which may result in its different NO reactivity.

The NO-induced fluorescence enhancement is a consequence of fluorophore dissociation upon formation of Co(II)-dinitrosyl adducts in the reaction. These reactions were monitored by IR and ¹H NMR spectroscopy. Several hours after addition of excess NO to CH₂Cl₂ solutions of **1**, two IR bands at 1838 and 1760 cm⁻¹ appeared, indicating the formation of dinitrosyl complexes.²⁸ The ¹H NMR spectrum after NO reaction revealed two sets of resonances for diamagnetic compounds corresponding to the free ligand H^{iPr}DATI and the {Co(NO)₂}¹⁰ species [Co(NO)₂(^{iPr}DATI)].²⁸ Thus, the NO reaction proceeds by a reductive nitrosylation mechanism (Scheme 1.2), consistent with a fluorescence increase resulting from fluorophore dissociation upon NO binding to Co(II) (Scheme 1.1c.i).

Dicobalt(II) Tetracarboxylate Complex. A dicobalt(II) tetracarboxylate complex with *N*-donor ligands, [Co₂(μ-O₂CAr^{Tol})₂(O₂CAr^{Tol})₂(py)₂], where O₂CAr^{Tol} = 2,6-di(*p*-tolyl)benzoate and py = pyridine, was previously reported by our laboratory.³⁶ The properties of this complex, such as air-stability and *N*-donor ligand binding to the metal core, inspired us to examine a carboxylate-bridged dimetallic complex with fluorophore-appended nitrogen bases coordinated to the metal center as a fluorescent NO sensor. A dicobalt(II) complex, with dansyl-piperazine (Ds-pip) as the fluorophore, was prepared and demonstrated to exist in solution as an equilibrium mixture of

windmill $[\text{Co}_2(\mu\text{-O}_2\text{CAr}^{\text{Tot}})_2(\text{O}_2\text{CAr}^{\text{Tot}})_2(\text{Ds-pip})_2]$ (5) and paddlewheel $[\text{Co}_2(\mu\text{-O}_2\text{CAr}^{\text{Tot}})_4(\text{Ds-pip})_2]$ (6) geometric isomers, the ratio of which depends on temperature (Figure 1.5).³² Complex 6 is the predominant species in solution at room temperature.

When non-fluorescent 6 (100 μM) was allowed to react with 150 equiv of NO, a 9.6-fold fluorescence increase occurred within 1 h in CH_2Cl_2 , and emission maximum shifted from 503 nm to 513 nm ($\lambda_{\text{ex}} = 350$ nm).³² IR spectroscopy *in situ* revealed, two noticeable bands at 1864 and 1783 cm^{-1} , consistent with the formation of a Co(I) dinitrosyl adduct. The band attributed to a carboxylate C=O stretching mode at 1610 cm^{-1} in 6 disappeared and was replaced by a new band at 1745 cm^{-1} assigned to the free carboxylic acid during the NO reaction. These results indicate a structural change at the metal center involving the carboxylate ligands.³² X-ray crystallographic analysis of a dicobalt tetranitrosyl complex $[\text{Co}_2(\mu\text{-O}_2\text{CAr}^{\text{Tot}})_2(\text{NO})_4]$ and *N*-nitroso dansyl-piperazine formed during the reaction indicate that NO reductively nitrosylates 6 at the dicobalt(II) core to generate NO^+ , which in turn nitrosates the ligand with concomitant dissociation from cobalt and turn-on fluorescence emission (Scheme 1.3). The observed formation of the *N*-nitrosated fluorophore ligand helps to explain the emission maximum shift after the NO reaction.³² Thus, the fluorophore dissociation strategy (Scheme 1.1c.i), involving *N*-nitrosation of the fluorophore ligand during reductive nitrosylation at the metal center, is responsible for the increase of fluorescence upon treatment of these dicobalt systems with NO.

Other Cobalt Dansyl Complexes. To improve the aqueous solubility as well as the kinetics of fluorescence turn-on by NO in the Co(II) systems, we synthesized the non-fluorescent air-stable Co(II) complexes $[\text{Co}(\text{Ds-AMP})_2]$ (7) and $[\text{Co}(\text{Ds-AQ})_2]$ (8) (Figure 1.6), where Ds-AMP and Ds-AQ are the conjugate bases of dansyl-

aminomethylpyridine (Ds-HAMP) and dansyl-aminoquinoline (Ds-HAQ). These Co(II) complexes were obtained in high yield and only two steps.³⁷ X-ray crystal structure determinations of both complexes revealed a pseudotetrahedral geometry with a dihedral angle ($\Theta = 76.8^\circ$ for both 7 and 8) similar to those of the Co-DATI complexes (Figure 1.6).

Fluorescence enhancement of 7 and 8 upon NO treatment was observed in both CH₃CN and CH₃OH solvents, which are more similar to aqueous media than less polar CH₂Cl₂. For example, upon admission of NO to CH₃CN solutions of Co(II) complexes (10 μ M), the fluorescence was increased by 2.1-fold within 35 min for 7 and by 3.6-fold within 20 min for 8, restoring half of that displayed by two equiv of the free ligands, Ds-HAMP or Ds-HAQ ($\lambda_{\text{ex}} = 342$ nm).³⁷ To understand further the mechanism of the NO-induced fluorescence increase, we investigated the NO reaction with 7 *in situ* by IR ($\{\text{Co}(\text{NO})_2\}$, $\nu_{\text{NO}} = 1766$ and 1693 cm⁻¹) and ¹H NMR (two sets of diamagnetically shifted peaks) spectroscopy.³⁷ A diamagnetic dinitrosyl adduct, presumably [Co(Ds-AMP)(NO)₂], and one free Ds-HAMP ligand were formed in the NO reaction of 7, analogous to the reaction of Co-DATI complexes with NO (Scheme 1.2). Thus, NO sensing by turn-on fluorescence of 7 and 8 occurs by ejection of one fluorophore ligand from the cobalt coordination sphere via reductive nitrosylation, as described in Scheme 1.1c.i.

Co-FATI Systems. The dansyl group that was used in the cobalt complexes above is not optimal for *in vivo* imaging of NO because it requires high excitation energy, which can damage cells. We therefore designed two Co(II) complexes with fluorescein-based ligands, each with an aminotroponimate moiety, [Co(^{iPr}FATI-3)] (9) and [Co(^{iPr}FATI-4)] (10) (Figure 1.7).³⁸ Although X-ray structure determinations of 9 and

10 were not obtained, both complexes are expected to be mononuclear based on mass spectrometric analysis. Compound **10** might have a dinuclear structure by analogy to that of the related complex $[\text{Co}_2(\text{ipr}^{\text{r}}\text{SATI-4})_2]$ (SATI = salicylaldimine) (Figure 1.8), however.³⁸

Addition of excess NO to CH₃OH solutions of both **9** and **10** (10 μM) showed a fluorescence increase of only 20% over 4 h for **9** and 3-fold over 22 h for **10** ($\lambda_{\text{ex}} = 503$ nm, $\lambda_{\text{em}} = 530$ nm), which is significantly slower than encountered with the previous Co(II) systems.^{27,28,32,37,38} Infrared studies of the reaction of **9** with NO indicates that mononitrosyl (1630 cm⁻¹) and dinitrogen (2114 cm⁻¹) adducts were formed.³⁸ We cannot rule out the formation of dinitrosyl species, however, since an intense band for the fluorescein carboxylic acid at 1759 cm⁻¹ overlaps with the IR bands of ν_{NO} in {Co(NO)₂}. Complex **10** also formed the 2117 cm⁻¹ band which most likely corresponds to a dinitrogen adduct. Since multiple products are formed during the reaction, it is not clear from which species fluorescence enhancement arises. Based on IR studies of **9** and **10**, emission may be increased due to the formation of mononitrosyl or dinitrogen adducts.

Iron(II) Complexes

Iron(II) Mmc-cyclam. An Fe(II) methoxycoumarinomethyl-cyclam (Mmc-cyclam) scaffold containing a fluorescamine-PROXYL group (**11**, Scheme 1.4) was synthesized as a ratiometric fluorescent NO sensor with the aim of utilizing the fluorophore-displacement strategy (Scheme 1.1a).²¹ When **11** is excited at 360 nm, fluorescence resonance energy transfer (FRET) occurs from Mmc-cyclam ($\lambda_{\text{ex}} = 360$ nm, $\lambda_{\text{em}} = 410$ nm) to fluorescamine-PROXYL ($\lambda_{\text{ex}} = 385$ nm, $\lambda_{\text{em}} = 470$ nm). Treatment of **11**

in a pH 7.4 buffered solution (40 μM) with the NO-releasing agent NOC-7 produced an increase in emission intensity over 1 h at 410 nm and 470 nm by 1.17-fold and 0.75-fold, respectively.²¹ The NO detection limit for **11** is less than 100 nM. The fluorescence turn-on of **11** by NO arises from dissociation of fluorescamine-PROXYL upon NO binding to the iron center, showing the restored fluorescence of Mmc-cyclam (Scheme 1.4). Although **11** is capable of monitoring NO by fluorescence turn-on at a physiological pH, it is not practical for the bio-imaging of NO due to its sensitivity to O₂, slow response to NO, and small increase in fluorescence intensity.

Diiron(II) Tetracarboxylate Complex. Several diiron(II) terphenylcarboxylato complexes with *N*-donor ligands have been reported.³⁹⁻⁴¹ We prepared a diiron(II)-based NO sensor [Fe₂(μ -O₂CAr^{Tol})₄(Ds-pip)₂] (**12**, Figure 1.9) by an approach similar to that used for dicobalt(II) complexes **5** and **6**.³² Exposure of **12** (0.1 mM) to 1 equiv of NO in CH₂Cl₂ elicited a 4-fold increase in emission intensity within 5 min ($\lambda_{\text{ex}} = 350 \text{ nm}$).³² The reaction of **12** with O₂, however, also led to fluorescence enhancement by 2.8-fold over 15 min. Infrared spectroscopic studies of **12** (0.5 mM) with 10 equiv of NO revealed two new IR bands at 1797 and 1726 cm⁻¹, consistent with formation of an Fe(NO)₂ unit, and concomitant loss of the carboxylate stretching band at 1605 cm⁻¹. These observations possibly indicate generation of a diiron tetranitrosyl complex with two bridging carboxylate ligands during the reaction.³² Thus, the NO-induced fluorescence increase would occur by ligand dissociation from the diiron core. Although **12**, like **11**, reacts with NO resulting in a fluorescence increase, the O₂-sensitivity of **12** renders it unsuitable as a NO sensor.

Ruthenium(II) Tetraphenylporphyrins

Ruthenium(II) porphyrins form stable nitrosyl complexes upon exposure to NO.²⁹ The axial positions on the Ru(II) center are available for fluorophore ligands as well. The affinity of NO for the Ru(II) porphyrins was therefore utilized to devise a new NO sensor based on the fluorophore-displacement strategy (Scheme 1.1a). We constructed ruthenium carbonyl tetraphenylporphyrin complexes with a dansyl-derivatized axial base, imidazole (Ds-im) or thiomorpholine (Ds-tm), [Ru(TPP)(CO)(Ds-im)] (**13**) and [Ru(TPP)(CO)(Ds-tm)] (**14**) (Figure 1.10). These compounds are expected to detect NO via the fluorophore-displacement strategy.²² The fluorophores are coordinated to the axial site of the Ru(II) center *trans* to CO via the nitrogen atom of imidazole or sulfur atom of thiomorpholine, as confirmed by an X-ray structure determination (Figure 1.10).

Reaction of **13** and **14** (10 μ M) with 100 equiv of NO in CH₂Cl₂ afforded a 19-fold increase in fluorescence within 20 min and an immediate 1.3-fold increase in fluorescence, respectively ($\lambda_{\text{ex}} = 368$ nm for Ds-im, $\lambda_{\text{ex}} = 345$ nm for Ds-tm). Isolation and characterization of the Ru-containing product in the NO reactions of **13** revealed that both CO and dansyl-containing fluorophore ligands dissociate from the Ru(II) center during the reaction. The product isolated is [Ru(TPP)(NO)(ONO)].^{29,42,43} Release of the free fluorophore ligand from Ru(II) formed during the NO reaction of **13** was monitored by ¹H NMR spectroscopy.²² Thus, the fluorescence enhancement that occurs upon addition of NO to **13** and **14** arises from displacement of Ds-im or Ds-tm from the axial sites, restoring their turn-on emission (Scheme 1.1a).

Dirhodium(II) Tetracarboxylates

Various ligands including nitric oxide can be coordinated as axial ligands to a tetra-bridged dirhodium core.⁴⁴ A nitrosyl adduct obtained from the reaction of NO with solid $[\text{Rh}_2(\mu\text{-O}_2\text{CMe})_4]$ can be reversed upon heating to 120 °C,⁴⁵ suggesting that a dirhodium fluorophore complex might potentially be a reversible NO sensor. We designed dirhodium tetracarboxylate scaffolds containing bound fluorophores $[\text{Rh}_2(\mu\text{-O}_2\text{CMe})_4(\text{Ds-pip})]$ (**15**) and $[\text{Rh}_2(\mu\text{-O}_2\text{CMe})_4(\text{Ds-im})]$ (**16**) (Figure 1.11). These compounds were synthesized *in situ* by the reaction of $[\text{Rh}_2(\mu\text{-O}_2\text{CMe})_4]$ of Ds-pip or Ds-im.²³ X-ray crystallographic studies of the isolated dirhodium tetracarboxylate complexes with Ds-pip and Ds-im revealed coordination to the axial positions of the dirhodium core by the piperazine and imidazole nitrogen atoms, respectively.²³

When **15** was exposure to 100 equiv of NO in 1,2-dichloroethane (DCE), there was an immediate 26-fold increase in fluorescence ($\lambda_{\text{ex}} = 345 \text{ nm}$).²³ A 16-fold increased fluorescence was observed upon addition of 100 equiv of NO to a DCE solution of **16** ($\lambda_{\text{ex}} = 365 \text{ nm}$).²³ The fluorescence response of both compounds was reversible and their sensitivity to NO extended to $\sim 4 \mu\text{M}$ solutions.

NO sequentially generates mono- and dinitrosyl adducts with dirhodium tetracarboxylates. Although the mononitrosyl species has not been isolated, dirhodium dinitrosyl complexes were obtained and characterized by IR spectroscopy ($[\text{Rh}_2(\mu\text{-O}_2\text{CMe})_4(\text{NO})_2]$, $\nu_{\text{NO}} = 1729$ and 1698 cm^{-1} in KBr, $\nu_{\text{NO}} = 1702 \text{ cm}^{-1}$ in DCE) and X-ray crystallography (Figure 1.12).²³ Thus, the NO-induced fluorescence turn-on is due to the formation of metal nitrosyl species with concomitant dissociation of dansyl fluorophores from the quenching environment of the Rh_2 core (Scheme 1.1a).

A kinetic study of the reaction at $-80 \text{ }^\circ\text{C}$ revealed it to be complete within the 1-ms mixing time of the stopped-flow experiment, corresponding to an on-rate of at least

$4 \times 10^6 \text{ s}^{-1}$ at $40 \text{ }^\circ\text{C}$.²³ Fast and reversible NO detection utilizing dirhodium complexes **15** and **16** suggests their potential value as real-time imaging agents for NO in biological systems. They are incompatible with aqueous media, however, since water itself can displace the fluorophore ligand and bind to the dirhodium core. One approach to achieve water-compatibility is to isolate a solution of the dirhodium sensor behind a Silastic membrane that is impermeable to water, but permits NO gas transport. In one such experiment, the fluorescence of a $20 \text{ }\mu\text{M}$ Ds-pip and $40 \text{ }\mu\text{M}$ $[\text{Rh}_2(\mu\text{-O}_2\text{CMe})_4]$ solution in CH_2Cl_2 , which was sequestered from a saturated aqueous NO solution by the membrane, immediately increased upon application of the nitric oxide (Figure 1.13a).²³ In a separate strategy the dirhodium sensor was embedded within the Silastic membrane. When membrane-encapsulated $[\text{Rh}_2(\mu\text{-O}_2\text{CPr})_4(\text{Ds-pip})]$ was treated with an aqueous solution of NO, an immediate fluorescence increase was observed (Figure 1.13b).⁴⁶ These experiments illustrate a potential approach to fascinating fiber-optic or film-based NO sensing devices for study in biological fluids using dirhodium-containing polymers.

Copper(II) Complexes

Copper(II) Dansyl Complexes. Nitric oxide reduces Cu(II) to Cu(I), a process that has been well-investigated.²⁴ Quenching of the fluorescence of the luminescent ligand by coordination to a paramagnetic Cu(II) center can be restored by NO-induced reduction to diamagnetic Cu(I) (Scheme 1.1b). We applied this strategy to develop two water-soluble Cu(II) complexes $[\text{Cu}(\text{Ds-en})_2]$ (**17**) and $[\text{Cu}(\text{Ds-AMP})_2]$ (**18**) (Figure 1.14), where Ds-en is the conjugate base of dansyl ethylenediamine.^{25,47,48} X-ray crystal

structures of both **17** and **18** indicate that the Cu(II) center is coordinated by two dansyl-containing ligands (Figure 1.14).^{25,48}

The fluorescence response of **17** and **18** to NO was monitored with 10 nM sensitivity in both organic and aqueous buffered solutions. Fluorescence experiments demonstrated significant Cu(II)-induced quenching in both organic (4:1 CH₃OH:CH₂Cl₂) and aqueous buffered solutions, compared to the free ligands ($\lambda_{\text{ex}} = 342$ nm).²⁵ Upon addition of NO to an organic solution of **17** and **18** (20 μ M, 4:1 CH₃OH:CH₂Cl₂), emission intensity was immediately increased by 6.1-fold for **17** and 8.8-fold for **18** with a sensitivity of 10 nM.²⁵ Addition of NO to an aqueous buffered solution (50 mM CHES, pH 9, 100 mM KCl) of **17** or **18** (10 μ M) also caused a fluorescence increase by 2.3- or 2.0-fold, respectively.²⁵ Although this pH is not within the typical physiological range, these complexes allowed for the first time NO sensing in purely aqueous solutions with significant fluorescence turn-on at physiological relevant concentrations.

NO-induced fluorescence enhancement in these Cu(II) systems occurs by formation of a diamagnetic Cu(I) species, as mentioned previously, as well as dissociation of the sulfonamide functionality by protonation. Evidence that a Cu(I) species forms in the NO reactions of the Cu(II) complexes was provided by EPR spectroscopy, which displayed a decrease in the Cu(II) EPR signal.²⁵ The protonation of the sulfonamide functionality was observed by IR spectroscopy ($\nu_{\text{N-H}} = 3083$ cm⁻¹).²⁵ A proton was generated from the reaction of ROH, either CH₃OH or H₂O, with NO⁺ produced during the course of the NO reactions. Further support for the proposed mechanism was provided by the reactions of NO in the absence of ROH and of ROH with NOBF₄. The ¹H NMR spectrum indicated that complete dissociation of dansyl

ligands does not occur after the NO reaction.²⁵ Therefore, fluorescence is increased by NO-induced reduction of Cu(II) to Cu(I) without complete dissociation of fluorophore ligand from the Cu center (Scheme 1.1b).

Copper(II) Conjugated Polymer. A conjugated polymer (CP1a), composed of a bipyridyl-substituted poly(*p*-phenylene vinylene), was prepared as a fluorophore ligand for Cu(II) (Figure 1.15).²⁶ The fluorescence of CP1a was significantly quenched in the presence of Cu(II). Addition of 300 equiv of NO to Cu(II)-CP1a (**19**) in 4:1 CH₂Cl₂:CH₃CH₂OH immediately induced a 2.8-fold fluorescence enhancement ($\lambda_{\text{ex}} = 462$ nm, $\lambda_{\text{em}} = 542$ nm).²⁶ This fluorescence response is caused by reduction of Cu(II) to Cu(I) without fluorophore release (Scheme 1.1b), as described above for **17** and **18**. The fluorescence increase by NO was not observed in the absence of added ROH. Selectivity studies versus other reactive nitrogen species such as nitrosothiol (RSNO), NO⁺, and HNO, were performed and revealed that only nitroxyl elicited an immediate 2.8-fold increase in fluorescence.²⁶ The detection limit for NO by **19** is 6.3 nM, which was measured by using the NO-releasing agent *S*-nitroso-*N*-acetylpenicillamine (SNAP).²⁶

Copper(II) Anthracenyl-Cyclam. A copper(II) complex of a cyclam derivative having pendent anthracyl groups, Cu(DAC)²⁺ (**20**) (DAC = bis(9-anthracylmethyl)cyclam), was recently reported (Figure 1.16).³¹ Addition of excess NO to the weakly-fluorescent **20** in aqueous CH₃OH (10:1 CH₃OH:H₂O) solution resulted in slow restoration of anthracene emission over 45 min.³¹ This increase in fluorescence occurs by release of the *N*-nitrosated DAC ligand from the Cu center with concomitant reduction of Cu(II) to Cu(I) (Scheme 1.1c.ii). The presence of a Cu(I) species during the NO reaction was determined by UV-vis spectroscopy (disappearance of a d-d absorption band at 566 nm) and electrochemical studies.³¹ Formation of the *N*-nitrosated

DAC ligand during the reaction was confirmed by ESI-MS ($m/z = 610$ corresponding to $[\text{DAC} + \text{NO}]^+$) and ^1H COSY NMR spectroscopy (1:1 *E:Z* isomers).³¹ The ligand dissociation in the NO reaction of **20** may be explained by the less basic nature of the *N*-nitrosoamine and the geometric mismatch between the cyclam ring and Cu(I), which prefers a tetrahedral coordination environment.

Copper(II) Fluorescein Complex. For intracellular NO sensing we applied the strategy described in Scheme 1.1c.ii to design a Cu(II) fluorescein complex. The Cu(II) fluorescein-based NO sensor CuFL (**21**) (FL = 2-(2-chloro-6-hydroxy-5-[(2-methylquinolin-8-ylamino)-methyl]-3-oxo-3*H*-xanthen-9-yl)benzoic acid) was formed *in situ* by reacting FL with CuCl₂ in a 1:1 ratio at pH 7.0 (50 mM PIPES, 100 mM KCl) (Figure 1.17).³³ Introduction of NO to a non-fluorescent buffered solution of **21** (1 μM) at 37 °C led to an immediate 11-fold fluorescence enhancement, which continued to rise to 16-fold over 5 min with a sensitivity of 5 nM.³³ Compound **21** is highly specific for NO over other biologically relevant species such as HNO, NO₂⁻, NO₃⁻, ONOO⁻, and H₂O₂.³³

As described in Schemes 1.1c.ii and 1.5, NO-induced metal reduction of Cu(II) to Cu(I), forming the *N*-nitrosamine of FL (FL-NO), occurs in the NO reaction of **21**. Reduction of Cu(II) to Cu(I) by NO during the reaction was confirmed by following the decrease of Cu(II) EPR signals.³³ The formation of the *N*-nitrosated FL ligand was proved by product analysis using LC-MS and comparison with independently prepared FL-NO. The red-shifted UV-vis spectrum observed following the addition of excess NO to **21** is the same as that of free FL and different from the spectrum observed upon mixing free FL with the Cu(I) salt $[\text{Cu}(\text{CH}_3\text{CN})_4](\text{BF}_4)$, indicating that FL-NO dissociates from the Cu center.³³ Thus, the turn-on fluorescence is a result of *N*-nitrosated fluorophore displacement via reduction of the metal center (Scheme 1.1c.ii).

The ability of **21** to detect NO directly, rapidly, and specifically at a physiological pH encouraged us to apply it to image NO production in live cells. We tested **21** for its ability to visualize biological NO in Raw 264.7 murine macrophage cells, for iNOS-generated NO, and in SK-N-SH human neuroblastoma cells, for cNOS-produced NO. Time-dependent NO generation in Raw 264.7 cells stimulated with bacterial lipopolysaccharide and interferon- γ was monitored by **21** using fluorescence microscopy (Figure 1.18).³³ The fluorescence intensity derived from **21** was diminished in Raw 264.7 cells in which iNOS silenced by RNA interference (Figure 1.18), or in the presence of N^G -methyl-*L*-arginine (*L*-NMA), a known inhibitor of iNOS.³³ These control experiments indicate that the observed results originate from the reaction of **21** with NO. We also investigated the ability of **21** to detect NO produced by cNOS in SK-N-SH cells. The NO-induced fluorescence response, monitored after simultaneous administration of 17β -estradiol and **21** to the cells, was complete within 5 min (Figure 1.19).³³ A diminished fluorescence response occurred in the presence of the cNOS inhibitor N^G -nitro-*L*-arginine (*L*-NNA) (Figure 1.19), confirming that NO generation is responsible for the fluorescence increase.³³ Cytotoxicity assays of Raw 264.7 and SK-N-SH cells treated with **21** for 5 days demonstrated > 80% cell survival, proving **21** to be non-toxic to live cells and an excellent candidate for bio-imaging studies of nitric oxide.³³

Summary

Nitric oxide, being a reactive and unstable species, mediates beneficial and harmful biological events in the cardiovascular, immune, and nervous systems. Fluorescent probes have been developed for visualizing nitric oxide in biology. The

commonly used organic molecule-based sensors are not capable of direct NO detection, a requirement for understanding fully the activity of NO in bioorganisms. Metal-based NO sensors are promising candidates for direct and specific NO detection, utilizing NO binding to the metal center. We and other groups have devised a variety of metal complexes described here as fluorescent NO sensors. Cobalt(II) complexes containing dansyl and fluorescein moiety (1 – 10), iron(II) complexes (11 and 12), ruthenium(II) porphyrins (13 and 14), and dirhodium(II) tetracarboxylates (15 and 16) clearly afford direct NO detection by fluorescence turn-on through interaction of nitric oxide with the metal centers. NO chemistry at the copper(II) centers also provides a valuable approach to fluorescence-based NO sensing (17-21). Very recently, the Cu(II) complex of a fluorescein-based ligand (21) has made NO detection at pH 7.0 and in live cells a reality. As summarized here, strategies for NO sensing by metal complexes include fluorophore displacement without metal reduction and metal reduction with or without fluorophore displacement. These approaches have facilitated novel for NO detection. Taken together, the metal complexes described here unequivocally demonstrate that fluorescent complexes of transition metal ions are appropriate and practical for investigating the roles of NO itself in biology. We anticipate significant advances in this new area in the near future.

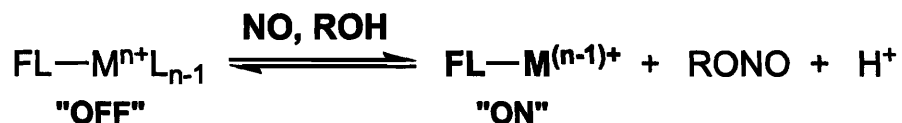
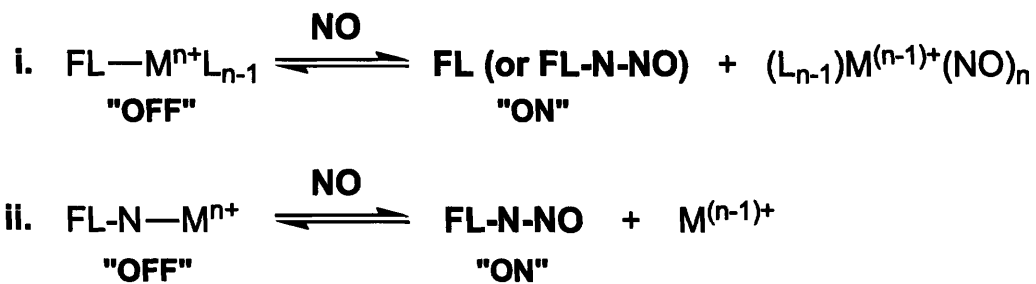
References

- (1) Murad, F., *Angew. Chem. Int. Ed.* **1999**, *38*, 1856-1868.
- (2) Furchgott, R. F., *Angew. Chem. Int. Ed.* **1999**, *38*, 1870-1880.
- (3) Ignarro, L. J., *Angew. Chem. Int. Ed.* **1999**, *38*, 1882-1892.
- (4) Moncada, S.; Palmer, R. M. J.; Higgs, E. A., *Pharmacol. Rev.* **1991**, *43*, 109-142.

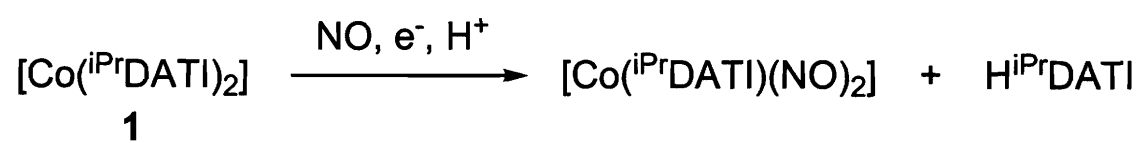
- (5) Ricciardolo, F. L. M.; Sterk, P. J.; Gaston, B.; Folkerts, G., *Physiol. Rev.* **2004**, *84*, 731-765.
- (6) Conner, E. M.; Grisham, M. B., *Methods Enzymol.* **1995**, *7*, 3-13.
- (7) Marletta, M. A.; Hurshman, A. R.; Rusche, K. M., *Curr. Opin. Chem. Biol.* **1998**, *2*, 656-663.
- (8) Wink, D. A.; Vodovotz, Y.; Laval, J.; Laval, F.; Dewhirst, M. W.; Mitchell, J. B., *Carcinogenesis* **1998**, *19*, 711-721.
- (9) Laval, F.; Wink, D. A., *Carcinogenesis* **1994**, *15*, 443-447.
- (10) Calabrese, V.; Bates, T. E.; Stella, A. M. G., *Neurochem. Res.* **2000**, *25*, 1315-1341.
- (11) Lancaster, J. R., Jr., *Nitric Oxide: Biol. and Chem.* **1997**, *1*, 18-30.
- (12) Wood, J.; Garthwaite, J., *Neuropharm.* **1994**, *33*, 1235-1244.
- (13) Nagano, T.; Yoshimura, T., *Chem. Rev.* **2002**, *102*, 1235-1269 and references cited therein.
- (14) Hilderbrand, S. A.; Lim, M. H.; Lippard, S. J., *In Topics in Fluorescence Spectroscopy*, Geddes, C. D.; Lakowicz, J. R., Eds. Springer: 2005; pp 163-188 and references cited therein.
- (15) Hampl, V.; Walters, C. L.; Archer, S. L., *In Methods in Nitric Oxide Research*, Feelisch, M.; Stamler, J. S., Eds. John Wiley & Sons: New York, 1996; pp 309-318.
- (16) Malinski, T.; Mesaros, S.; Tomboulian, P., *Methods Enzymol.* **1996**, *268*, 58-69.
- (17) Miles, A. M.; Chen, Y.; Owens, M. W.; Grisham, M. B., *Methods Enzymol.* **1995**, *7*, 40-47.
- (18) Katayama, Y.; Takahashi, S.; Maeda, M., *Anal. Chim. Acta* **1998**, *365*, 159-167.
- (19) Soh, N.; Katayama, Y.; Maeda, M., *Analyst* **2001**, *126*, 564-566.
- (20) Bergonzi, R.; Fabbri, L.; Licchelli, M.; Mangano, C., *Coord. Chem. Rev.* **1998**, *170*, 31-46.

- (21) Soh, N.; Imato, T.; Kawamura, K.; Maeda, M.; Katayama, Y., *Chem. Commun.* **2002**, 2650-2651.
- (22) Lim, M. H.; Lippard, S. J., *Inorg. Chem.* **2004**, *43*, 6366-6370.
- (23) Hilderbrand, S. A.; Lim, M. H.; Lippard, S. J., *J. Am. Chem. Soc.* **2004**, *126*, 4972-4978.
- (24) Ford, P. C.; Fernandez, B. O.; Lim, M. D., *Chem. Rev.* **2005**, *105*, 2439-2455 and references cited therein.
- (25) Lim, M. H.; Lippard, S. J., *J. Am. Chem. Soc.* **2005**, *127*, 12170-12171.
- (26) Smith, R. C.; Tennyson, A. G.; Lim, M. H.; Lippard, S. J., *Org. Lett.* **2005**, *7*, 3573-3575.
- (27) Franz, K. J.; Singh, N.; Lippard, S. J., *Angew. Chem. Int. Ed.* **2000**, *39*, 2120-22.
- (28) Franz, K. J.; Singh, N.; Spingler, B.; Lippard, S. J., *Inorg. Chem.* **2000**, *39*, 4081-4092.
- (29) Ford, P. C.; Lorkovic, I. M., *Chem. Rev.* **2002**, *102*, 993-1017 and references cited therein.
- (30) Lee, J.; Chen, L.; West, A. H.; Richter-Addo, G. B., *Chem. Rev.* **2002**, *102*, 1019-1065 and references cited therein.
- (31) Tsuge, K.; DeRosa, F.; Lim, M. D.; Ford, P. C., *J. Am. Chem. Soc.* **2004**, *126*, 6564-6565.
- (32) Hilderbrand, S. A.; Lippard, S. J., *Inorg. Chem.* **2004**, *43*, 5294-5301.
- (33) Lim, M. H.; Xu, D.; Lippard, S. J., *Nat. Chem. Biol.* **2006**, in press.
- (34) Franz, K. J.; Doerrer, L. H.; Spingler, B.; Lippard, S. J., *Inorg. Chem.* **2001**, *40*, 3774-3780.
- (35) Liu, Z.-H.; Duan, C.-Y.; Hu, J.; You, X.-Z., *Inorg. Chem.* **1999**, *38*, 1719-1724.
- (36) Lee, D.; Hung, P.-L.; Spingler, B.; Lippard, S. J., *Inorg. Chem.* **2002**, *41*, 521-531.
- (37) Lim, M. H.; Kuang, C.; Lippard, S. J., *ChemBioChem* **2006**, in press.

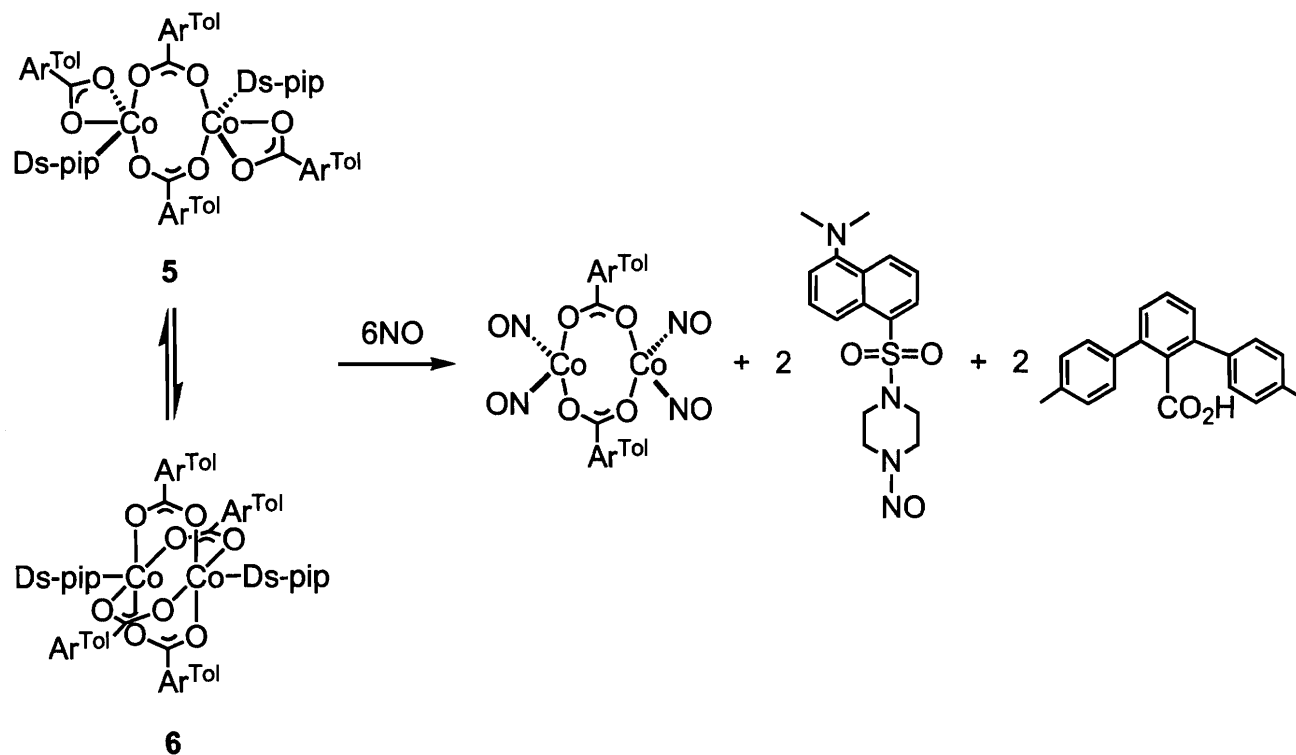
- (38) Hilderbrand, S. A.; Lippard, S. J., *Inorg. Chem.* **2004**, *43*, 4674-4682.
- (39) Lee, D.; Lippard, S. J., *J. Am. Chem. Soc.* **2001**, *123*, 4611-4612.
- (40) Yoon, S.; Lippard, S. J., *Inorg. Chem.* **2003**, *42*, 8606-8608.
- (41) Lee, D.; Lippard, S. J., *Inorg. Chem.* **2002**, *41*, 2704-2719.
- (42) Miranda, K. M.; Bu, X.; Lorkovic, I.; Ford, P. C., *Inorg. Chem.* **1997**, *36*, 4838-4848.
- (43) Kadish, K. M.; Adamian, V. A.; Van Caemelbecke, E.; Tan, Z.; Tagliatesta, P.; Bianco, P.; Boschi, T.; Yi, G.-B.; Khan, M. A.; Richter-Addo, G. B., *Inorg. Chem.* **1996**, *35*, 1343-1348.
- (44) Boyar, E. B.; Robinson, S. D., *Coord. Chem. Rev.* **1983**, *50*, 109-208.
- (45) Johnson, S. A.; Hunt, H. R.; Neumann, H. M., *Inorg. Chem.* **1963**, *2*, 960-962.
- (46) Lim, M. H.; Lippard, S. J., **2005**, unpublished results.
- (47) Prodi, L.; Bolletta, F.; Montalti, M.; Zaccheroni, N., *Eur. J. Inorg. Chem.* **1999**, 455-460.
- (48) Prodi, L.; Montalti, M.; Zaccheroni, N.; Dallavalle, F.; Folesani, G.; Lanfranchi, M.; Corradini, R.; Pagliari, S.; Marchelli, R., *Helv. Chim. Acta* **2001**, *84*, 690-706.

(a) Fluorophore Displacement without Metal Reduction**(b) Metal Reduction without Fluorophore Displacement****(c) Metal Reduction with Fluorophore Displacement**

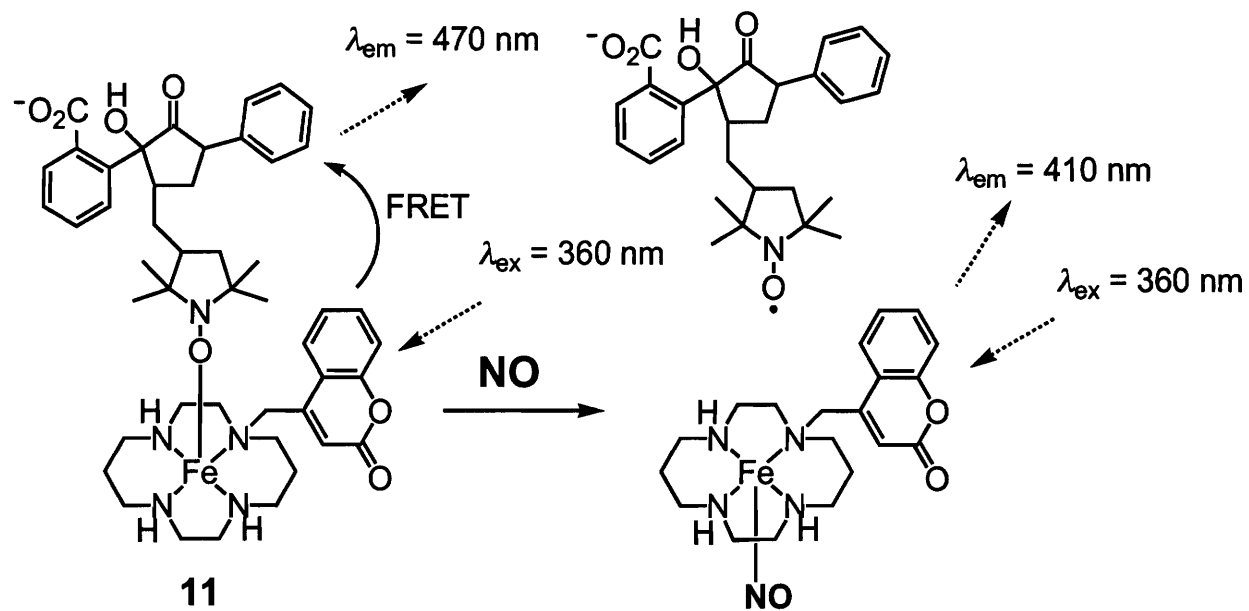
Scheme 1.1. Strategies for Metal-Based Nitric Oxide Sensing.



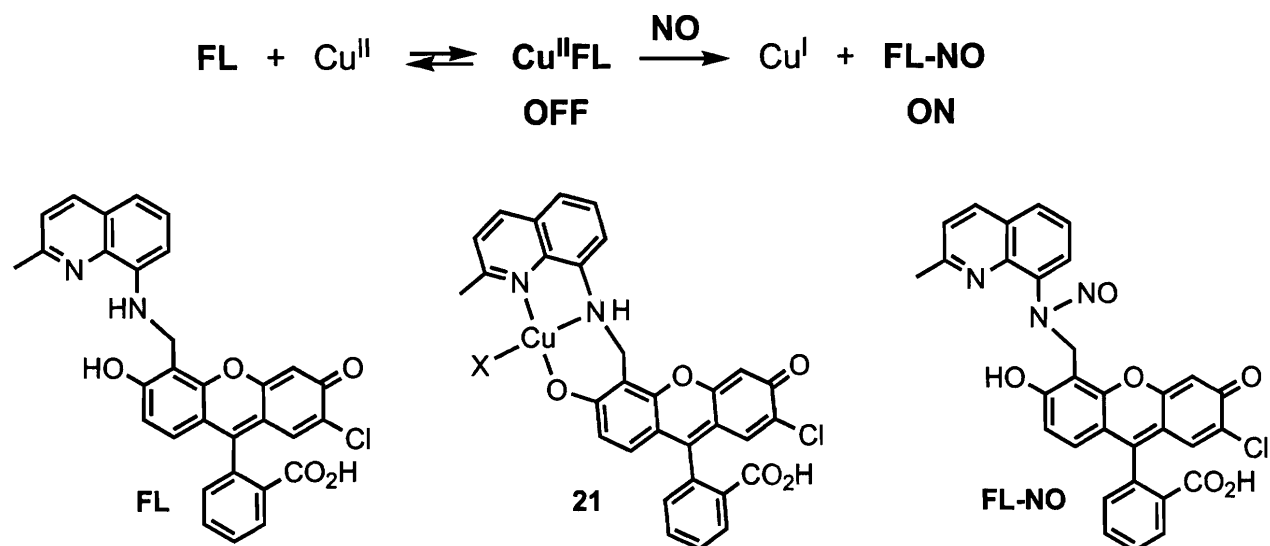
Scheme 1.2. NO Reactivity of Co-DATI Complexes.



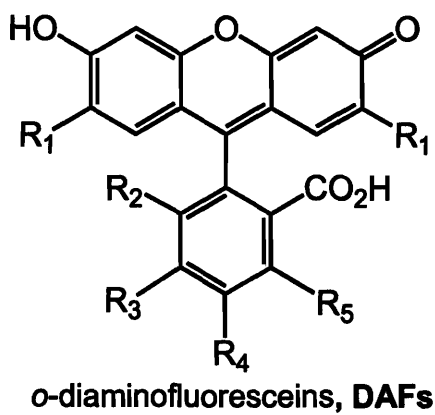
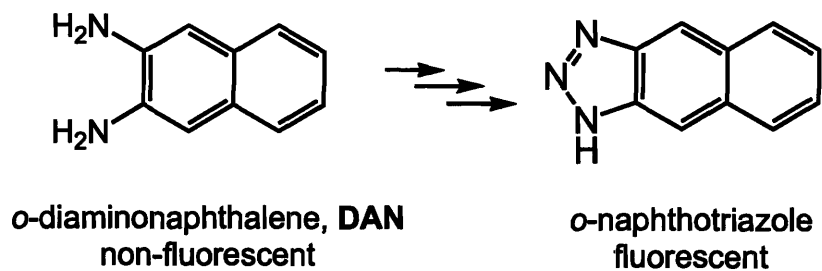
Scheme 1.3. Nitric Oxide Reactivity of 5 and 6.



Scheme 1.4. Nitric Oxide Detection by **11**.



Scheme 1.5. Nitric Oxide Sensing by 21.



DAFs	R ₁	R ₂	R ₃	R ₄	R ₅
DAF-1	H	H	H	NH ₂	NH ₂
DAF-2	H	H	NH ₂	NH ₂	H
DAF-3	H	NH ₂	NH ₂	H	H
DAF-4	Cl	H	H	NH ₂	NH ₂
DAF-5	Cl	H	NH ₂	NH ₂	H
DAF-6	Cl	NH ₂	NH ₂	H	H

Figure 1.1. Schematic drawings of DAN and DAFs.

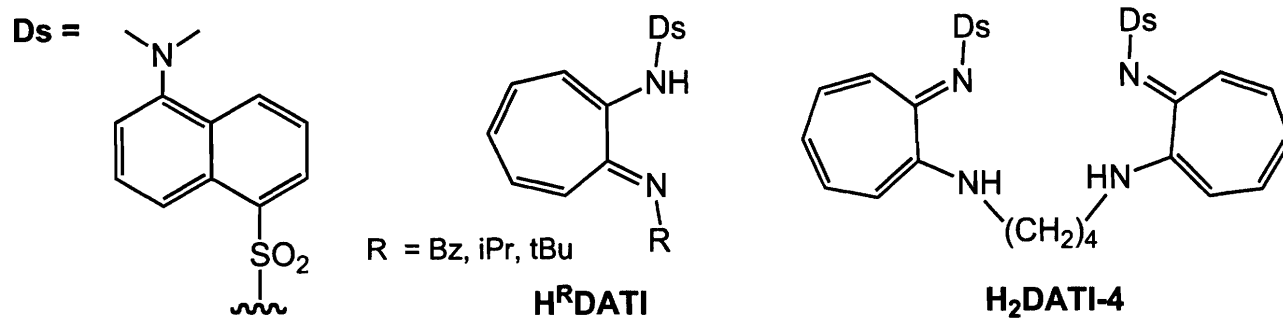


Figure 1.2. Schematic drawings of H^RDATI and H₂DATI-4.

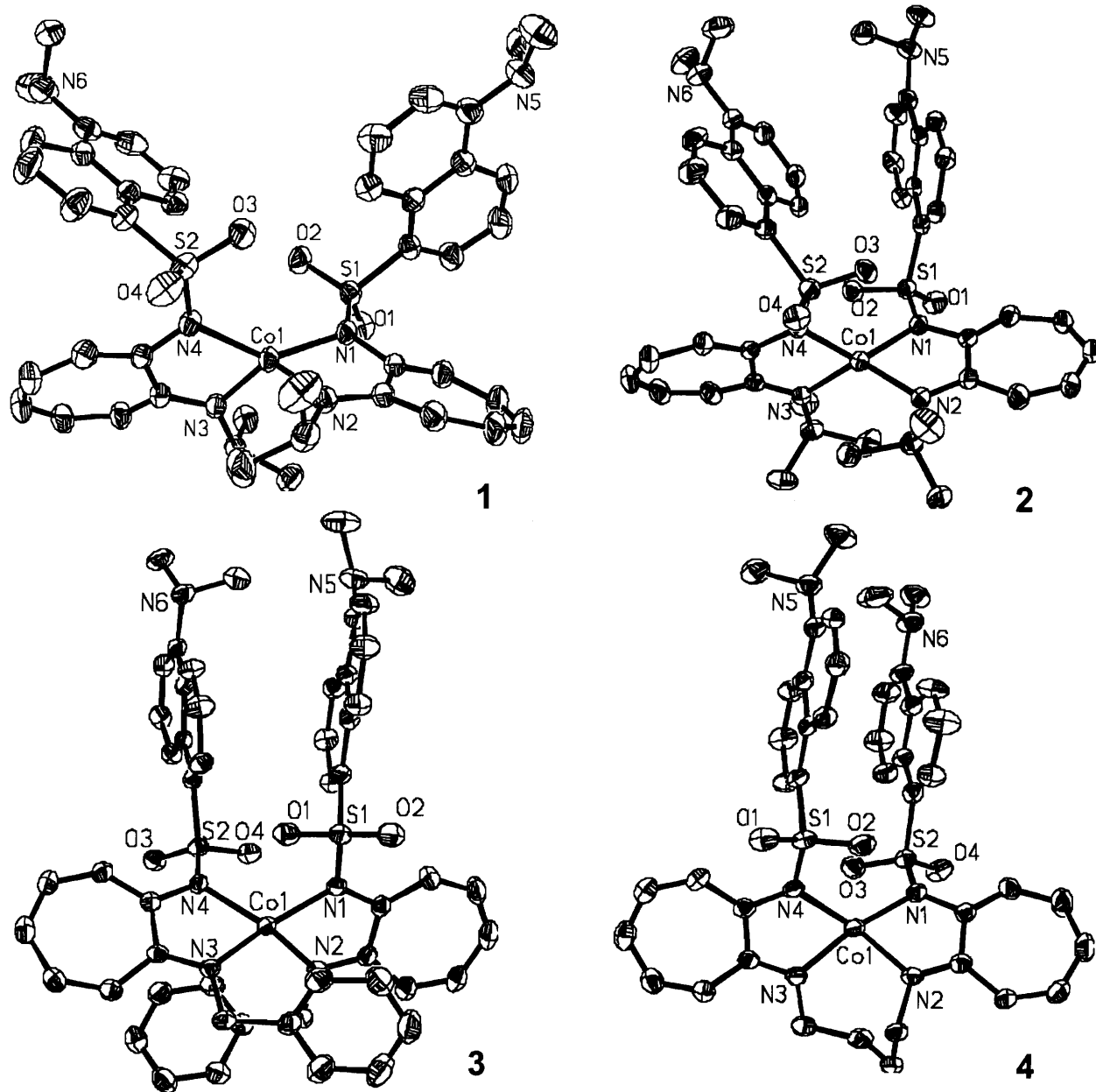


Figure 1.3. ORTEP diagrams of $[\text{Co}(\text{iPrDATI})_2]$ (1), $[\text{Co}(\text{tBuDATI})_2]$ (2), $[\text{Co}(\text{BzDATI})_2]$ (3), and $[\text{Co}(\text{DATI-4})]$ (4) showing 50% probability thermal ellipsoids. The figure adopted from ref. 28 was modified.

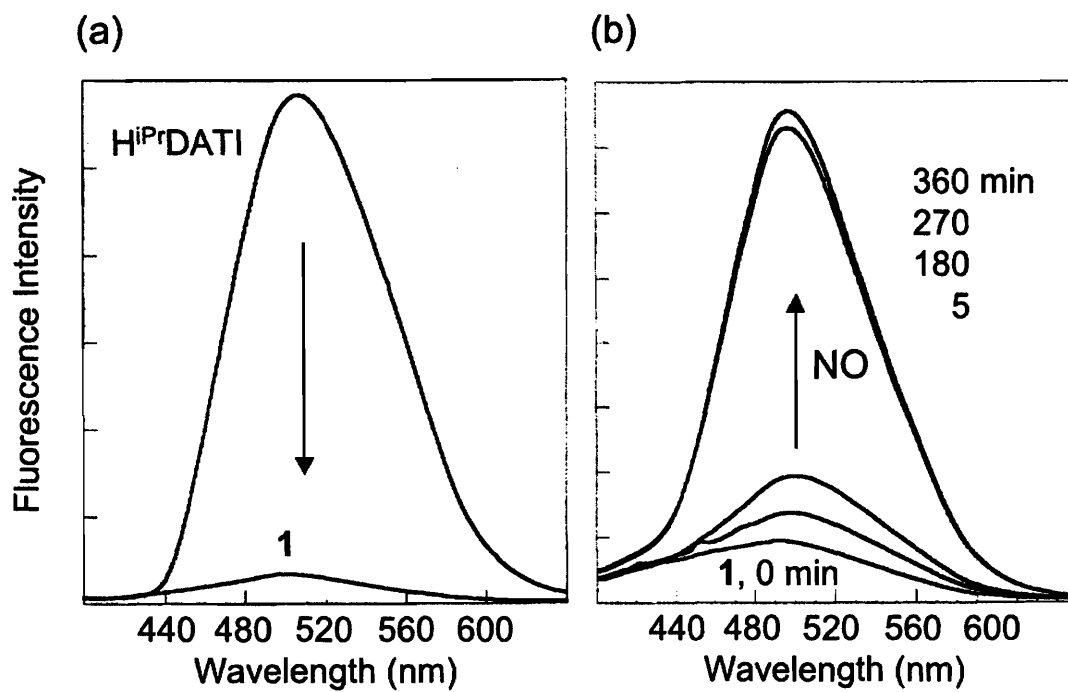


Figure 1.4. Fluorescence responses of (a) $\text{H}^{\text{iPr}}\text{DATI}$ and $[\text{Co}(\text{iPr}^{\text{DATI}})_2]$ (**1**) and (b) of **1** upon addition of excess NO, excited at 350 nm. The figure adopted from ref. 28 was modified.

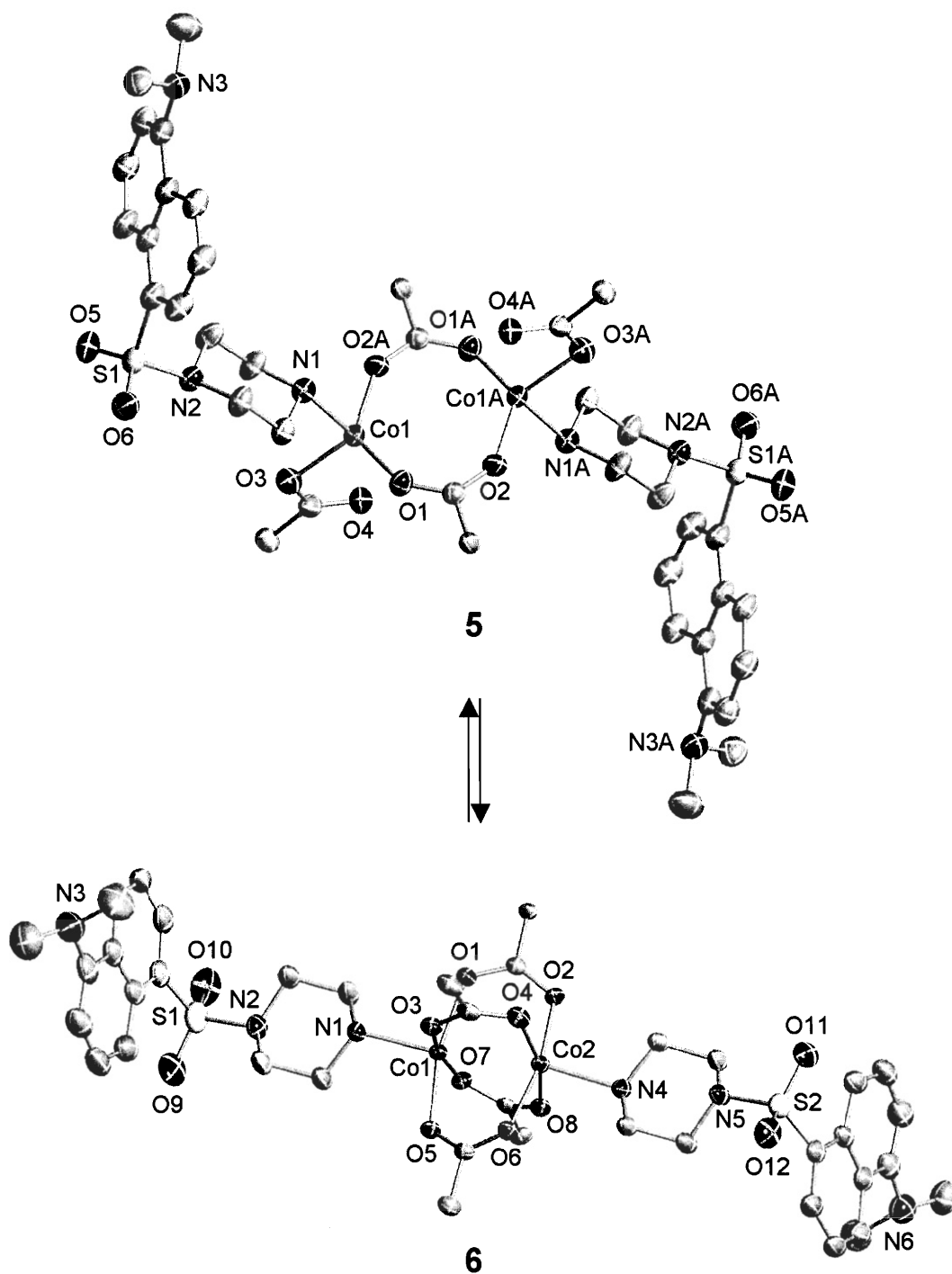


Figure 1.5. ORTEP diagrams of windmill $[\text{Co}_2(\mu\text{-O}_2\text{CAr}^{\text{Tol}})_2(\text{O}_2\text{CAr}^{\text{Tol}})_2(\text{Ds-pip})_2]$ (5) and paddlewheel $[\text{Co}_2(\mu\text{-O}_2\text{CAr}^{\text{Tol}})_4(\text{Ds-pip})_2]$ (6) showing 50% probability thermal ellipsoids. The phenyl rings of $\text{Ar}^{\text{Tol}}\text{CO}_2^-$ ligands have been omitted for clarity. The figure adopted from ref. 32 was modified.

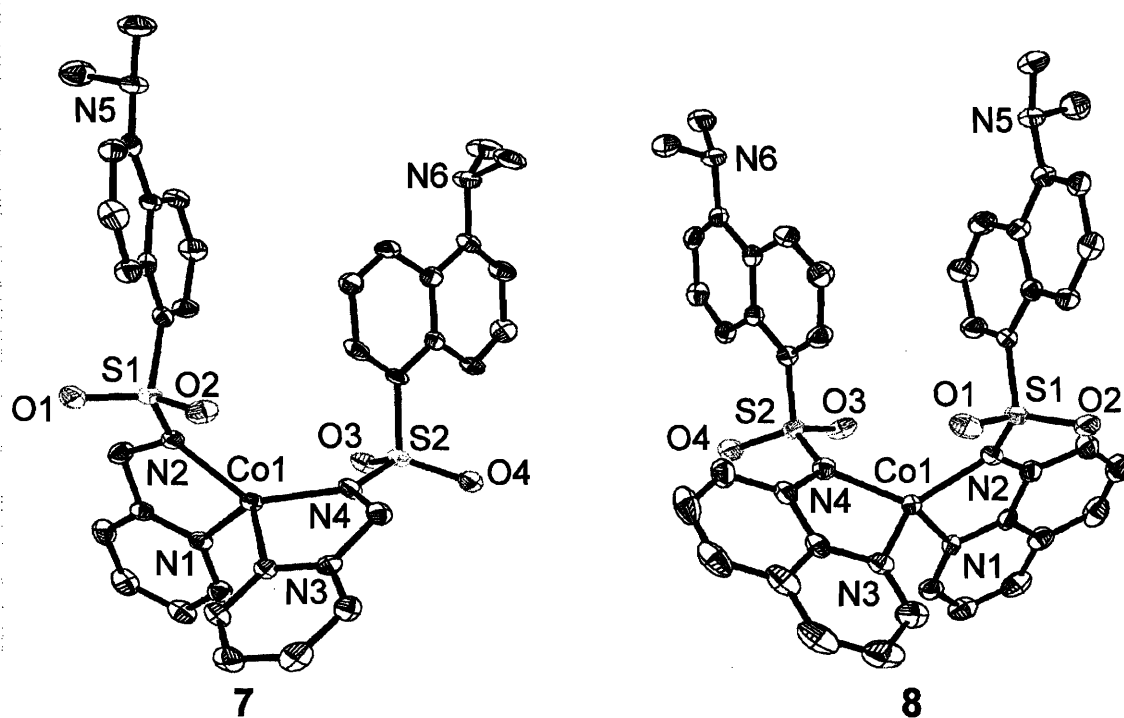
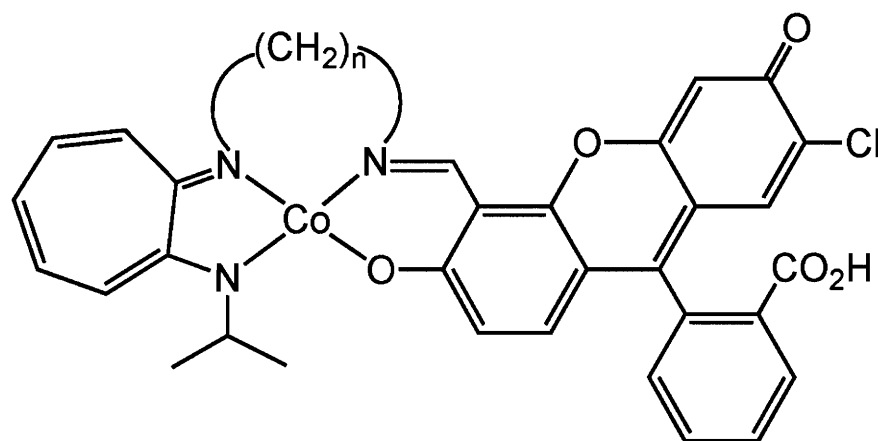


Figure 1.6. ORTEP diagrams of $[\text{Co}(\text{Ds-AMP})_2]$ (7) and $[\text{Co}(\text{Ds-AQ})_2]$ (8) showing 50% probability thermal ellipsoids. The figure adopted from ref. 37 was modified.

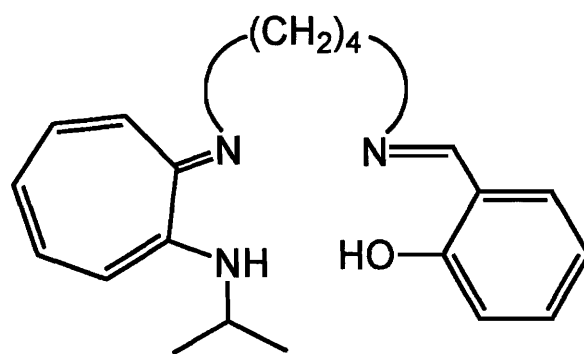
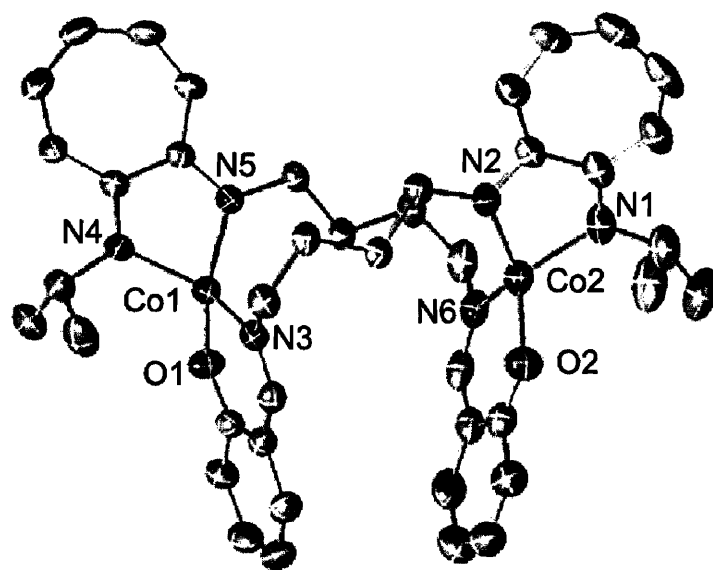


[Co(ⁱPrFATI-*n*)]

9, *n* = 3

10, *n* = 4

Figure 1.7. Schematic drawings of [Co(ⁱPrFATI-3)] (9) and [Co(ⁱPrFATI-4)] (10).



H₂^{iPr}SATI

Figure 1.8. ORTEP diagram of [Co₂(^{iPr}SATI-4)₂] showing 50% probability thermal ellipsoids (top) and schematic drawing of H₂^{iPr}SATI (bottom). The figure adopted from ref. 38 was modified.

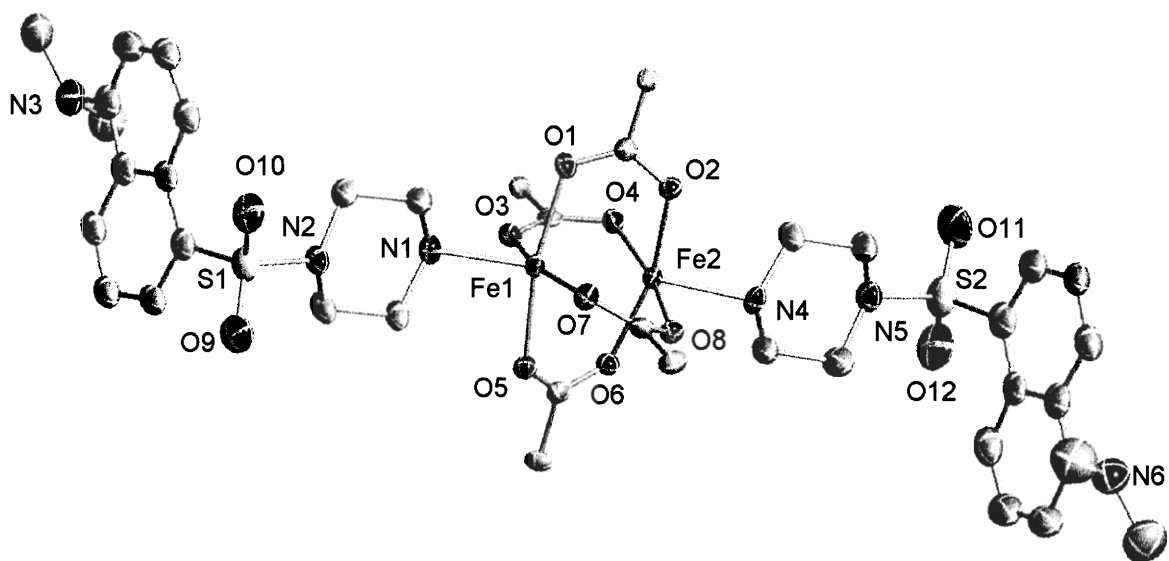
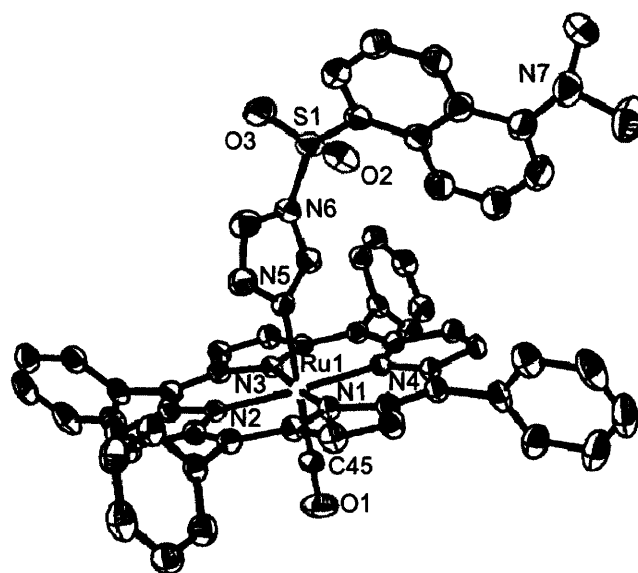
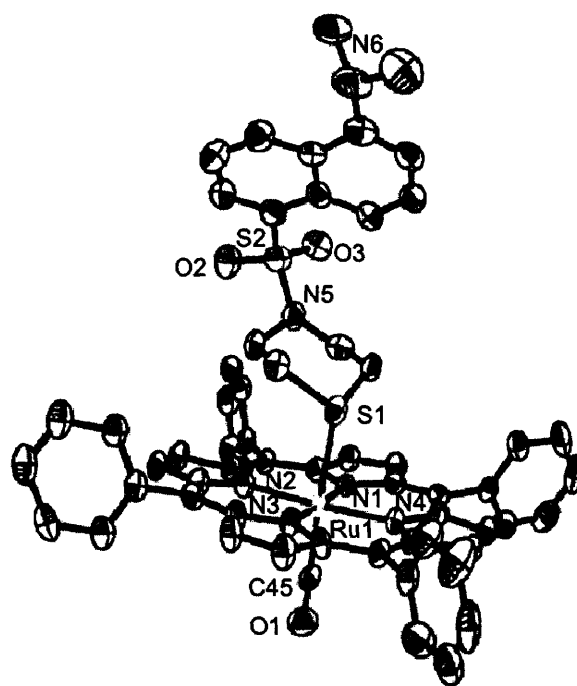


Figure 1.9. ORTEP diagram of $[\text{Fe}_2(\mu\text{-O}_2\text{CAR}^{\text{Tol}})_4(\text{Ds-pip})_2]$ (**12**) showing 50% probability thermal ellipsoids. The phenyl rings of $\text{Ar}^{\text{Tol}}\text{CO}_2^-$ ligands are omitted for clarity. The figure adopted from ref. 32 was modified.



13



14

Figure 1.10. ORTEP diagrams of [Ru(TPP)(CO)(Ds-im)] (13) and [Ru(TPP)(CO)(Ds-tm)] (14) showing 50% probability thermal ellipsoids. The figure adopted from ref. 22 was modified.

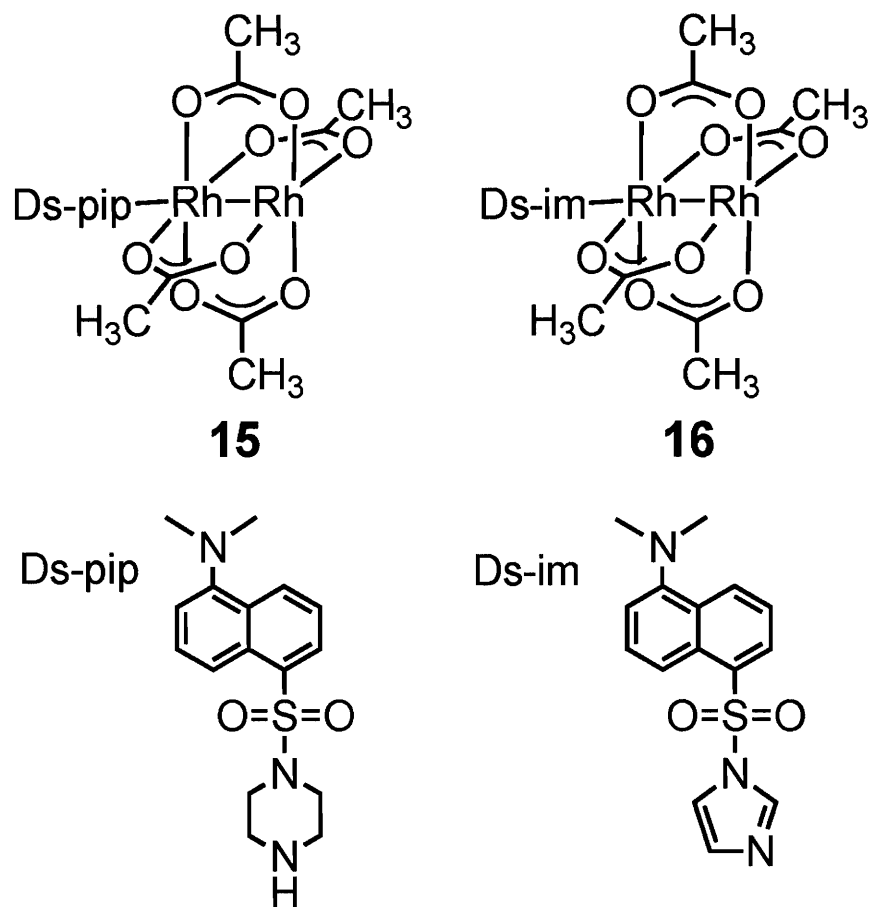


Figure 1.11. Schematic drawings of $[\text{Rh}_2(\mu\text{-O}_2\text{CMe})_4(\text{Ds-pip})]$ (15) and $[\text{Rh}_2(\mu\text{-O}_2\text{CMe})_4(\text{Ds-im})]$ (16).

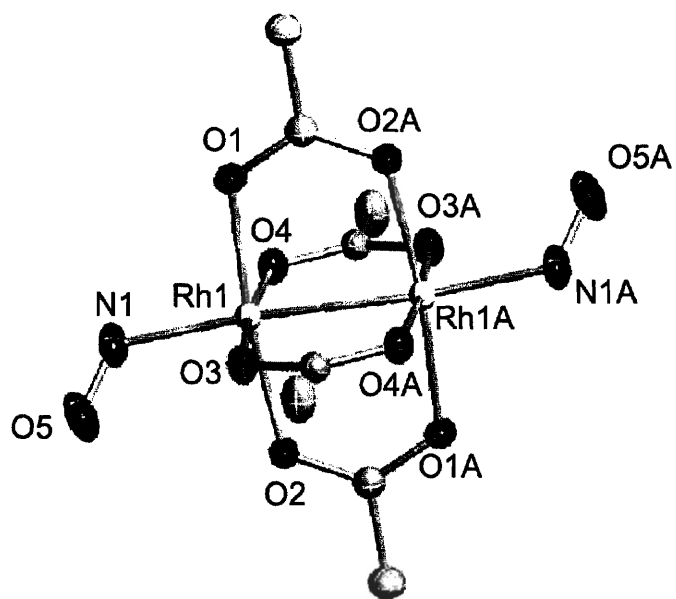


Figure 1.12. ORTEP diagram of $[\text{Rh}_2(\mu\text{-O}_2\text{CMe})_4(\text{NO})_2]$ showing 50% probability thermal ellipsoids. The figure adopted from ref. 23 was modified.

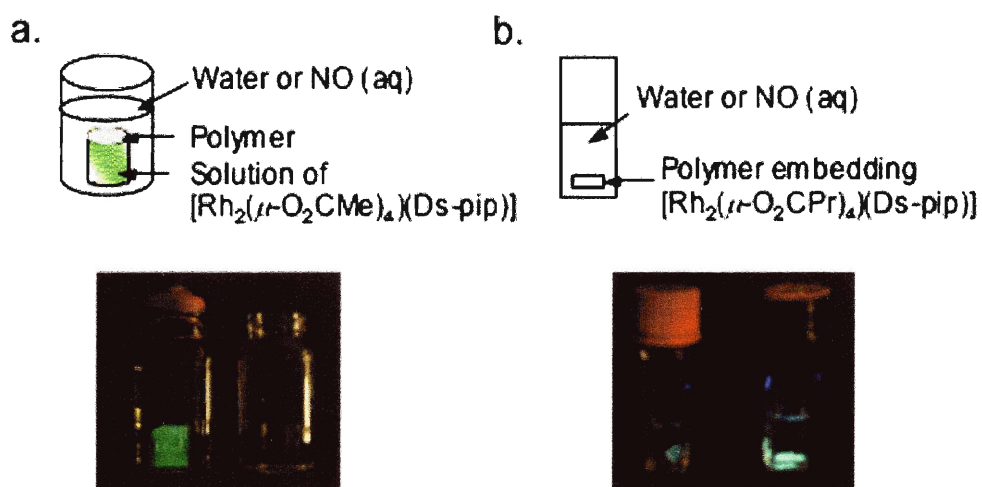


Figure 1.13. (a) Fluorescence response of a CH_2Cl_2 solution of **15** protected by a Silastic membrane against water in the outer vial (right) and upon introduction of 1.9 mM aqueous NO (aq) into outer vial (left). (b) Fluorescence response of Silastic membrane-embedded $[\text{Rh}_2(\mu\text{-O}_2\text{CPr})_4(\text{Ds-pip})]$ in water (left) and after exposure to a saturated NO aqueous solution (right). The figure (a) taken from ref. 23 was modified.

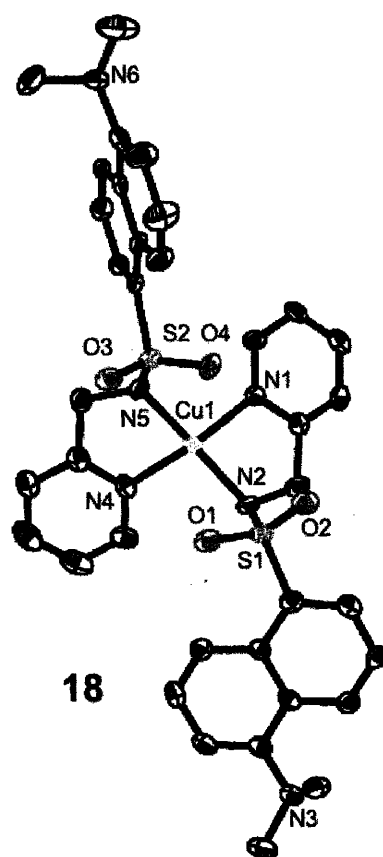
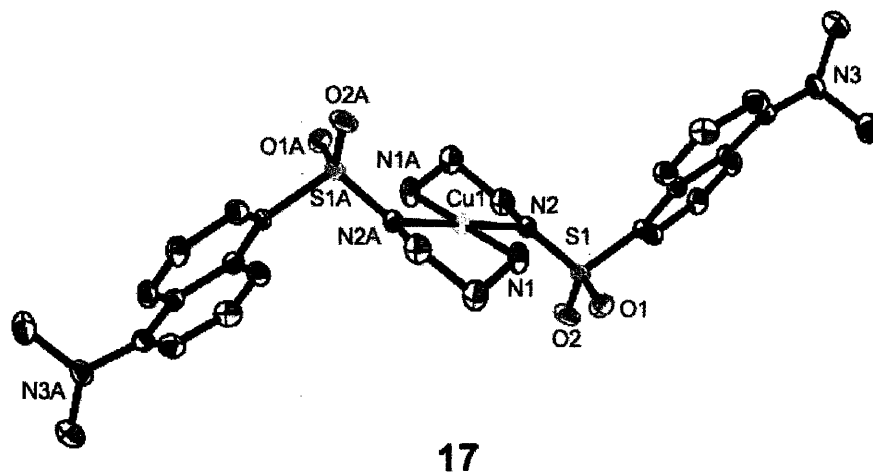


Figure 1.14. ORTEP diagrams of [Cu(Ds-en)₂] (17) and [Cu(Ds-AMP)₂] (18) showing 50% probability thermal ellipsoids. The figure adopted from refs. 25 and 48 was modified.

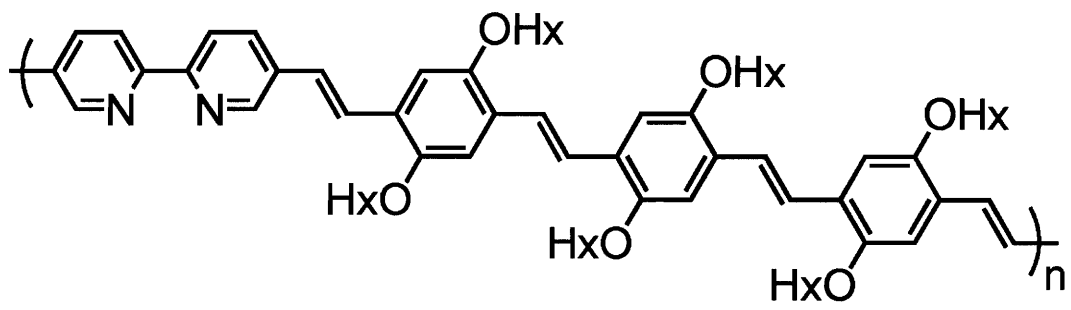
**CP1a**

Figure 1.15. Schematic drawing of CP1a.

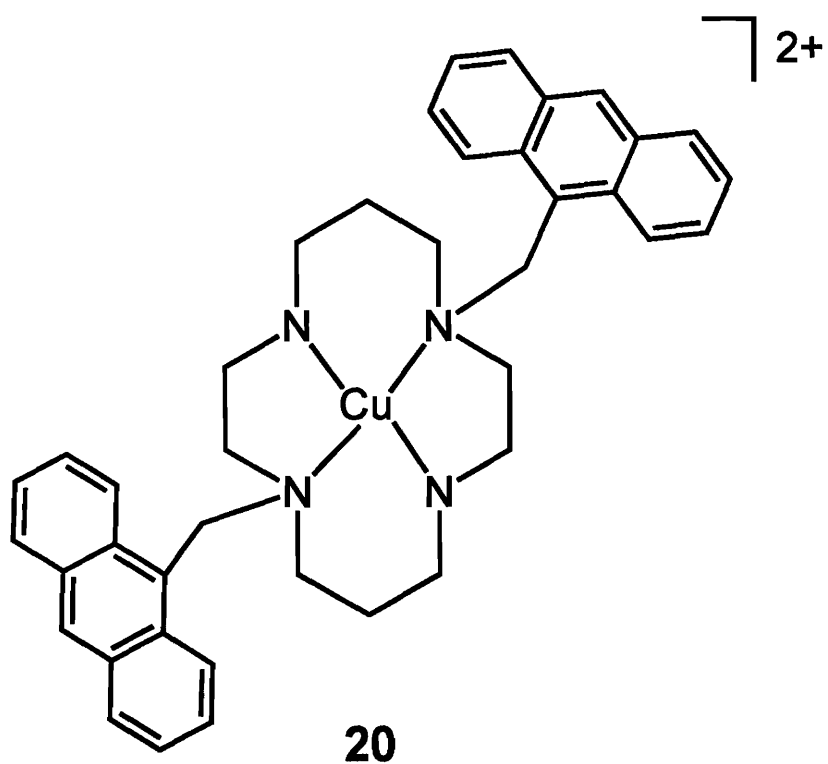


Figure 1.16. Schematic drawing of $[\text{Cu}(\text{DAC})]^{2+}$ (20).

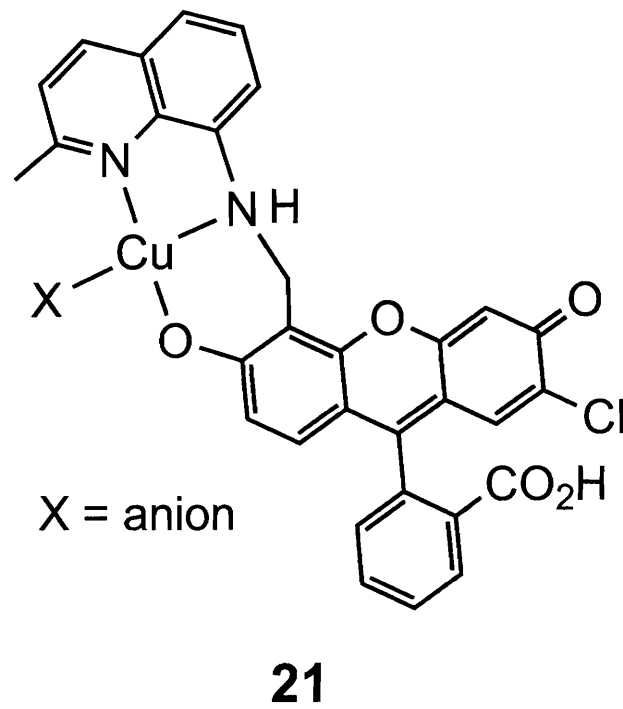


Figure 1.17. Schematic drawing of CuFL (21).

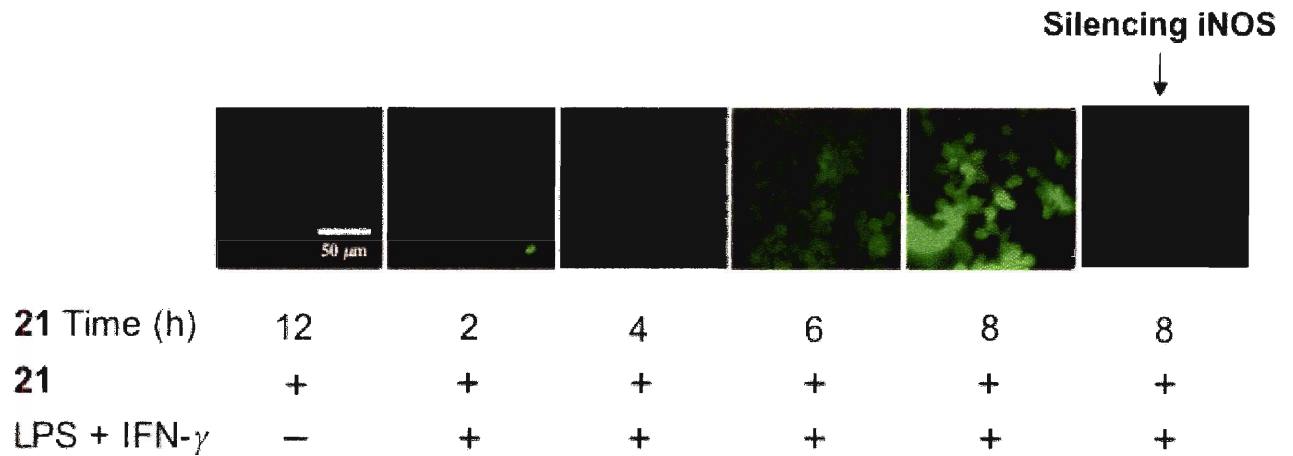


Figure 1.18. Detection by **21** of NO produced in Raw 264.7 cells activated by LPS and IFN- γ or in Raw 264.7 cells silenced with iNOS. Time depicted in the figure is the total incubation of time of **21** with only cells or with cells pre-treated with LPS and IFN- γ for 4 h. The figure adopted from ref. 33 was modified.

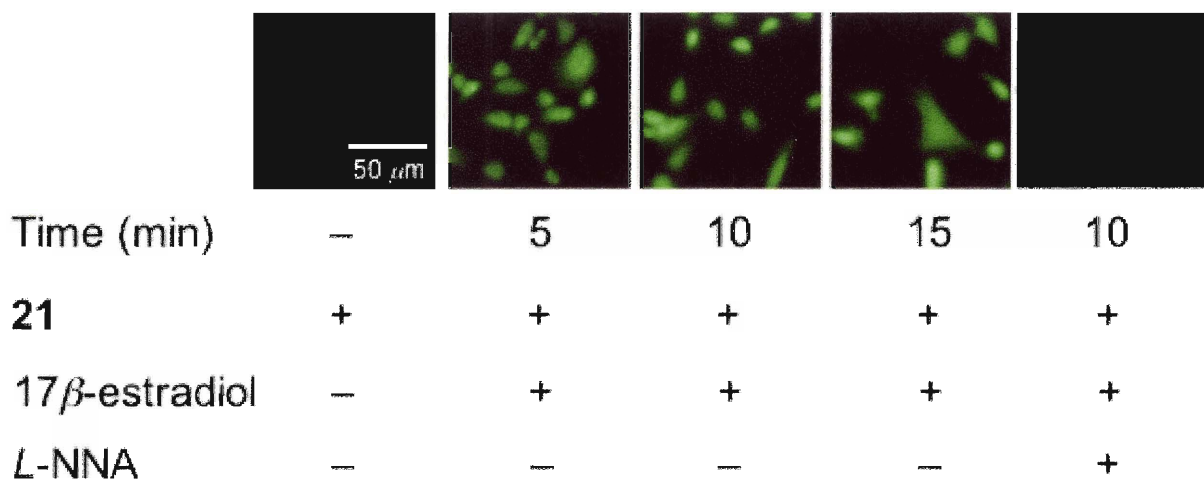


Figure 1.19. Detection by **21** of NO produced in SK-N-SH cells activated by 17 β -estradiol in the absence or presence of inhibitor (*L*-NNA). Time depicted in the figure is the total time of co-treatment of **21** and 17 β -estradiol. The figure adopted from ref. 33 was modified.

Chapter 2

Fluorescence-Based Nitric Oxide Detection by Ruthenium Porphyrin Fluorophore Complexes

This chapter is based on previously published work (Lim, M. H.; Lippard, S. J., *Inorg. Chem.* **2004**, *43*, 6366-6370). This work was supported by NSF grant CHE-0234951. We thank Dr. Sumitra Mukhopadhyay for assistance with the X-ray structure determinations and Dr. Scott A. Hilderbrand for helpful discussions. The MIT DCIF NMR spectrometer was funded through NSF grants CHE-9808061 and DBI-9729592.

Introduction

Nitric oxide, well known as an atmospheric pollutant, also serves as a messenger in the cardiovascular, immune, and nervous systems.¹⁻⁵ To understand these diverse biological functions, direct sensing of NO in a manner that maps its spatial and temporal distribution would be most valuable. Currently, NO can be monitored^{6,7} by chemiluminescence,⁵ amperometry,⁸ EPR spectroscopy,⁹⁻¹¹ or fluorescence.¹²⁻¹⁶ Research in our laboratory focuses on the synthesis of fluorescence-based sensors in which NO-induced displacement of a fluorophore, quenched when bound to a metal center, is accompanied by light emission upon excitation at a proper wavelength. Previous applications of this strategy revealed that $[\text{Co}(\text{R}^{\text{D}}\text{ATI})_2]$, $[\text{Co}(\text{DATI-4})]$ and $[\text{Rh}_2(\mu\text{-OAc})_4(\text{Ds-R})]$ complexes, where DATI is dansyl aminotroponimate and Ds-R is an imidazole or piperazine derivatized dansyl group, display dramatic increases in fluorescence upon exposure to NO.^{17,18} These complexes are stable in the presence of O_2 , an important requirement for biological applications, but additional tactics are required, including faster response rates and water compatibility. We have therefore been exploring other synthetic platforms to approach these goals.

Nitric oxide binds to the heme iron of soluble guanylyl cyclase (sGC) selectively over O_2 .^{19,20} The coordination environment of this NO-binding iron center has inspired the fabrication of fiber optic probes that are embedded with a fluorescent dye-labeled heme domain of sGC or cytochrome *c'* to detect NO.^{21,22} These probes, however, report only local NO concentrations at their tips and are unsuitable for intracellular work. An iron complex of a methoxycoumarin-pendant cyclam and 2,2,5,5-tetramethylpyrrolidine-*N*-oxide covalently linked to fluorescamine was designed as a fluorescent model of sGC. Unfortunately, this sensor is unstable in air and displays only a weak fluorescent response to NO.²³

The reactivity of nitric oxide with metalloporphyrins has been extensively investigated.^{24,25} Ruthenium porphyrins form stable nitrosyl adducts upon exposure to NO.²⁵⁻³⁰ In this chapter we describe the synthesis and characterization of ruthenium porphyrin complexes with axially bound fluorophores. We demonstrate that a fluorophore coordinated to ruthenium in this manner can be released by NO, resulting in turn-on fluorescence upon excitation. This ruthenium porphyrin fluorophore scaffold is the first example of a fluorescent NO sensor incorporating a metalloporphyrin.

Experimental

General Considerations. All reagents for syntheses were purchased from Aldrich and used without further purification. Dichloromethane (CH_2Cl_2) and tetrahydrofuran (THF) were purified by passage through alumina columns under an Ar atmosphere. Diethyl ether (Et_2O), hexanes, and ethyl acetate (EtOAc) were used as received. Compound dansyl-imidazole (Ds-im) was synthesized as previously reported.¹⁸ Nitric oxide (Matheson 99%) was purified as described.^{18,31} NO was transferred by a gastight syringe in a glove box. NO reactions were performed under anaerobic conditions to avoid adventitious reactions of the gas with O_2 . Fluorescence emission spectra were recorded at 25.0 ± 0.2 °C on a Hitachi F-3010 spectrophotometer. NMR spectra were measured on a Varian 300 spectrometer or an Inova 500 MHz spectrometer at ambient temperature and referenced to internal ^1H and ^{13}C solvent peaks. FT-IR spectra were obtained on an Avatar 360 spectrophotometer and UV-vis spectra on a Hewlett-Packard 8453 diode array spectrophotometer. ESI-MS analysis was performed on an Agilent 1100 series instrument.

X-ray Crystallographic Studies. A suitable crystal was mounted in Paratone N oil on the tip of a glass capillary and frozen in a -100 °C nitrogen cold stream. Data were

collected on a Bruker APEX CCD X-ray diffractometer with Mo K α radiation ($\lambda = 0.71073 \text{ \AA}$) controlled by the SMART software package and refined and solved with the SAINTPLUS and SHELXTL software packages.³²⁻³⁴ The general procedures used for data collection are reported elsewhere.³⁵ Empirical absorption corrections were calculated with the SADABS program.³⁶ The structures of **1** and **2** were solved by the Patterson method. All non-hydrogen atoms were refined anisotropically and the structure solution was checked for higher symmetry with PLATON.³⁷ In the crystal structure of **1**, a disordered Et₂O molecule in the lattice was refined over two positions, each with a 0.5 occupancy factor. One and one-half CH₂Cl₂ molecules in the structure of **2** were disordered. In the first disordered CH₂Cl₂, one of the chlorine atoms resides in two positions, each assigned an occupancy factor of 0.5. In the remaining 0.5 CH₂Cl₂, the carbon atom was disordered over two sites modeled with 0.5 occupancy factors each. The highest electron density in the final difference Fourier maps for **1** and **2** was 1.573 and 1.542 e/ \AA^3 , respectively, in the vicinity of the ruthenium atom.

Dansyl-thiomorpholine (Ds-tm). To a solution of dansyl chloride (2.9 g, 11 mmol) in 200 mL of THF were added thiomorpholine (1.1 g, 11 mmol) and Cs₂CO₃ (4.2 g, 13 mmol). The reaction was allowed to stir overnight, filtered, and the solvent was removed by rotary evaporation. The crude solids were purified by column chromatography (silica, 6:1 hexanes:EtOAc; $R_f = 0.29$ by TLC), yielding a yellow product (2.8 g, 8.4 mmol, 77%): mp: 144-146 °C. ¹H NMR (500 MHz, CDCl₃): δ (ppm) 8.56 (1H, d, $J = 5$ Hz), 8.3 (1H, d, $J = 10$ Hz), 8.19 (1H, dd, $J = 7.25, 1.5$ Hz), 7.57-7.51 (2H, m), 7.19 (1H, dd, $J = 7.5, 0.5$ Hz), 3.55-3.53 (4H, m), 2.89 (6H, s), 2.67-2.64 (4H, m). ¹³C NMR (125 MHz, CDCl₃): δ (ppm) 152.0, 133.6, 130.9, 130.5, 130.3, 130.2, 128.3, 123.3, 119.5, 115.5, 47.5, 45.6, 27.5. FTIR (KBr; cm⁻¹): 2985 (w), 2953 (w), 2917 (w), 2862 (w), 2825 (w), 2783

(w), 1612 (w), 1590 (m), 1579 (m), 1572 (m), 1501 (w), 1478 (w), 1463 (w), 1443 (w), 1411 (m), 1401 (m), 1379 (w), 1355 (m), 1319 (m), 1288 (m), 1228 (w), 1199 (w), 1183 (w), 1171 (w), 1140 (m), 1102 (w), 1080 (m), 1043 (w), 1018 (w), 965 (m), 942 (w), 914 (s), 835 (w), 814 (w), 801 (w), 789 (m), 775 (w), 689 (s), 659 (m), 623 (m), 569 (s), 530 (w), 502 (w), 452 (m). ESI(+)MS (m/z): [M+H]⁺ Calcd. for C₁₆H₂₁N₂O₂S₂, 337.1; Found 337.4.

[Ru(TPP)(CO)(Ds-im)] (1). A portion of Ds-im (55 mg, 0.18 mmol) was added to a solution of [Ru(TPP)(CO)] (45 mg, 0.060 mmol) in 2 mL of CH₂Cl₂, after which Et₂O was slowly diffused into the solution at 0 °C. Purple crystals of X-ray quality were grown over one day and isolated in 93% yield (0.058 g, 0.056 mmol): mp > 260 – 262 °C (decomp). FTIR (KBr; cm⁻¹): 3164 (w), 3144 (w), 3126 (w), 3103 (w), 3074 (w), 3045 (w), 3022 (w), 2972 (w), 2945 (w), 2971 (w), 2945 (w), 2864 (w), 2830 (w), 2788 (w), 2771 (w), 1938 (s), 1593 (m), 1568 (w), 1437 (m), 1387 (m), 1350 (m), 1304 (m), 1261 (w), 1202 (w), 1176 (m), 1163 (m), 1062 (m), 1008 (s), 934 (w), 834 (w), 796 (m), 757 (m), 751 (m), 736 (w), 717 (m), 700 (m), 677 (w), 664 (w), 636 (m), 591 (m), 559 (w), 538 (w), 525 (w), 492 (w), 461 (w). UV-vis in CH₂Cl₂ [λ_{max} /nm (ϵ , M⁻¹ cm⁻¹): 313 (2.0 × 10⁴), 413 (2.3 × 10⁵), 534 (2.0 × 10⁴), 567 (4.6 × 10³), 601 (1.3 × 10³). ¹H NMR (300 MHz, CD₂Cl₂): δ (ppm) 8.60 (8H, s), 8.43 (1H, d, J = 8.5 Hz), 8.26-8.22 (4H, m), 7.90 (4H, dm, J = 7.3 Hz), 7.78-7.64 (14H, m), 7.52 (1H, dd, J = 7.6, 1.1 Hz), 7.32-7.19 (3H, m), 7.13 (1H, d, J = 7.7 Hz), 6.46 (1H, d, J = 8.8 Hz), 2.83 (6H, s). ¹³C NMR (100 MHz, CDCl₃): δ (ppm) 180.1, 152.3, 143.3, 142.4, 134.0, 133.8, 133.1, 131.4, 131.2, 130.0, 129.9, 129.1, 128.1, 127.0, 126.3, 126.0, 123.4, 122.4, 121.2, 115.5, 115.3, 114.3, 45.1. Anal. Calcd. for C₆₀H₄₃N₇O₃RuS: C, 69.08; H, 4.15; N, 9.40; Found: C, 68.78; H, 4.21; N, 9.09.

[Ru(TPP)(CO)(Ds-tm)] (2). A portion of Ds-tm (9.1 mg, 0.027 mmol) was added to a solution of [Ru(TPP)(CO)] (10 mg, 0.013 mmol) in 2 mL of CH₂Cl₂. The resulting

solution was layered with hexanes and cooled to 0 °C. Purple crystals of X-ray quality were grown over 4 days and collected (0.013 g, 0.012 mmol, 91%): mp > 255 – 257 °C (decomp). UV-vis in CH₂Cl₂ [λ_{max} / nm (ϵ , M⁻¹ cm⁻¹): 312 (2.5 x 10⁴), 412 (2.1 x 10⁵), 531 (2.1 x 10⁴), 569 (5.1 x 10³), 602 (2.0 x 10³). FTIR (KBr; cm⁻¹): 3104 (w), 3075 (w), 3052 (w), 3022 (w), 2985 (w), 2943 (w), 2937 (w), 2865 (w), 2832 (w), 2790 (w), 1951 (s), 1595 (m), 1574 (w), 1568 (w), 1527 (m), 1503 (w), 1486 (w), 1477 (w), 1453 (w), 1440 (m), 1405 (w), 1394 (w), 1373 (w), 1350 (m), 1320 (w), 1305 (m), 1282 (w), 1264 (w), 1230 (w), 1216 (w), 1201 (w), 1175 (m), 1157 (w), 1141 (m), 1094 (w), 1071 (s), 1008 (s), 962 (w), 945 (w), 909 (m), 885 (m), 846 (w), 834 (w), 793 (s), 754 (m), 737 (m), 716 (m), 700 (s), 672 (w), 664 (w), 637 (w), 619 (w), 595 (w), 577 (w), 567 (m), 540 (w), 527 (w), 499 (w), 462 (w), 452 (w), 415 (w). ¹H NMR (500 MHz, CD₂Cl₂): δ (ppm) 8.64 (8H, s), 8.51 (1H, s), 8.22 (4H, br, s), 8.00 (4H, br, s), 7.76-7.64 (14H, m), 7.36 (2H, s), 7.16 (1H, s), 2.86 (6H, s), 1.11 (4H, br, s), -2.23 (4H, br, s). Anal. Calcd. for C₆₁H₄₈N₆O₃RuS₂·CH₂Cl₂: C, 64.02; H, 4.33; N, 7.22; Found: C, 64.47; H, 4.29; N, 7.21.

Results and Discussion

Syntheses of Fluorophore-Derived Ruthenium Porphyrin Complexes.

Ruthenium carbonyl tetraphenylporphyrin complexes [Ru(TPP)(CO)(L)], with L = Ds-im (1) or Ds-tm (2), were readily prepared from solutions of [Ru(TPP)(CO)] and the dansyl-derivatized axial base, imidazole or thiomorpholine, in CH₂Cl₂. Crystals of 1 were grown by vapor diffusion of Et₂O into the resulting solution over one day at 0 °C and isolated in 93% yield. When a CH₂Cl₂ solution of [Ru(TPP)(CO)] and Ds-tm was layered with hexanes, X-ray quality crystals of 2 were grown over 4 days at 0 °C in 91% yield.

X-ray Crystal Structure Determinations of [Ru(TPP)(CO)(Ds-im)] (1) and [Ru(TPP)(CO)(Ds-tm)] (2).

Crystallographic data for 1 and 2 are summarized in Table 2.1, and selected bond distances and angles are contained in Table 2.2. The crystal structures of 1 and 2 indicate that the fluorophores are coordinated to the axial site of the ruthenium center trans to the carbonyl group via the nitrogen atom of imidazole and the sulfur atom of thiomorpholine, respectively (Figure 2.1). In the crystal structure of 1, the Ru–C_{CO} and Ru–N_{im} distances, 1.834(4) Å and 2.166(3) Å, and the Ru–C–O and N_{im}–Ru–C_{CO} angles, 179.2(3)° and 179.54(16)°, are consistent with those in the [Ru(TPP)(CO)(1-MeIm)] analogue reported previously.^{38,39} Compound 2 is the first crystallographically characterized ruthenium porphyrin complex that contains a sulfur-donor axial ligand trans to a carbonyl group. The Ru–S bond length, 2.499(2) Å, is the longest reported for ruthenium porphyrin complexes containing S-donor axial ligands,^{40,41} reflecting the strong trans influence of the carbonyl ligand.

Fluorescence Properties.

Fluorescence studies revealed 39-fold and 2.0-fold quenching of the dansyl group fluorescence in 1 and 2, respectively, when compared to that of the free Ds-im or Ds-tm ligands (Figures 2.2a & 2.2b). In the solid state, 1 and 2 are not fluorescent. Upon addition of NO to solutions of these compounds, an increase in fluorescence was observed. Reaction of a 10 μM dichloromethane solution of 1 with 100 equiv of NO afforded a 19-fold increase in the integrated fluorescence emission (Figure 2.3a). The fluorescence response was complete in less than 20 min. Restoration of fluorescence to the value of free Ds-im in the reaction of 1 with NO does not occur, most likely due to an inner filter effect. Ruthenium porphyrin complexes have strong absorption bands at

the same wavelengths where excitation and emission of the fluorophore occurs, thus absorbing some of the light excitation and emission, resulting in a diminished fluorescence response. A similar effect was observed in the reaction of **2** with NO. When 100 equiv of NO were introduced into a 10 μ M dichloromethane solution of **2**, a 1.3-fold increase in fluorescence was exhibited (Figure 2.3b). The response is much more rapid, however, being complete in 3 min. Compounds **1** and **2** display turn-on fluorescent detection of NO 1-2 orders of magnitude more rapid than our previously reported Co(II) sensors.¹⁷

Nature of the Reaction of [Ru(TPP)(CO)(Ds-im)] (**1**) with Nitric Oxide.

When [Ru(TPP)(CO)] is treated with excess NO, the product is [Ru(TPP)(NO)(ONO)].^{26,30} In order to determine whether similar chemistry might apply in the present case, the Ru-containing product from the reaction of **1** with NO was isolated from a CH₂Cl₂/pentane solution under anaerobic conditions and characterized by IR and UV-vis spectroscopy. The IR spectrum displayed bands at 1854 cm⁻¹ (vs, ν_{NO}), 1520 (m, $\nu_{\text{as}}(\text{ONO})$), and 932 (m, $\nu_{\text{s}}(\text{ONO})$) cm⁻¹ in KBr (Figure 2.4). In addition, the product exhibited an optical spectrum with λ_{max} values of 411 (Soret band), 563, and 607 (sh) nm (Q bands) in CH₂Cl₂ (Figure 2.5). These data are consistent with those previously reported for [Ru(TPP)(NO)(ONO)].^{26,30} An X-ray analysis of crystals grown by the slow evaporation of a CH₂Cl₂ solution of the complex isolated from the NO reaction revealed the presence of [Ru(TPP)(NO)(ONO)] (57% yield), with an 8-fold rotational disorder of the axial ligands about the Ru-O bond. The X-ray crystal structure (Figure 2.6) is consistent with those previously reported in the literature.²⁶ In addition, the ¹H NMR spectrum of the reaction of **1** with NO indicated the presence of free Ds-im (Figure 2.7).

Taken together, these results demonstrate that nitric oxide treatment causes both Ds-im and CO to dissociate from the axial sites of the Ru(II) center (Scheme 2.1). We therefore conclude that the fluorescence enhancement of 1 and 2 observed upon reaction with NO arises from displacement of Ds-im or Ds-tm from their axial positions, liberating the fluorophores from the quenching environment of the Ru(II) center and restoring fluorescence.

Conclusions

New fluorophore-derived ruthenium porphyrin complexes have been prepared, which can be used for direct fluorescence-based detection of NO. The fluorescence increase observed during the reaction of these non-fluorescent complexes with NO is the result of the dissociation of fluorophore from the axial site of the ruthenium center. This study further demonstrates the value of fluorophore displacement as a valid strategy for the development of NO sensors and paves the way for the development of water-soluble, even more rapidly responding metalloporphyrins toward the ultimate goal of sensing nitric oxide in living cells.

References

- (1) Furchgott, R. F., *Angew. Chem. Int. Ed.* **1999**, *38*, 1870-1880.
- (2) Ignarro, L. J., *Angew. Chem. Int. Ed.* **1999**, *38*, 1882-1892.
- (3) Palmer, R. M. J.; Ferrige, A. G.; Moncada, S., *Nature* **1987**, *327*, 524-6.
- (4) Wink, D. A.; Vodovotz, Y.; Laval, J.; Laval, F.; Dewhirst, M. W.; Mitchell, J. B., *Carcinogenesis* **1998**, *19*, 711-721.
- (5) Hampl, V.; Walters, C. L.; Archer, S. L., *In Methods in Nitric Oxide Research*, Feelisch, M.; Stamler, J. S., Eds. Wiley: New York, 1996; pp 309-318.

- (6) Nagano, T.; Yoshimura, T., *Chem. Rev.* **2002**, *102*, 1235-1270.
- (7) Hilderbrand, S. A.; Lim, M. H.; Lippard, S. J., *In Topics in Fluorescence Spectroscopy*, Geddes, C. D.; Lakowicz, J. R., Eds. Springer: 2005; pp 163-188.
- (8) Mao, L.; Tian, Y.; Shi, G.; Liu, H.; Jin, L.; Yamamoto, K.; Tao, S.; Jin, J., *Anal. Lett.* **1998**, *31*, 1991-2007.
- (9) Kotake, Y.; Tanigawa, T.; Tanigawa, M.; Ueno, I.; Allen, D. R.; Lai, C.-S., *Biochim. Biophys. Acta* **1996**, *1289*, 362-8.
- (10) Yoshimura, T.; Fujii, S.; Yokoyama, H.; Kamada, H., *Chem. Lett.* **1995**, 309-10.
- (11) Komarov, A. M.; Lai, C.-S., *Biochim. Biophys. Acta* **1995**, *1272*, 29-36.
- (12) Kojima, H.; Nakatsubo, N.; Kikuchi, K.; Kawahara, S.; Kirino, Y.; Nagoshi, H.; Hirata, Y.; Nagano, T., *Anal. Chem.* **1998**, *70*, 2446-2453.
- (13) Kojima, H.; Urano, Y.; Kikuchi, K.; Higuchi, T.; Hirata, Y.; Nagano, T., *Angew. Chem. Int. Ed.* **1999**, *38*, 3209-3212.
- (14) Miles, A. M.; Wink, D. A.; Cook, J. C.; Grisham, M. B., *In Methods in Enzymology*, Packer, L., Ed. Academic Press: Boston, MA, 1996; Vol. 268, pp 105-120 and references therein.
- (15) Bätz, M.; Korth, H.-G.; Sustmann, R., *Angew. Chem. Int. Ed.* **1997**, *36*, 1501-1503.
- (16) Meineke, P.; Rauen, U.; de Groot, H.; Korth, H.-G.; Sustmann, R., *Chem. Eur. J.* **1999**, *5*, 1738-1747.
- (17) Franz, K. J.; Singh, N.; Spingler, B.; Lippard, S. J., *Inorg. Chem.* **2000**, *39*, 4081-4092.
- (18) Hilderbrand, S. A.; Lim, M. H.; Lippard, S. J., *J. Am. Chem. Soc.* **2004**, *126*, 4972-4978.
- (19) Kim, S.; Deinum, G.; Gardner, M. T.; Marletta, M. A.; Babcock, G. T., *J. Am. Chem. Soc.* **1996**, *118*, 8769-8770 and references cited therein.

- (20) Burstyn, J. N.; Yu, A. E.; Dierks, E. A.; Hawkins, B. K.; Dawson, J. H., *Biochemistry* 1995, 34, 5896-903.
- (21) Barker, S. L. R.; Zhao, Y.; Marletta, M. A.; Kopelman, R., *Anal. Chem.* 1999, 71, 2071-2075.
- (22) Barker, S. L. R. C., Heather A.; Swallen, Stephen F.; Kopelman, Raoul; Tsang, Albert W.; Swanson, Joel A., *Anal. Chem.* 1999, 71, 1767-1772.
- (23) Soh, N.; Imato, T.; Kawamura, K.; Maeda, M.; Katayama, Y., *Chem. Commun.* 2002, 2650-2651.
- (24) Hoshino, M.; Laverman, L.; Ford, P. C., *Coord. Chem. Rev.* 1999, 187, 75-102 and references therein.
- (25) Ford, P. C.; Lorkovic, I. M., *Chem. Rev.* 2002, 102, 993-1017.
- (26) Miranda, K. M.; Bu, X.; Lorkovic, I.; Ford, P. C., *Inorg. Chem.* 1997, 36, 4838-4848.
- (27) Lorkovic, I. M.; Miranda, K. M.; Lee, B.; Bernhard, S.; Schoonover, J. R.; Ford, P. C., *J. Am. Chem. Soc.* 1998, 120, 11674-11683.
- (28) Lorkovic, I. M.; Ford, P. C., *Inorg. Chem.* 1999, 38, 1467-1473.
- (29) Lorkovic, I. M.; Ford, P. C., *Chem. Commun.* 1999, 1225-1226.
- (30) Kadish, K. M.; Adamian, V. A.; Van Caemelbecke, E.; Tan, Z.; Tagliatesta, P.; Bianco, P.; Boschi, T.; Yi, G.-B.; Khan, M. A.; Richter-Addo, G. B., *Inorg. Chem.* 1996, 35, 1343-8.
- (31) Lorkovic, I. M.; Ford, P. C., *Inorg. Chem.* 2000, 39, 632-633.
- (32) SMART: Software for the CCD Detector System, version 5.626; Bruker AXS: Madison, WI, 2000.
- (33) SAINTPLUS: Software for the CCD Detector System, version 5.01; Bruker AXS: Madison, WI, 1998.

- (34) *SHELXTL: Program Library for Structure Solution and Molecular Graphics*, version 6.1; Bruker AXS: Madison, WI, 2001.
- (35) Kuzelka, J.; Mukhopadhyay, S.; Spingler, B.; Lippard, S. J., *Inorg. Chem.* **2004**, *43*, 1751-1761.
- (36) Sheldrick, G. M. *SADABS: Area-Detector Absorption Correction*, University of Göttingen: Göttingen, Germany, 2001.
- (37) Spek, A. L., *PLATON, A Multipurpose Crystallographic Tool*. Utrecht University: Utrecht, The Netherlands, 2000.
- (38) Slebodnick, C.; Seok, W. K.; Kim, K.; Ibers, J. A., *Inorg. Chim. Acta* **1996**, *243*, 57-65.
- (39) Salzmann, R.; Ziegler, C. J.; Godbout, N.; McMahon, M. T.; Suslick, K. S.; Oldfield, E., *J. Am. Chem. Soc.* **1998**, *120*, 11323-11334.
- (40) James, B. R.; Pacheco, A.; Rettig, S. J.; Ibers, J. A., *Inorg. Chem.* **1988**, *27*, 2414-2421.
- (41) Yi, G.-B.; Khan, M. A.; Richter-Addo, G. B., *Chem. Commun.* **1996**, 2045-2046.

Table 2.1. Summary of X-ray Crystallographic Data

	[Ru(TPP)(CO)(Ds-im)] ·0.5 Et ₂ O (1·0.5 Et ₂ O)	[Ru(TPP)(CO)(Ds-tm)] ·1.5 CH ₂ Cl ₂ (2·1.5 CH ₂ Cl ₂)
Formula	C ₆₂ H ₄₃ N ₇ O _{3.5} RuS	C _{62.5} H ₄₈ Cl ₃ N ₆ O ₃ RuS ₂
formula weight	1075.16	1202.61
space group	P2 ₁ /c	P1
a, Å	12.773(3)	11.241(2)
b, Å	20.264(4)	15.233(3)
c, Å	20.711(4)	16.615(3)
α, deg		97.00(3)
β, deg	107.79(3)	97.90(3)
γ, deg		103.00(3)
V, Å ³	5104.3(18)	2711.2(9)
Z	4	2
ρ _{calc} g/cm ³	1.399	1.473
crystal size (mm ³)	0.15 x 0.08 x 0.06	0.10 x 0.08 x 0.05
T, °C	-100	-100
μ(Mo Kα), mm ⁻¹	0.405	0.568
total no. of data	37390	19865
no. of unique data	9005	9446
no. of params	684	714
GOF ^a	1.099	1.032
R ^b	0.0510	0.0795
wR ^{2c}	0.1271	0.1729
max, min peaks, e/Å ³	1.573, -0.573	1.542, -0.979

^a GOF (Goodness of fit on F²) = {Σ[w(F_o²-F_c²)²]/(m-n)}^{1/2} (m = number of reflections, n = number of parameters refined)

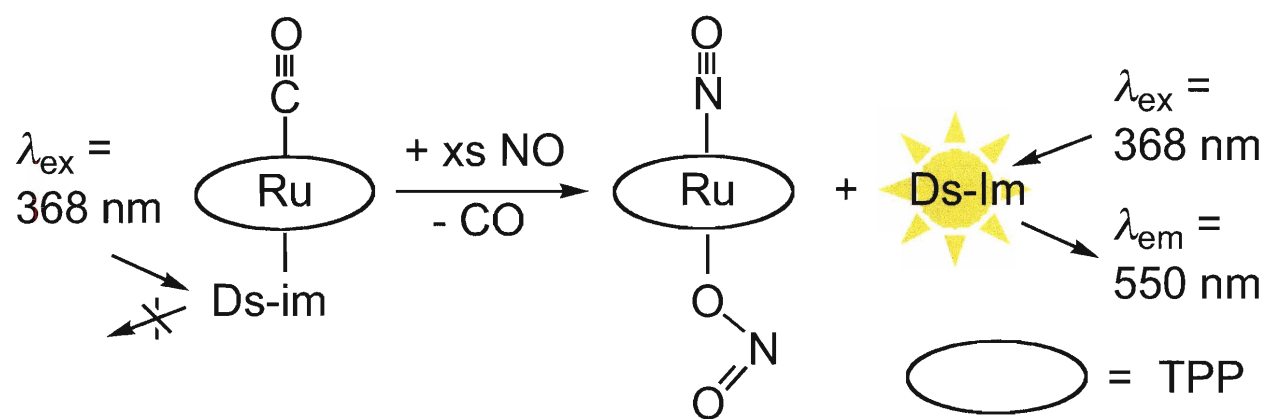
^b R = Σ||F_o|-|F_c||/Σ|F_o|

^c wR² = {w(F_o²-F_c²)²/Σ[w(F_o²)²]}^{1/2}

Table 2.2. Selected Bond Distances (Å) and Angles (deg)^a

[Ru(TPP)(CO)(Ds-im)] (1)			
Ru1-N1	2.056(3)	Ru1-C45	1.834(4)
Ru1-N2	2.048(3)	C45-O1	1.139(5)
Ru1-N3	2.044(3)	C45-Ru1-N5	179.54(16)
Ru1-N4	2.055(3)	O1-C45-Ru1	179.2(3)
Ru1-N5	2.166(3)		
[Ru(TPP)(CO)(Ds-tm)] (2)			
Ru1-N1	2.042(6)	Ru1-C45	1.826(9)
Ru1-N2	2.048(6)	C45-O1	1.133(9)
Ru1-N3	2.038(6)	C45-Ru1-S1	173.1(2)
Ru1-N4	2.054(6)	O1-C45-Ru1	177.4(7)
Ru1-S1	2.499(2)		

^a Numbers in parentheses are estimated standard deviations of the last significant figures. Atoms are labeled as indicated in Figure 2.1. The full list of bond lengths and angles is in the supporting information of the previous reference, which is available at <http://pubs.acs.org> (Lim, M. H.; Lippard, S. J., *Inorg. Chem.* **2004**, *43*, 6366-6370).



Scheme 2.1. Nitric Oxide Chemistry of **1**.

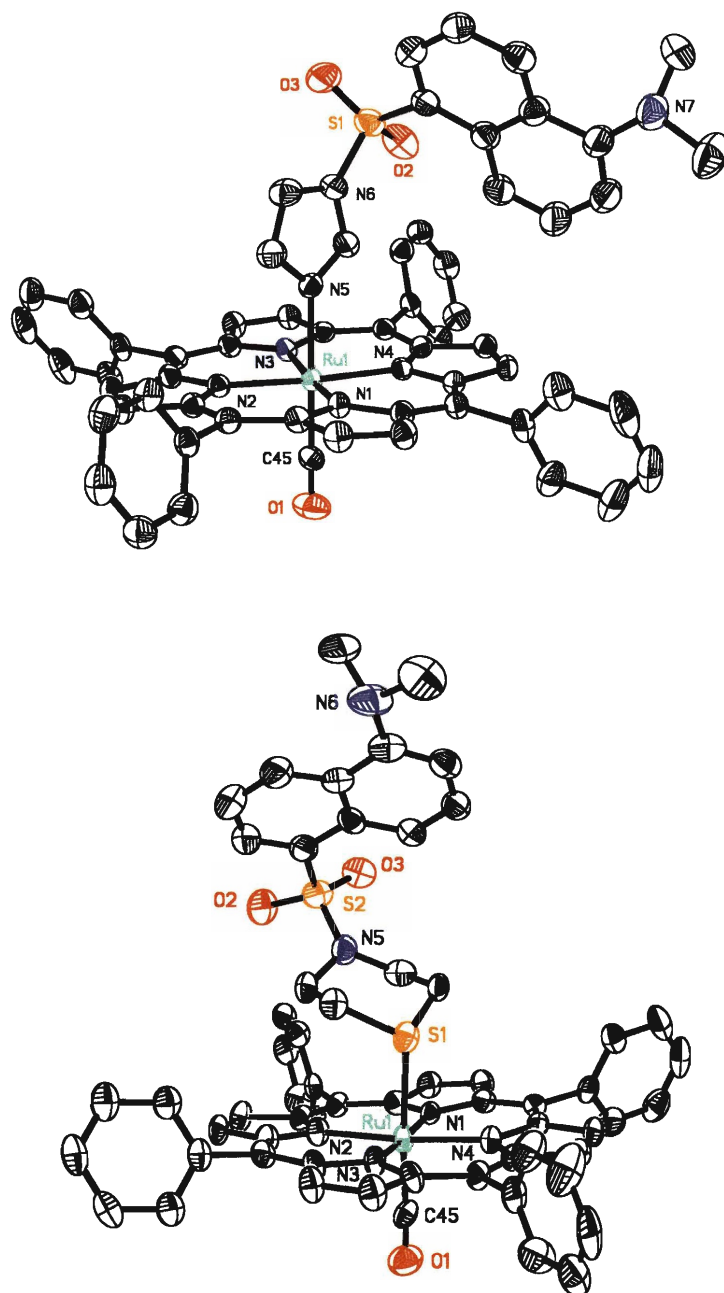


Figure 2.1. ORTEP diagrams of [Ru(TPP)(CO)(Ds-im)] (1, top) and [Ru(TPP)(CO)(Ds-tm)] (2, bottom) showing 50% probability thermal ellipsoids.

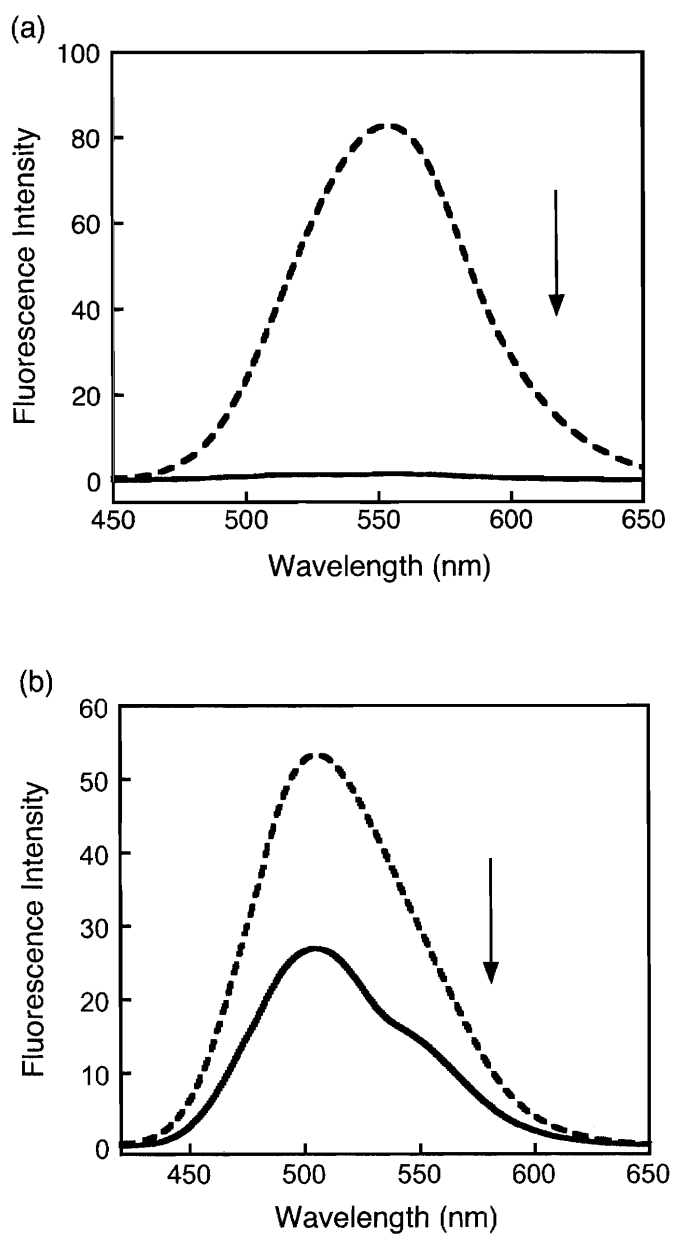


Figure 2.2. Fluorescence emission spectra of (a) **1** (10 μM , solid line) and Ds-im (10 μM , dashed line) and of (b) **2** (10 μM , solid line) and Ds-tm (10 μM , dashed line) in CH_2Cl_2 .

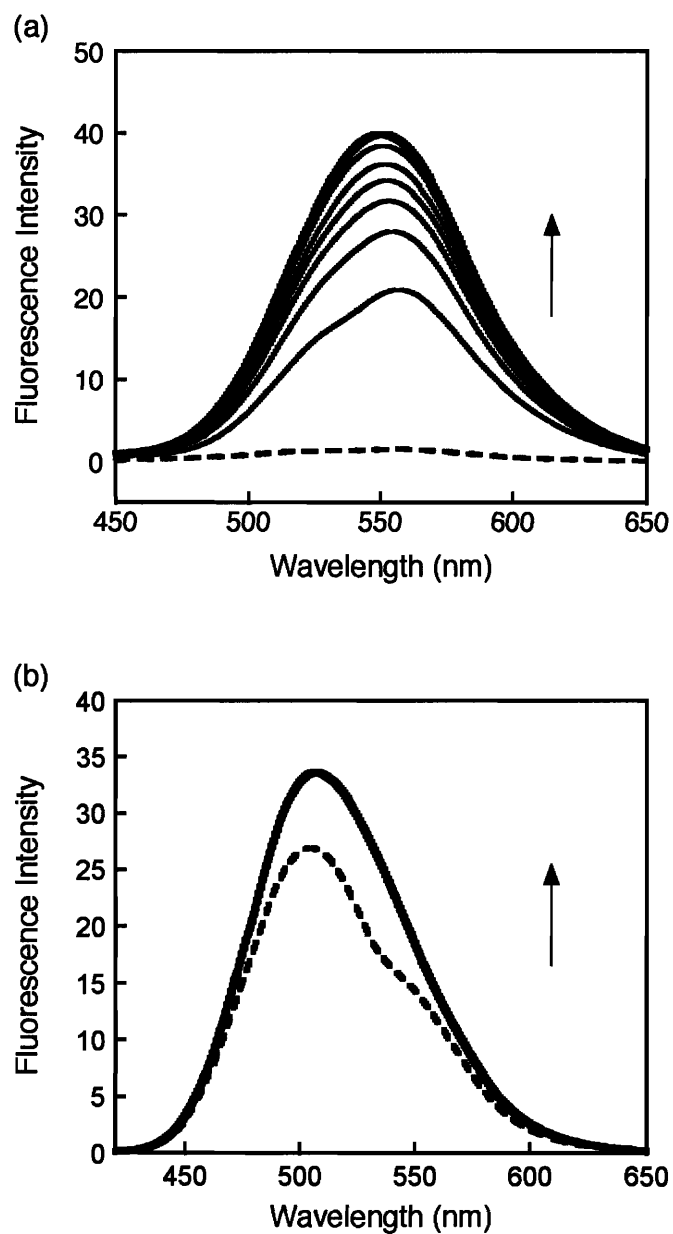


Figure 2.3. Fluorescence response of [Ru(TPP)(CO)(Ds-im)] (1) and [Ru(TPP)(CO)(Ds-tm)] (2) to NO. (a) Upon addition of 100 equiv of NO to a CH₂Cl₂ solution of 1 (10 μM), individual spectra (solid lines) were recorded at 1, 3, 5, 10, 15, and 20 min. Dashed line is at 0 min. (b) Spectrum 3 min after addition of 100 equiv of NO (solid line) to a CH₂Cl₂ solution of 2 (10 μM). Dashed line is at 0 min.

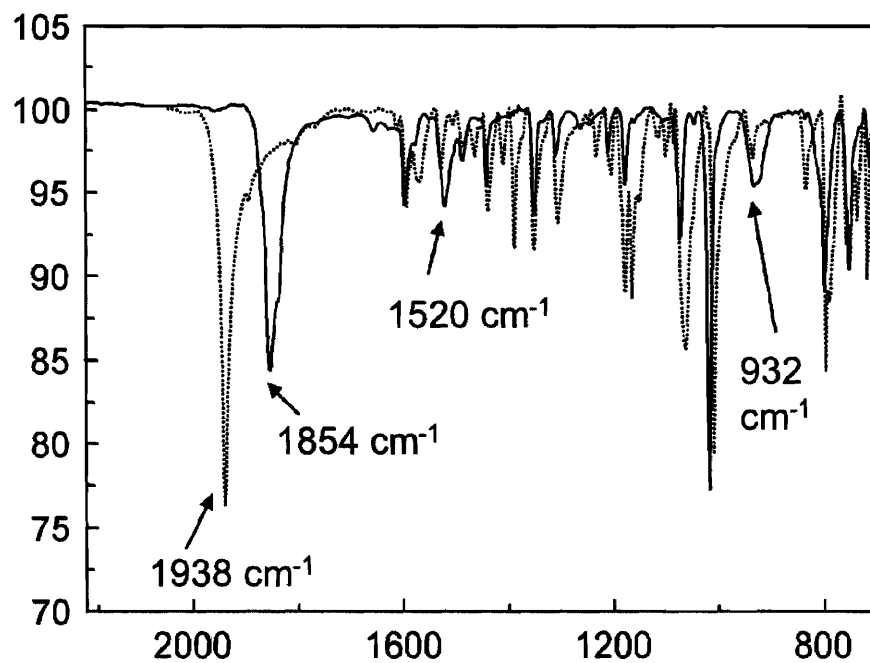


Figure 2.4. IR spectra (in KBr) of [Ru(TPP)(CO)(Ds-im)] (1, dotted line) and [Ru(TPP)(NO)(ONO)] (solid line). The IR bands at 1938 cm⁻¹ and 1854 cm⁻¹ correspond to ν_{CO} and ν_{NO} of 1 and [Ru(TPP)(NO)(ONO)], respectively. The features of ν_{as}(ONO) and ν_s(ONO) were displayed at 1520 and 932 cm⁻¹, respectively.

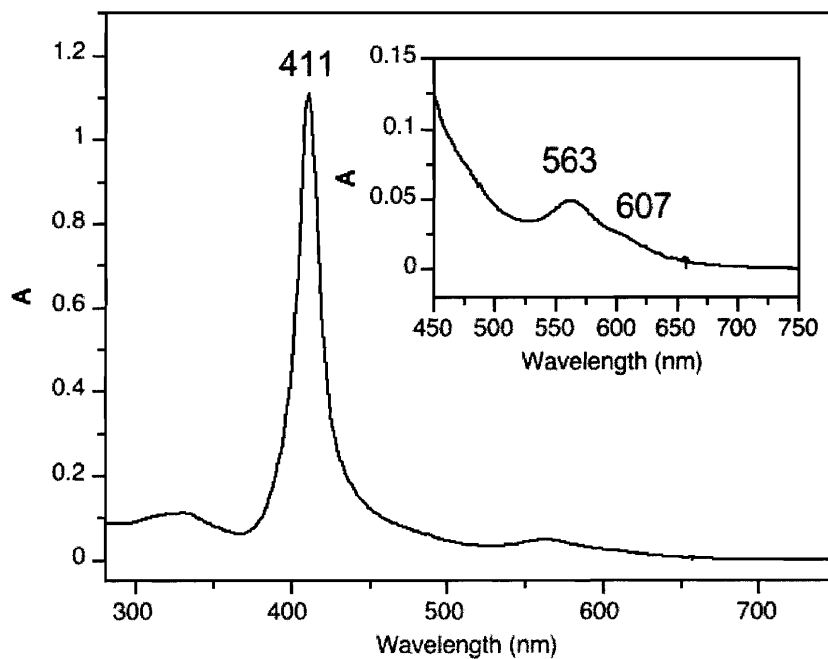


Figure 2.5. UV-vis spectrum of the isolated NO reaction product in CH_2Cl_2 . The spectra match those reported for $[\text{Ru}(\text{TPP})(\text{NO})(\text{ONO})]$, as described in refs. 26 and 30 of the text. Inset: expanded spectrum from 450 nm to 750 nm.

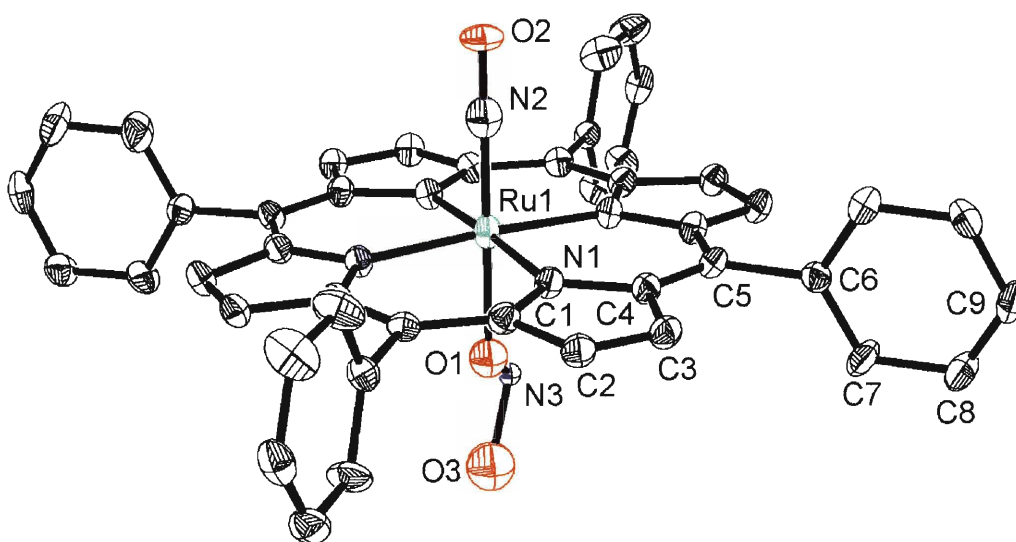


Figure 2.6. ORTEP diagram of $[\text{Ru}(\text{TPP})(\text{NO})(\text{ONO})]$ showing 20% probability thermal ellipsoid. Crystal data for $[\text{Ru}(\text{TPP})(\text{NO})(\text{ONO})]$ (-60 °C): $M = 789.79$, space group $I4/m$ (No. 87), $a = 13.6428(17) \text{ \AA}$, $c = 9.7359(17) \text{ \AA}$, $V = 1812.1(4) \text{ \AA}^3$, $Z = 2$, $\rho = 1.447 \text{ g/cm}^3$, dark red plate, $R(F) = 5.75\%$ ($I > 2\sigma(I)$). The crystal structure of $[\text{Ru}(\text{TPP})(\text{NO})(\text{ONO})]$ was consistent with that previously reported in the literature.²⁶

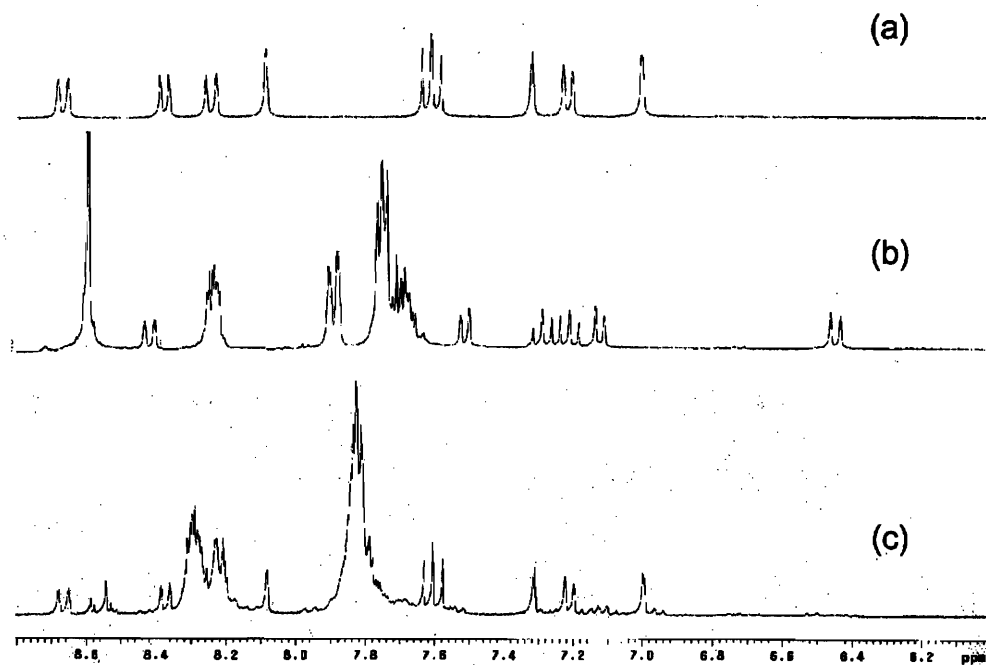


Figure 2.7. Expanded ^1H NMR spectra (6.0 ppm – 8.8 ppm) of CD_2Cl_2 solutions of (a) Ds-im, (b) 1 (2 mM), and (c) 1 (2 mM) upon addition of 10 equiv of NO (g).

Chapter 3

Nitric Oxide-Induced Fluorescence Enhancement by Displacement of Dansylated Ligands from Cobalt

This chapter is based on previously published work (Lim, M. H.; Kuang, C.; Lippard, S. J., *ChemBioChem* 2006, in press). This work was supported by NSF grant CHE-0234951. The MIT DCIF NMR spectrometer was funded through NSF Grant CHE-9808061. We thank Chaoyuan Kuang for his assistance with preparing the cobalt complex 2.

Introduction

The study of nitric oxide (NO), a reactive gaseous free radical, is of interest in biological chemistry, where it regulates a variety of important signaling processes.¹⁻³ Investigations of the biological functions of NO would significantly benefit from a method that allows for its direct and selective detection with simultaneous spatial and temporal resolution. Fluorescence-based NO sensing is a suitable methodology to satisfy these requirements.^{4,5} Organic molecule-based fluorescent NO sensors are currently available, but most only exhibit fluorescence turn-on with an oxidized NO species such as N_2O_3 rather than NO itself. Consequently, they are not capable of providing spatiotemporal details about NO production in biological systems.^{4,6-9} In previous work we described cobalt-based fluorescent sensors for direct NO detection by a fluorophore-displacement strategy (Scheme 3.1).¹⁰⁻¹³ Formation of a metal nitrosyl species causes dissociation of the fluorophore from the quenching environment of the paramagnetic Co(II) ion with concomitant fluorescence emission.

Figure 3.1 depicts the dansyl-containing aminotroponimine ligands, $H^R\text{DATI}$ ($R = \text{Bz}, \text{'Pr}, \text{and 'Bu}$; DATI = dansyl-aminotroponimine) and $H_2\text{DATI-4}$ employed in our earlier studies.^{10,11} The fluorescence of the Co(II) complexes, $[\text{Co}(^R\text{DATI})_2]$ and $[\text{Co}(\text{DATI-4})]$, is significantly quenched relative to that of the free ligands in CH_2Cl_2 solution. Treatment of the cobalt complexes with excess NO for several hours leads to an increase in fluorescence due to release of the fluorophore-appended ligand and formation of a cobalt dinitrosyl species. Additional Co(II) complexes were prepared to improve the fluorescence properties by replacing the dansyl groups with fluorescein emitting units.¹² The resulting Co(II) aminotroponimate complexes, $[\text{Co}(\text{FATI-n})]$ ($n = 3$ or 4), displayed increased fluorescence emission over the course of several hours following addition of excess NO in CH_3OH , accompanied by the formation of

mononitrosyl and dinitrogen adducts.¹² In the case of [Co(FATI-4)], a 3-fold increase in fluorescence occurred 22 h after NO introduction. A dicobalt tetracarboxylate system gave a 9.6-fold fluorescence increase in 1 h, but only in non-coordinating solvents such as CH₂Cl₂.¹³

The goal of the present study was to investigate further the fluorophore-displacement strategy discovered in our previous work to obtain more advanced systems, ultimately for use in biological samples. Our specific aim was to achieve solubility in aqueous media and to improve the kinetics of turn-on emission by NO utilizing non-fluorescent Co(II) complexes. We therefore synthesized and characterized two new air-stable Co(II) complexes, [Co(Ds-AMP)₂] (1) and [Co(Ds-AQ)₂] (2), where Ds-AMP and Ds-AQ are the conjugate bases of dansyl aminomethylpyridine (Ds-HAMP) and dansyl aminoquinoline (Ds-HAQ). These complexes bear a dansyl emitting unit and pyridine or quinoline metal-binding units. They can be prepared in high yield in only two steps and can detect NO (g) in CH₃CN. Their rate of response to NO is >10 times faster than those of the previously described Co(DATI) and Co(FATI) systems.¹⁰⁻¹² The synthesis, characterization, and mechanism of fluorescence enhancement, which involves NO-induced release of one of the ligands from the cobalt center with formation of a dinitrosyl species, are described herein.

Experimental Section

Materials and Procedures

All reagents were purchased from commercial suppliers and used without further purification. Acetonitrile (CH₃CN) and dichloromethane (CH₂Cl₂) were purified by passage through alumina columns under an Ar atmosphere. 5-Dimethylamino-*N*-(2-pyridylmethyl)-1-naphthalenesulfonamide (Ds-HAMP) was prepared as described

elsewhere.¹⁴ Nitric oxide (Matheson 99%) was purified by a method adapted from the literature.^{15,16} For fluorescence experiments, NO (g) was transferred to an anaerobic fluorescence cuvette by using a gastight syringe in the glove box. Fluorescence emission spectra were recorded at 25.0 ± 0.2 °C on a Hitachi F-3010 spectrophotometer. NMR spectra were collected on a Varian 500 spectrometer operating at ambient temperature and referenced to internal ¹H and ¹³C solvent peaks. IR spectra were obtained on an Avatar 360 FTIR instrument and ESI-MS analyses were performed on an Agilent 1100 series instrument.

X-ray Crystallographic Studies. A single crystal suitable for data collection was mounted in Infineum V8512 on the tip of a glass capillary and frozen in a -100 °C nitrogen cold stream. Data were collected on a Bruker APEX CCD X-ray diffractometer with Mo K α radiation ($\lambda = 0.71073$ Å) controlled by the SMART software package.¹⁷ The general procedures used for data collection are reported elsewhere.¹⁸ Empirical absorption corrections were calculated with the SADABS program.¹⁹ Structures were solved by direct methods and refined with the SAINTPLUS and SHELXTL software packages.^{20,21} All non-hydrogen atoms were refined anisotropically. Hydrogen atoms were assigned idealized positions and given a thermal parameter equivalent to 1.2 times the thermal parameter of the atoms to which they were attached. All structure solutions were checked for higher symmetry with PLATON.²² In the structure of **2**, two CH₂Cl₂ molecules per molecule of **2** were assigned. The carbon atom of one CH₂Cl₂ molecule was disordered over two positions with 0.5 occupancy factors. The highest electron density in the final difference Fourier maps for **2** was 1.224 e/Å³ in the vicinity of the cobalt atom.

[Co(Ds-AMP)₂] (**1**). To a CH₃OH solution (5.0 mL) of Ds-HAMP¹⁴ (0.17 g, 0.50 mmol) was added a 0.1 M aqueous solution of KOH (5.0 mL, 5.0 mmol). The solvent

was evaporated under reduced pressure. The resulting residue was dissolved in CH₃OH (10 mL) and cobaltous acetate (44 mg, 0.25 mmol) was added. The solution was refluxed for 7 h and slowly cooled to room temperature over a 2 h period. X-ray quality purple crystals were obtained, collected by filtration, and washed with cold CH₃OH (0.12 g, 0.17 mmol, 67%): m.p. > 230 °C (decomp). FTIR (KBr, cm⁻¹): 3111 (vw), 3085 (vw), 3071 (vw), 3031 (vw), 3018 (vw), 2994 (vw), 2950 (vw), 2937 (vw), 2903 (vw), 2873 (vw), 2836 (w), 2802 (vw), 2788 (vw), 1609 (m), 1588 (m), 1566 (m), 1500 (w), 1488 (m), 1458 (m), 1437 (m), 1411 (w), 1402 (m), 1391 (m), 1329 (m), 1302 (m), 1291 (m), 1272 (vs), 1224 (w), 1212 (w), 1196 (w), 1180 (s), 1151 (s), 1111 (m), 1070 (m), 1055 (m), 1026 (m), 995 (w), 977 (vw), 967 (w), 949 (vw), 923 (s), 910 (s), 888 (m), 836 (m), 817 (m), 785 (s), 763 (m), 733 (m), 721 (m), 682 (w), 655 (w), 637 (s), 620 (s), 575 (s), 555 (s), 538 (w), 529 (w), 499 (w), 484 (m), 463 (vw), 413 (vw). Anal. Calcd. for CoC₃₆H₃₆S₂O₄N₆·0.5H₂O: C, 57.75; H, 4.98; N, 11.22; Found C, 58.20; H, 4.96; N, 11.09.

5-Dimethylamino-N-(8-quinolinyl)-1-naphthalenesulfonamide, (Ds-HAQ).

Triethylamine (0.51 mL, 3.7 mmol) was added to a CH₂Cl₂ solution (20 mL) of 8-aminoquinoline (0.27 g, 1.9 mmol) and dansyl chloride (0.50 g, 1.9 mmol). The mixture was stirred for 2 h at room temperature and was washed with an aqueous saturated NaHCO₃ solution. The aqueous solution was extracted with CH₂Cl₂ (3 × 10 mL) and the organic phase was dried over anhydrous magnesium sulfate. The final product was purified by column chromatography (SiO₂, 3:1 hexanes:ethyl acetate; R_f = 0.25 by TLC) and isolated as a yellow powder (0.41 g, 1.1 mmol, 59%): m.p. 147 – 151 °C. ¹H NMR (500 MHz, CDCl₃): δ (ppm) 2.81 (s, 6H), 7.12 (d, J = 7.5, 1H), 7.34 – 7.37 (m, 3H), 7.45 – 7.48 (m, 1H), 7.56 – 7.59 (m, 1H), 7.69 – 7.71 (m, 1H), 8.02 (dd, J = 8.25, J = 1.5, 1H), 8.38 (dd, J = 7.25, J = 1.0, 1H), 8.46 (dd, J = 8.5, 1H), 8.50 (dd, J = 8.5, 1H), 8.72 (dd, J

= 4.5, $J = 2.0$, 1H), 9.56 (s, 1H). ^{13}C NMR (75 MHz, CDCl_3): δ (ppm) 151.9, 148.7, 138.3, 136.3, 134.5, 134.2, 130.9, 130.3, 130.0, 129.8, 128.6, 128.2, 126.9, 123.1, 122.1, 121.7, 119.3, 115.4, 114.0, 45.6. FTIR (KBr, cm^{-1}): 3256 (m), 3131 (w), 3071 (vw), 2995 (w), 2956 (w), 2876 (vw), 2842 (vw), 2787 (vw), 1611 (m), 1585 (m), 1573 (m), 1504 (s), 1482 (w), 1472 (m), 1456 (m), 1430 (vw), 1411 (m), 1403 (vw), 1392 (w), 1383 (w), 1363 (m), 1333 (m), 1305 (s), 1256 (w), 1232 (m), 1200 (m), 1180 (w), 1146 (vs), 1105 (w), 1088 (m), 1070 (ww), 1060 (w), 1045 (vw), 962 (w), 946 (m), 927 (m), 887 (w), 850 (m), 821 (m), 791 (vs), 753 (m), 735 (w), 685 (m), 627 (s), 594 (w), 580 (m), 557 (m), 569 (s), 538 (m), 497 (w), 486 (m), 418 (w). ESI(+)-MS (m/z): $[\text{M}+\text{H}]^+$ Calcd for $\text{C}_{21}\text{H}_{19}\text{N}_3\text{O}_2\text{S}$, 378.1; Found, 378.1.

[Co(Ds-AQ)₂] (2). To a CH_3OH solution (5.0 mL) of Ds-HAQ (0.10 g, 0.26 mmol) was added a 0.1 M aqueous solution of KOH (2.6 mL, 0.26 mmol). The solvent was evaporated under reduced pressure. The resulting residue was dissolved in CH_3OH (5.0 mL) and cobaltous acetate (0.023 g, 0.13 mmol) was added. The solution was refluxed for 6 h and slowly cooled to room temperature over 1 h. A purple solid was collected and washed with diethyl ether (0.092 g, 0.11 mmol, 87%): m.p. 309 – 310 °C. X-ray quality purple crystals were obtained by the vapor diffusion of hexanes into a CH_2Cl_2 solution of the purple complex at room temperature. FTIR (KBr, cm^{-1}): 3111 (vw), 3085 (vw), 3071 (vw), 3068 (vw), 3011 (vw), 2997 (vw), 2948 (w), 2867 (vw), 2831 (w), 2788 (w), 2768 (w), 1604 (w), 1583 (m), 1474 (w), 1465 (s), 1436 (w), 1419 (vw), 1382 (s), 1355 (w), 1319 (s), 1287 (vs), 1272 (m), 1245 (w), 1231 (w), 1190 (m), 1178 (w), 1156 (w), 1129 (vs), 1116 (s), 1071 (m), 1059 (w), 1040 (w), 957 (m), 941 (m), 869 (s), 839 (w), 831 (m), 805 (m), 788 (vs), 762 (m), 736 (vw), 685 (w), 666 (vw), 627 (vs), 582 (vs), 569 (m), 551 (w), 539 (w), 525 (w), 496 (w), 491 (w), 450 (w). Anal. Calcd. for $\text{CoC}_{42}\text{H}_{36}\text{S}_2\text{O}_4\text{N}_6\cdot\text{H}_2\text{O}$: C, 60.79; H, 4.62; N, 10.13; Found C, 60.73; H, 4.49; N, 10.21.

Results and Discussion

Syntheses and Structural Characterization of Cobalt Complexes

The main goal in the present study was to investigate cobalt(II) complexes as fluorescent NO sensors. To improve the solubility of complexes in this class, we synthesized $[\text{Co}(\text{Ds-AMP})_2]$ (**1**) and $[\text{Co}(\text{Ds-AQ})_2]$ (**2**). These compounds, which contain *N*-donor atoms as metal-binding units and a dansyl group for emitting light (Ds-HAMP¹⁴ or Ds-HAQ, **1** and **2**, respectively; Figure 3.2), can be prepared in only two steps in good yield by combining $\text{Co}(\text{OAc})_2$ with two equiv of the ligand in CH_3OH in the presence of a base. Both compounds are air-stable.

X-ray quality purple crystals of the cobalt complexes were obtained by slowly cooling a CH_3OH solution of **1** and layering hexanes on a CH_2Cl_2 solution of **2**. Crystallographic data for **1** and **2** are summarized in Table 3.1, and their molecular structures with the atom-labeling schemes are depicted in Figure 3.3. Selected bond lengths and angles are listed in Table 3.2. In each complex, the cobalt center is four-coordinate with the nitrogen atoms supplied by the two bidentate ligands. In the structure of **1**, the $\text{Co-N}_{\text{amide}}$ bonds (1.941(4) Å and 1.956(4) Å) are shorter than those of $\text{Co-N}_{\text{pyridine}}$ (2.020(3) Å and 2.043(3) Å). Similarly, the $\text{Co-N}_{\text{amide}}$ bonds (1.956(4) Å and 1.959(4) Å) are shorter than those of $\text{Co-N}_{\text{quinoline}}$ (2.028(4) Å and 2.033(4) Å) in the structure of **2**. Highly distorted tetrahedral geometries about the Co(II) centers in **1** and **2** are revealed by the relevant bond angles of the complexes. For example, the $\text{N}(1)\text{-Co-N}(2)$ and $\text{N}(3)\text{-Co-N}(4)$ angles (81.95(15)° and 81.66(14)° for **1**; 82.66(16)° and 82.46(16)° for **2**) in both structures are significantly less than the 109.5° expected for a perfect tetrahedron. The $\text{N}(1)\text{-Co-N}(3)$ (107.76(14) for **1** and 114.17(16) for **2**) angle is significantly smaller than the $\text{N}(2)\text{-Co-N}(4)$ angle (127.98(15) for **1** and 121.06(16) for **2**), presumably, due to steric repulsion between the dansyl substituents of the ligand

framework. The dihedral angle, Θ , measured between the planes of the two five-membered chelate rings is 76.8° in both structures. These geometric features are similar to those observed in other four-coordinate Co(II) complexes with sulfonamide nitrogen donors.^{23,24}

Fluorescence Spectroscopic Measurements

Fluorescence studies of **1** and **2** ($10 \mu\text{M}$) were conducted in the polar coordinating solvent CH_3CN and indicated $4.7(\pm 1.2)$ -fold and $7.9(\pm 0.9)$ -fold quenching ($\lambda_{\text{ex}} = 342 \text{ nm}$), respectively, compared to the free ligands (Figure 3.4). Upon addition of 100 equiv of NO to these CH_3CN solutions of the weakly emissive cobalt complexes, the fluorescence intensity increased by $2.1(\pm 0.3)$ -fold within 35 min for **1** and $3.6(\pm 0.1)$ -fold within 20 min for **2** (Figure 3.5). In a polar protic solvent such as CH_3OH , $1.6(\pm 0.3)$ -fold and $16(\pm 3)$ -fold quenching in fluorescence were observed for **1** and **2**, respectively (Figure 3.6). When the CH_3OH solutions of these cobalt complexes ($10 \mu\text{M}$) were allowed to react with 100 equiv of NO, a $1.4(\pm 0.1)$ -fold (**1**) and $6.5(\pm 1.4)$ -fold (**2**) fluorescence increase in integrated emission occurred within 60 min (Figure 3.7). These fluorescence studies demonstrate that the two cobalt complexes **1** and **2** can sense NO using the fluorophore-displacement strategy, with a significantly faster fluorescence response than previously obtained by the related cobalt systems Co(II)-DATI^{10,11} and Co(II)-FATI (Table 3.3).¹² The successful fluorescence-based NO detection was performed in both CH_3CN and CH_3OH solvents that have dielectric constants closer to that of water (37.5 for CH_3CN and 32.6 for CH_3OH , versus 80.2 for water) than CH_2Cl_2 (9.1).

Investigation of the Chemistry of the Cobalt Complexes with Nitric Oxide

In order to gain an understanding of the underlying mechanism of the NO-induced fluorescence turn-on we examined the reactivity of these cobalt systems more closely. Formation of a Co-nitrosyl species was monitored by following the reactions of **1** and **2** with NO using vibrational spectroscopy.

The time-dependent IR spectra of a CH₃CN solution of **1** following addition of 100 equiv of NO were recorded (Figure 3.8). The initial purple solution turned brown upon exposure to NO. After five minutes after NO introduction, the IR spectrum displayed a band at 1693 cm⁻¹, indicating formation of a Co-mononitrosyl species, and two bands at 1766 and 1847 cm⁻¹, indicating the presence of a Co-dinitrosyl adduct. The mononitrosyl appears to be the first species formed, and the intensities of the two bands at 1766 and 1847 cm⁻¹ slowly increased over 60 min, while that associated with the mononitrosyl disappeared during this time period. The appearance of two stretching bands at 1766 and 1847 cm⁻¹ is consistent with the IR spectra of other Co-dinitrosyl complexes, which exhibit symmetric and asymmetric stretching modes between 1750 – 1798 and 1820 – 1876 cm⁻¹.^{10,11,13,25-32} These observations suggest stepwise coordination of NO to the cobalt center.

When no further changes in the IR spectra were observed, the reaction mixture was examined by ¹H NMR spectroscopy. The ¹H NMR spectrum revealed resonances consistent only with the presence of diamagnetic species in solution (Figure 3.9). For example, proton resonances corresponding to the dimethylamino functionality (–N(CH₃)₂–) of the dansyl group were distinguished at 2.83 δ for the dissociated ligand and at 2.85 δ for the ligand bound to cobalt.

As discussed above, when excess NO was allowed to react with **1**, the

fluorescence was enhanced by half the value corresponding to Ds-HAMP emission from two equiv of free ligand (Figure 3.10). This result demonstrates that NO binding releases one ligand from the cobalt center with corresponding restoration of emission. When **1** was exposed to 5 equiv of NO in CH₃CN, only a 1.4-fold increase in fluorescence intensity was observed. The low sensitivity of **1** to small amounts of NO may reflect the need for multiple steps required to reduce Co(II) to Co(I) in order to generate the final product [Co(Ds-AMP)(NO)₂]. This process is depicted in Scheme 3.2, which parallels that previously proposed for the reaction of dicobalt(II) complexes with NO.¹³

Taken together, the fluorescence, IR, and ¹H NMR spectroscopic results for the reaction of **1** with NO indicate that excess NO displaces one Ds-AMP ligand from the metal center, forming a diamagnetic dinitrosyl adduct, presumably [Co(Ds-AMP)(NO)₂], {Co(NO)₂}¹⁰ (Scheme 3.2). Attempts to separate and isolate the Ds-HAMP ligand and [Co(Ds-AMP)(NO)₂] complex from the resulting solution in order to assess whether the fluorescence increase is caused by the dinitrosyl cobalt species, the dissociated ligand, or both were unsuccessful. We, however, have previously characterized the related dinitrosyl cobalt complex obtained from the reaction of [Co(ⁱPrDATI)Cl₂] with NO (g), which was not fluorescent.³³ We therefore conclude that the dansyl moiety released from cobalt in the present reactions is the source of the NO-induced fluorescence enhancement.

Conclusions

Two cobalt complexes containing dansyl-functionalized bidentate ligands were synthesized and characterized. Both complexes are air-stable and show significant fluorescence quenching in CH₃CN and CH₃OH, compared to the emission of the free

ligands. Upon addition of excess NO, fluorescence is restored. The fluorescence-based NO response of both complexes in coordinating solvents such as CH₃CN and CH₃OH is faster than that of other cobalt sensors previously reported. Nitric oxide replaces one ligand from the cobalt center forming a dinitrosyl cobalt complex with turn-on emission, as demonstrated by IR and ¹H NMR spectroscopy. Although the response represents an improvement over previous cobalt-based systems, the reaction is still slow for some bioimaging applications. In addition, solubility in aqueous media would be required for most studies of this kind. These efforts were an important step in the evolution of fluorescein-based ligands for metal-mediated NO sensing to monitor nitric oxide production in living cells.³⁴

References

- (1) Furchgott, R. F., *Angew. Chem. Int. Ed.* **1999**, *38*, 1870-1880.
- (2) Murad, F., *Angew. Chem. Int. Ed.* **1999**, *38*, 1856-1868.
- (3) Ignarro, L. J., *Angew. Chem. Int. Ed.* **1999**, *38*, 1882-1892.
- (4) Nagano, T.; Yoshimura, T., *Chem. Rev.* **2002**, *102*, 1235-1269 and references cited therein.
- (5) Hilderbrand, S. A.; Lim, M. H.; Lippard, S. J., *In Topics in Fluorescence Spectroscopy*, Geddes, C. D.; Lakowicz, J. R., Eds. Springer: 2005; pp 163-188 and references cited therein.
- (6) Kojima, H.; Sakurai, K.; Kikuchi, K.; Kawahara, S.; Kirino, Y.; Nagoshi, H.; Hirata, Y.; Akaike, T.; Maeda, H.; Nagano, T., *Biol. Pharm. Bull.* **1997**, *20*, 1229-1232.
- (7) Kojima, H.; Nakatsubo, N.; Kikuchi, K.; Kawahara, S.; Kirino, Y.; Nagoshi, H.; Hirata, Y.; Nagano, T., *Anal. Chem.* **1998**, *70*, 2446-2453.

- (8) Nakatsubo, N.; Kojima, H.; Kikuchi, K.; Nagoshi, H.; Hirata, Y.; Maeda, D.; Imai, Y.; Irimura, T.; Nagano, T., *FEBS Lett.* **1998**, *427*, 263-266.
- (9) Sasaki, E.; Kojima, H.; Nishimatsu, H.; Urano, Y.; Kikuchi, K.; Hirata, Y.; Nagano, T., *J. Am. Chem. Soc.* **2005**, *127*, 3684-3685.
- (10) Franz, K. J.; Singh, N.; Lippard, S. J., *Angew. Chem. Int. Ed.* **2000**, *39*, 2120-2122.
- (11) Franz, K. J.; Singh, N.; Spingler, B.; Lippard, S. J., *Inorg. Chem.* **2000**, *39*, 4081-4092.
- (12) Hilderbrand, S. A.; Lippard, S. J., *Inorg. Chem.* **2004**, *43*, 4674-4682.
- (13) Hilderbrand, S. A.; Lippard, S. J., *Inorg. Chem.* **2004**, *43*, 5294-5301.
- (14) Lim, M. H.; Lippard, S. J., *J. Am. Chem. Soc.* **2005**, *127*, 12170-12171.
- (15) Lorkovic, I. M.; Ford, P. C., *Inorg. Chem.* **2000**, *39*, 632-633.
- (16) Hilderbrand, S. A.; Lim, M. H.; Lippard, S. J., *J. Am. Chem. Soc.* **2004**, *126*, 4972-4978.
- (17) *SMART: Software for the CCD Detector System*, version 5.626; Bruker AXS: Madison, WI, 2000.
- (18) Kuzelka, J.; Mukhopadhyay, S.; Spingler, B.; Lippard, S. J., *Inorg. Chem.* **2004**, *43*, 1751-1761.
- (19) Sheldrick, G. M. *SADABS: Area-Detector Absorption Correction*, University of Göttingen: Göttingen, Germany, 1996.
- (20) *SAINTPLUS: Software for the CCD Detector System*, version 5.01; Bruker AXS: Madison, WI, 1998.
- (21) *SHELXTL: Program Library for Structure Solution and Molecular Graphics*, version 6.1; Bruker AXS: Madison, WI, 2001.
- (22) Spek, A. L. *PLATON, A Multipurpose Crystallographic Tool*, Utrecht University: Utrecht, The Netherlands, 2000.

- (23) Congreve, A.; Katakya, R.; Knell, M.; Parker, D.; Puschmann, H.; Senanayake, K.; Wylie, L., *New J. Chem.* **2003**, *27*, 98-106.
- (24) Durán, M. L.; García-Vázquez, J. A.; Gómez, C.; Sousa-Pedrares, A.; Romero, J.; Sousa, A., *Eur. J. Inorg. Chem.* **2002**, 2348-2354.
- (25) Field, J. S.; Wheatley, P. J.; Bhaduri, S., *J. Chem. Soc., Dalton Trans.* **1974**, 74-8.
- (26) Haymore, B. L.; Huffman, J. C.; Butler, N. E., *Inorg. Chem.* **1983**, *22*, 168-70.
- (27) Kaduk, J. A.; Ibers, J. A., *Inorg. Chem.* **1977**, *16*, 3283-3287.
- (28) Reichert, B. E., *Acta Cryst.* **1976**, *B32*, 1934-1936.
- (29) Roustan, J.-L.; Ansari, N.; Le Page, Y.; Charland, J.-P., *Can. J. Chem.* **1992**, *70*, 1650-1657.
- (30) Aresta, M.; Ballivet-Tkatchenko, D.; Bonnet, M. C.; Faure, R.; Loiseleur, H., *J. Am. Chem. Soc.* **1985**, *107*, 2994-2995.
- (31) Hendrickson, A. R.; Ho, R. K. Y.; Martin, R. L., *Inorg. Chem.* **1974**, *13*, 1279-1281.
- (32) Martin, R. L.; Taylor, D., *Inorg. Chem.* **1976**, *15*, 2970-2976.
- (33) Hilderbrand, S. A.; Lippard, S. J., unpublished results.
- (34) Lim, M. H.; Xu, D.; Lippard, S. J., *Nat. Chem. Biol.* **2006**, in press.

Table 3.1. Summary of X-ray Crystallographic Data

	[Co(Ds-AMP) ₂] (1)	[Co(Ds-AQ) ₂] · 2CH ₂ Cl ₂ (2·2CH ₂ Cl ₂)
formula	C ₃₆ H ₃₆ CoN ₆ O ₄ S ₂	C ₄₄ H ₃₉ Cl ₄ CoN ₆ O ₄ S ₂
formula weight	739.76	980.68
space group	P2 ₁ /c	P1
a, Å	19.533(3)	9.998(2)
b, Å	11.0613(18)	10.852(2)
c, Å	16.975(3)	22.118(4)
α, deg	–	89.26(3)
β, deg	113.733(3)	88.94(3)
γ, deg	–	64.35(3)
V, Å ³	3357.4(10)	2162.9(7)
Z	4	2
ρ _{calc} g/cm ³	1.463	1.506
crystal size (mm ³)	0.10 x 0.06 x 0.05	0.10 x 0.07 x 0.03
T, °C	-100	-100
μ(Mo Kα), mm ⁻¹	0.686	0.792
θ limits, deg	1.14 – 26.49	1.84 – 25.50
total no. of data	26959	16660
no. of unique data	6946	7945
no. of params	446	597
GOF ^a	1.268	1.169
R ^b	0.0788	0.0726
wR ^{2 c}	0.1473	0.1824
max, min peaks, e/Å ³	0.596, -0.507	1.224, -0.561

^a GOF (Goodness of fit on F²) = {Σ[w(F_o²-F_c²)²]/(m-n)}^{1/2} (m = number of reflections, n = number of parameters refined)

^b R = Σ||F_o| - |F_c||/Σ|F_o|

^c wR² = {Σ[w(F_o²-F_c²)²]/Σ[w(F_o²)²]}^{1/2}

Table 3.2. Selected Bond Distances (Å) and Angles (deg)^a

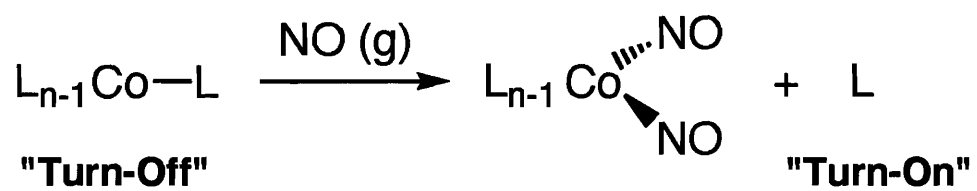
1			
Co1-N1	2.043(3)	N1-Co1-N3	107.76(14)
Co1-N2	1.956(4)	N1-Co1-N4	136.34(15)
Co1-N3	2.020(3)	N2-Co1-N3	125.34(15)
Co1-N4	1.941(4)	N2-Co1-N4	127.98(15)
N1-Co1-N2	81.95(15)	N3-Co1-N4	81.66(14)
		Θ^b	76.8
2·2CH ₂ Cl ₂			
Co1-N1	2.033(4)	N1-Co1-N3	114.17(16)
Co1-N2	1.959(4)	N1-Co1-N4	134.08(16)
Co1-N3	2.028(4)	N2-Co1-N3	129.01(16)
Co1-N4	1.956(4)	N2-Co1-N4	121.06(16)
N1-Co1-N2	82.66(16)	N3-Co1-N4	82.46(16)
		Θ^b	76.8

^a Numbers in parentheses are estimated standard deviations of the last significant figures. Atoms are labeled as indicated in Figure 3.3. The full list of bond lengths and angles is in the supporting information of the previous report, which is available at <http://www.chembiochem.org> (Lim, M. H.; Kuang, C.; Lippard, S. J., *ChemBioChem* 2006, in press).

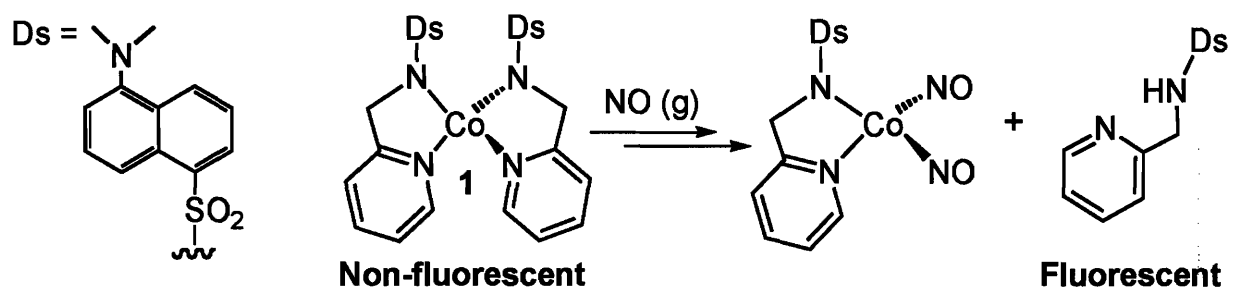
^b The angle Θ is the dihedral angle between the planes of the two five-membered chelate rings.

Table 3.3. NO Detection Times of Cobalt Complexes

Complex	Solvent	NO detection time (min, h)	Reference
[Co(ⁱ PrDATI) ₂]	CH ₂ Cl ₂	6 h	11
[Co(DATI-4)]	CH ₂ Cl ₂	6 h	10, 11
[Co ₂ (μ-O ₂ CAr ^{tol}) ₄ (Ds-pip) ₂]	CH ₂ Cl ₂	1 h	13
[Co(ⁱ PrFATI-4)]	CH ₃ OH	22 h	12
[Co(Ds-AMP) ₂]	CH ₃ CN, CH ₃ OH	35 min, 1 h	this work
[Co(Ds-AQ) ₂]	CH ₃ CN, CH ₃ OH	20 min, 1 h	this work



Scheme 3.1. Fluorophore Displacement Strategy.



Scheme 3.2. Nitric Oxide Detection of **1**.

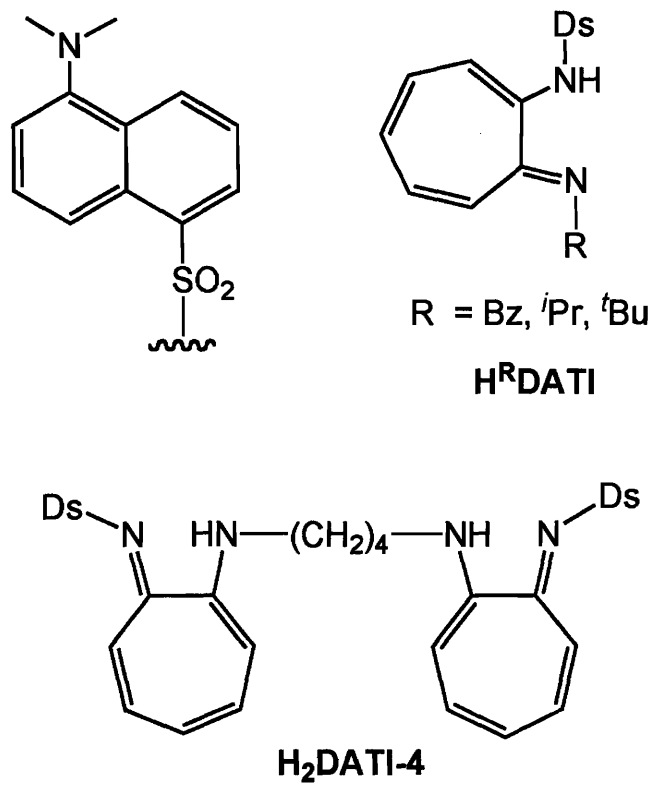


Figure 3.1. Schematic drawings of H^RDATI and H₂DATI-4.

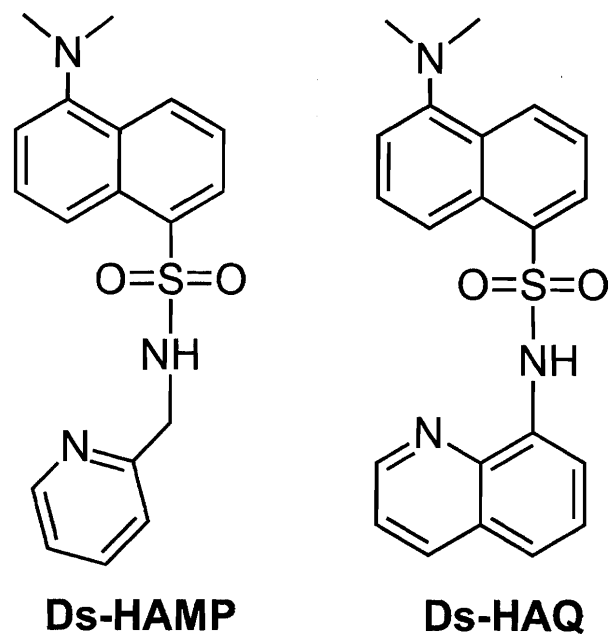


Figure 3.2. Schematic drawings of Ds-HAMP and Ds-HAQ.

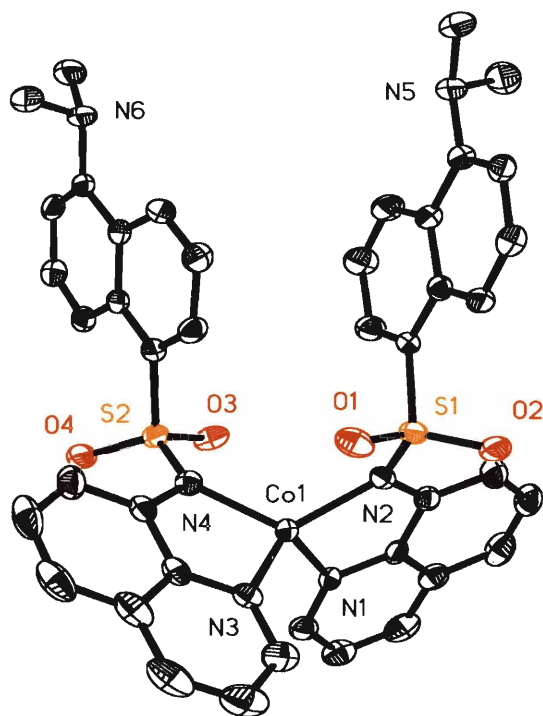
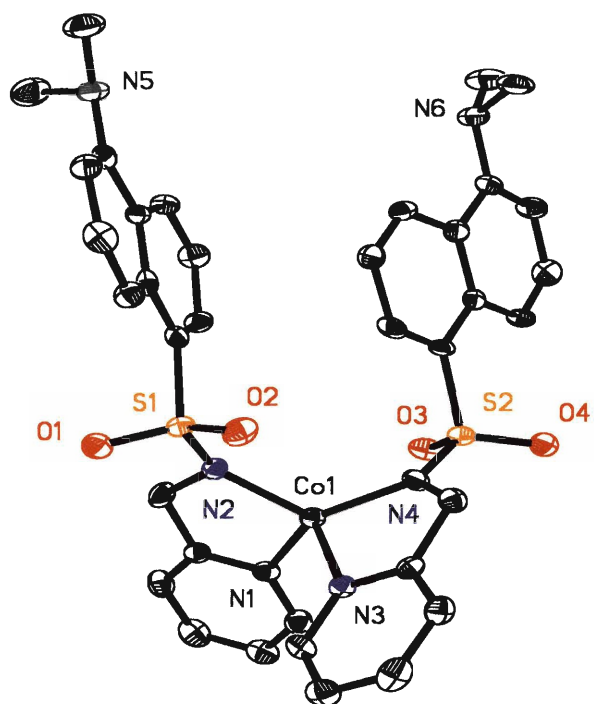


Figure 3.3. ORTEP diagrams of [Co(Ds-AMP)₂] (1, left) and [Co(Ds-AQ)₂] (2, right) showing 50% probability thermal ellipsoids.

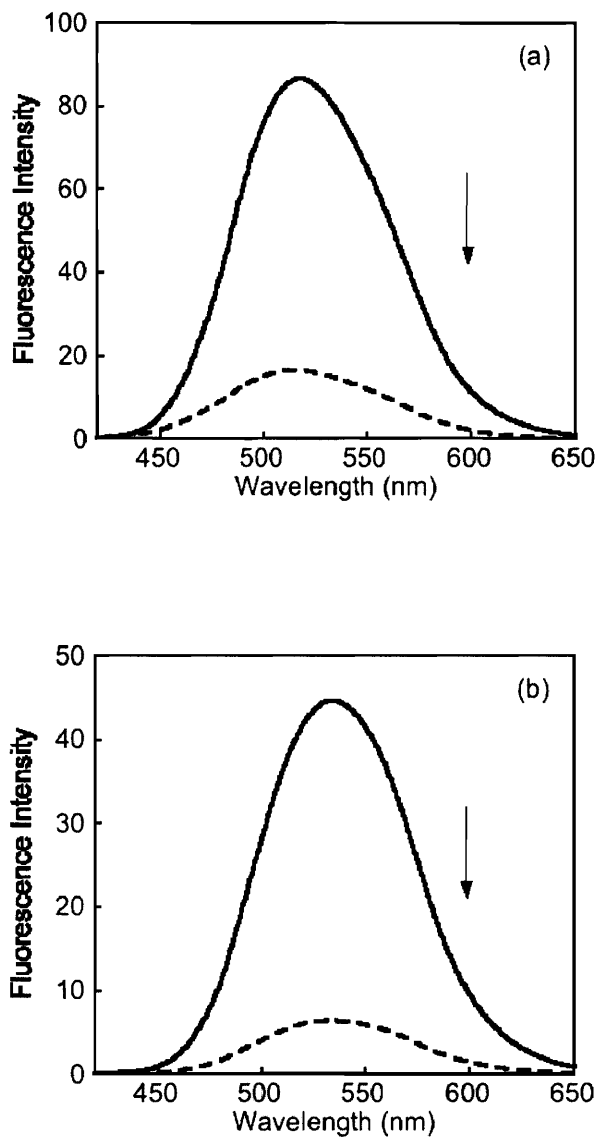


Figure 3.4. Fluorescence emission spectra in CH_3CN : (a) **1** ($10\ \mu\text{M}$, dotted line) and Ds-HAMP ($20\ \mu\text{M}$, solid line); (b) **2** ($10\ \mu\text{M}$, dotted line) and Ds-HAQ ($20\ \mu\text{M}$, solid line). Excitation is at 342 nm.

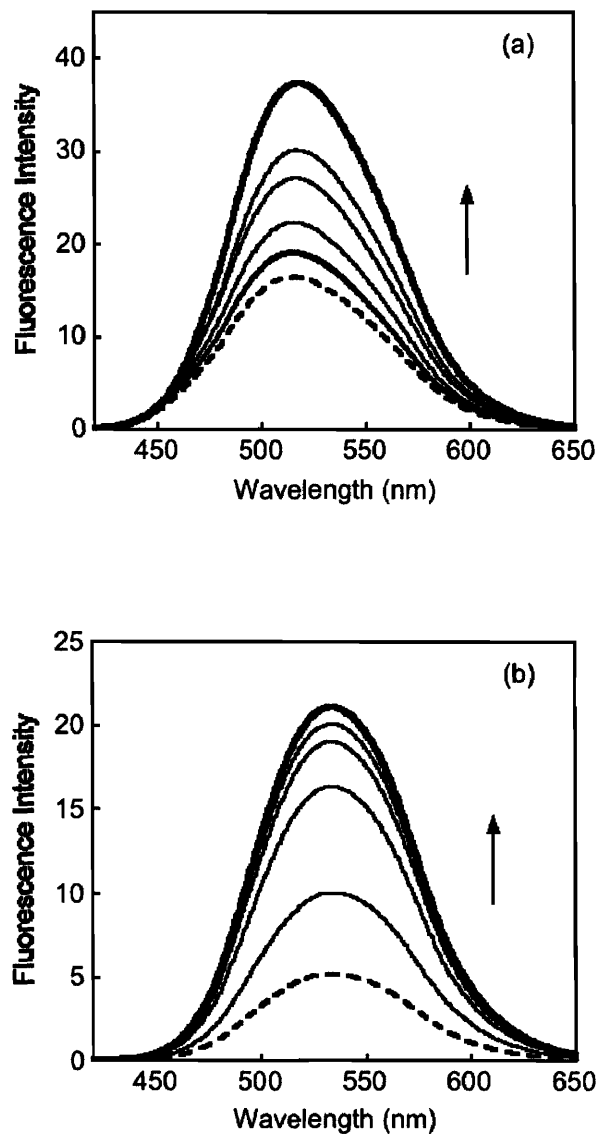


Figure 3.5. Fluorescence responses of a CH_3CN solution of **1** ($10\ \mu\text{M}$, dotted line) upon addition of 100 equiv of NO (5, 10, 15, 20, 25, 30, 35 min, solid lines) (left, a). Right: fluorescence response of a CH_3CN solution of **2** ($10\ \mu\text{M}$, dotted line) after introduction of 100 equiv of NO (3, 6, 10, 15, 20 min, solid lines) (right, b). Excitation is at 342 nm.

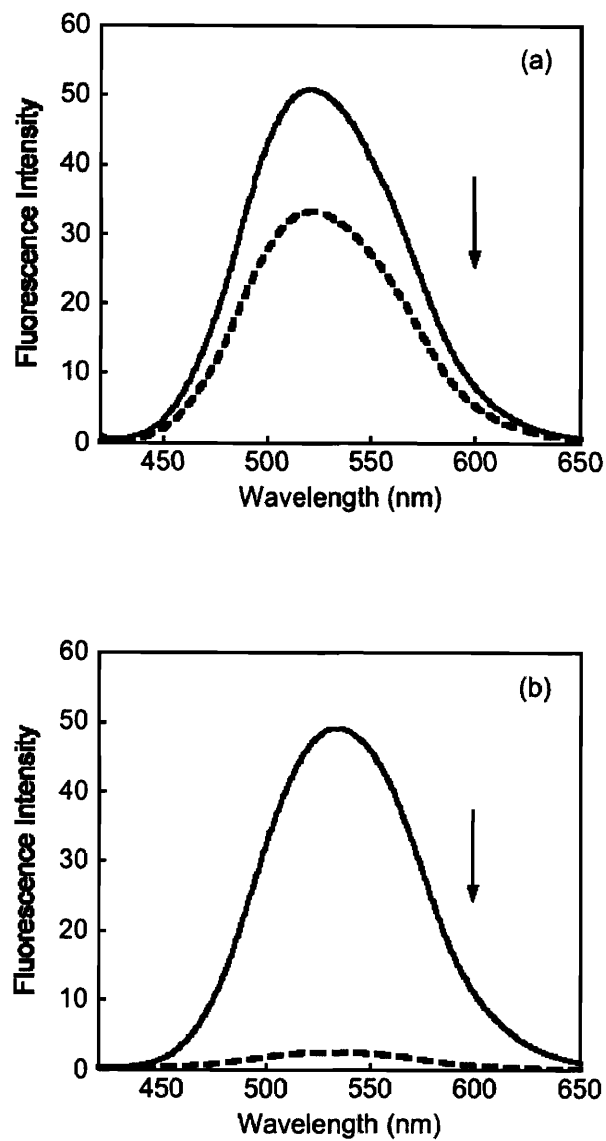


Figure 3.6. Fluorescence emission spectra in CH_3OH . (a) 1 ($10 \mu\text{M}$, dotted line) and Ds-HAMP ($20 \mu\text{M}$, solid line); (b) 2 ($10 \mu\text{M}$, dotted line) and Ds-HAQ ($20 \mu\text{M}$, solid line). Excitation is at 342 nm.

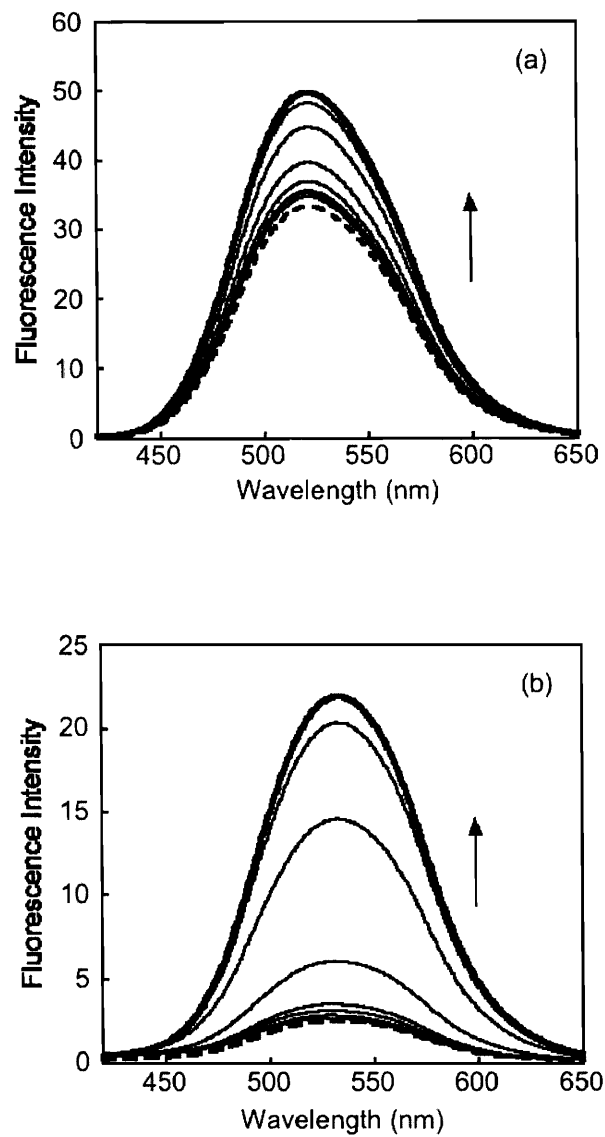


Figure 3.7. Fluorescence response of a CH₃OH solution of (a) 1 (10 μM, dotted line) upon addition of 100 equiv of NO (6, 10, 15, 20, 30, 40, 50, 60 min, solid lines) and (b) a 10 μM solution of 2 in CH₃OH (dotted line) after admission of 100 equiv of NO (6, 10, 15, 20, 30, 40, 50, 60 min, solid lines).

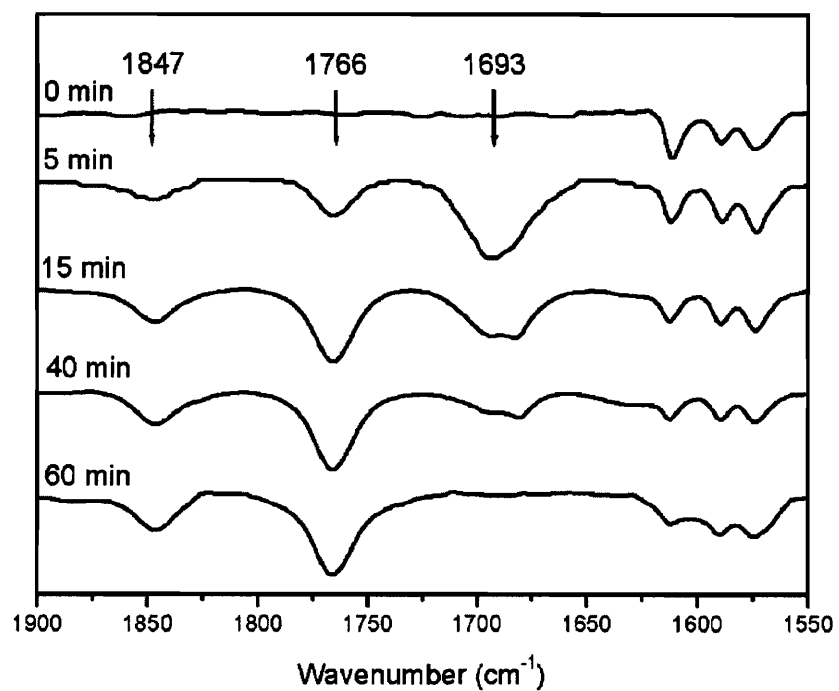


Figure 3.8. Solution IR spectra of the reaction of **1** (2 mM) and 100 equiv of NO in CH_3CN (0, 5, 15, 40, 60 min).

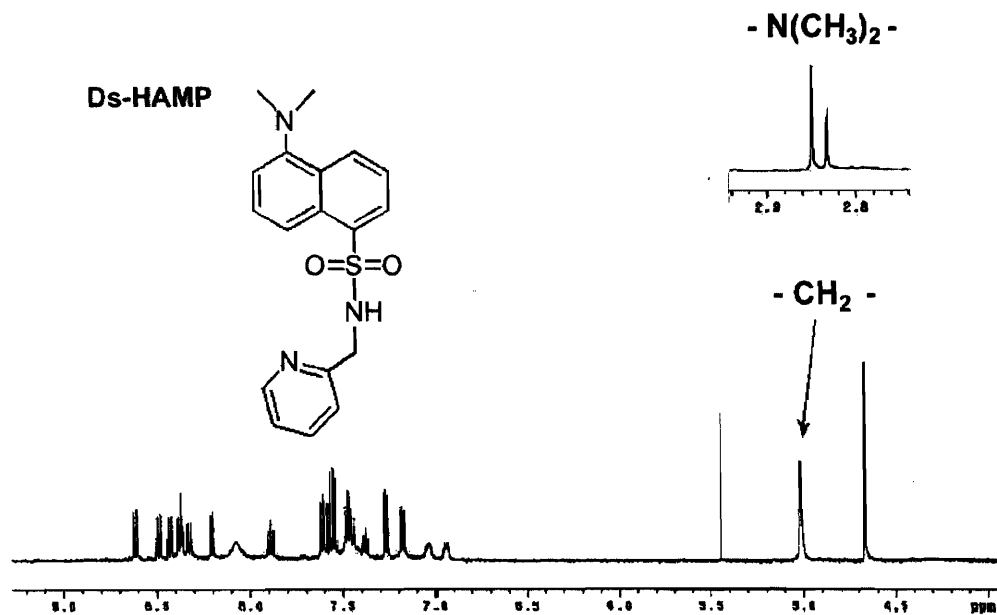


Figure 3.9. ¹H NMR spectrum taken 2 h after the reaction of 1 (1 mM) with 10 equiv of NO in CD₃CN: (500 MHz, CD₃CN): δ = 2.83 (s, 6H), 2.85 (s, 6H), 4.63 (s, 2H), 5.04 (s, 2H), 6.95 (d, J = 7.5, 1H), 7.03 – 7.05 (m, 1H), 7.18 (d, J = 8.0, 1H), 7.27 (d, J = 7.5, 1H), 7.38 (t, J = 7.5, 1H), 7.43 – 7.49 (m, 3H), 7.56 (t, J = 7.0, 2H), 7.61 (t, J = 8.0, 1H), 7.89 (t, J = 7.5, 1H), 8.08 (s, 1H), 8.20 (dd, J = 6.5, J = 1.0, 1H), 8.32 (d, J = 9.0, 1H), 8.38 (t, J = 6.0, 2H), 8.42 (d, J = 1.5, 1H), 8.49 (d, J = 3.5, 1H), 8.62 (d, J = 8.0, 1H).

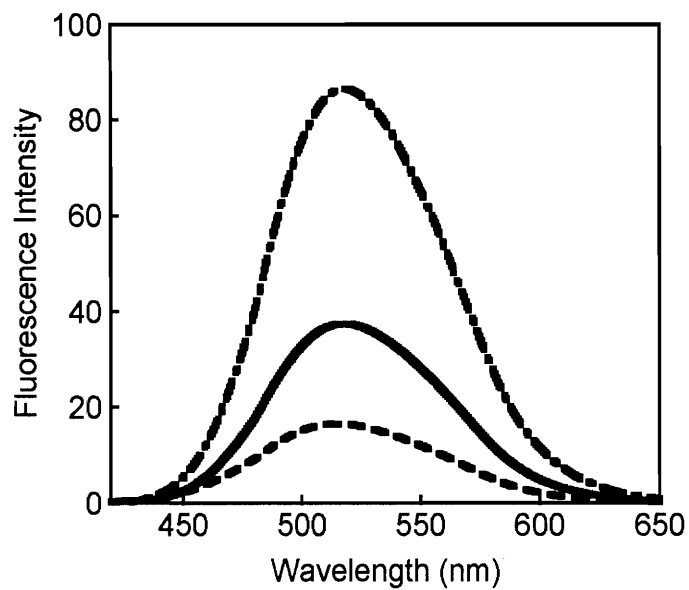


Figure 3.10. Fluorescence emission spectra in CH_3CN : **1** ($10 \mu\text{M}$, dotted line), Ds-HAMP ($20 \mu\text{M}$, dash-dotted line), and **1** ($10 \mu\text{M}$) with 100 equiv of NO at 35 min (solid line).

Chapter 4

Fluorescent Nitric Oxide Detection by Copper Complexes Bearing Anthracenyl and Dansyl Fluorophore Ligands

A portion of this chapter has appeared previously in Lim, M. H.; Lippard, S. J., *J. Am. Chem. Soc.* **2005**, *127*, 12170-12171. This work was supported by NSF grant CHE-0234951. The MIT DCIF NMR spectrometer was funded through NSF Grant CHE-9808061. I thank the Martin Family Society at MIT for fellowship funding. We thank Professor Daniel G. Nocera and Mr. Joel Rosenthal for assistance with the spectroelectrochemistry experiments of compound 6.

Introduction

The discovery of nitric oxide (NO) as a biological signaling messenger stimulated to a wide range of NO-related research activities with the ultimate aim of elucidating the precise biological functions of NO.¹⁻⁵ This goal is very challenging, however, since NO is a highly reactive free radical. A critical mission of the research is to pinpoint the location of NO formation and NO-induced events at the cellular level. Thus, an indicator to visualize NO in biological systems is desired, which can provide selective and direct NO detection with spatiotemporal resolution. The most promising approach for sensing the presence of NO is the use of fluorescence methodologies.

An early small-molecule fluorescent probe for NO detection is *o*-diaminonaphthalene (DAN, Figure 4.1), which responds to the presence of NO oxidation products (e.g. NO_2^- , N_2O_3) with an increase of the fluorescence intensity. As such, it can serve only as an indirect NO sensor.⁶ Moreover, DAN requires high-energy excitation for fluorescence imaging, which can damage cells. To improve upon the properties of DAN, several *o*-diaminofluorescein compounds (DAFs, Figure 4.1) were prepared as fluorescent NO indicators. These compounds have been used for imaging NO in biological media, but the increased fluorescence of these compounds still requires an oxidized NO species. Like DAN, DAFs are also indirect NO sensors.^{6,7}

Our approach to obtain a probe for detecting NO directly has been utilize the chemistry of transition metal complexes. Rapid interaction of the metal center with NO initiates subsequent chemistry leading to the desired sensing. We have reported several metal complexes as fluorescent NO indicators following this strategy, including fluorophore-displacement by NO from the metal center with concomitant fluorescence turn-on (Scheme 4.1a).^{6,8-13} Although this initial tactic allows us to detect NO directly based on fluorescence with metal complexes, it occurs only in organic solvents. In

aqueous environments, water molecules can replace the fluorophore ligand from the metal center, leading to fluorescence turn-on in the absence of NO. On the basis of these discoveries, we devised another strategy for NO detection, which involves the reduction of a metal center by NO. Nitric oxide reduces a paramagnetic metal center to a diamagnetic state, restoring the quenched fluorescence of a ligand fluorophore, which remains coordinated to metal (Scheme 4.1b).^{14,15}

This chemistry is exemplified by reduction of a Cu(II) dithiocarbamate complex to the Cu(I) form with NO (Scheme 4.1b).¹⁶ The Cu(II) phen or dmp complexes (phen = 1,10-phenanthroline, dmp = 2,9-dimethyl-1,10-phenanthroline) were reported similarly to react with NO in alcoholic and aqueous media to yield the corresponding Cu(I) compounds (Scheme 4.1b).¹⁷ In the present work we have utilized this chemistry to detect NO by preparing copper(II) complexes with a dansyl or an anthracenyl group as the fluorophore. These complexes can detect NO by fluorescence turn-on in both organic and pH 7.0 or 9.0 buffered aqueous solutions. The only prior example of fluorescent NO detection with a Cu(II) complex occurs in aqueous methanol by a different mechanism, reduction of Cu(II) by NO followed by dissociation of the *N*-nitrosated ligand (Scheme 4.1c).¹⁸ The Cu(II)-based NO sensors presented here broadened the scope of metal coordination chemistry for NO detection.

Experimental

Materials and Procedures

All reagents were purchased from commercial suppliers and used as received unless stated otherwise. Acetonitrile (CH₃CN), dichloromethane (CH₂Cl₂), tetrahydrofuran (THF), and toluene were purified by passage through alumina columns under an Ar atmosphere. Methanol (CH₃OH), ethyl acetate (EtOAc), ethanol

(CH₃CH₂OH), diethyl ether (Et₂O), and hexanes were used as received. Nitric oxide (NO) (Matheson 99%) was purified by the method reported previously.¹⁰ NO was transferred to the reaction solutions by a gastight syringe in the glove box. All NO reactions were performed under anaerobic conditions. Fluorescence emission spectra were recorded at 25.0 ± 0.2 °C or 37.0 ± 0.2 °C on a Hitachi F-3010 or a Photon Technology International fluorescence spectrophotometer. NMR spectra were obtained on a Varian 300 or 500 spectrometer and IR spectra were recorded on an Avatar 360 FTIR Instrument. ESI-MS analyses were performed on an Agilent 1100 series instrument.

X-ray Crystallography. Suitable crystals were mounted in Paratone N oil on the tips of glass capillaries and frozen under a -100 or -123 °C nitrogen cold stream. Data were collected on a Bruker APEX CCD X-ray diffractometer with Mo K α radiation (λ = 0.71073 Å) controlled by the SMART software package.¹⁹ The general procedures used for data collection are reported elsewhere.²⁰ Empirical absorption corrections were applied with the SADABS program.²¹ Data were processed using the SAINTPLUS and SHELXTL software packages.^{22,23} The structures were solved by direct method. All non-hydrogen atoms were refined anisotropically. Hydrogen atoms were assigned idealized positions and given a thermal parameter of 1.2 times the thermal parameter of the atom to which they were attached. The structure solutions were checked for higher symmetry with PLATON.²⁴ In the structure of **9**, one DMF and 0.5 CH₃OH solvent molecules are included. In the 0.5 CH₃OH molecule, a disordered carbon atom was refined isotropically. The highest electron density in the final difference Fourier maps for **9** was 1.215 e/Å³, in the vicinity of this disordered methanol.

Electrochemistry. Cyclic voltammograms were recorded in an MBraun glovebox under N₂ with an EG&G model 263 potentiostat. A three-electrode setup was employed,

consisting of a Ag/AgNO₃ reference electrode (0.01 M in CH₃CN with 0.5 M (Bu₄N)(PF₆), a platinum mesh auxiliary electrode, and a platinum disk working electrode. The supporting electrolyte was 0.1 M or 0.5 M (Bu₄N)(PF₆) in CH₃CN or CH₂Cl₂. Cyclic voltammograms were externally referenced to the Cp₂Fe/Cp₂Fe⁺ couple (Conversion Cp₂Fe/Cp₂Fe⁺ scale to NHE scale, Cp₂Fe/Cp₂Fe⁺ = +460 mV vs SCE ((Bu₄N)PF₆ in CH₂Cl₂), SCE = +242 mV vs NHE).^{25,26}

Spectroelectrochemistry. A three-electrode setup was used consisting of a Ag/AgCl reference electrode, a platinum mesh working electrode, and a platinum wire auxiliary electrode. The supporting electrolyte was 0.1 M (Bu₄N)PF₆ in CH₂Cl₂. The copper sample solutions (0.2 mM) were prepared in air and purged with N₂ for 20 min before electrolysis in a 1 mm UV-vis cell containing the three electrodes. Optical spectra were obtained with a Spectral Instruments 440 Series spectrophotometer with continuously flowing current from a Bioanalytical Systems (BAS) Model CV-50W potentiostat/galvanostat.

EPR Spectroscopy. X-band EPR spectra were recorded on a Bruker EMX EPR spectrometer (9.37 GHz). Temperature control was performed with an Oxford Instruments ESR900 liquid-helium cryostat and an ITC503 controller. Nitric oxide gas (1 equiv) was directly transferred by a gastight syringe into a 4 mM CH₂Cl₂/CH₃OH (1/4) solution of copper complexes in an EPR tube. The solution was then frozen at liquid N₂ and the sample measured at 50 K.

Syntheses. The ligand Ds-Hen (5-Dimethylamino-*N*-(2-aminoethyl)-1-naphthalenesulfonamide, **2**) and copper complex [Cu(Ds-en)₂] (**7**) were prepared by previously reported methods.^{27,28} The synthesis of 5-dimethylamino-*N*-(8-quinolinyl)-1-naphthalenesulfonamide (Ds-HAQ, **4**) is described elsewhere.¹²

Potassium 4-(Anthracen-9-ylmethyl)piperazine-1-dithiocarbamate (An-CH₂pipCS₂K, 1). A portion of 1-anthracen-9-ylmethyl-piperazine·2HCl²⁹ (0.056 g, 0.16 mmol) was added to an aqueous solution of KOH (0.033 g, 0.59 mmol, 4.0 mL). The produced yellow solids were collected, dried *in vacuo*, and redissolved in diethyl ether (10 mL). Upon addition of potassium hydroxide (9.0 mg, 0.16 mmol) and carbon disulfide (9.7 μ L, 0.16 mmol) to the reaction solution, a pale yellow precipitate immediately formed. The mixture was stirred overnight at room temperature. The solid was filtered, washed with Et₂O, and dried *in vacuo* (0.046 mmol, 0.12 mmol, 73%): mp = 240 – 242 °C (decomp). ¹H NMR (500 MHz, d₆-DMSO): δ (ppm) 2.46 (4H, t, *J* = 4.5), 4.24 (4H, s), 4.41 (2H, s), 7.51 (2H, t, *J* = 7.0), 7.56 (2H, t, *J* = 7.0), 8.08 (2H, *J* = 8.5), 8.50 (2H, d, *J* = 9.0), 8.57 (1H, s). ¹³C NMR (125 MHz, d₆-DMSO): δ (ppm) 213.7, 130.9, 130.9, 129.7, 128.8, 127.2, 125.8, 125.1, 125.0, 53.2, 53.0, 49.0. FTIR (KBr, cm⁻¹): 3082 (vw), 3051 (w), 3047 (vw), 2991 (w), 2923 (w), 2904 (w), 2857 (vw), 2857 (w), 2799 (w), 2766 (vw), 1624 (w), 1525 (w), 1493 (w), 1465 (m), 1454 (sh, vw), 1444 (m), 1411 (s), 1356 (w), 1338 (w), 1295 (w), 1273 (m), 1251 (m), 1213 (vs), 1182 (w), 1160 (vw), 1135 (m), 1118 (m), 1102 (w), 1026 (m), 1005 (w), 992 (m), 981 (m), 922 (s), 899 (vw), 881 (m), 866 (w), 857 (w), 836 (w), 802 (m), 774 (m), 774 (w), 756 (w), 727 (vs), 707 (w), 655 (w), 634 (w), 602 (w), 559 (w), 517 (w), 485 (w), 443 (vw), 417 (w). ESI(-)MS (*m/z*): [M-K]⁻ Calcd for C₂₀H₁₉N₂S₂, 351.1; Found, 351.5.

5-Dimethylamino-*N*-(2-pyridylmethyl)-1-naphthalenesulfonamide (Ds-HAMP, 3). A 0.55 g (5.0 mmol) portion of 2-(aminomethyl)pyridine was added to an aqueous solution of NaOH (0.20 g, 5.0 mmol, 5.0 mL). To this solution was added slowly over 15 min a THF (10 mL) solution of dansyl chloride (1.4 g, 5.0 mmol) with stirring. The resulting mixture was stirred for 4 h at room temperature and the THF solution was

removed under reduced pressure. The yellow oil thus obtained was purified by column chromatography (SiO₂, 4:3 hexanes:ethyl acetate; R_f = 0.22 by TLC), yielding a pale yellow product (1.2 g, 3.6 mmol, 73%): mp = 122 – 124 °C. ¹H NMR (300 MHz, CDCl₃): δ (ppm) 2.87 (6H, s), 4.23 (2H, d, J = 5.4), 6.27 (1H, m), 7.03 (2H, d, J = 7.5), 7.16 (1H, d, J = 7.5), 7.45 – 7.59 (3H, m), 8.24 – 8.36 (3H, m), 8.47 (1H, d, J = 8.4). ¹³C NMR (125 MHz, CDCl₃): δ (ppm) 154.9, 152.0, 149.0, 136.6, 134.7, 130.6, 130.0, 129.8, 129.8, 128.5, 123.2, 122.5, 121.9, 119.1, 115.4, 47.8, 45.6. FTIR (KBr, cm⁻¹): 3071 (br, m), 2971 (w), 2939 (w), 2860 (w), 2826 (w), 2783 (w), 2660 (vw), 1615 (vw), 1591 (m), 1575 (m), 1502 (vw), 1479 (m), 1463 (m), 1451 (m), 1443 (m), 1403 (w), 1358 (vw), 1325 (vs), 1311 (m), 1294 (w), 1256 (vw), 1228 (w), 1199 (w), 1176 (vw), 1152 (s), 1143 (s), 1105 (vw), 1094 (vw), 1074 (m), 1045 (w), 1005 (w), 976 (vw), 966 (vw), 943 (w), 927 (vw), 897 (w), 851 (m), 838 (w), 830 (w), 824 (w), 790 (s), 767 (m), 693 (w), 680 (w), 636 (s), 628 (s), 606 (m), 581 (vw), 569 (s), 537 (m), 516 (w), 499 (w), 483 (m), 444 (w), 405 (w). ESI(+)MS (m/z): [M+H]⁺ for C₁₈H₂₀N₃O₂S, 342.1; Found, 342.4.

5-Dimethylamino-{3-[4-(3-amino-propyl)-piperazin-1-yl]-propyl}-1 naphthalenesulfonamide (Ds-HAPP, 5). To a CH₂Cl₂ solution (120 mL) of 3-[4-(3-amino-propyl)-piperazin-1-yl]-propylamine (1.2 mL, 5.6 mmol) at 0 °C was added dropwise a CH₂Cl₂ solution (20 mL) of dansyl chloride (0.30 g, 1.1 mmol) over 1 h. The solution was allowed to warm slowly to room temperature as it was stirred overnight. A white solid was filtered and the filtrate was collected. A pH 2 aqueous solution (50 mL) was added to the filtrate and the aqueous layer was collected. The pH of the solution was adjusted to 11 by addition of sodium hydroxide. The solution was extracted three times with CH₂Cl₂. Removal of the CH₂Cl₂ solvent gave a viscous yellow oil (0.32 g, 0.72 mmol, 65%). ¹H NMR (300 MHz, CD₃OD): δ (ppm) 1.45 (2H, p, J = 6.9), 1.60 (2H, p, J = 7.2),

2.03 – 2.40 (12H, m), 2.61 (2H, t, $J = 6.9$), 2.84 – 2.88 (8H, m), 7.25 (1H, d, $J = 7.8$), 7.52 – 7.59 (2H, m), 8.17 (1H, dd, $J = 7.2$, $J = 1.2$), 8.31 (1H, d, $J = 8.7$), 8.53 (1H, d, $J = 8.4$). ^{13}C NMR (125 MHz, CDCl_3): δ (ppm) 153.3, 137.1, 131.3, 131.2, 131.0, 130.5, 129.3, 124.5, 120.6, 116.5. FTIR (KBr, cm^{-1}): 3435 (br, m), 3064 (vw), 2941(m), 2872 (w), 2811 (m), 2770 (m), 1612 (w), 1588 (m), 1575 (m), 1503 (w), 1474 (sh, w), 1462 (m), 1406 (w), 1392 (sh, w), 1369 (vw), 1353 (m), 1311 (s), 1269 (sh, vw), 1231 (w), 1201 (w), 1161 (sh, w), 1142 (vs), 1092 (w), 1072 (vw), 1059 (vw), 1043 (vw), 1008 (vw), 986 (vw), 971 (vw), 944 (w), 899 (vw), 836 (vw), 824 (vw), 791 (s), 740 (w), 682 (w), 623 (s), 571 (s), 499 (vw), 486 (vw), 461 (vw), 435 (vw). ESI(+)-MS (m/z): $[\text{M}+\text{H}]^+$ Calcd for $\text{C}_{22}\text{H}_{36}\text{N}_5\text{O}_2\text{S}$, 434.3; Found, 434.2.

[Cu(AnCH₂pipCS₂)₂] (6). A dark brown solid was obtained from an aqueous solution (10 mL) of **1** (30 mg, 0.077 mmol) and copper(II) nitrate (8.9 mg, 0.038 mmol). The residue was filtered, washed with water and Et₂O several times, and dried *in vacuo* (28 mg, 0.037 mmol, 97%): mp = 260 – 260 °C. X-ray quality crystals were obtained by vapor diffusion ($\text{CH}_2\text{Cl}_2/\text{Et}_2\text{O}$) at room temperature. FTIR (KBr, cm^{-1}): 3433 (br, w), 3080 (vw), 3048 (w), 2923 (w), 2900 (w), 2850 (w), 2801 (w), 2766 (w), 1622 (w), 1492 (s), 1434 (m), 1382 (vw), 1363 (w), 1336 (w), 1294 (w), 1274 (w), 1250 (vw), 1232 (vs), 1180 (vw), 1124 (w), 1093 (vw), 1019 (w), 989 (m), 946 (vw), 925 (vw), 886 (w), 864 (vw), 843 (vw), 801 (vw), 775 (vw), 730 (s), 706 (vw), 656 (vw), 635 (vw), 602 (vw), 59 (vw), 446 (vw), 430 (vw). Anal. Calcd. for $\text{CuC}_{40}\text{H}_{38}\text{S}_4\text{N}_4 \cdot 0.5\text{H}_2\text{O}$: C, 61.95; H, 5.07; N, 7.22; Found: C, 62.33; H, 5.09; N, 7.03.

[Cu(Ds-AMP)₂] (8). To a CH_3OH solution (5.0 mL) of **3** (0.11 g, 0.31 mmol) was added a 0.1 M KOH solution (3.1 mL, 0.31 mmol). The solvent was evaporated under reduced pressure. The resulting residue was dissolved in CH_3OH (10 mL) and copper acetate (32 mg, 0.16 mmol) was added. The solution was refluxed for 7 h and slowly

cooled to room temperature. The blue microcrystalline powder (97 mg, 0.13 mmol, 81%) was collected and washed with cold CH_3OH and Et_2O : mp = 213 – 215 °C. X-ray quality blue crystals were obtained by slow evaporation of CH_3CN . FTIR (KBr, cm^{-1}): 3068 (w), 2978 (w), 2933 (w), 2824 (w), 2824 (w), 2783 (w), 1608 (m), 1589 (m), 1570 (m), 1502 (w), 1474 (m), 1456 (m), 1439 (m), 1425 (m), 1408 (m), 1392 (m), 1357 (w), 1329 (w), 1281 (vs), 1271 (vs), 1229 (m), 1206 (w), 1197 (w), 1186 (w), 1136 (m), 1112 (w), 1101 (w), 1091 (w), 1073 (w), 1060 (w), 1046 (m), 1028 (w), 1005 (w), 998 (w), 970 (vw), 945 (m), 908 (m), 897 (w), 887 (w), 861 (m), 834 (w), 825 (w), 815 (w), 800 (m), 780 (w), 764 (m), 735 (w), 716 (m), 687 (w), 655 (w), 632 (s), 603 (w), 578 (s), 559 (s), 536 (w), 515 (vw), 488 (m), 467 (vw), 457 (vw), 420 (w). Anal. Calcd. for $\text{CuC}_{36}\text{H}_{36}\text{S}_2\text{O}_4\text{N}_6 \cdot 0.5\text{H}_2\text{O}$: C, 57.39; H, 4.95; N, 11.15; Found: C, 57.01; H, 4.70; N, 11.07.

[Cu(Ds-AQ)₂] (9). To a CH_3OH solution (5.0 mL) of 4^{12} (0.10 g, 0.26 mmol) was added a 0.1 M KOH solution (2.6 mL, 0.26 mmol). The solvent was evaporated under reduced pressure. The resulting residue was dissolved in CH_3OH (5.0 mL) and copper acetate (26 mg, 0.13 mmol) was added. The solution was refluxed for 6 h and slowly cooled to room temperature. A dark brown solid was collected and washed with Et_2O (0.088 g, 0.11 mmol, 83%): mp = 199 – 201 °C (decomp). X-ray quality brown crystals were obtained by vapor diffusion ($\text{DMF}/\text{Et}_2\text{O}$). FTIR (KBr, cm^{-1}): 3108 (w), 2988(w), 2940 (w), 2866 (w), 2830 (w), 2787 (w), 1610 (w), 1578 (m), 1502 (vs), 1467 (m), 1382 (s), 1355 (w), 1322 (vs), 1296 (s), 1273 (w), 1239 (w), 1228 (w), 1189 (m), 1132 (vs), 1114 (w), 1090 (w), 1072 (w), 1060 (w), 1045 (w), 957 (m), 942 (m), 870 (m), 825 (m), 787 (s), 752 (w), 685 (w), 628 (s), 585 (s), 567 (m), 544 (w), 527 (w), 494 (w), 461 (vw). Anal. Calcd. for $\text{CuC}_{42}\text{H}_{36}\text{S}_2\text{O}_4\text{N}_6 \cdot \text{H}_2\text{O}$: C, 60.45; H, 4.59; N, 10.07; Found: C, 59.99; H, 4.50; N, 9.98.

[Cu(Ds-APP)(OTf)] (10). A portion of 5 (50 mg, 0.12 mmol) was added to a CH₃OH solution (3.0 mL) of copper(II) triflate (42 mg, 0.12 mmol). The solution was stirred for 1 h and removed. The residues were dissolved in CH₂Cl₂ (5.0 mL) and a white solid was removed by filtration. Evaporation of solvent from the filtrate provided a blue solid (67 mg, 0.10 mmol, 90%): mp = 116 – 119 °C (decomp). X-ray quality blue crystals were obtained by vapor diffusion (CH₂Cl₂/Et₂O) at room temperature. FTIR (KBr, cm⁻¹): 3306 (w), 3258 (w), 2944 (w), 2873 (w), 2836 (vw), 2789 (w), 1610 (vw), 1590 (w), 1575 (w), 1500 (vw), 1461 (w), 1439 (vw), 1407 (w), 1391 (vw), 1352 (vw), 1287 (s), 1243 (s), 1225 (w), 1162 (m), 1146 (m), 1116 (w), 1090 (vw), 1070 (vw), 1062 (vw), 1029 (s), 965 (vw), 946 (vw), 928 (vw), 899 (vw), 839 (w), 792 (m), 760 (vw), 740 (vw), 683 (vw), 638 (s), 573 (m), 517 (m). Anal. Calcd. for CuC₂₃H₃₄F₃N₅O₅S₂·2CH₂Cl₂: C, 36.84; H, 4.70; N, 8.59; Found: C, 37.09; H, 4.67; N, 8.73 (¹H NMR spectrum also presented CH₂Cl₂ molecules in the material).

Results

Syntheses of Ligands.

Potassium 4-(anthracen-9-ylmethyl)piperazine-1-dithiocarbamate (AnCH₂pipCS₂ K, 1, Figure 4.2) was synthesized from the reaction of 1-anthracen-9-ylmethyl-piperazine·2HCl²⁹ and carbon disulfide in the presence of a base. Bidentate ligands bearing dansyl groups (2 – 4) were prepared by the reaction of the amines and dansyl chloride according to previously reported procedures.^{12,27} A tetradentate ligand (5) was also obtained, which contains the dansyl group as a light-emitting unit (Figure 4.2). Slow addition of the precursor amine, 3-[4-(3-amino-propyl)-piperazin-1-yl]-

propylamine, to the solution of dansyl chloride over 1 h at 0 °C afforded the desired product 5 in moderate yield without further purification.

Synthesis and Structural Characterization of Copper Complexes.

$[Cu(AnCH_2pipCS_2)_2]$ (6). The copper complex 6 was prepared from an aqueous solution of $Cu(NO_3)_2$ and 1 in the ratio of 1:2. X-ray quality brown crystals were obtained by vapor diffusion of Et_2O into a CH_2Cl_2 solution of 6. The compound crystallizes in the monoclinic space group $P2_1/c$ with $Z = 2$. Crystallographic data for 6 are summarized in Table 4.1 and the molecular structure with the atomic labeling scheme is shown in Figure 4.3. The copper atom occupies a special position requiring a center of inversion and is coordinated by the four sulfur atoms in a square planar geometry. One of the two Cu–S distances, 2.2694(13) Å, is the shortest reported for copper dithiocarbamate complexes, which fall in the range of ~2.28 Å – ~2.32 Å.^{30,31} The C–S bond lengths, 1.713(5) Å and 1.715(5) Å, lie between the values of a C–S single bond, ~1.81 Å, and a C=S double bond, ~1.69 Å.^{30,32} Similarly, the C–N bond length, 1.323(6) Å,³² has significant double bond character, indicating delocalization of the π -electrons over the S_2CN moiety. Thus, the S_2CN groups are coplanar with the CuS_4 core. Selected bond lengths and angles are listed in Table 4.2 and are consistent with those of previously reported analogous copper complexes.^{30,31}

$[Cu(Ds-AMP)_2]$ (8) and $[Cu(Ds-AQ)_2]$ (9). The copper(II) complexes 8 and 9 (Ds-AMP and Ds-AQ are the conjugate bases of 3 and 4¹²) were prepared from a methanol solution of $Cu(OAc)_2$ and the appropriate ligand in the ratio of 1:2 in the presence of a base. X-ray quality blue crystals of 8 were obtained by slowly evaporating a CH_3CN solution. Dark brown crystals of 9 were grown by vapor diffusion of Et_2O into a DMF solution. Crystallographic data for 8 and 9 are summarized in Table 4.1. The molecular

structures with the atomic labeling schemes are presented in Figure 4.3 and selected bond lengths and angles are listed in Table 4.2. The copper centers of **8** and **9** are coordinated by four nitrogen atoms from bidentate Ds-AMP or Ds-AQ ligands. In the structure of **8**, the Co–N_{amide} bonds (1.949(4) Å and 1.979(4) Å) are shorter than those of Co–N_{pyridine} (1.992(4) Å and 2.003(4) Å). Like **8**, the Co–N_{amide} bonds (1.943(3) Å and 1.944(3) Å) are shorter than those of Co–N_{quinoline} (1.993(3) Å and 2.001(3) Å) in the structure of **9**. The dihedral angles for **8** and **9**, Θ , measured between the planes of the two five-membered chelate rings, are 39.3° and 45.8°, respectively, indicating distorted tetrahedral copper coordination geometry. Comparison of the dihedral angles of **7**,²⁸ **8** and **9** ($\Theta = 3.9^\circ$, 39.3° and 45.8°) suggests that the copper complex **9** would be easier to reduce to a Cu(I) species anticipated as its NO reaction product, since it needs less reorganization than **7** and **8**. The bond lengths and angles of **8** or **9** are consistent with those of the previously reported [Cu(L)₂] compounds, where L = *N*-(2-pyridylmethyl)-toluenesulfonamide or *N*-(2-pyridylmethyl)trifluoromethylsulfonamide, and of [Cu(qnsa)₂] (qnsa = *N*-quinolin-8-yl-naphthalenesulfonamide).^{33,34}

[Cu(Ds-APP)(OTf)] (**10**). Vapor diffusion of Et₂O into a CH₂Cl₂ solution of copper(II) triflate and **5** in a ratio of 1:1 produced blue X-ray quality crystals of **10**. The molecular structure of **10** with the atomic labeling scheme is shown in Figure 4.3 and crystallographic data are summarized in Table 4.1. The copper center is pentacoordinate with four nitrogen atoms from the tetradetate Ds-APP ligand (Ds-APP is the conjugate base of **5**) and one oxygen atom from a triflate anion, arranged in an axially elongated square-pyramidal geometry. The bond lengths of Cu1–N1, Cu1–N2, Cu1–N3, and Cu1–N4 are 1.983(3), 2.071(3), 2.028(3), and 1.987(2) Å, respectively. The Cu1–O3 distance is 2.364(2) Å, which is within the range of ~2.34 Å to ~2.53 Å for Cu(II)–OTf in

the Cambridge Structural Database (CSD version 5.26). The ratio of the two basal angles ($168.26(11)^\circ$ and $159.67(11)^\circ$) in a square-pyramidal structure, τ (an index of the degree of trigonality, 0.14),³⁵ is close to 0, indicating nearly idealized geometry. The copper center lies slightly above the basal plane. The bond lengths and angles of **10** are similar to those of the previously published copper complexes $[\text{Cu}(\text{bapp})(\text{Cl})]\text{Cl}$ and $[\text{Cu}(\text{bapp})(\text{ClO}_4)] (\text{ClO}_4)$ (bapp = 1,4-bis(3-aminopropyl)piperazine).³⁶ Selected bond lengths and angles are provided in Table 4.2.

Electrochemistry of Copper Complexes.

The electrochemical behavior of **6** was studied by cyclic voltammetry in CH_2Cl_2 . The copper complex **6** undergoes both a one-electron oxidation ($\text{Cu}(\text{II})/\text{Cu}(\text{III})$) and a one-electron reduction ($\text{Cu}(\text{II})/\text{Cu}(\text{I})$) processes at a platinum electrode, which is consistent with the previously reported studies of copper dithiocarbamate complexes (Scheme 4.2).³⁷ A representative cyclic voltammogram of **6** is shown in Figure 4.4. A reversible oxidation at +0.10 V ($\Delta E = 0.083$ V in Figure 4.4b) and a quasi-reversible reduction at -0.87 V ($\Delta E = 0.55$ V in Figure 4.4c) were observed in CH_2Cl_2 (vs $\text{Cp}_2\text{Fc}/\text{Cp}_2\text{Fc}^+$).

The reduction potentials of **7**, **8** and **9** (vs Fc/Fc^+) in CH_3CN for the $\text{Cu}(\text{II})/\text{Cu}(\text{I})$ couple are of -1.5 V (irrev), -0.82 V (rev, $\Delta E = 0.13$ V) and -0.70 V (rev, $\Delta E = 0.12$ V), respectively, confirming that **9** is more easily reduced than **7** and **8** (Figure 4.5a). This trend is predicted based on the above comparison of the dihedral angles in the crystal structures of **7**, **8**, and **9**. The $\text{Cu}(\text{II})$ complex **10** showed a reduction wave ($\text{Cu}(\text{II})/\text{Cu}(\text{I})$) vs Fc/Fc^+ of -1.32 V in CH_2Cl_2 (Figure 4.5b).

Fluorescence Studies.

[Cu(*AnCH₂pipCS₂*)₂] (**6**). An initial fluorescence study of **6** indicated 3.1(±0.3)-fold quenching in CH₂Cl₂/CH₃OH (1:1) relative to the free ligand (**1**) at an excitation wavelength of 370 nm (Figure 4.6a). Administration of excess NO (g) to a solution (CH₂Cl₂:CH₃OH, 1:1) of **6** resulted in a 5.5(±0.6)-fold fluorescence increase within 60 min (Figure 4.6b).

[Cu(*Ds-en*)₂] (**7**), [Cu(*Ds-AMP*)₂] (**8**), [Cu(*Ds-AQ*)₂] (**9**), and [Cu(*Ds-APP*)(OTf)] (**10**). Coordination to Cu(II) quenched the fluorescence of the ligands in solutions of **7**, **8**, and **9**. A 31(±2)-, 23(±0.5)- or 61(±1)-fold decrease in fluorescence compared to that of the free ligands **2**, **3** or **4** was observed in CH₃OH:CH₂Cl₂ solutions of **7**, **8**, or **9** (20 μM) (Figures 4.7a, 4.7b, and 4.7c). Upon addition of 100 equiv of NO to CH₃OH solutions of **7**, **8**, and **9**, the fluorescence of the **2**, **3**, and **4** ligands was restored. The respective increases in integrated fluorescence were 6.1(±0.2)-, 8.8(±0.1)- and 3.0(±0.4)-fold, respectively within less than 3 min (Figures 4.7a, 4.7b, and 4.7c). The NO detection limit of 10 nM for **8** was obtained by fluorescence measurements of solutions treated with decreasing concentrations of NO. Compound **8** therefore has a significantly improved detection limit relative to that of our previous metal complexes, which have μM NO detection limits.^{9,10}

Additional fluorescence measurements indicated that the water-soluble Cu(II) complexes **7** and **8** are capable of NO detection at pH 9.0. A 4.3(±0.5)-fold or 4.5(±0.6)-fold decrease in the fluorescence intensity of **2** and **3**, respectively, was observed in aqueous buffered solutions (50 mM CHES, pH 9.0, 100 mM KCl) of **7** and **8** (10 μM) at 37 °C (Figures 4.8a and 4.8b). A fluorescence increase of 2.3(±0.2)-fold or

2.0(\pm 0.2)-fold was exhibited upon administration of 100 equiv of NO to the pH 9.0 buffered solutions of **7** or **8**, respectively, within 30 min (Figures 4.8a and 4.8b).

A methanol solution of **10** (20 μ M) displayed a 10(\pm 0.6)-fold quenching in fluorescence, relative to the free ligand **5** (20 μ M) (Figure 4.9a). The fluorescence was immediately increased by 2.3(\pm 0.1)-fold after addition of excess NO (Figure 4.9a). Moreover, **10** (10 μ M) showed a 2.6(\pm 0.2)-fold decrease in fluorescence in pH 7.0 buffered solution (50 mM PIPES and 100 mM KCl), compared to the ligand **5** (Figure 4.9b). Upon addition of excess NO, the fluorescence of **10** was enhanced by 1.6(\pm 0.3)-fold over 10 min (Figure 4.9b). Although the fluorescence change is not large following addition of NO to the pH 7.0 buffered solution of **10**, these observations suggest that a copper complex containing dansyl fluorophore could be designed for NO detection at a physiological pH.

NO Reactivity of Copper Anthrancenyyl Complex **6**.

To investigate further the species responsible for the fluorescence enhancement upon the reaction of **6** with NO, spectroelectrochemical, infrared, and fluorescence studies were carried out. The optical spectrum of **6** (20 μ M) with 682 equiv of added NO in CH₂Cl₂/CH₃OH (1:1) showed a decrease of the charge transfer band at $\lambda_{\text{max}} = 436$ nm ($\epsilon = 1.3 \times 10^4$ M⁻¹cm⁻¹ for **6**) (Figure 4.10a), which suggests the formation of a Cu(I) species. To help identify the NO-induced transformation, spectroelectrochemical studies were first carried out. As shown in Figure 4.4, cyclic voltammogram of **6** revealed reversible one electron oxidation (Cu(II)/Cu(III)) and quasi-reversible reduction (Cu(II)/Cu(I)). Two potentials, +0.50 V and -0.75 V, were selected to electrolytically generate Cu(III) and Cu(I) species from the Cu(II) complex **6**, which was

monitored by UV-vis spectroscopy during electrolysis. A progress of the electrolysis at +0.50 V was accompanied by a change in the optical spectrum from that of **6** to $[\text{Cu}(\text{AnCH}_2\text{pipCS}_2)_2]^+$ (**6**⁺), shifting the maximum wavelength of its charge transfer band from 436 nm to 426 nm (Figure 4.10b). In addition, the charge transfer band of **6** at $\lambda_{\text{max}} = 436$ nm was slowly abolished upon the reduction at -0.75 V (Figure 4.10c), which indicates the formation of a Cu(I) species similar to that observed in the NO reaction of **6**. These spectroelectrochemical features of **6** are similar to those of previously described copper dithiocarbamate complexes.³⁷

Based on these results, we conclude that a diamagnetic Cu(I) species forms in reaction of **6** with NO. Addition of $[\text{Cu}(\text{CH}_3\text{CN})_4](\text{BF}_4)$ to ligand **1** in a ratio of 1:2 produces a fluorescence intensity the same as that in the NO-induced fluorescence increase of **6**, as shown in Figure 4.11. This result lends further support to be proposed mechanism for the fluorescence enhancement that accompanies the reaction of **6** with NO. The Cu(I) species generated by reacting NO with **6** in $\text{CH}_3\text{OH}/\text{CH}_2\text{Cl}_2$ may exist in two different forms in solution: a copper nitrosyl adduct ($\text{Cu}(\text{II})\text{-NO} \leftrightarrow \text{Cu}(\text{I})\text{-NO}^+$) or a Cu(I) compound without a bound nitrosyl. We ruled out the formation of a copper nitrosyl compound in the NO reaction of **6** ($\text{CH}_3\text{OH}/\text{CH}_2\text{Cl}_2$) by the absence of any IR band (KBr) in the 1600 - 1900 cm^{-1} region.^{16,38} Thus, introduction of NO reduces the copper center, forming NO^+ , which can react with solvent molecules CH_3OH or with the ligand **1**, possibly at the sulfur atoms of the dithiocarbamate moiety. Such a nitrosothiol (RS-NO) or thiol (RS-H) group, however, is also not consistent with the IR spectrum of the product ($\nu_{\text{SN-O}} = 1400 - 1600 \text{ cm}^{-1}$; $\nu_{\text{S-H}} = 2500 - 2600$),^{39,40} suggesting either that it is not generated during the reaction or that it might overlap with other IR bands of the copper complex. Nitric oxide in the absence of CH_3OH did not enhance the fluorescence

intensity of **6** in the same manner as that in the presence of the alcohol, which suggests that the NO^+ cation, generated in the reaction of NO with **6**, may react with solvent CH_3OH molecules, forming RONO species (Figure 4.12). Therefore, the reaction of **6** and NO would appear to occur by reduction of Cu(II) to Cu(I), forming NO^+ in solution, as shown in Scheme 4.3. This conclusion is supported by previously reported nitric oxide studies of the Cu(II) complexes $[\text{Cu}(\text{phen})_2]^{2+}$ and $[\text{Cu}(\text{dmp})_2]^{2+}$.¹⁷

NO Reactivity of Copper Dansyl Complex **8**.

An anticipated mechanism of the fluorescence enhancement of **7**, **8**, **9**, and **10** by NO (Scheme 4.3) is that nitric oxide induces the formation of a diamagnetic Cu(I) species with partial dissociation of the sulfonamide functionality due to protonation by H^+ formed during the reaction. To investigate this possibility the reaction of **8** with NO was examined in depth. A significant fluorescence increase of **8** occurs in the presence of NO and protonation of its sulfonamide functionality would be readily observable by IR spectroscopy without overlap with another N–H functionality on the ligand (Figure 4.2).

The formation of a Cu(I) species in the reaction of **8** with one equiv of NO in 4:1 $\text{CH}_3\text{OH}:\text{CH}_2\text{Cl}_2$ was indicated by the observation of a ~15% decrease in the initial Cu(II) EPR signal intensity at 50 K (Figure 4.13). Since only a ~40% reduction in fluorescence was observed upon addition of the Cu(I) complex $[\text{Cu}(\text{CH}_3\text{CN})_4](\text{BF}_4)$ to **3** in the presence of a base ($\text{N}(\text{Et})_3$) in 4:1 $\text{CH}_3\text{OH}:\text{CH}_2\text{Cl}_2$ (Figure 4.14), the Cu(I) formed in the reaction with NO would restore some fluorescence of ligand **3**. Reduction of Cu(II) therefore cannot be completely responsible for the fluorescence rise in the reaction of **8** with NO, however.

As with the Cu(II) complex **6**, the NO-triggered fluorescence enhancement does not occur in a pure CH₂Cl₂ solution of the copper complex **8** (Figure 4.15), which suggests that a protic solvent such as methanol or water is required (Scheme 4.3). In addition, there was no IR (KBr) signal in the 1600 – 1900 cm⁻¹ region that could be ascribed a copper nitrosyl functionality.^{16,38} Upon reduction of Cu(II) to Cu(I) by NO in the reaction of **8**, one equiv of NO⁺ and H⁺ appear to form. Both the NO⁺ and H⁺ cations can react with a sulfonamide functionality, causing its dissociation from the copper center with a concomitant turn-on emission. The infrared spectrum of the reaction product of NO with **8** in 4:1 CH₃OH:CH₂Cl₂ following solvent removal did not reveal an IR band corresponding to $\nu_{\text{NN-O}}$ ⁴¹ but a band at 3083 cm⁻¹ (in KBr) appeared (Figure 4.16). We assign this feature to $\nu_{\text{N-H}}$ arising from the protonation of ligand at the sulfonamide functionality. The ¹H NMR spectrum of the reaction solution of **8** and NO did not reveal complete dissociation of the protonated ligand **3** from the copper center (Figure 4.17), however. Thus, the protonated sulfonamide group, generated from the NO reaction of **8**, might be partially bound to, or dangling from, the coordination sphere, causing an increase in fluorescence intensity.

The Cu(II) complex **8** was also allowed to react with an NO⁺ source, NOBF₄. Upon addition of 1 equiv of NO⁺ to a CH₃OH/CH₂Cl₂ solution of **8**, the fluorescence increased by half that obtained in the NO-triggered emission turn-on (Figure 4.18). A band at 3083 cm⁻¹ (in KBr), arising from $\nu_{\text{N-H}}$ was also observed in the reaction of **8** with NO⁺, but a feature due to $\nu_{\text{NN-O}}$ of a sulfonamide functionality or ν_{NO} of a copper nitrosyl species was not observed (Figure 4.16). These results are consistent with NO⁺ reacting with methanol to form CH₃ONO and H⁺. The latter can protonate the sulfonamide

functionality with partial release from the copper center, providing fluorescence turn-on.

Discussion

To achieve the direct NO detection based on fluorescence we prepared copper(II)-based sensors. Copper anthracenyl and dansyl complexes examined in the present work display a significant fluorescence turn-on in the presence of NO, which clearly suggests that these Cu(II)-based probes are capable of its direct detection. Only the Cu(II) complexes 7, 8, and 10 were tested for fluorescent NO response in aqueous media due to the poor solubility of 6 and 9. Compounds 7 and 8 could detect NO in pH 9.0 buffered solutions. At pH 7.0, ligands 2 and 3 bound to the Cu(II) center become protonated at the sulfonamide functionality and as a result there is no fluorescence quenching in 7 (10 μ M) or 8 (10 μ M) under these conditions.^{27,28} They cannot, therefore, be used to sense NO at a physiologically relevant pH. To improve the affinity of the fluorophore ligands for the Cu(II) center, additional N-donor atoms were introduced. As anticipated, the Cu(II) complex 10 of the tetradentate ligand 5 exhibits quenched fluorescence in both organic and pH 7.0 buffered solutions that is resorted when NO is introduced. Although only a 1.6-fold fluorescence enhancement of 10 occurs upon treatment of NO, this observation demonstrates the potential utility of metal-based sensors for NO in biological media and contributed significantly to our development of a better nitric oxide sensor (see chapter 5).

Nitric oxide detection occurs by the Cu(II) reduction in both the copper anthracenyl and dansyl systems. Spectroscopic studies revealed that NO reduces Cu(II), forming NO⁺. The resultant Cu(I) species is responsible for the fluorescence increase in the NO reaction. Free ligands such as 1 and 3 in the presence of [Cu(CH₃CN)₄](BF₄) are

fluorescent, compared to their properties with Cu(II), as shown in Figs. 4.11 and 4.14. Although, we were unable to characterize the Cu(I) species by X-ray structural analyses, infrared studies showed no formation of copper nitrosyl complexes during the NO reactions. We can therefore rule out Cu–NO compounds as the species responsible for the fluorescence turn-on in the present work. A protic solvent is required for the NO-induced fluorescence increase, suggesting that the nitrosonium ion formed during the reaction reacts with the solvent molecules, CH₃OH or H₂O, driving the formation of fluorescent species and the final Cu(I) compound (Scheme 4.4),¹⁷ Thus, introduction of NO may cause fluorescence enhancement of the copper complexes via reduction followed by the formation of NO⁺, which in turn reacts with solvent molecules such as methanol and water.

Summary

Five copper(II) complexes (6 – 10) were synthesized and characterized as fluorescent nitric oxide sensors. Copper(II)-induced fluorescence quenching was observed in all five compounds, relative to that of the free ligands. A significant turn-on emission was observed upon addition of NO (g) to an organic or aqueous solution of all the Cu(II) complexes. Interestingly, 7, 8, and 10 exhibited a fluorescence increase in a pH 7.0 or 9.0 buffered aqueous solution upon treatment with NO. Mechanistic studies indicate that the fluorescence enhancement is basically caused by NO-triggered copper(II) reduction and generation of a diamagnetic Cu(I) species. This work demonstrates that Cu(II) complexes can function as a fluorescence-based turn-on NO sensors in both organic and aqueous environments. This discovery forms the foundation for developing metal-based probes for NO detection in biological systems.

References

- (1) Furchgott, R. F., *Angew. Chem. Int. Ed.* **1999**, *38*, 1870-1880.
- (2) Ignarro, L. J., *Angew. Chem. Int. Ed.* **1999**, *38*, 1882-1892.
- (3) Murad, F., *Angew. Chem. Int. Ed.* **1999**, *38*, 1856-1868.
- (4) Bon, C. L. M.; Garthwaite, J., *J. Neurosci.* **2003**, *23*, 1941-1948.
- (5) Pepicelli, O.; Raiteri, M.; Fedele, E., *Neurochem. Int.* **2004**, *45*, 787-797.
- (6) Hilderbrand, S. A.; Lim, M. H.; Lippard, S. J., *In Topics in Fluorescence Spectroscopy*, Geddes, C. D.; Lakowicz, J. R., Eds. Springer: 2005; pp 163-188 and references cited therein.
- (7) Nagano, T.; Yoshimura, T., *Chem. Rev.* **2002**, *102*, 1235-1270 and references cited therein.
- (8) Franz, K. J.; Singh, N.; Lippard, S. J., *Angew. Chem. Int. Ed.* **2000**, *39*, 2120-2122.
- (9) Franz, K. J.; Singh, N.; Spingler, B.; Lippard, S. J., *Inorg. Chem.* **2000**, *39*, 4081-4092.
- (10) Hilderbrand, S. A.; Lim, M. H.; Lippard, S. J., *J. Am. Chem. Soc.* **2004**, *126*, 4972-4978.
- (11) Lim, M. H.; Lippard, S. J., *Inorg. Chem.* **2004**, *43*, 6366-6370.
- (12) Lim, M. H.; Kuang, C.; Lippard, S. J., *ChemBioChem* **2006**, in press.
- (13) Hilderbrand, S. A.; Lippard, S. J., *Inorg. Chem.* **2004**, *43*, 5294-5301.
- (14) Lim, M. H.; Lippard, S. J., *J. Am. Chem. Soc.* **2005**, *127*, 12170-12171.
- (15) Smith, R. C.; Tennyson, A. G.; Lim, M. H.; Lippard, S. J., *Org. Lett.* **2005**, *7*, 3573-3575.
- (16) Díaz, A.; Ortiz, M.; Sánchez, I.; Cao, R.; Mederos, A.; Sanchiz, J.; Brito, F., *J. Inorg. Biochem.* **2003**, *95*, 283-290.
- (17) Tran, D.; Skelton, B. W.; White, A. H.; Laverman, L. E.; Ford, P. C., *Inorg. Chem.* **1998**, *37*, 2505-2511.

- (18) Tsuge, K.; DeRosa, F.; Lim, M. D.; Ford, P. C., *J. Am. Chem. Soc.* **2004**, *126*, 6564-6565.
- (19) *SMART: Software for the CCD Detector System*, version 5.626; Bruker AXS: Madison, WI, 2000.
- (20) Kuzelka, J.; Mukhopadhyay, S.; Spingler, B.; Lippard, S. J., *Inorg. Chem.* **2004**, *43*, 1751-1761.
- (21) Sheldrick, G. M. *SADABS: Area-Detector Absorption Correction*, University of Göttingen: Göttingen, Germany, 1996.
- (22) *SAINTPPLUS: Software for the CCD Detector System*, version 5.01; Bruker AXS: Madison, WI, 1998.
- (23) *SHELXTL: Program Library for Structure Solution and Molecular Graphics*, version 6.1; Bruker AXS: Madison, WI, 2001.
- (24) Spek, A. L. *PLATON, A Multipurpose Crystallographic Tool*, Utrecht University: Utrecht, The Netherlands, 2000.
- (25) Connelly, N. G.; Geiger, W. E., *Chem. Rev.* **1996**, *96*, 877-910.
- (26) Bard, A. J.; Faulkner, L. R., *Electrochemical Methods Fundamentals and Applications*. John Wiley & Sons: New York, 1980.
- (27) Prodi, L.; Bolletta, F.; Montalti, M.; Zaccheroni, N., *Eur. J. Inorg. Chem.* **1999**, 455-460.
- (28) Prodi, L.; Montalti, M.; Zaccheroni, N.; Dallavalle, F.; Folesani, G.; Lanfranchi, M.; Corradini, R.; Pagliari, S.; Marchelli, R., *Helv. Chim. Acta* **2001**, *84*, 690-706.
- (29) Akkaya, E. U.; Huston, M. E.; Czarnik, A. W., *J. Am. Chem. Soc.* **1990**, *112*, 3590-3593.
- (30) Mederos, A.; Cachapa, A.; Hernandez-Molina, R.; Teresa Armas, M.; Gili, P.; Sokolov, M.; Gonzalez-Platas, J.; Brito, F., *Inorg. Chem. Commun.* **2003**, *6*, 498-502.

- (31) Jian, F.; Wang, Z.; Bai, Z.; You, X.; Fun, H.-K.; Chinnakali, K.; Razak, I. A., *Polyhedron* **1999**, *18*, 3401-3406.
- (32) Greenwood, N. N.; Earnshaw, A., *Chemistry of the Elements*. Elsevier: 1997.
- (33) Congreve, A.; Katakya, R.; Knell, M.; Parker, D.; Puschmann, H.; Senanayake, K.; Wylie, L., *New J. Chem.* **2003**, *27*, 98-106.
- (34) Macías, B.; Villa, M. V.; García, I.; Castiñeiras, A.; Borrás, J.; Cejudo-Marin, R., *Inorg. Chim. Acta* **2003**, *342*, 241-246.
- (35) Addison, A. W.; Rao, T. N.; Reedijk, J.; van Rijn, J.; Verschoor, G. C., *J. Chem. Soc., Dalton Trans.* **1984**, 1349-1355.
- (36) Kwak, C.-H.; Jee, J.-E.; Pyo, M.; Kim, J.; van Eldik, R., *Inorg. Chim. Acta* **2004**, *357*, 2643-2649.
- (37) Hendrickson, A. R.; Ho, R. K. Y.; Martin, R. L., *Inorg. Chem.* **1974**, *13*, 1279-1281.
- (38) Park, S.-K.; Kurshev, V.; Luan, Z.; W, L. C.; Kevan, L., *Microporous Mesoporous Mater.* **2000**, *38*, 255-266.
- (39) Williams, D. L. H., *Acc. Chem. Res.* **1999**, *32*, 869-876.
- (40) Pavia, D. L.; Lampman, G. M.; Kriz, G. S., *Introduction to Spectroscopy*. 2 ed.; Saunders College: 1996.
- (41) Lee, J.; Chen, L.; West, A. H.; Richter-Addo, G. B., *Chem. Rev.* **2002**, *102*, 1019-1065.

Table 4.1. Summary of X-ray Crystallographic Data

	6	8	9-DMF·0.5CH ₃ OH	10
formula	C ₄₀ H ₃₈ CuN ₄ S ₄	C ₃₆ H ₃₆ CoN ₆ O ₄ S ₂	C _{45.5} H ₄₄ CuN ₇ O _{5.5} S ₂	C ₂₃ H ₃₄ CuF ₃ N ₅ O ₅ S ₂
formula weight	766.52	744.37	904.54	645.24
space group	P2 ₁ /c	P2 ₁ /c	P2 ₁ /n	Pī
a, Å	21.418(4)	7.6658(18)	13.851(7)	8.272(5)
b, Å	8.5585(17)	16.540(4)	23.123(12)	12.900(7)
c, Å	10.154(2)	26.737(6)	13.958(7)	13.942(8)
α, deg	-	-	-	84.277(10)
β, deg	102.08(3)	91.558(5)	100.181(8)	84.374(9)
γ, deg	-	-	-	71.511(9)
V, Å ³	1820.1(6)	3388.9(14)	4400(4)	1400.4(14)
Z	2	4	4	2
ρ _{calc} g/cm ³	1.399	1.459	1.367	1.530
crystal size (mm ³)	0.10 x 0.05 x 0.03	0.10 x 0.05 x 0.03	0.20 x 0.08 x 0.04	0.15 x 0.10 x 0.08
T, °C	-100	-100	-100	-123
μ(Mo Kα), mm ⁻¹	0.865	0.818	0.646	0.992
θ limits, deg	1.94 – 25.50	1.45 – 25.50	1.76 – 25.03	1.47 – 25.50
total no. of data	13611	25691	38868	10731
no. of unique data	3395	6302	7764	5150
no. of params	223	446	569	386
GOF ^a	1.147	1.126	1.098	1.080
R ^b	0.0738	0.0730	0.0568	0.0434
wR ^{2c}	0.1324	0.1350	0.1462	0.1029
max, min peaks, e/Å ³	0.469, -0.494	0.460, -0.547	1.215, -0.537	0.621, -0.300

^a GOF (Goodness of fit on F²) = {Σ[w(F_o²-F_c²)²]/(m-n)}^{1/2} (m = number of reflections, n = number of parameters refined)

^b R = Σ||F_o|-|F_c||/Σ|F_o|

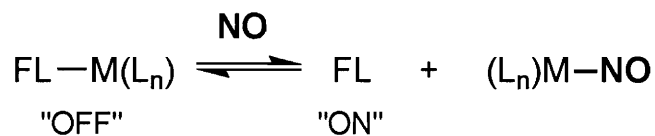
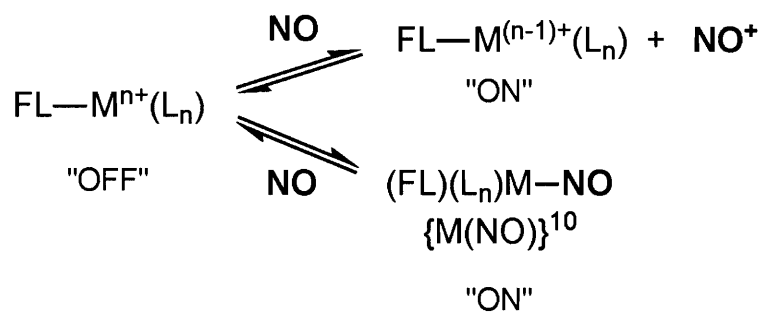
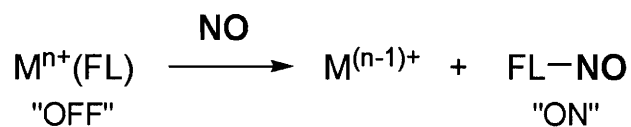
^c wR² = {w(F_o²-F_c²)²/Σ[w(F_o²)²]}^{1/2}

Table 4.2. Selected Bond Distances (Å) and Angles (deg)^a

6			
Cu1-S1	2.2694(13)	S1-Cu1-S2	77.68(5)
Cu1-S2	2.3008(14)	S1A-Cu1-S2	102.32(5)
S1-C1	1.713(5)	C1-S1-Cu1	84.90(16)
S2-C1	1.715(5)	C1-S2-Cu1	83.88(16)
N1-C1	1.323(6)	N1-C1-S1	123.0(4)
S1-Cu1-S1A	180.0(6)	N1-C1-S2	123.5(4)
		S1-C1-S2	113.4(3)
8			
Cu1-N1	1.992(4)	N1-Cu1-N4	150.38(17)
Cu1-N2	1.979(4)	N1-Cu1-N5	101.78(17)
Cu1-N4	2.003(4)	N2-Cu1-N4	100.92(18)
Cu1-N5	1.949(4)	N2-Cu1-N5	162.10(17)
N1-Cu1-N2	83.91(17)	N4-Cu1-N5	82.61(17)
		Θ ^b	39.3
9·DMF·0.5CH ₃ OH			
Cu1-N1	1.993(3)	N1-Cu1-N4	146.48(13)
Cu1-N2	1.943(3)	N1-Cu1-N5	103.75(13)
Cu1-N4	2.001(3)	N2-Cu1-N4	102.16(13)
Cu1-N5	1.944(3)	N2-Cu1-N5	160.34(13)
N1-Cu1-N2	82.78(13)	N4-Cu1-N5	82.77(13)
		Θ ^b	45.8
10			
Cu1-N1	1.983(3)	N1-Cu1-N4	98.39(11)
Cu1-N2	2.071(3)	N2-Cu1-N3	73.20(11)
Cu1-N3	2.028(3)	N2-Cu1-N4	159.67(11)
Cu1-N4	1.987(2)	N3-Cu1-N4	90.66(11)
Cu1-O3	2.364(2)	O3-Cu1-N1	92.93(10)
N1-Cu1-N2	96.27(10)	O3-Cu1-N2	94.38(10)
N1-Cu1-N3	168.28(11)	O3-Cu1-N3	93.06(9)
		O3-Cu1-N4	98.84(10)

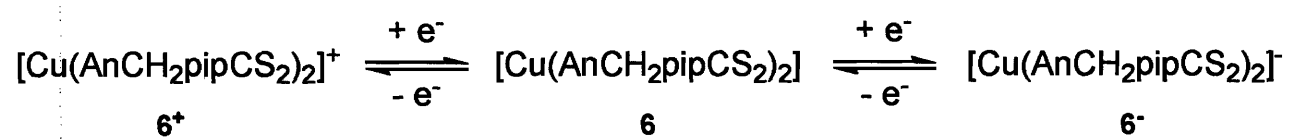
^a Numbers in parentheses are estimated standard deviations of the last significant figures. Atoms are labeled as indicated in Figure 4.3.

^b The angle Θ is the dihedral angle between the planes of the two five-membered chelate rings.

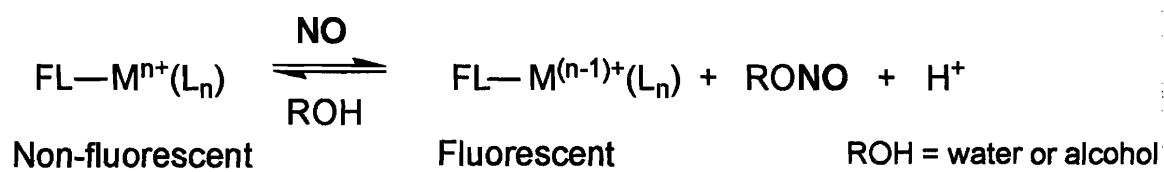
(a) Fluorophore Displacement**(b) Metal Reduction****(c) Metal Reduction and Ligand Nitrosation**

FL = Fluorophore ligand, M = Metal, L = Ligand

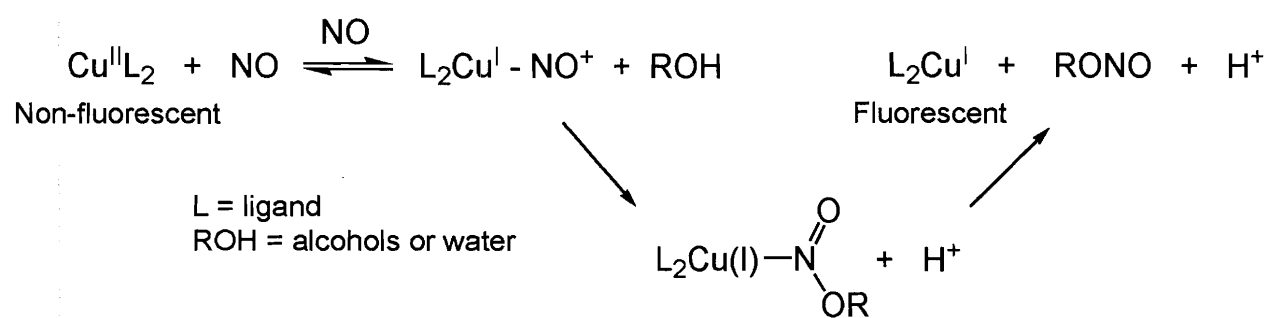
Scheme 4.1. Strategies of Nitric Oxide Detection Using Transition Metal Complexes.



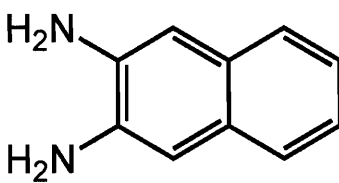
Scheme 4.2. One-Electron Oxidation/Reduction of **6**.



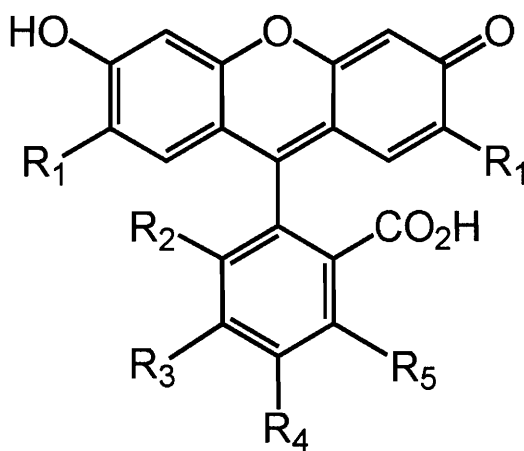
Scheme 4.3. NO Reactivity of Cu(II) Complexes.



Scheme 4.4. Proposed Reaction Pathways of Cu(II) Complexes with NO.



o-diaminonaphthalene, **DAN**



$\text{R}_1 = \text{H}, \text{Cl}$
 $\text{R}_2 = \text{H}, \text{NH}_2$
 $\text{R}_3 = \text{H}, \text{NH}_2$
 $\text{R}_4 = \text{H}, \text{NH}_2$
 $\text{R}_5 = \text{H}, \text{NH}_2$

o-diaminofluoresceins, **DAFs**

Figure 4.1. Schematic drawings of DAN and DAFs.

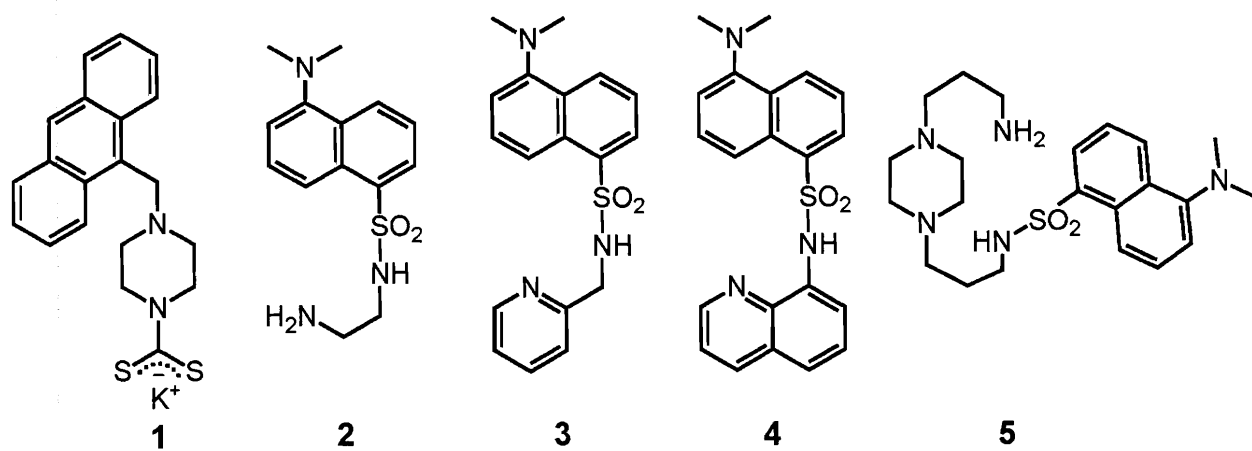
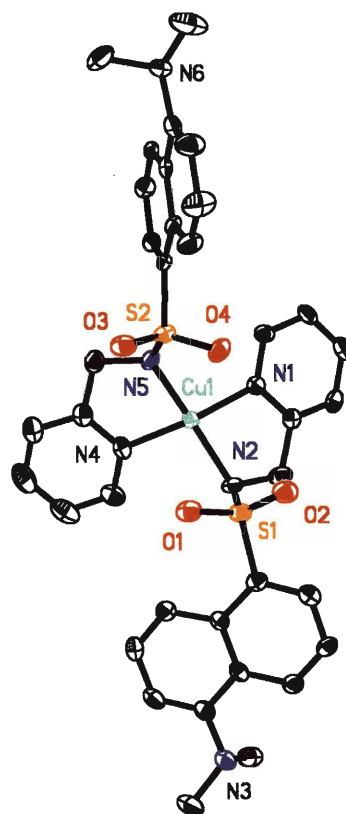
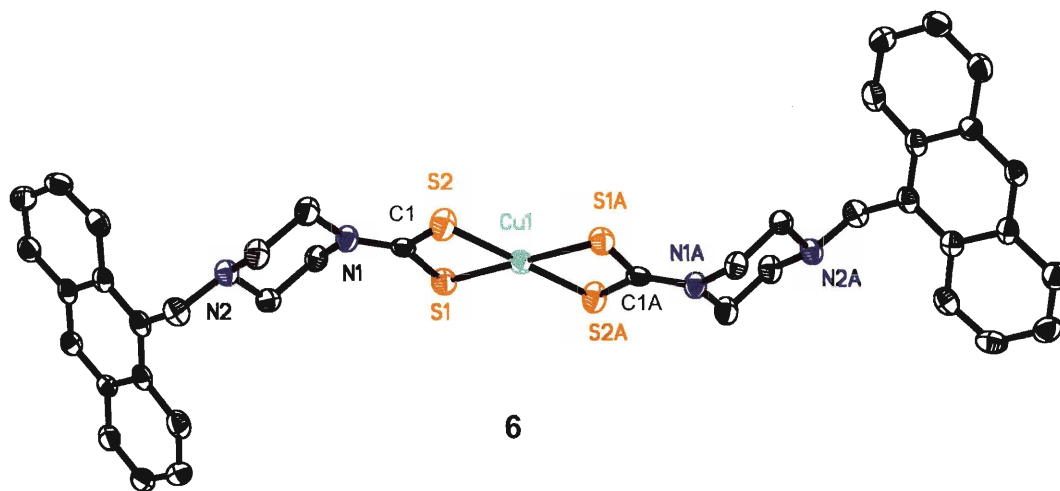
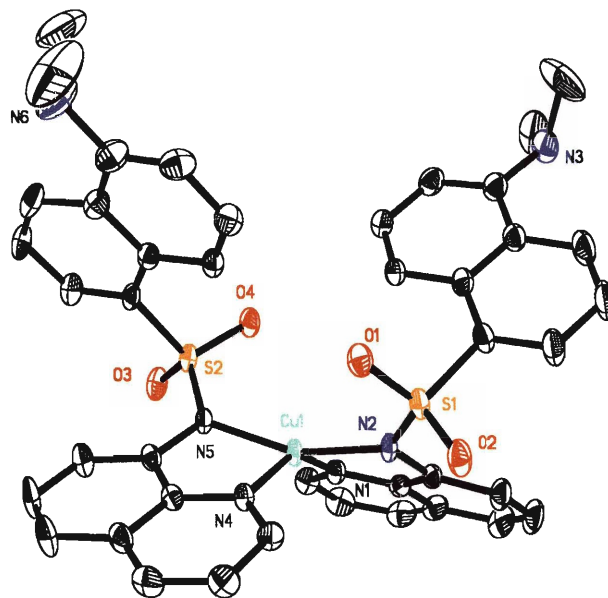
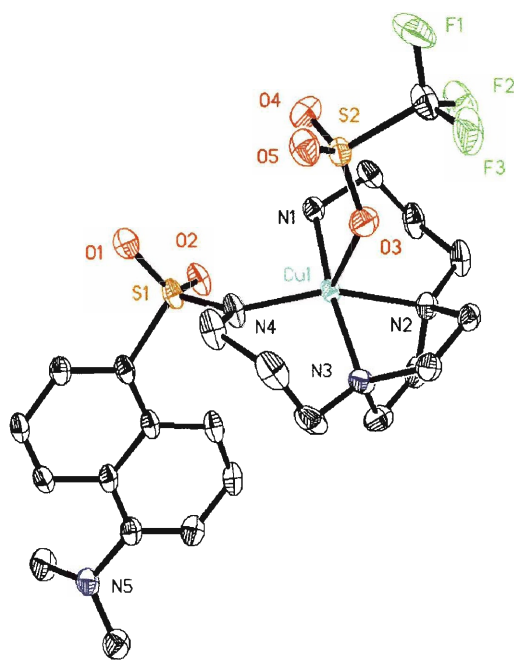


Figure 4.2. Schematic drawings of AnCH₂pipCS₂K (1), Ds-HAQ (2), Ds-HAMP (3), Ds-Hen (4), and Ds-HAPP (5).





9



10

Figure 4.3. ORTEP diagrams of 6, 8, 9, and 10 showing 50% probability thermal ellipsoids.

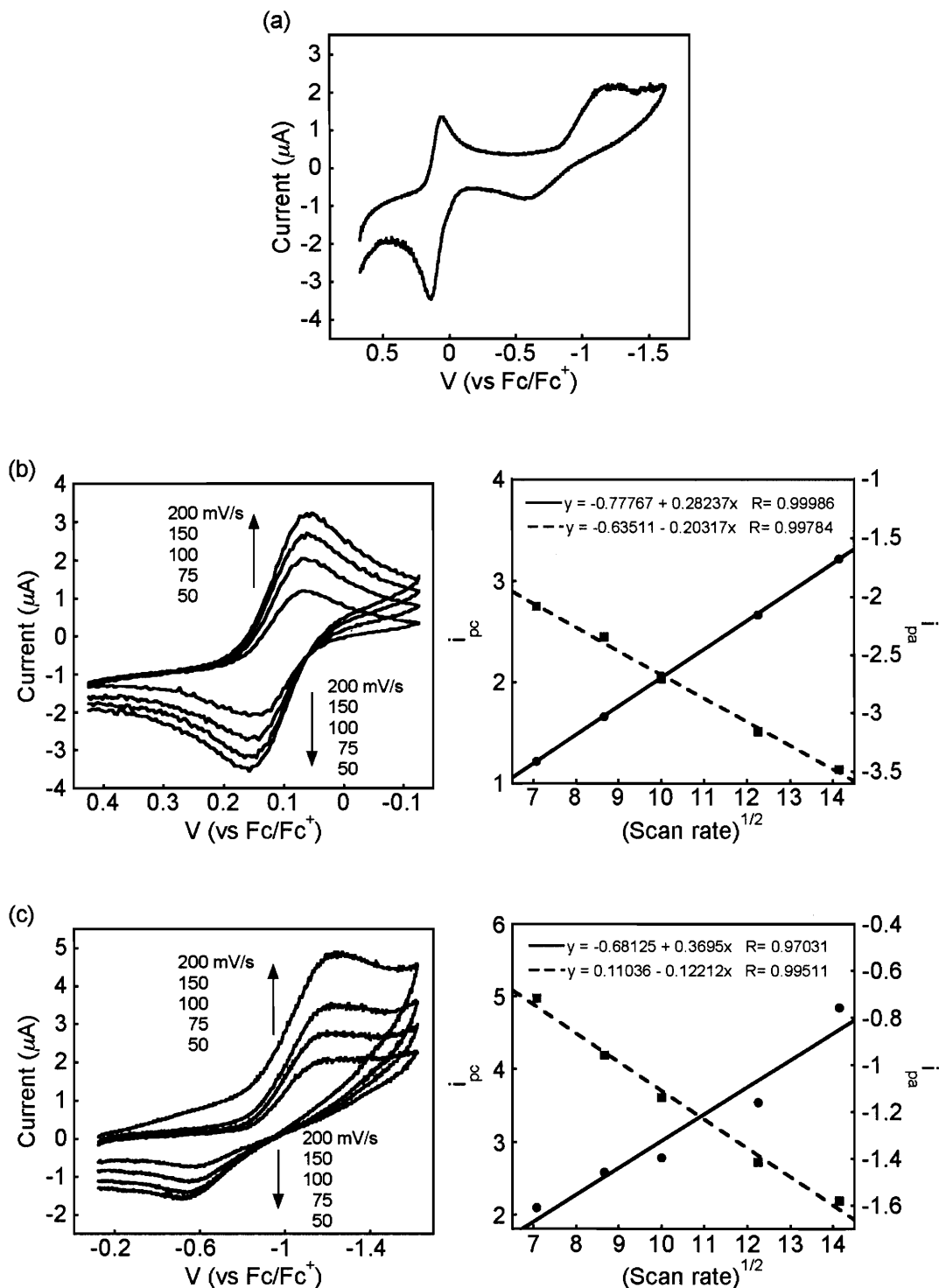
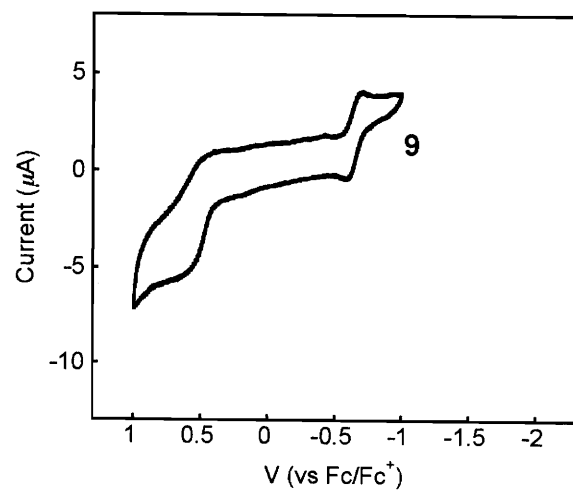
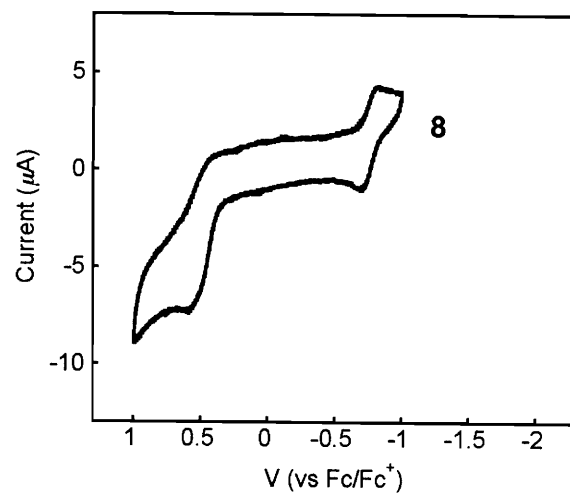
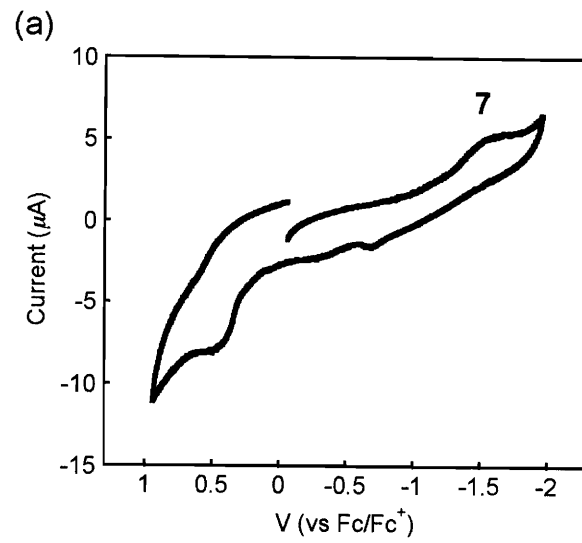


Figure 4.4. Cyclic voltammogram of 6 in CH_2Cl_2 (1 mM) with 0.5 M $(\text{Bu}_4\text{N})(\text{PF}_6)$ as supporting electrolyte and a scan rate of 50 mV/s (a, +1.0 V to -1.5 V) and variable scan rates (b (left), 0.0 V to -1.5 V and c (left) +0.55 V to 0.0 V). The right panels of b and c plot current as a function of $(\text{scan rate})^{1/2}$.



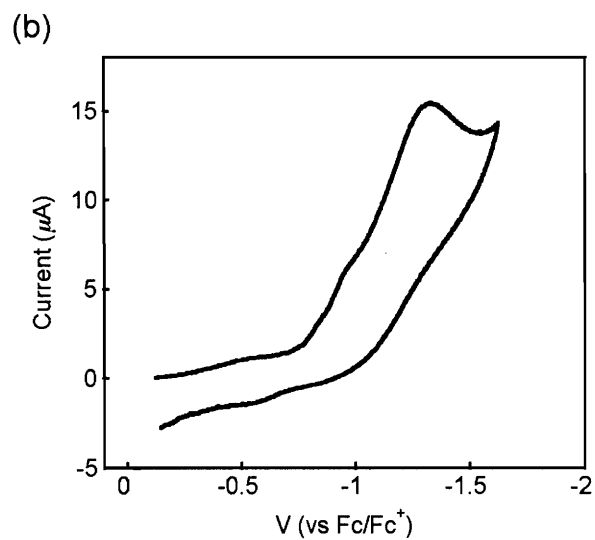


Figure 4.5. Cyclic voltammograms of (a) 7, 8, and 9 in CH_3CN (2 mM) and (b) 10 in CH_2Cl_2 (4 mM) with 0.5 M $(\text{Bu}_4\text{N})(\text{PF}_6)$ as supporting electrolyte with a scan rate of 50 mV/s.

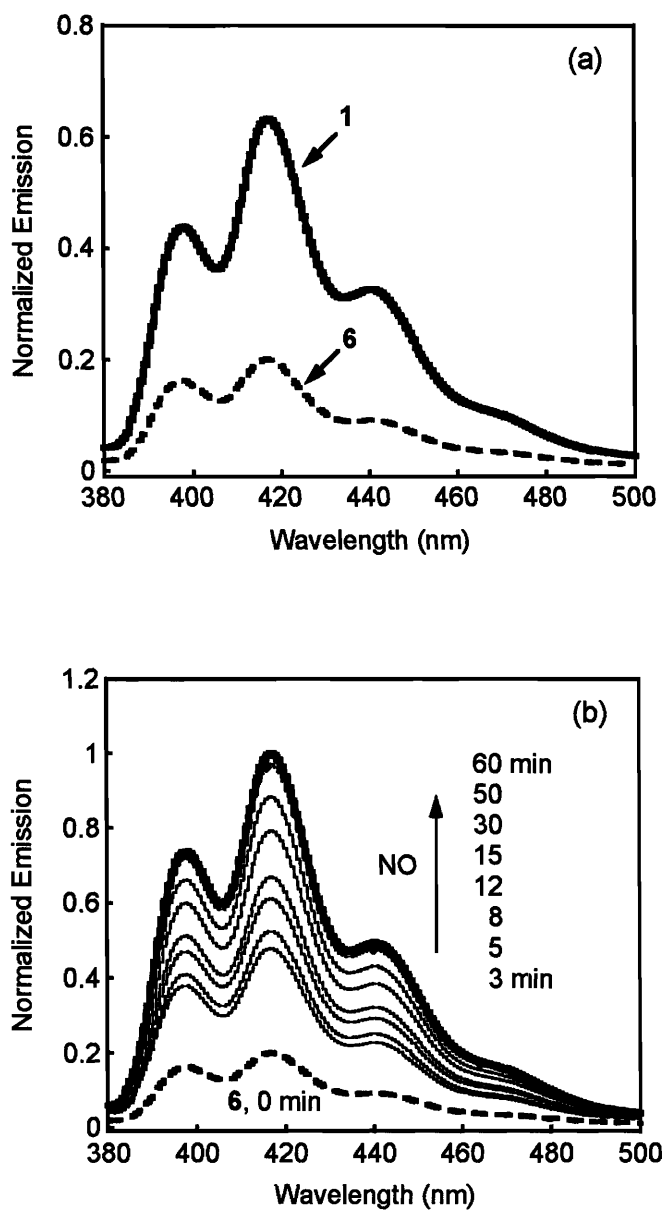


Figure 4.6. (a) Fluorescence emission spectra of 1 ($20 \mu\text{M}$, solid line) and 6 ($20 \mu\text{M}$, dashed line) in $\text{CH}_3\text{OH}/\text{CH}_2\text{Cl}_2$ (1:1) ($\lambda_{\text{ex}} = 370 \text{ nm}$). (b) Fluorescence response of 6 (dashed line, 0 min) upon addition of 682 equiv of NO (g) (solid lines) at 3, 5, 8, 12, 15, 30, 50, and 60 min.

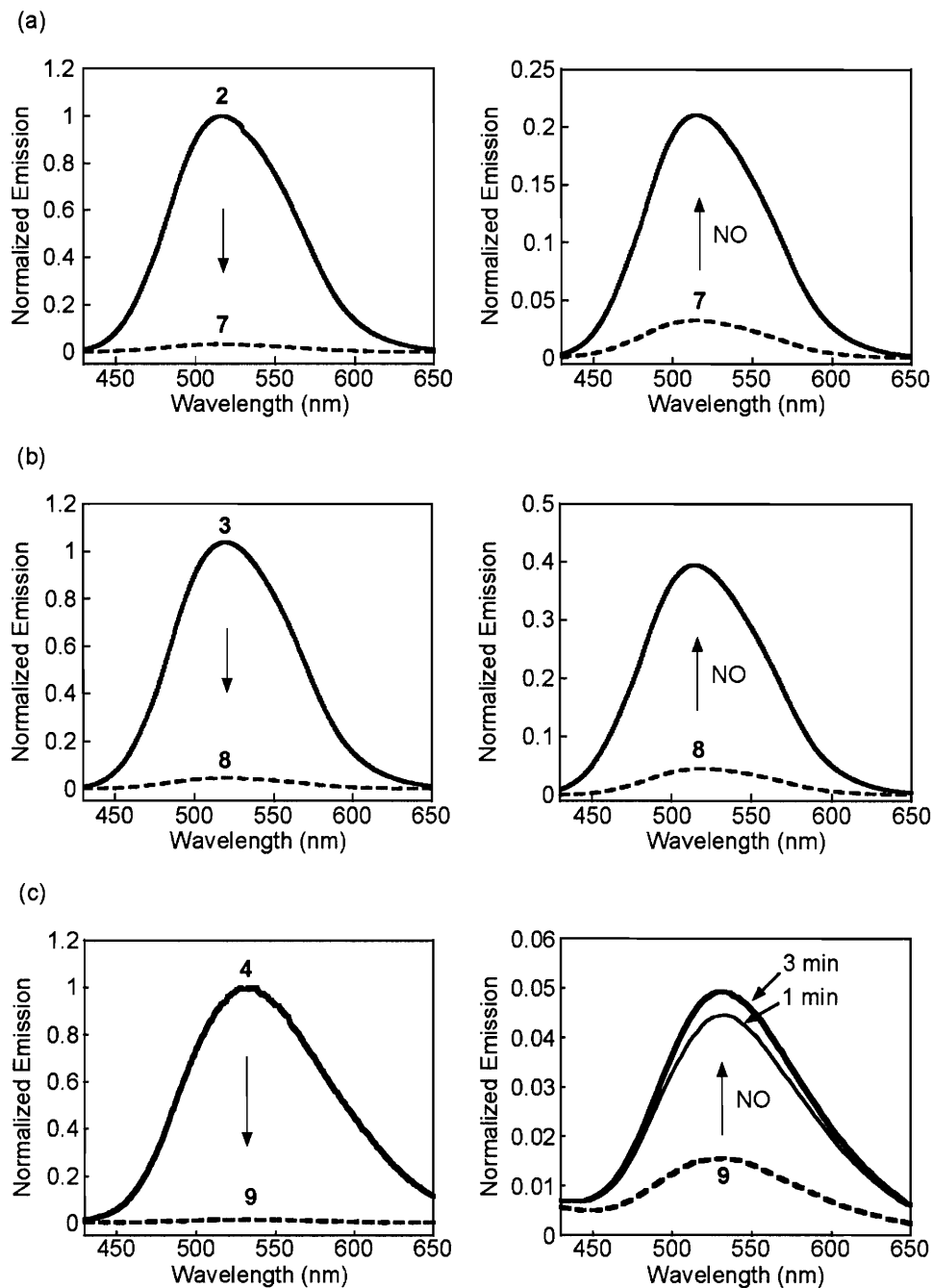


Figure 4.7. Left: emission spectra of 2 (a), 3 (b), and 4 (c) ($40 \mu\text{M}$, solid line) and 7 (a), 8 (b), and 9 (c) ($20 \mu\text{M}$, dashed line) in $\text{CH}_3\text{OH}/\text{CH}_2\text{Cl}_2$ (4:1) at 25°C . Right: emission spectra of 7 (a) and 8 (b) ($20 \mu\text{M}$, dashed line) upon immediate addition of 100 equiv of NO (g) (solid lines). (c) Fluorescence response of 9 ($20 \mu\text{M}$, dashed line) to 100 equiv of NO (g) (solid lines) at 1 and 3 min at 25°C (right). Excitation wavelength is at 342 nm.

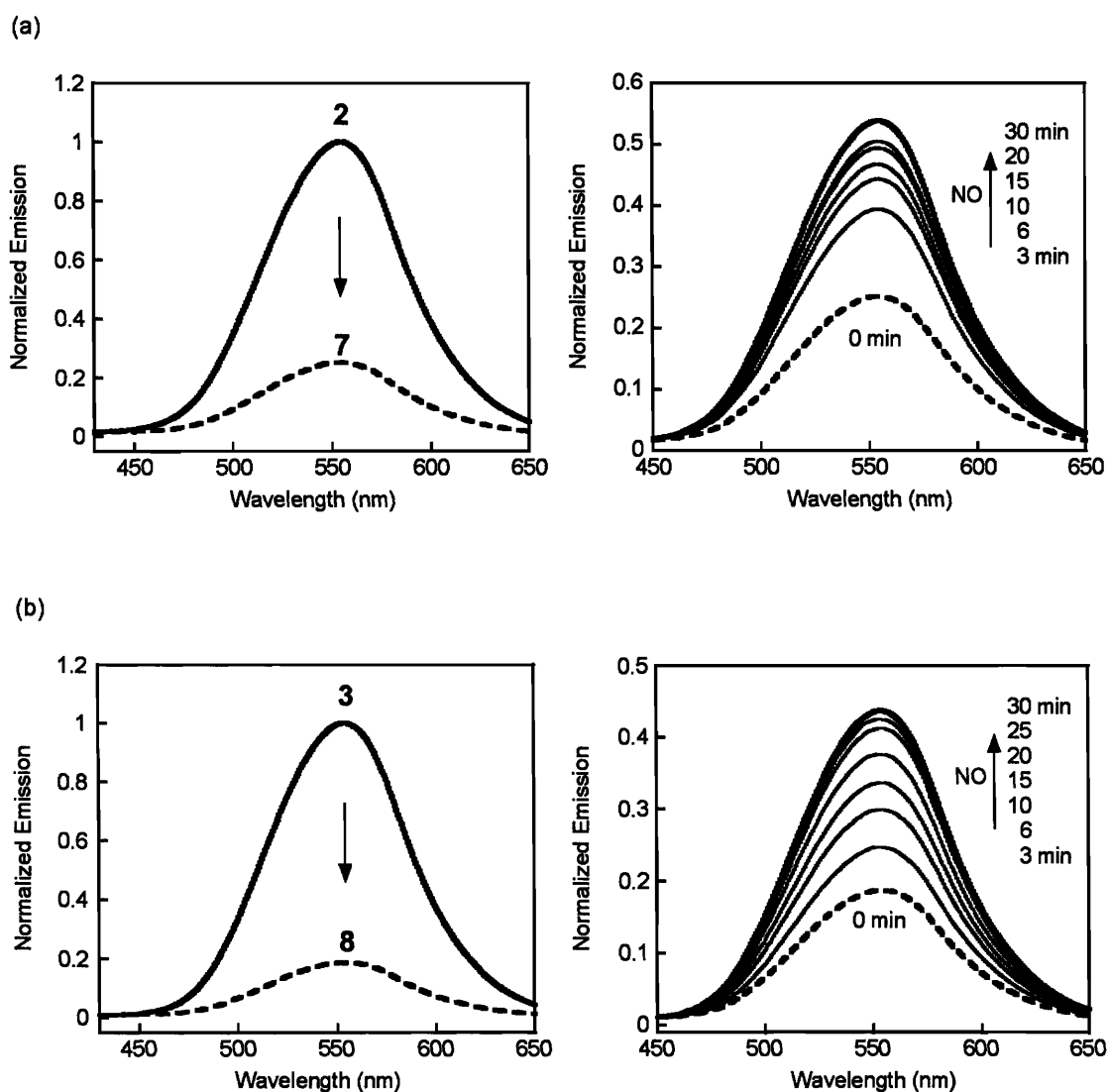


Figure 4.8. (a) Left: fluorescence emission spectra of 2 (20 μM , solid line) and 7 (10 μM , dashed line) at pH 9.0 (50 mM CHES, 100 mM KCl). Right: fluorescence response to of 7 (10 μM , dashed line) to 100 equiv of NO (g) at 3, 6, 10, 15, 20, and 30 min (solid lines) at 37 °C. (b) Left: emission spectra of 3 (20 μM , solid line) and 8 (10 μM , dashed line) in pH 9.0 CHES buffered solution. Right: fluorescence response of 8 (10 μM , dashed line) to 100 equiv of NO (g) at 3, 6, 10, 15, 20, 25, and 30 min (solid lines) 37 °C. Excitation wavelength is at 342 nm.

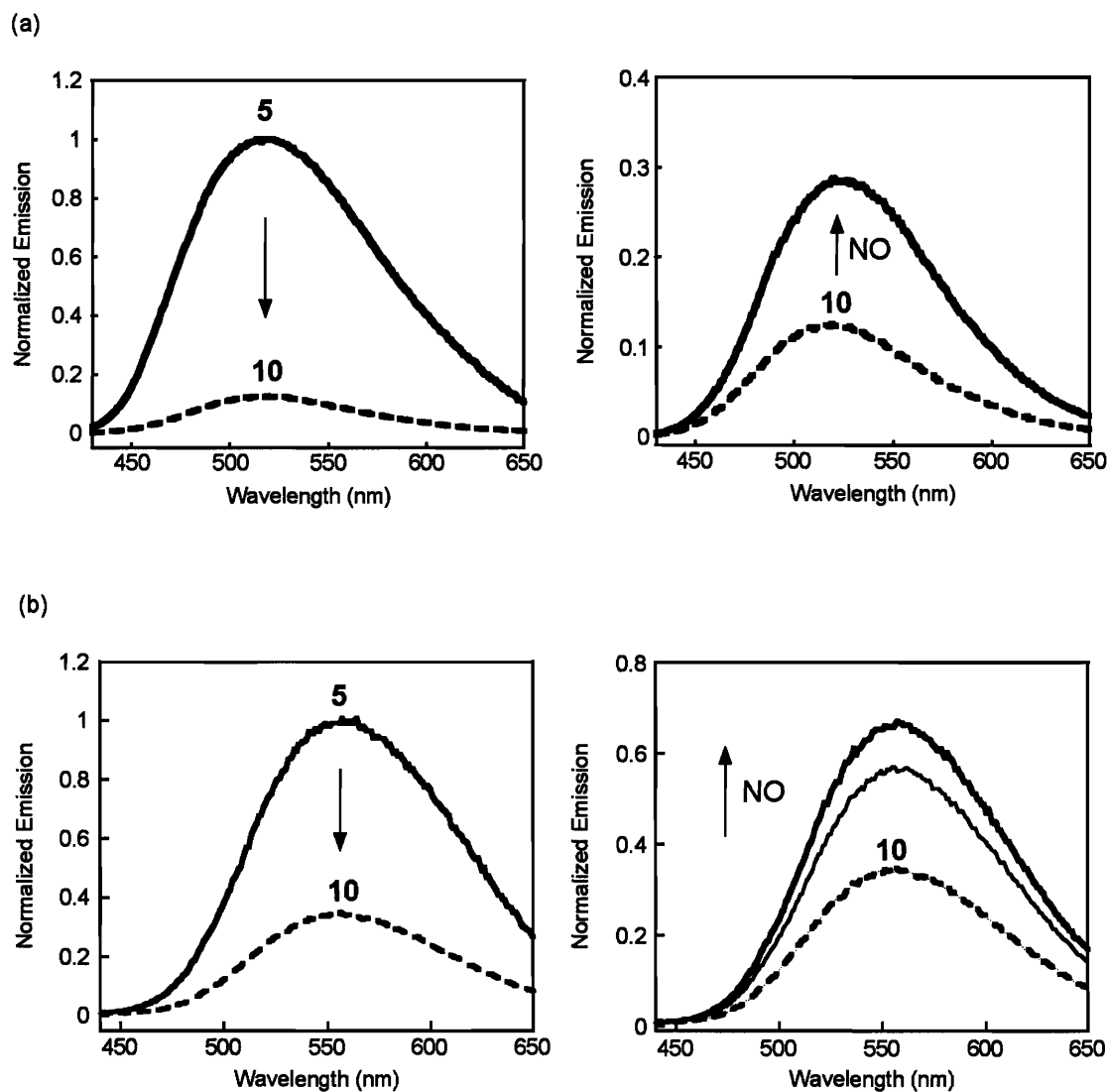


Figure 4.9. (a) Right: emission spectra of 5 (20 μM , solid line) and 10 (20 μM , dashed line) in CH_3OH at 25 $^\circ\text{C}$. Left: fluorescence response to of 10 (20 μM , dashed line) to 682 equiv of NO (g) within 5 min (solid line) at 25 $^\circ\text{C}$. (b) Right: emission spectra of 5 (10 μM , solid line) and 10 (10 μM , dashed line) at pH 7.0 (50 mM PIPES, 100 mM KCl). Left: fluorescence response of 10 (10 μM , dashed line) to 682 equiv of NO (g) at 2 and 6 min (solid lines) 37 $^\circ\text{C}$. Excitation wavelength is at 342 nm.

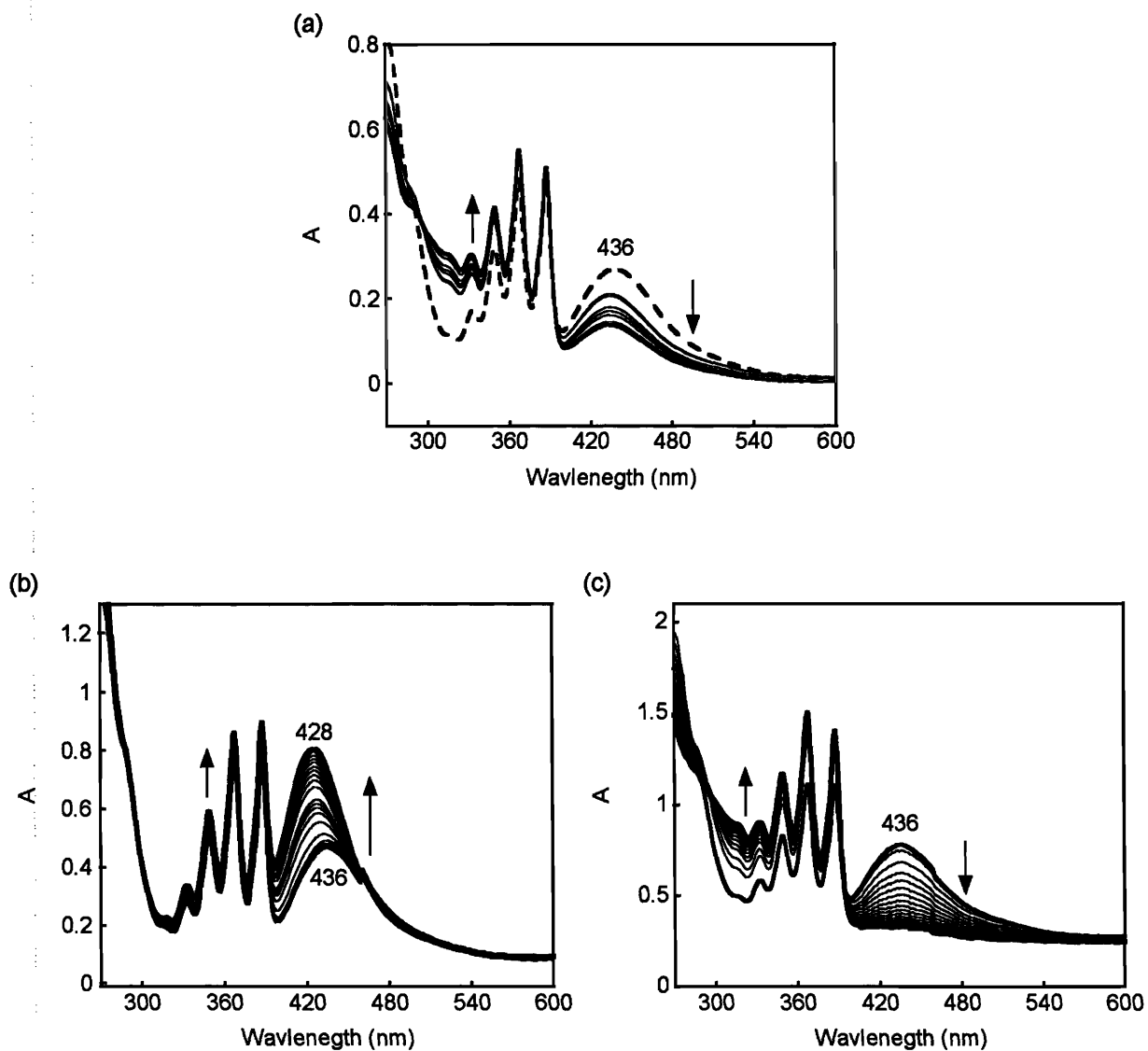


Figure 4.10. Optical spectra (a) from the reaction of 6 (20 μM) (dotted line) with 682 equiv of NO (solid line) over 60 min in $\text{CH}_2\text{Cl}_2/\text{CH}_3\text{OH}$ (1/1). Spectra of a solution of 6 (200 μM in CH_2Cl_2 with 0.1 M $(\text{Bu}_4\text{N})\text{PF}_6$, 1 mm UV-vis cell) during oxidation (b) and reduction (c). The current at +0.50 V (b) or -0.75 V (c) is continually provided when optical spectra were collected for 40 min.

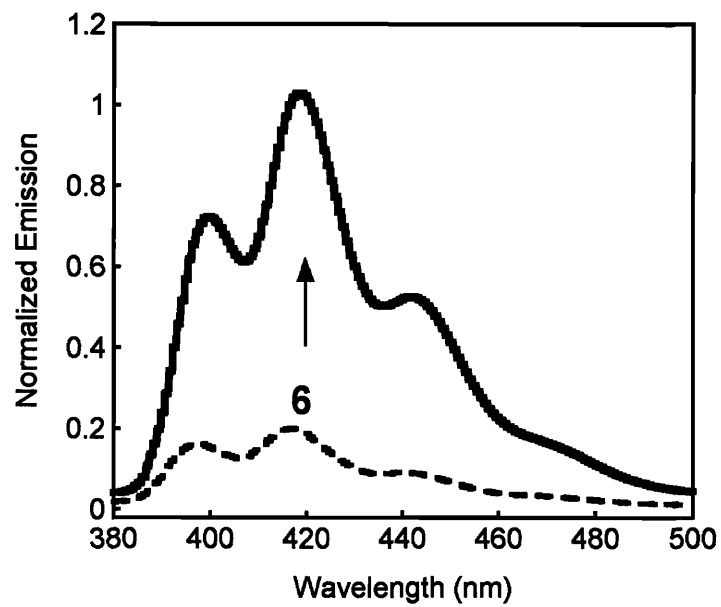


Figure 4.11. Fluorescence spectra of a 1:1 CH₃OH:CH₂Cl₂ solution of 6 (20 μ M, dashed line) and 1 (40 μ M) with [Cu(CH₃CN)₄](BF₄) (20 μ M) (solid line).

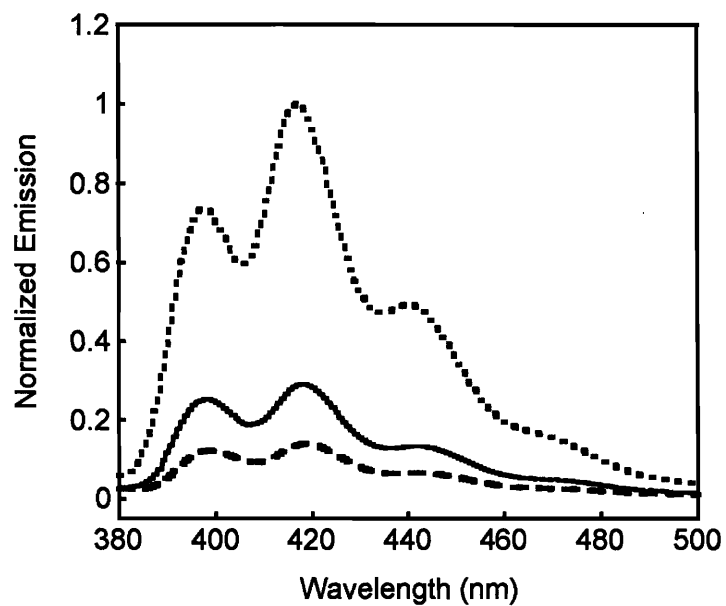


Figure 4.12. Fluorescence response of a 20 μM solution of 6 in CH_2Cl_2 (dashed line) upon addition of 100 equiv of NO (solid line). The dotted line is the fluorescence spectrum of 6 in $\text{CH}_3\text{OH}/\text{CH}_2\text{Cl}_2$ (1:1) at 60 min after administration of 682 equiv of NO (g).

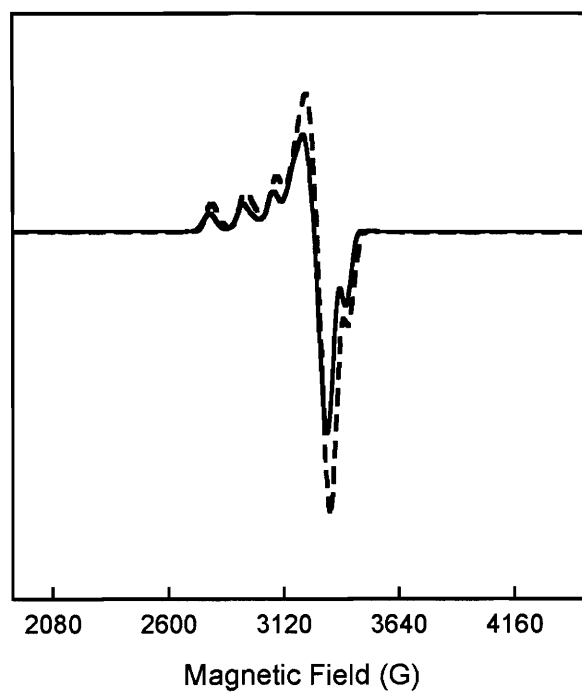


Figure 4.13. EPR spectra of a 4 mM solution of **8** in 4:1 CH₃OH:CH₂Cl₂ (dashed line) after addition of 1 equiv of NO (solid line). One equiv was used to avoid contamination by the EPR signal of free NO.

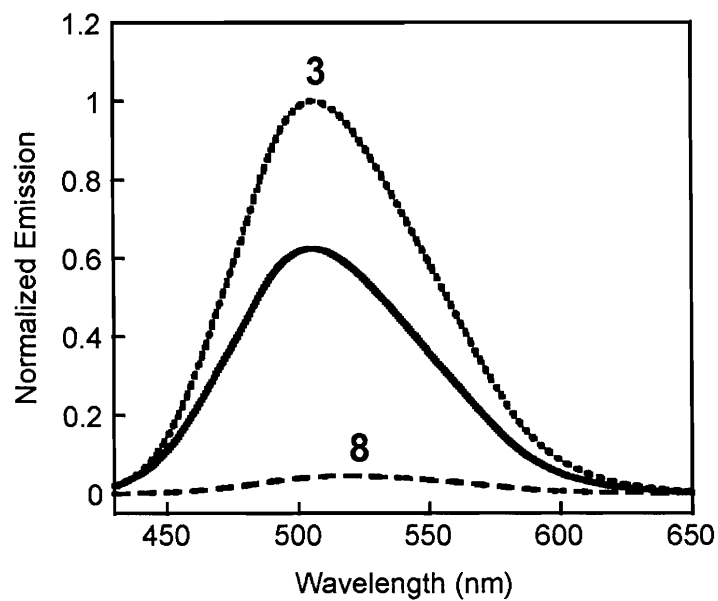


Figure 4.14. Fluorescence spectra of a 4:1 $\text{CH}_3\text{OH}:\text{CH}_2\text{Cl}_2$ solution of **3** ($40 \mu\text{M}$) without (dotted line) and with (solid line) $[\text{Cu}(\text{CH}_3\text{CN})_4](\text{BF}_4)$ ($20 \mu\text{M}$) in the presence of triethylamine ($40 \mu\text{M}$).

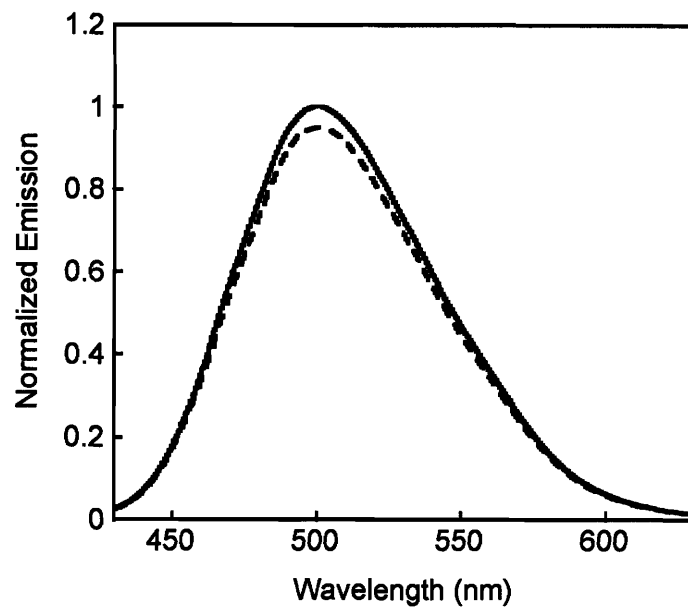


Figure 4.15. Fluorescence response of a 20 μM solution of **8** in CH_2Cl_2 (dashed line) upon addition of 100 equiv of NO (solid line).

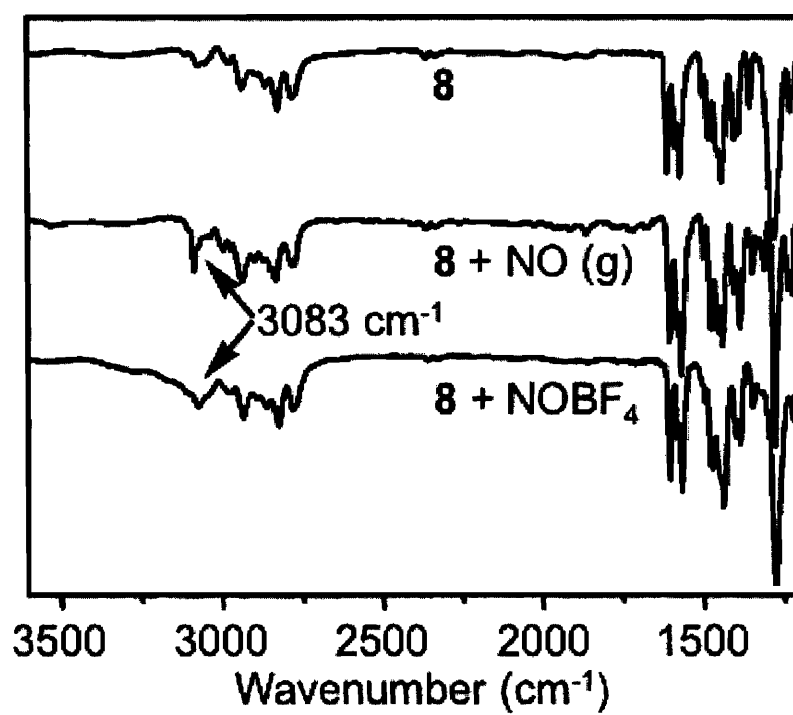


Figure 4.16. IR spectra of **8** (top), **8** with 10 equiv of NO (middle), and **8** with one equiv of NOBF₄ (bottom) in KBr.

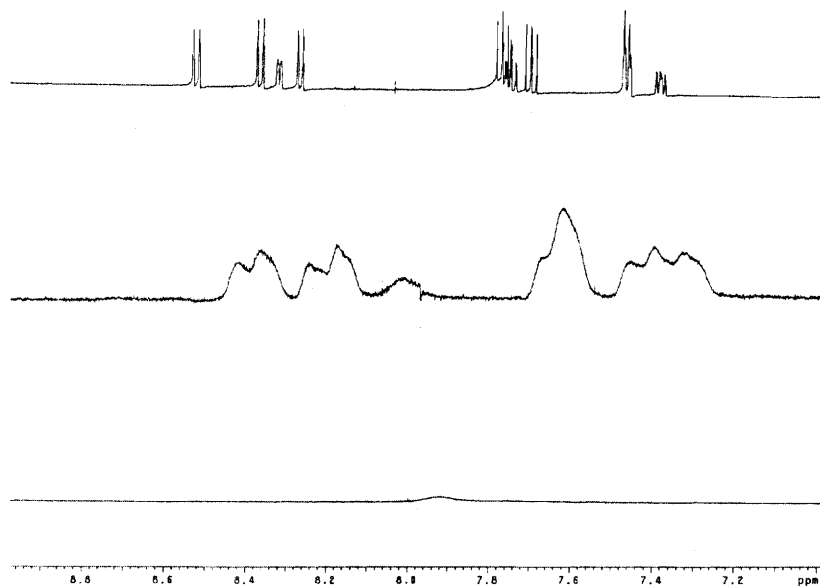


Figure 4.17. ^1H NMR spectra (6.6 – 9.0 ppm) of Ds-HAMP (4 mM in 4:1 $\text{CH}_3\text{OH}:\text{CD}_2\text{Cl}_2$, top), a reaction solution of **2** (4 mM in 4:1 $\text{CH}_3\text{OH}:\text{CD}_2\text{Cl}_2$) with 10 equiv of NO (bottom), and the latter solution to which was added Ds-HAMP (0.6 mM, middle).

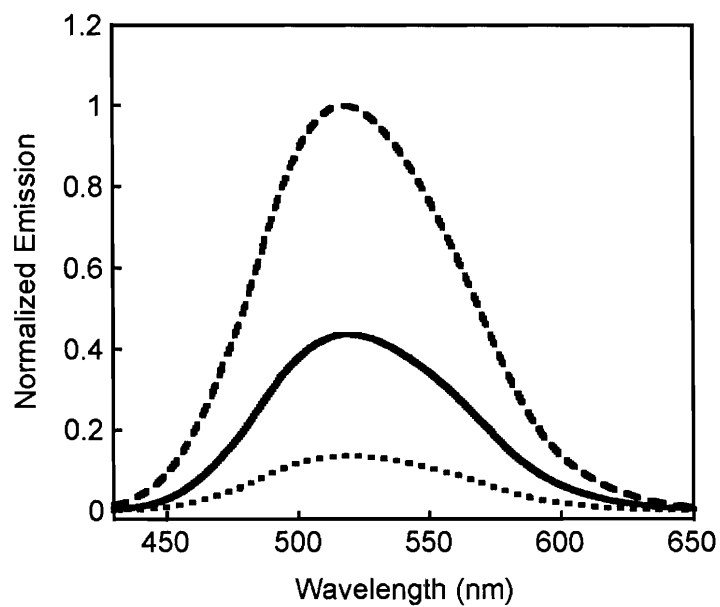


Figure 4.18. Fluorescence spectra of 4:1 $\text{CH}_3\text{OH}:\text{CH}_2\text{Cl}_2$ solution of 8 (dotted line), 8 with NOBF_4 (solid line), and 2 with NO (dashed line).

Chapter 5

Direct Nitric Oxide Detection In Aqueous Solution by Copper(II) Fluorescein Complexes

A portion of this chapter has appeared previously in Lim, M. H.; Xu, D.; Lippard, S. J., *Nat. Chem. Biol.* 2006, in press. This work was supported by grant CHE-0234951 from the National Science Foundation. I thank the Martin Family Society at MIT for fellowship funding. Spectroscopic instrumentation at the MIT DCIF is maintained with funding from NIH Grant 1S10RR13886-01 and NSF Grants CHE-9808063, DBI9729592, and CHE-9808061. We thank Professor M.-H. Baik, Mr. Brian A. Wong, and Mr. William H. Pitcock for DFT calculations. We thank Professor Daniel G. Nocera, Dr. Dong Xu and Dr. Datong Song for helpful discussions. We also thank Ms. E. M. Nolan for helping the synthesis of FL_n and providing FL₄ (QZ1) and Ms. Deepa Mokshagundam for absorption and emission measurements of FL₁ – FL₄.

Introduction

Nitric oxide (NO) is produced in a biological context by nitric oxide synthases.¹⁻⁶ The properties of NO allow for its varied involvement in physiological and pathophysiological pathways,^{3,4,6,7} but the details of how it performs its biological roles are not fully understood. The development of a method capable of detecting NO in biology has been an intriguing challenge for chemists, biologists and engineers. Small-molecule fluorescent sensors for NO have the potential to provide a practical method for visualizing its presence and movement *in vitro* and *in vivo*.^{8,9}

A few basic requirements are necessary for the design of biologically useful NO fluorescent probes,^{8,9} including water-solubility, cell-membrane permeability, and visible or near-IR excitation and emission wavelengths. Most importantly, these sensors must have the capability for direct, specific and rapid detection of NO. In addition, sensors that give fluorescence enhancement by reaction with NO are preferred for imaging NO in biological systems over those that respond to NO with a fluorescence decrease.

The commonly used, current generation of NO probes is based on organic molecules.^{8,10} Although these probes satisfy the basic requirements for bioimaging NO, they have the critical limitation that their fluorescence response is not driven by NO, but by an oxidized NO species. This requirement means that the most available sensors cannot provide direct, real-time imaging of NO. Since NO is relatively stable under physiological conditions,¹¹ new sensors for direct NO detection are desired for better exploration of NO-signaling in biology.

To achieve direct detection of nitric oxide, our laboratory has designed NO sensors employing transition metal complexes. Interaction of these complexes with NO offers the promise of investigating nitric oxide itself in biological media. In the past few

years, we have constructed several metal-fluorophore scaffolds as potential NO sensors including those based on cobalt,¹²⁻¹⁶ copper,¹⁷⁻¹⁹ iron,¹⁵ rhodium,²⁰ and ruthenium chemistry.²¹ Our general strategy for NO sensing is to coordinate a fluorophore ligand to a metal ion to quench its fluorescence, which is restored by the interaction of NO with the metal center, sometimes with release of the fluorophore and concomitant emission turn-on (Scheme 5.1a).⁹ Although all of the metal complexes reported by our laboratory can directly interact with NO, most of the metal-fluorophore platforms are not stable in aqueous solutions. In some case, water can outcompete the fluorophore for coordination to the metal center.

Recently, we have been exploring Cu(II)-based probes for NO detection. The strategy behind these Cu(II)-based sensors is that formation of a diamagnetic Cu(I) species via NO-triggered reduction alleviates the fluorescence quenching associated with coordination to a paramagnetic Cu(II) center (Scheme 5.1b).^{17,18} Utilizing this strategy, we constructed Cu(II) complexes containing dansyl groups as the fluorophore, which are able to detect NO in pH 9.0 buffered solutions.¹⁷ Unfortunately, these Cu(II) dansyl compounds did not show successful NO sensing at a physiologically more relevant pH. Recently, a Cu(II) cyclam complex was reported that demonstrated the potential of Cu(II) systems as suitable NO indicators by a strategy different from that used for the Cu(II) dansyl compounds.²² This complex exhibited fluorescence emission turn-on via NO-induced nitrosation of the fluorophore, which dissociated from the reduced Cu(I) in the buffered methanolic solution (Scheme 5.1c). Although the Cu(II)-based systems discussed here are not satisfactory as biological NO sensors, the studies formed the basis of a successful approach for developing metal-based sensors to image NO production in live cells.

To achieve NO sensing in a physiological context, five fluorescein derivatives (Figure 5.1) were prepared for binding Cu(II). These ligands were based on molecules previously described for zinc-sensing bio-applications by our laboratory.²³ The copper(II) fluorescein complexes of these ligands react directly with NO with concomitant emission increase in pH 7.0 buffered solutions. Moreover, the detection of NO by these Cu(II) probes is specific over other reactive nitrogen or oxygen species including HNO, NO₂⁻, NO₃⁻, ONOO⁻, H₂O₂ and O₂⁻. To our knowledge, Cu(II) probes are the first complexes that are capable of the direct and specific NO detection at pH 7.0. The synthesis, NO-sensing ability, and mechanism of fluorescence turn-on of the copper-fluorescein complexes are described in this chapter. Density functional theory (DFT) calculations of the species responsible for fluorescence turn-on are also presented.

Experimental

Materials and Procedures

All chemical reagents and solvents were obtained from commercial suppliers and used as received. Angeli's salt (Na₂N₂O₃) and sodium peroxyxynitrite (NaOONO) were purchased from Cayman Chemical Co. and used without further purification. Sodium nitrite (Na¹⁴NO₂ and Na¹⁵NO₂), xanthine oxidase and xanthine were obtained from Sigma-Aldrich. Whatman F254 silica gel-60 plates of 1 mm thickness were used for preparative TLC. Nitric oxide (NO) (Matheson, 99%) was purified by a previously reported method.²⁰ NO was transferred to the reaction solutions by a gastight syringe in an anaerobic chamber. Fluorescence emission spectra were recorded on a Photon Technology International fluorescence spectrophotometer at 25 °C or 37 °C. The lower detection limit of the copper fluorescein complexes for NO was determined by monitoring the fluorescence intensity (1 μM CuCl₂ and 1 μM fluorescein ligand)

following treatment of decreasing volumes of a 1.9 mM NO-saturated aqueous solution or a 10 mM SNAP solution (50 mM PIPES, pH 7.0, 100 mM KCl). We assigned a 15% increase of the integrated emission to be the lowest detectable change on our instrument. A Varian 300 or 500 NMR spectrometer was used to record ^1H and ^{13}C NMR spectra. IR spectra were measured on an Avatar 360 FTIR instrument. UV-vis spectra were obtained on a Hewlett-Packard 8453 diode array or a Cary 1E spectrophotometer. LC-MS analyses were performed on an Agilent Technologies 1100 Series LC-MS with a Zorbax Extend C-18 column using a linear gradient of 100% A (95:5 $\text{H}_2\text{O}:\text{CH}_3\text{CN}$; 0.05% HCO_2H) to 100% B (95:5 $\text{CH}_3\text{CN}:\text{H}_2\text{O}$; 0.05% HCO_2H) (3 min, 100% A; 15 min, 100% B; 20 min 100% B; 30 min 100% A) at a flow rate of 0.20 mL/min (detector wavelength = 280 nm). The MS detector was set to negative ion mode scanning in the range of $m/z = 100 - 2000$. High-resolution mass spectrometric measurements were performed by staff at the MIT Department of Chemistry Instrumentation Facility (DCIF).

EPR Spectroscopy. X-band EPR spectra were recorded on a Bruker EMX EPR spectrometer (9.37 GHz). The temperature was maintained with an Oxford Instruments ESR900 liquid-helium cryostat and ITC503 controller. Nitric oxide (five equiv) was directly transferred by a gastight syringe into a 2.5 mM DMF solution of the copper fluorescein complex in an EPR tube. The solution was then frozen with liquid N_2 and the spectrum was acquired at 5 K.

X-ray Crystallographic Studies. Single crystals suitable for data collection were mounted in Infineum V8512 on the tip of a glass capillary and frozen in a $-100\text{ }^\circ\text{C}$ nitrogen cold stream. Data were collected on a Bruker APEX CCD X-ray diffractometer with $\text{Mo K}\alpha$ radiation ($\lambda = 0.71073\text{ \AA}$) controlled by the SMART software package.²⁴ The general procedures used for data collection are reported elsewhere.²⁵ Empirical absorption corrections were calculated with the SADABS program.²⁶ Structures were

solved by direct methods and refined with the SAINTPLUS and SHELXTL software packages.^{27,28} All non-hydrogen atoms were refined anisotropically. Hydrogen atoms were assigned idealized positions and each was given a thermal parameter equivalent to 1.2 times the thermal parameter of the atom to which it was attached. All structure solutions were checked for higher symmetry with PLATON.²⁹ In the structure of $[\text{Cu}(\text{modL})_2](\text{BF}_4)_2 \cdot 2\text{CH}_3\text{OH}$, the oxygen atom of a CH_3OH molecule was disordered over two positions and assigned occupancy factors of 0.15 and 0.85, respectively. Four fluorine atoms of three BF_4^- anions were also disordered over two positions (0.35 and 0.65, 0.40 and 0.6, 0.32 and 0.68 occupancy factors, respectively) in the structure of $[\text{Cu}_2(\text{modL}')_2(\text{CH}_3\text{OH})](\text{BF}_4)_2 \cdot \text{CH}_3\text{OH}$. A hydrogen atom was not assigned to the oxygen atom of a solvent CH_3OH molecule, which forms a hydrogen bond to another CH_3OH molecule that is coordinated to the copper center.

Calculation Methods. All calculations were performed by Professor M.-H. Baik (Indiana University) with either the Jaguar 5.5 (Schrodinger, Inc.) or the Amsterdam Density Function (ADF) 200.01 software package. Gas phase molecular geometries were optimized by the density functional method utilizing the B3LYP functional and 6-31G** basis set. Single point energy calculations were performed from the optimized structures using the cc-pVTZ(-f) basis set, which accounts for electron correlation and provides reliable energies. Refinements to account for energy changes due to solvation were also carried out.

Syntheses. Precursors of FL_1 and FL_2 were synthesized by modification of a previously reported method.³⁰ The compound 2-[2-chloro-6-hydroxy-5-(quinolin-8-ylaminomethyl)-3-oxo-3H-xanthen-9-yl]-benzoic acid ($\text{FL}_4 = \text{QZ1}$) was prepared as described in the literature.³¹

8-Nitro-2-quinolinecarboxylic acid methyl ester (1). To a solution (20 mL CH₃OH and 50 mL Et₂O) of 8-nitro-2-quinolinecarboxylic acid (1 g, 4.27 mmol) was added Me₃SiCHN₂ (15 mL, 2.0 M in Et₂O) until the color of the solution became light yellow. The reaction solution was stirred for 4 h at room temperature. Removal of the solvent provided a light brown solid. The product (0.47 g, 2.0 mmol, 47%) was purified by column chromatography (SiO₂, 1:1 hexanes:EtOAc; *R_f* = 0.55 by TLC). ¹H NMR (500 MHz, CD₂Cl₂): δ (ppm) 4.05 (3H, s), 7.74 (1H, t, *J* = 7.5), 8.11 – 8.15 (2H, m), 8.31 (1H, d, *J* = 8.5), 8.43 (1H, d, *J* = 8.0). HRMS (*m/z*): [M+Na]⁺ Calcd. for C₁₁H₈N₂NaO₄, 255.0382; Found 255.0374.

8-Amino-2-quinolinecarboxylic acid methyl ester (2). Ethyl acetate (20 mL) was added to a mixture of 8-nitro-2-quinolinecarboxylic acid methyl ester (0.18 g, 0.76 mmol) and 10% Pd/C (63 mg) and the solution was degassed with Ar for 20 min. One atmosphere of H₂ (g) was introduced to the degassed solution overnight. The solid residues were removed by filtration over celite. Concentration of the filtrate produced the desired product (0.13 g, 0.66 mmol, 86%). ¹H NMR (500 MHz, CDCl₃): δ (ppm) 4.05 (3H, s), 6.97 (1H, dd, *J* = 7.5, *J* = 1.5), 7.18 (1H, dd, *J* = 8.3, *J* = 0.5), 7.44 (1H, t, *J* = 8.0), 8.13 (1H, d, *J* = 8.5), 8.19 (1H, d, *J* = 8.5). HRMS (*m/z*): [M+Na]⁺ Calcd. for C₁₁H₁₀N₂NaO₂, 225.0640; Found 225.0638.

(8-Amino-2-quinolinyl)-methanol (3). To an ethanol (8 mL) solution of NaBH₄ (0.19 g, 4.9 mmol) at 0 °C was added dropwise a THF solution (8 mL) of 8-amino-2-quinolinecarboxylic acid methyl ester (0.10 g, 0.50 mmol) over 5 min. The solution was allowed to warm to room temperature with stirring overnight. A saturated aqueous NaHCO₃ solution (3 mL) and water (2 mL) were added to the reaction, and the solution was extracted with CHCl₃ three times. The collected CHCl₃ layer was washed with

brine and water and dried with MgSO_4 . Removal of the solvent provided the desired product (63 mg, 0.36 mmol, 73 %). $^1\text{H NMR}$ (500 MHz, CDCl_3): δ (ppm) 4.95 (2H, s), 7.00 (1H, dd, $J = 7.5$, $J = 1.5$), 7.20 (1H, dd, $J = 8.0$, $J = 1.0$), 7.29 (1H, d, $J = 8.5$), 7.36 (1H, t, $J = 7.5$), 8.12 (1H, d, $J = 8.5$). HRMS (m/z): $[\text{M}+\text{Na}]^+$ Calcd. for $\text{C}_{10}\text{H}_{10}\text{N}_2\text{NaO}$, 197.0691; Found 197.0676.

2-[2-Chloro-6-hydroxy-5-[(2-(methylcarboxy)quinolin-8-ylamino)methyl]-3-oxo-3H-xanthen-9-yl]benzoic acid (FL₁). An ethyl acetate (3 mL) solution of 8-amino-2-quinolinecarboxylic acid methyl ester (15 mg, 0.076 mmol) and 7'-chloro-4'-fluoresceincarboxaldehyde³² (30 mg, 0.076 mmol) was stirred overnight at room temperature. The resulting red residue was collected, dried *in vacuo*, and dissolved in dichloroethane (2 mL). To this solution was added $\text{NaB}(\text{OAc})_3\text{H}$ (19 mg, 0.15 mmol) and the reaction solution was stirred overnight at room temperature. A portion of crude materials was purified by preparative TLC on reverse phase silica gel ($R_f = 0.32$, $\text{MeOH}/\text{H}_2\text{O} = 3 : 0.7$) to yield a red solid (16 mg, 27 μmol , 36%): mp = 155 – 157 °C (decomp). $^1\text{H NMR}$ (500 MHz, CD_3OD): δ (ppm) 3.97 (3H, s), 4.79 (2H, s), 6.53 (1H, d, $J = 9$), 6.61 (1H, s), 6.63 (1H, d, $J = 8.5$), 6.99 (1H, s), 7.04 (1H, d, $J = 8.0$), 7.12 (1H, d, $J = 8.0$), 7.19 (1H, d, $J = 7.5$), 7.46 (1H, t, $J = 8$), 7.68 (1H, t, $J = 7.5$), 7.73 (1H, t, $J = 7.5$), 7.99 (2H, t, $J = 8.5$), 8.15 (1H, d, $J = 9.5$). FTIR (KBr, cm^{-1}): 3421 (br, m), 2962 (w), 2917 (vw), 2849 (vw), 1759 (m), 1722 (m), 1627 (m), 1610 (m), 1577 (w), 1565 (w), 1519 (m), 1489 (w), 1445 (w), 1427 (m), 1377 (w), 1283 (w), 1263 (s), 1217 (w), 1149 (w), 1100 (m), 1092 (m), 1063 (w), 1027 (m), 873 (w), 803 (s), 769 (w), 701 (w), 617 (vw), 575 (vw), 545 (vw), 469 (vw), 403 (vw). HRMS (m/z): $[\text{M}-\text{H}]^-$ Calcd. for $\text{C}_{32}\text{H}_{20}\text{ClN}_2\text{O}_7$, 579.0959; Found 579.0963. Anal. Calcd. for $\text{C}_{32}\text{H}_{21}\text{ClN}_2\text{O}_7$: C, 66.16; H, 3.64; N, 4.82; Found: C, 66.18; H, 3.53; N, 4.98.

2-[2-Chloro-6-hydroxy-5-[(2-(carboxy)quinolin-8-ylamino)methyl]-3-oxo-3H-xanthen-9-yl]benzoic acid (FL₂). Portions of 8-aminoquinoline-2-carboxylic acid (14 mg, 0.076 mmol) and 7'-chloro-4'-fluoresceincarboxaldehyde³² (30 mg, 0.076 mmol) were added to 2 mL of EtOAc and the reaction solution was stirred overnight at room temperature. After removing the solvent, the resulting red residue was collected and dissolved in dichloroethane (2 mL) followed by the addition of NaB(OAc)₃H (19 mg, 0.15 mmol). The reaction solution was stirred and the solvent was removed after 1 d. The crude product was purified by preparative TLC on silica gel (1st purification: R_f = 0.11, 5:1 MeOH/CH₂Cl₂, 2nd purification: R_f = 0.61, 3:0.5 MeOH/0.1 M HCl), affording a red solid (9.7 mg, 17 μ mol, 23%): mp = 240 – 242 °C (decomp). ¹H NMR (300 MHz, CD₃OD/CD₂Cl₂): δ (ppm) 4.72 (2H, s), 6.57 (1H, d, J = 8.1), 6.68 (1H, s), 6.93 (0.5H, d, J = 7.5), 7.00 – 7.13 (3H, m), 7.20 (1H, d, J = 6.3), 7.32 (0.5H, t, J = 7.5), 7.48 (1H, t, J = 8.1), 7.53 – 7.61 (2H, m), 8.03 – 8.14 (3H, m). FTIR (KBr, cm⁻¹): 3404 (br, m), 3048 (vw), 2962 (w), 2923 (w), 2845 (w), 1635 (m), 1609 (m), 1576 (s), 1512 (w), 1459 (m), 1340 (w), 1303 (w), 1261 (m), 1221 (w), 1148 (s), 1094 (s), 1015 (s), 938 (vw), 878 (vw), 859 (vw), 821 (m), 796 (s), 745 (vw), 713 (vw), 690 (vw), 661 (vw), 628 (w), 599 (w), 582 (vw), 550 (w), 527 (vw), 516 (vw), 492 (w), 472 (m), 460 (w), 442 (w), 435 (w), 422 (w), 413 (w), 405 (w). HRMS (m/z): [M+Na]⁺ Calcd. for C₃₁H₁₉ClN₂O₇, 589.07785; Found 589.0786. Anal. Calcd. for C₃₁H₁₉ClN₂O₇: C, 65.67; H, 3.38; N, 4.94; Found: C, 65.58; H, 3.32; N, 4.79.

2-[2-Chloro-6-hydroxy-5-[(2-hydroxymethyl-quinolin-8-ylamino)-methyl]-3-oxo-3H-xanthen-9-yl]benzoic acid (FL₃). A solution (EtOAc, 3 mL) of (8-aminoquinolin-2-yl)-methanol (33 mg, 0.19 mmol) and 7'-chloro-4'-fluoresceincarboxaldehyde³² (75 mg, 0.19 mmol) was stirred overnight at room temperature. The resulting red residue was collected, dried *in vacuo*, and dissolved in

dichloroethane (2 mL). To the dichloroethane solution was added a portion of $\text{NaB(OAc)}_3\text{H}$ (48 mg, 0.23 mmol). The solution was stirred overnight and purified by preparative silica TLC ($R_f = 0.22$, 1:1:0.9 EtOAc/Hx/MeOH), affording a red solid (23 mg, 42 μmol , 22%): mp = 230 – 231 °C (decomp). $^1\text{H NMR}$ (500 MHz, CD_3OD): δ (ppm) 4.74 (2H, s), 4.77 (2H, s), 6.53 (1H, d, $J = 9.5$), 6.73 (1H, s), 6.97 – 7.00 (2H, m), 7.09 – 7.17 (3H, m), 7.32 (1H, t, $J = 8.0$), 7.45 (1H, d, $J = 8.0$), 7.49 – 7.56 (2H, m), 7.99 (1H, d, $J = 9.0$), 8.05 (1H, d, $J = 10.5$). FTIR (KBr, cm^{-1}): 3427 (br, m), 3059 (vw), 2996 (vw), 2963 (w), 2932 (vw), 2900 (vw), 1634 (vw), 1575 (s), 1519 (w), 1457 (m), 1419 (w), 1376 (m), 1342 (w), 1305 (vw), 1263 (m), 1223 (w), 1151 (w), 1092 (w), 1039 (vw), 925 (vw), 881 (vw), 822 (m), 806 (m), 712 (vw), 649 (vw), 619 (vw), 600 (vw), 550 (vw), 469 (vw). HRMS (m/z): $[\text{M-H}]^-$ Calcd. for $\text{C}_{31}\text{H}_{20}\text{ClN}_2\text{O}_6$, 551.1010; Found 551.1003. Anal. Calcd. for $\text{C}_{31}\text{H}_{21}\text{ClN}_2\text{O}_6 \cdot 2\text{H}_2\text{O} \cdot 2\text{CHCl}_3 \cdot \text{CH}_2\text{Cl}_2$: C, 44.74; H, 3.20; N, 3.07; Found: C, 46.46; H, 3.29; N, 2.84 ($^1\text{H NMR}$ spectrum also presented two CHCl_3 and one CH_2Cl_2 molecules per FL_5 in the material).

2-{2-Chloro-6-hydroxy-5-[(2-methyl-quinolin-8-ylamino)-methyl]-3-oxo-3H-xanthen-9-yl}benzoic acid (FL_5). To 2 mL of EtOAc were added 7'-chloro-4'-fluoresceincarboxaldehyde (30 mg, 0.076 mmol)³² and 8-aminoquinaldine (12 mg, 0.076 mmol). After the reaction was stirred overnight at room temperature, the solvent was removed under reduced pressure. The residue was dissolved in 2 mL of MeOH and the reaction solution was cooled to 0 °C. A portion of NaBH_4 (14 mg, 0.38 mmol) was added and the reaction was stirred at 0 °C for 1 h before being allowed to come slowly to room temperature, followed by stirring overnight. The solvent was evaporated under reduced pressure and the crude material was purified by preparative TLC on silica gel ($R_f = 0.34$, 20:1 $\text{CH}_2\text{Cl}_2/\text{MeOH}$), affording the FL_5 product as a magenta solid (9 mg, 17

μmol , 22%): mp = 190 – 192 °C (decomp). ^1H NMR (500 MHz, CD_3OD): δ (ppm) 2.61 (3H, s), 4.75 (2H, s), 6.50 (1H, d, $J = 9.5$), 6.76 (1H, s), 6.94 – 7.01 (2H, m), 7.10 – 7.15 (3H, m), 7.20 (1H, d, $J = 8.5$), 7.27 – 7.30 (1H, m), 7.52 – 7.58 (2H, m), 7.90 (1H, d, $J = 8.0$), 8.02 (1H, d, $J = 7.5$). ^{13}C NMR (125 MHz, CD_3OD): δ (ppm) 181.53, 174.38, 173.44, 159.42, 157.67, 157.31, 156.08, 145.00, 140.59, 138.63, 136.52, 133.77, 131.01, 130.17, 129.94, 129.50, 129.37, 129.05, 127.38, 127.34, 127.10, 123.99, 122.18, 114.33, 113.49, 112.79, 111.48, 106.68, 104.26, 36.43, 24.44. FTIR (KBr, cm^{-1}): 3390 (br, w), 3044 (vw), 2961 (w), 2920 (w), 2848 (w), 1636 (m), 1606 (m), 1575 (s), 1515 (m), 1460 (s), 1374 (s), 1342 (sh, w), 1304 (w), 1258 (vw), 1221 (w), 1149 (m), 1119 (vw), 1092 (vw), 1007 (m), 937 (vw), 883 (vw), 828 (m), 795 (vw), 745 (vw), 714 (vw), 686 (vw), 659 (vw), 627 (w), 599 (w), 549 (w), 520 (vw), 471 (m), 449 (vw). HRMS (m/z): $[\text{M}-\text{H}]^-$ and $[2\text{M}-\text{H}]^-$: Calcd, for $\text{C}_{31}\text{H}_{20}\text{ClN}_2\text{O}_5$, 535.1061 and for $\text{C}_{62}\text{H}_{41}\text{Cl}_2\text{N}_4\text{O}_{10}$ 1071.2200; Found, 535.1044 and 1071.2147.

2-[2-Chloro-6-hydroxy-5-[(2-methylquinolin-8-yl)(nitroso)amino)methyl]-3-oxo-3H-xanthen-9-yl]benzoic acid (FL₅-NO). Sodium nitrite ($\text{Na}^{14}\text{NO}_2$ or $\text{Na}^{15}\text{NO}_2$, 5 mg, 72 μmol , in 100 μL dd H_2O) was added to a mixture of FL₅ (1.5 mg, 2.8 μmol , in 200 μL CH_3OH) and 0.3 M NaOH (aq, 100 μL) on ice. Hydrochloric acid (100 μL , 6 M aq) was slowly introduced to the reaction solution on ice, affording a reddish precipitate. After the solution was centrifuged, LC-MS analyses of both supernatant and precipitate were performed. The precipitate included a mixture of FL₅-NO and FL₅. The collected supernatant mostly contained the desired product, confirmed by LC-MS. Excess sodium nitrite was removed by dialysis of the supernatant using Spectra/Pro[®] CE (Spectrum[®]) membrane and an orange solid (0.6 mg, 1.1 μmol , 39%) was obtained by solvent removal using a lyophilizer and characterized without further purification. TLC (silica, 1:9 $\text{CH}_3\text{OH}/\text{CH}_2\text{Cl}_2$) showed only one compound with $R_f = 0.6$: mp = 120 – 123 °C

(decomp). FTIR (KBr, cm^{-1}): 3419 (br, s), 3060 (vw), 2958 (vw), 2922 (w), 2846 (vw), 1762 (m), 1725 (vw), 1704 (vw), 1689 (vw), 1642 (m), 1630 (m), 1608 (m), 1580 (sh, w), 1542 (W), 1452 (s), 1428 (m), 1384 (m), 1303 (sh, w), 1285 (m), 1253 (sh, w), 1222 (w), 1151 (m), 1109 (m), 1087 (br, w), 1065 (w), 1017 (m), 952 (w), 605 (vw), 874 (vw), 842 (vw), 803 (w), 763 (w), 703 (w), 672 (vw), 621 (vw), 605 (vw), 579 (vw). It was not possible to identify ν_{NO} unambiguously in the IR spectrum, probably due to overlap with other peaks in the expected region (1200 – 1600 cm^{-1}). Several possible intramolecular hydrogen bonding interactions involving the nitrosyl group may also attenuate its position and intensity. HRMS (m/z): $[\text{M}-\text{H}+\text{Cl}]^-$: Calcd, for $\text{C}_{31}\text{H}_{20}\text{Cl}_2\text{N}_3\text{O}_6$, 600.0729; Found, 600.0729. ^{15}N NMR (50.71 MHz, CD_3OD) for $\text{FL}_5\text{-}^{15}\text{NO}$: δ (ppm) 167.33 and 169.61 (relative to CH_3NO_2 as external standard). ^1H NMR (500 MHz, CD_3OD , ca. 7:3 isomer mixture) selected peaks for $\text{FL}_5\text{-}^{15}\text{NO}$: δ (ppm) 2.67 (0.9H, s), 2.71 (2.1H, s), 7.83 (0.3H, dd, $J = 8.0$, $J = 1.0$), 7.91 (0.7H, dd, $J = 7.5$, $J = 1.5$), 7.96 (0.7H, d, $J = 7.5$), 8.0 (0.3H, d, $J = 7.5$), 8.19 (0.3H, d, $J = 8.5$), 8.23 (0.7H, d, $J = 8.5$). HRMS (m/z): $[\text{M}-\text{H}+\text{Cl}]^-$: Calcd, for $\text{C}_{31}\text{H}_{20}\text{Cl}_2\text{}^{14}\text{N}_2\text{}^{15}\text{NO}_6$, 601.0700; Found, 601.0736.

$[\text{Cu}_2(\text{modL}')_2(\text{CH}_3\text{OH})](\text{BF}_4)_2 \cdot \text{CH}_3\text{OH}$ and $[\text{Cu}(\text{modL})_2](\text{BF}_4)_2 \cdot 2\text{CH}_3\text{OH}$. Two kinds of crystals were grown by vapor diffusion of Et_2O into a methanol solution (3 mL) of 2-[(quinolin-8-ylamino)methyl]phenol (modL) (10 mg, 40 μmol) and copper(II) tetrafluoroborate (9.5 mg, 40 μmol) at room temperature overnight. Violet (major product, $[\text{Cu}(\text{modL})_2](\text{BF}_4)_2 \cdot 2\text{CH}_3\text{OH}$) and green (minor product, $[\text{Cu}_2(\text{modL}')_2(\text{CH}_3\text{OH})](\text{BF}_4)_2 \cdot \text{CH}_3\text{OH}$) colored crystals were manually separated for characterization. Quantities of $[\text{Cu}_2(\text{modL}')_2(\text{CH}_3\text{OH})](\text{BF}_4)_2 \cdot \text{CH}_3\text{OH}$ sufficient for full characterization were not obtained. FTIR (KBr, cm^{-1}): 3485 (br, w), 3216 (m), 3071 (vw), 2952 (vw), 2931 (vw), 2849 (vw), 1617 (vw), 1598 (vw), 1570 (vw), 1513 (m), 1485 (m),

1454 (m), 1384 (m), 1322 (w), 1265 (s), 1199 (vw), 1130 (sh, w), 1081 (br, vs), 1042 (br, vs), 936 (sh, vw), 903 (vw), 881 (w), 859 (vw), 834 (w), 804 (w), 764 (s), 730 (w), 656 (vw), 633 (vw), 618 (vw), 598 (vw), 581 (vw), 551 (w), 519 (w), 504 (w), 463 (w), 415 (w). Characterization of $[\text{Cu}(\text{modL})_2](\text{BF}_4)_2 \cdot 2\text{CH}_3\text{OH}$: mp = 223 – 225 °C (decomp). FTIR (KBr, cm^{-1}): 3379 (br, m), 3246 (m), 3119 (vw), 3070 (w), 3056 (w), 3026 (vw), 2940 (vw), 2864 (vw), 1616 (w), 1596 (m), 1516 (s), 1479 (w), 1462 (s), 1400 (w), 1382 (w), 1358 (w), 1332 (w), 1316 (vw), 1270 (w), 1248 (w), 1188 (w), 1175 (w), 1162 (sh, w), 1133 (sh, w), 1100 (br, vs), 1080 (br, vs), 1039 (sh, vw), 936 (sh, vw), 885 (w), 867 (w), 848 (w), 832 (m), 794 (w), 763 (s), 731 (w), 721 (w), 664 (vw), 559 (vw), 519 (w), 491 (vw). Anal. Calcd. for $\text{CuC}_{32}\text{H}_{28}\text{B}_2\text{F}_8\text{N}_4\text{O}_2 \cdot 2\text{H}_2\text{O}$: C, 49.67; H, 4.17; N, 7.24; Found: C, 50.41; H, 4.18; N, 6.98.

Results and Discussion

Design Considerations for Cu(II)-Based NO Sensors.

Several metal-based fluorescent sensors for nitric oxide have been developed in our laboratory.^{9,12-21} Most recently, we succeeded in fluorescent NO sensing using Cu(II) dansyl complexes in pH 9.0 buffered solution, which results in the formation of a diamagnetic Cu(I) species (Scheme 5.1b).¹⁷ In addition, a Cu(II) anthracenyl cyclam complex showed an NO-triggered fluorescence increase in a buffered methanol solution by fluorophore ligand dissociation from copper following *N*-nitrosation (Scheme 5.1c).²² Both observations demonstrate that a Cu(II)-based sensor could be designed for NO detection in a physiologically relevant setting. To achieve this goal, fluorescein-based ligands for Cu(II) were prepared, since fluorescein is water-soluble, highly emissive ($\Phi = 0.95$) and has excitation and emission in the visible region,³³ which is not harmful for cellular components during NO imaging. Incorporation of a metal-binding unit to a

fluorescein backbone provides small-molecule, metal-ion sensors, as previously demonstrated for Zn(II).²³ Similarly, a copper-binding site was linked to fluorescein to obtain a copper-fluorescein compound as an NO indicator at pH 7.0 (Figure 5.1).

Synthesis of Fluorescein-Based Ligands (FL_n).

The general assembly of fluorescein-based sensors with one metal ion binding site containing two nitrogen and one or more oxygen donor atoms (N₂O_n, n = 1 or 2) has been previously achieved in our laboratory by using 7'-chloro-4'-fluoresceincarboxaldehyde.³² This general synthesis was adopted to prepare copper(II)-based NO sensors in the present study.

The synthesis of amine ligands 8-amino-2-quinolinecarboxylic acid methyl ester (**2**) and (8-amino-2-quinolinyl)-methanol (**3**) was achieved by modification of a previously reported method, as shown in Scheme 5.2.³⁰ 8-Nitro-2-quinolinecarboxylic acid was generated by bromination of 8-nitroquinoline followed by hydrolysis as described.³⁰ To prepare 8-nitro-2-quinolinecarboxylic acid methyl ester (**1**), trimethylsilyldiazomethane Me₃SiCHN₂, which is a safer alternative to the use of diazomethane, was employed in the present work, affording **1** as a light-brown solid in moderate yield (47%) after purification on silica gel (1:1 hexanes/EtOAc). Hydrogenation of **1** in EtOAc using 10% Pd/C gave pure **2** in 86% yield without further manipulation. Upon reduction of **2** with sodium borohydride in a mixture of THF and EtOH, **3** was obtained in 73% yield without purification.

Scheme 5.3 illustrates the syntheses of fluorescein-based ligands FL₁ – FL₅. Combination of **2** or **3** with 7'-chloro-4'-fluoresceincarboxaldehyde³² in dry EtOAc resulted in precipitates of the respective intermediate imines, as shown in the scheme. The imines were reduced under mild conditions by using NaB(OAc)₃H in

dichloroethane. A portion of the crude materials was purified by preparative TLC, affording desired products FL₁ and FL₃ respectively in moderate yield. Commercially available amine moieties were assembled with 7'-chloro-4'-fluoresceincarboxaldehyde³² to obtain pure FL₂, FL₄,³¹ and FL₅ by a similar procedure. The spectroscopic properties of the FL_n (n = 1 – 5) compounds are summarized in Table 5.1.

Preparation and Fluorescence Studies of Copper Fluorescein Compounds.

The Cu(II) fluorescein-based NO sensors Cu(FL_n) (n = 1 – 5, Figure 5.1) were generated *in situ* by combining the FL_n ligand with CuCl₂ in a 1:1 ratio in pH 7.0 buffered solution (50 mM PIPES, 100 mM KCl). Upon Cu(II) binding to the fluorescein ligands FL_n, a blue-shifted absorption band was observed, compared to that of free FL_n, as summarized in Table 5.1. UV-visible spectroscopy was employed to verify the binding stoichiometry of the FL_n:Cu(II) complexes at pH 7.0. For FL₁, FL₃, and FL₅, Job's plots of CuCl₂:ligand mixtures revealed a break at 0.5, indicating the formation of a 1:1 complexes (Figure 5.2). The reaction of FL₂ or FL₄ with CuCl₂, however, generated a mixture of 1:1 and 1:2 complexes in pH 7.0 buffered solution as revealed by analyses of the Job's plots (Figure 5.2). This mixed binding mode of FL₄ with Cu(II) was also observed in the reaction of Cu(BF₄)₂ with 2-[(quinolin-8-ylamino)methyl]phenol (modL) as a model for the reaction of FL₄. Two kinds of crystals [Cu(modL)₂](BF₄)₂ and [Cu₂(modL')₂(MeOH)](BF₄)₂ (modL' = 2-[(quinolin-8-ylamino)methyl]phenolate) were obtained by vapor diffusion of Et₂O into a methanol solution of Cu(BF₄)₂ and modL in a ratio of 1:1 (Figure 5.3). The observation of 1:1 and 1:2 complexes in the Cu(II) modL system suggests that a similar mixed binding mode for FL₂ and FL₄ with Cu(II). Also, these crystal structures reveal that one oxygen and two nitrogen atoms of the ligands FL_n might bind to Cu(II), as in the crystal structure of [Cu₂(modL')₂(CH₃OH)](BF₄)₂.

Crystallographic data for $[\text{Cu}(\text{modL})_2](\text{BF}_4)_2$ and $[\text{Cu}_2(\text{modL}')_2(\text{CH}_3\text{OH})](\text{BF}_4)_2$ are summarized in Table 5.2, and selected bond lengths and angles are listed in Table 5.3.

As shown in Table 5.1, the fluorescence emission intensities of 1 μM FL_n ($n = 1 - 5$) pH 7.0 buffered solutions at 37 °C are slightly diminished upon addition of one equivalent of CuCl_2 . Introduction of excess NO to buffered $\text{Cu}(\text{FL}_n)$ (1 μM FL_n and 1 μM CuCl_2) solutions (50 mM PIPES, pH 7.0, 100 mM KCl) causes an increase in fluorescence. A 2.5(± 0.1)- or 8.3(± 0.9)-fold increase in fluorescence was observed in the reaction of $\text{Cu}(\text{FL}_1)$ or $\text{Cu}(\text{FL}_2)$ with excess NO over 60 or 70 min (Figure 5.4a and b). Copper complexes $\text{Cu}(\text{FL}_3)$ and $\text{Cu}(\text{FL}_4)$ displayed 3.4(± 0.1)- and 31(± 1)-fold fluorescence enhancements upon treatment of excess NO over 15 and 20 min, respectively (Figure 5.4c and d). Lastly, a 16(± 1)-fold fluorescence increase was observed at 5 min when $\text{Cu}(\text{FL}_5)$ was allowed to react with excess NO (immediate 11(± 2)-fold increase in fluorescence, Figure 5.4e). The lower limit of $\text{Cu}(\text{FL}_5)$ for NO detection is 5 nM. The fluorescence response of the $\text{Cu}(\text{FL}_5)$ probe is specific for NO over other reactive species present in biological systems, including H_2O_2 (1.2(± 0.1)-fold increase), NO_2^- (1.2(± 0.2)-fold increase), NO_3^- (1.2(± 1.3)-fold increase), HNO (1.4(± 0.2)-fold increase) and ONOO^- (2.6(± 0.3)-fold increase) (Figure 5.5). A 2.0(± 0.2)-fold increase in fluorescence was observed when $\text{Cu}(\text{FL}_5)$ allowed to react with superoxide (O_2^-) that was generated by xanthine and xanthine oxidase.^{34,35} Although $\text{Cu}(\text{FL}_5)$ showed a slight fluorescence increase by peroxynitrite and superoxide, it is significantly less than that caused by NO.

Fluorescence enhancement in the NO reactions of $\text{Cu}(\text{FL}_n)$ is not significantly affected in the different buffered solutions and is independent on Cl^- ion. When 20 mM potassium phosphate buffer was used to follow the NO reaction of $\text{Cu}(\text{FL}_5)$, a 10(± 2)-

fold fluorescence increase was exhibited over 5 min (Figure 5.6a). When Cu(FL₅) was prepared *in situ* by the reaction of Cu(NO₃)₂ with FL₅ in a 1:1 ratio, a 12(±2)-fold increase was observed upon addition of excess NO over 5 min (50 mM PIPES, pH 7.0, 100 mM KNO₃), as shown in Figure 5.6b.

These results demonstrate that Cu(FL_n) can detect NO with significant emission turn-on at a physiologically relevant pH. A comparison of the NO reactions of Cu(FL_n) with those of a commercially available NO probe DAF-2 (*o*-diaminofluorescein) clearly highlights the unique ability of copper-based sensors for direct NO sensing (Figure 5.7). DAF-2 displays no increase in fluorescence upon addition of excess NO for 1 h in the absence of O₂ (Figure 5.7a). DAF-2 did exhibit fluorescence turn-on by using an aerobic pH 7.0 buffered solution, indicating that it is capable of detecting only oxidized NO species (Figure 5.7b). On the other hand, Cu(FL_n) showed immediate fluorescence enhancement by NO (Figure 5.4), which clearly indicates that it is a probe that can directly and rapidly visualize nitric oxide *in vitro* and *in vivo*.

Mechanism of Fluorescence Detection of NO by Cu(FL_n).

When FL₁ or FL₅ was titrated with CuCl₂ at 25 °C, the optical absorption spectral changes could be fit to a one-step binding equation affording a dissociation constant (K_d) of 0.25(±0.14) or 1.5(±0.3) μM for Cu(II) ion (Figure 5.8). These K_d values indicate that the reaction solution of FL₁ or FL₅ (1 μM) with CuCl₂ (1 μM) contains Cu(II) ion, free FL_n, and Cu(FL_n) (n = 1, 5). To identify the species responsible for NO detection, the fluorescence of a Cu(II)-free FL₅ solution was monitored upon treatment with excess NO. This solution exhibited only a small, 1.5 ± 0.2-fold increase in fluorescence over 30 min (Figure 5.9a), which suggests that Cu(II) ion is required for fluorescence increase in

the presence of NO. In addition, a slight, 1.3 ± 0.2 -fold, enhancement in fluorescence was observed upon addition of excess NO to a $\text{Cu}(\text{FL}_5)$ solution in the presence of a Cu(II) chelator such as *N,N'*-1,2-ethanediybis-(*N*-(carboxymethyl)glycine) (EDTA) (Figure 5.9b). This result indicates that the binding of FL_5 to Cu(II) is indispensable for NO-induced fluorescence increase. These findings demonstrate that $\text{Cu}(\text{FL}_5)$, and not FL_5 or Cu(II) ion alone, is the nitric oxide indicator showing a significant fluorescence turn-on in our studies.

The mechanism of turn-on emission of $\text{Cu}(\text{FL}_5)$ by NO requires NO-induced reduction of Cu(II) to Cu(I), forming NO^+ . The loss of Cu(II) was monitored by EPR spectroscopy. The Cu(II) EPR signal decreases by 2.9-fold upon introduction of 5 equiv of NO to a DMF solution of $\text{Cu}(\text{FL}_5)$, consistent with reduction to Cu(I) compound (Figure 5.10). It has been reported that the formation of a diamagnetic Cu(I) complex during NO reactions of Cu(II) complexes can restore the quenched fluorescence of a fluorophore coordinated to the paramagnetic metal.^{17,18,22} The fluorescence of FL_5 is unchanged when allowed to react with $[\text{Cu}(\text{CH}_3\text{CN})_4](\text{BF}_4)$ (Figure 5.11a). A mixture of FL_5 and Cu(I) also exhibited only a 1.3 ± 0.1 -fold increase in fluorescence over 30 min with the addition of excess NO over 30 min (Figure 5.11b). These results indicate that reduction of the copper center from Cu(II) to Cu(I) by NO alone does not cause fluorescence enhancement in the NO reaction of $\text{Cu}(\text{FL}_n)$ complexes, which differs from prior observation for Cu(II)-based systems.^{17,18}

The absorption of $\text{Cu}(\text{FL}_5)$ ($\lambda_{\text{max}} = 499$ nm) in pH 7.0 buffered solution red-shifted back to that characteristic of FL_5 ($\lambda_{\text{max}} = 504$ nm) upon treatment with excess NO, which is different from the λ_{max} (506 nm) value of $\text{Cu}^{\text{I}}(\text{FL}_5)$ that is generated *in situ* by reaction of FL_5 with 1 equiv of $[\text{Cu}(\text{CH}_3\text{CN})_4](\text{BF}_4)$ (Figure 5.12). This observation

indirectly suggests dissociation of the fluorescein ligand from copper during the NO reaction of $\text{Cu}(\text{FL}_5)$. The negative ion electrospray mass spectrum of the $\text{Cu}(\text{II})$ species, generated *in situ* by the reaction of a 1:1 ratio of CuCl_2 and FL_5 , displays a peak with m/z of 632.0 corresponding to $[\text{Cu}(\text{FL}_5)\text{Cl} - \text{H}]^-$ (Calcd. m/z 632.0) (Figure 5.13). The reaction of $\text{Cu}(\text{FL}_5)$ with NO in solution (50 mM PIPES, pH 7.0, 100 mM KCl) was monitored by liquid chromatography-mass spectrometry (LC-MS, low resolution MS). A major LC species ($93 \pm 3\%$), shown in Figure 5.14a, displayed three m/z peaks at 564.7, 600.5, and 1128.9, corresponding to the species $[\text{FL}_5 + \text{NO} - 2\text{H}]^-$ (Calcd. m/z 564.1), $[\text{FL}_5 + \text{NO} - \text{H} + \text{Cl}]^-$ (Calcd. m/z 600.1), and $[2(\text{FL}_5 + \text{NO}) - 3\text{H}]^-$, (Calcd. m/z 1129.2). This LC-MS analysis of the NO-induced compound suggests that nitrosation of the FL_5 ligand to create $\text{FL}_5\text{-NO}$ occurs during the reaction of $\text{Cu}(\text{FL}_5)$ with nitric oxide. The fluorescence intensity of the NO reaction solution of $\text{Cu}(\text{FL}_5)$ was unchanged 30 min after purging with Ar or after standing for several days in air. In addition, the $\text{FL}_5\text{-NO}$ species is stable in pH 7.0 buffered solution for several days, as monitored by LC-MS. These results indicate that the NO reaction of $\text{Cu}(\text{FL}_n)$ is irreversible.

To identify the FL_n nitrosation product in the reaction of $\text{Cu}(\text{FL}_n)$ with NO, $\text{FL}_5\text{-NO}$ was separately prepared by reacting FL_5 with sodium nitrite (NaNO_2) under the acidic conditions, which is a general procedure for producing nitroso compounds.³⁶ Treatment of a MeOH solution of FL_5 containing excess NaNO_2 (aq) over ice with HCl (aq) immediately induced a color change from red-orange to bright yellow. A precipitate immediately appeared and the supernatant was collected after 30 min by centrifuging the reaction mixture. Dialysis of the supernatant against water was performed to remove residual NaNO_2 . An orange solid was obtained in moderate yield upon lyophilization. The isolated solid was analyzed by LC-MS and its properties were compared with those of the material obtained in a reaction of $\text{Cu}(\text{FL}_5)$ with NO. LC-MS

analyses of synthetic $\text{FL}_5\text{-NO}$ showed only one LC peak with $m/z = 564.6, 600.1,$ and 1129.2 , which is consistent with the results of the NO reaction product at the identical retention time (Figures 5.14a and 5.14b), $[\text{FL}_5 + \text{NO} - 2\text{H}]^-$ (Calcd. m/z 564.1), $[\text{FL}_5 + \text{NO} - \text{H} + \text{Cl}]^-$ (Calcd. m/z 600.1), and $[2(\text{FL}_5 + \text{NO}) - 3\text{H}]^-$, (Calcd. m/z 1129.2)). In addition, $\text{FL}_5\text{-}^{15}\text{NO}$ was synthesized in an analogous manner by reacting FL_5 and ^{15}N -labeled sodium nitrite ($\text{Na}^{15}\text{NO}_2$). The electrospray-MS (ESI-MS) of $\text{FL}_5\text{-}^{15}\text{NO}$ exhibited m/z peaks at 565.8, 601.3, and 1131.2, as expected from the mass shift of $\Delta m/z$ between ^{14}NO and ^{15}NO (Figure 5.14c). ESI-MS/MS analysis of the major peaks with $m/z = 564.6$ or 565.8 showed that one of fragmentation products of $\text{FL}_5\text{-NO}$ having $m/z = 534.0$ (Calcd. m/z 534.1) derives from loss of the NO moiety of $\text{FL}_5\text{-NO}$ (Figure 5.15). These studies indicate that the NO functionality is incorporated in the final NO-induced reaction product of $\text{Cu}(\text{FL}_5)$.

Nitrosation of FL_n might occur at the secondary amine metal-binding site, as shown in Scheme 5.4, causing dissociation of nitrosated ligand from the copper center. The latter interpretation is based on indirect evidence provided by the optical changes that accompany the NO reaction of a solution of $\text{Cu}(\text{FL}_5)$ (Figure 5.12). There are two likely sites for nitrosation on the fluorophore, namely, the 3'-hydroxyl group of the xanthenone ring or the amino nitrogen atom at the 8-position of the quinoline ring. To determine the site of nitrosation of FL_5 , the $\text{FL}_5\text{-NO}$ species independently generated was investigated by UV-vis and NMR spectroscopy. The properties of fluorescein at different pH values are reflected in significant optical changes upon protonation or deprotonation of the hydroxyl group on the xanthenone ring.³³ Fluorescein generally has a dianionic form with deprotonated hydroxylate and carboxylate groups at pH 7.0.³³ The spectrum of FL_5 is dominated by the fluorescein absorptions in the 400 to 650 nm range. As shown in Figures 5.12 and 5.16, the optical spectrum of $\text{Cu}(\text{FL}_5)$ after reaction

with NO is consistent with that of FL₅, suggesting that a dianionic form of FL₅-NO exists at pH 7.0. The NO reaction product of Cu(FL₅) showed a similar optical changes of FL₅ upon lowering the pH from 7.0 to 5.0 (Figure 5.16), indicating the formation of monoanionic fluorescein.³³ This observation suggests that nitrosation of FL₅ does not occur at the hydroxyl group on the xanthenone ring of the fluorophore.

The ¹⁵N NMR spectrum of FL₅-¹⁵NO was also obtained to clarify further the position of nitrosation. The ¹⁵N NMR spectrum of FL₅-¹⁵NO, generated by reacting FL₅ with Na¹⁵NO₂, exhibited chemical shifts for the labeled ¹⁵NO group at 167.32 and 169.61 ppm in a ratio of 7:3 versus CH₃NO₂ as external reference. These ¹⁵N chemical shifts of FL₅-¹⁵NO are similar to those of previously reported *N*-nitrosamines.^{37,38} Two different chemical shifts might be indicative of the presence of isomers, which is well-known for *N*-nitrosamines.^{36,37} The difference of the two ¹⁵N chemical shifts, $\Delta\delta = 2.29$, is in the range of previously described values for *N*-nitrosamine isomers.³⁷ This distribution of isomers was confirmed by ¹H NMR spectroscopy. The NMR studies of FL₅-NO clearly indicate that FL₅ is *N*-nitrosated at the secondary amine functionality,³⁶ as shown in Scheme 5.4. Formation of an *N*-nitrosamine was previously reported in the reaction of NO with a Cu(II) complex in a mixed water/methanol solution.²² *N*-nitrosation of FL_n will weaken its binding affinity for the metal center. In short, Cu(FL_n) reacts with NO via NO-induced reduction of Cu(II) to Cu(I) forming NO⁺, which nitrosates the FL_n ligand with concomitant dissociation from the copper center. The MS/MS analysis of *N*-nitrosamines FL₅-¹⁴NO and FL₅-¹⁵NO shown in Figure 5.15 supports this conclusion.

One last question remains: Is FL₅-NO the species responsible for enhanced emission? The quantum yield of synthetic FL₅-NO was measured as $\Phi(\text{FL}_5\text{-NO}) = 0.58 \pm 0.02$ compared to fluorescein ($\Phi = 0.95$).³⁹ Thus, FL₅-NO is brighter than FL₅ or Cu(FL₅)

($\Phi(\text{FL}_5) = 0.077 \pm 0.002$ and $\Phi(\text{Cu}(\text{FL}_5)) = 0.063 \pm 0.002$ in Table 5.1). These mechanistic studies thus demonstrate that $\text{Cu}(\text{FL}_n)$ is capable of fluorescence-based NO sensing at pH 7.0 via NO-induced metal reduction followed by release of the *N*-nitrosated fluorescein ligand from the copper center, triggering concomitant fluorescence enhancement (Scheme 5.4). *N*-nitrosated FL_n ($\text{FL}_n\text{-NO}$) is the species responsible for fluorescence enhancement in the reaction of $\text{Cu}(\text{FL}_n)$ with NO, a conclusion supported by density functional theory (DFT) calculations of $\text{FL}_5\text{-NO}$ (*vide infra*).

The reaction pathway shown in Scheme 5.4 might explain the different observed fluorescence responses of $\text{Cu}(\text{FL}_n)$ ($n = 1 - 5$) to NO. Compound $\text{FL}_5\text{-NO}$ could be formed via several different reaction pathways. One such possibility (Scheme 5.5a) is initial NO coordination to Cu(II) followed by NO^+ migration from the copper center to the amine functionality to produce the *N*-nitrosamine. The last step would be dissociation of *N*-nitrosamine from the Cu(I) center. An alternative mechanism of *N*-nitrosamine formation is direct interaction of NO with the deprotonated amine via inner sphere electron transfer from the copper center to the ligand to form the *N*-nitrosamine, as described in a recent report (Scheme 5.5b).²²

A comparison of the NO reactions of the Cu(II) complexes with FL_1 , FL_3 , and FL_5 reveals that the NO-induced fluorescence increase is slower when FL_n has one additional donor atom coordinated to the Cu(II) center (Figure 5.4). Based on the mechanism proposed above, this observation might be explained by two possible factors. The Cu(II) complexes containing tetradentate ligands such as FL_1 and FL_3 may be less able to accommodate the structural rearrangements required for the planar to tetrahedral conversion upon Cu(I) complex formation as compared to the tridentate ligand FL_5 . As a result, the rate of the NO reactions of $\text{Cu}(\text{FL}_n)$ ($n = 1, 3$) compared with $\text{Cu}(\text{FL}_5)$ decreases and consequently reduces the rate of formation of the $\text{FL}_n\text{-NO}$ species

responsible for fluorescence enhancement. The second possibility concerns the dissociation of $\text{FL}_n\text{-NO}$ from copper. The presence of an additional donor atom in the FL_n chelate may decelerate the dissociation of $\text{FL}_n\text{-NO}$ from copper, which would also result in a slower fluorescence increase. A comparison of the K_d values for $\text{Cu}(\text{FL}_1)$ and $\text{Cu}(\text{FL}_5)$, $0.25(\pm 0.14) \mu\text{M}$ and $1.5(\pm 0.3) \mu\text{M}$ (Figure 5.8), respectively, supports this notion assuming that the K_d values for the *N*-nitrosated amine product follow this trend. At present, we are unable to determine whether one of these factors plays the main role in influencing the NO reactivity of $\text{Cu}(\text{FL}_n)$ or perhaps a combination of both.

Introduction of additional donor atoms to FL_n could also affect the electronic properties of the copper center. To address this issue, electrochemical studies were also attempted. The measurements of the $\text{Cu}(\text{FL}_n)$ redox potentials, however, was not successful and the redox potential of free Cu(II) ion was mainly observed. This might be a consequence of high K_d values for the equilibrium in Scheme 5.4, which is already shown for $\text{Cu}(\text{FL}_n)$ ($n = 1, 5$), and the corresponding presence of high concentrations of free Cu(II) ion in solution.

Although the mechanism of NO reaction with $\text{Cu}(\text{FL}_n)$ is not unequivocally proved by these experiments, the present work suggests that both electronic effects and binding equilibrium may affect the formation of *N*-nitrosamine. Moreover, the ability to detect NO as well as the different reactivity observed for the copper fluorescein compounds described herein represent an invaluable platform for devising improved NO sensors, suitable for the elucidation of NO function *in vivo*.

DFT Calculation of FL_5 versus $\text{FL}_5\text{-NO}$.

The “off-on” properties of fluorescence-based sensors such as FL_n are believed to operate by the well-established photoinduced electron transfer (PET) mechanism.^{40,41}

The presence of a covalently bound nitrogen atom with free lone pair electrons will quench the fluorescence of the sensor in the absence of analyte. Perturbation of this nitrogen atom lone pair, such as by binding of a diamagnetic metal ion,³¹ will alleviate this quenching process, causing fluorescence "turn-on." Note that binding to a paramagnetic metal ion such as Cu(II) is expected to preserve or enhance the quenching behavior of fluorophores.⁴²

For the FL₅/FL₅-NO system, it is interesting to note that both species have a nitrogen atom-based free electron lone pair that might be expected to contribute to fluorescence quenching. In order to provide some explanation for the fluorescence "turn-on" observed in the nitrosated species, density functional theory (DFT) calculations were performed. These calculations provide valuable information about the molecular orbitals (MOs) involved in the PET process. For a fluorophore to be quenched by an electron donor group, the MO associated with that donor must lie energetically within the region of the frontier orbitals associated with the fluorophore. For FL₅, the nitrogen atom lone pair is conjugated into the quinoline group, forming an antibonding interaction, as can be seen from the node between these two groups (Figure 5.17c), that generates a filled MO that lies just below the HOMO of the fluorophore (HOMO-1, Figure 5.18). Excitation of the fluorophore causes a reordering of these MOs due to electronic relaxation in the excited state, which does not affect the energy of the donor orbital. Electron transfer from the donor orbital into the now lower-lying, half-occupied MO of the fluorophore is expected to cause the observed quenching.

In the case of FL₅-NO, the donor nitrogen atom has a nearly planar geometry with a normal vector in the plane of the quinoline group (Figure 5.17d), thus preventing the same conjugation present in FL₅. Instead, the nitrogen atom lone pair interacts with the π -system of the NO group, producing a stabilized MO at a significantly lower

energy (Figure 5.19). This MO lies well below the frontier orbitals of the fluorophore and cannot act as an electron donor for purposes of quenching. This result is in agreement with the observed fluorescence "turn-on" of the nitrosated species.

Summary

Five fluorescein-based ligands (FL_n , $n = 1 - 5$) were synthesized as the framework for Cu(II)-based complexes that could serve as bio-sensors for nitric oxide. The Cu(II) species $Cu(FL_n)$ generated *in situ* by the reaction of FL_n with $CuCl_2$, exhibited a significant increase in fluorescence upon addition of NO in pH 7.0 buffered solution. Turn-on emission of $Cu(FL_n)$ by NO would occur by reduction of Cu(II) to Cu(I), forming NO^+ , which nitrosates FL_n to create FL_n-NO , as suggested by spectroscopic and product analyses of the reaction. Dissociation from the copper center leads to emission turn-on. DFT calculations of FL_5-NO relative to FL_5 also support that *N*-nitrosation of FL_n triggers fluorescence enhancement. The $Cu(FL_n)$ probes are the first examples of direct NO detection using metal complexes with fluorescence increase at pH 7.0, when excited at a visible wavelength. The fluorescence response to NO of $Cu(FL_n)$ is specific for NO over other biologically relevant reactive species such as O_2^- , H_2O_2 , NO_2^- , NO_3^- , HNO, and $ONOO^-$. Therefore, the Cu(II) fluorescent complexes can directly and specifically detect NO at a physiologically relevant pH.

References

- (1) Murad, F., *Angew. Chem. Int. Ed.* **1999**, *38*, 1856-1868.
- (2) Leone, A. M.; Palmer, R. M. J.; Knowles, R. G.; Francis, P. L.; Ashton, D. S.; Moncada, S., *J. Biol. Chem.* **1991**, *266*, 23790-23795.
- (3) Moncada, S.; Palmer, R. M. J.; Higgs, E. A., *Pharmacol. Rev.* **1991**, *43*, 109-142.

- (4) Conner, E. M.; Grisham, M. B., *Methods Enzymol.* **1995**, *7*, 3-13.
- (5) Marletta, M. A.; Hurshman, A. R.; Rusche, K. M., *Curr. Opin. Chem. Biol.* **1998**, *2*, 656-663.
- (6) Ricciardolo, F. L. M.; Sterk, P. J.; Gaston, B.; Folkerts, G., *Physiol. Rev.* **2004**, *84*, 731-765.
- (7) Packer, L., *Methods in Enzymology, Nitric Oxide. Part B, Physiological and Pathological Processes*. Academic Press: San Diego, CA, 1996; Vol. 269.
- (8) Nagano, T.; Yoshimura, T., *Chem. Rev.* **2002**, *102*, 1235-1269
- (9) Hilderbrand, S. A.; Lim, M. H.; Lippard, S. J., *In Topics in Fluorescence Spectroscopy*, Geddes, C. D.; Lakowicz, J. R., Eds. Springer: 2005; pp 163-188.
- (10) Gomes, A.; Fernandes, E.; Lima, J. L. F. C., *J Fluoresc.* **2006**, *16*, 119-139.
- (11) Wink, D. A.; Grisham, M. B.; Mitchell, J. B.; Ford, P. C., *Methods Enzymol.* **1996**, *268*, 12-31.
- (12) Franz, K. J.; Singh, N.; Spingler, B.; Lippard, S. J., *Inorg. Chem.* **2000**, *39*, 4081-4092.
- (13) Franz, K. J.; Singh, N.; Lippard, S. J., *Angew. Chem. Int. Ed.* **2000**, *39*, 2120-22.
- (14) Hilderbrand, S. A.; Lippard, S. J., *Inorg. Chem.* **2004**, *43*, 4674-4682.
- (15) Hilderbrand, S. A.; Lippard, S. J., *Inorg. Chem.* **2004**, *43*, 5294-5301.
- (16) Lim, M. H.; Kuang, C.; Lippard, S. J., *ChemBioChem* **2006**, in press.
- (17) Lim, M. H.; Lippard, S. J., *J. Am. Chem. Soc.* **2005**, *127*, 12170-12171.
- (18) Smith, R. C.; Tennyson, A. G.; Lim, M. H.; Lippard, S. J., *Org. Lett.* **2005**, *7*, 3573-3575.
- (19) Lim, M. H.; Xu, D.; Lippard, S. J., *Nat. Chem. Biol.* **2006**, in press.
- (20) Hilderbrand, S. A.; Lim, M. H.; Lippard, S. J., *J. Am. Chem. Soc.* **2004**, *126*, 4972-4978.
- (21) Lim, M. H.; Lippard, S. J., *Inorg. Chem.* **2004**, *43*, 6366-6370.

- (22) Tsuge, K.; DeRosa, F.; Lim, M. D.; Ford, P. C., *J. Am. Chem. Soc.* **2004**, *126*, 6564-6565.
- (23) Chang, C. J.; Lippard, S. J., *In Neurodegenerative Diseases and Metal Ions: Metal Ions in Life Sciences*, Sigel, A.; Sigel, H.; Sigel, R. K. O., Eds. John Wiley & Sons: 2006; Vol. 1, pp 321-370.
- (24) *SMART: Software for the CCD Detector System*, version 5.626; Bruker AXS: Madison, WI, 2000.
- (25) Kuzelka, J.; Mukhopadhyay, S.; Spingler, B.; Lippard, S. J., *Inorg. Chem.* **2004**, *43*, 1751-1761.
- (26) Sheldrick, G. M. *SADABS: Area-Detector Absorption Correction*, University of Göttingen: Göttingen, Germany, 1996.
- (27) *SAINTPLUS: Software for the CCD Detector System*, version 5.01; Bruker AXS: Madison, WI, 1998.
- (28) *SHELXTL: Program Library for Structure Solution and Molecular Graphics*, version 6.1; Bruker AXS: Madison, WI, 2001.
- (29) Spek, A. L. *PLATON, A Multipurpose Crystallographic Tool*, Utrecht University: Utrecht, The Netherlands, 2000.
- (30) Roth, R.; Erlenmeyer, H., *Helv. Chim. Acta* **1954**, *37*, 1064-1068.
- (31) Nolan, E. M.; Jaworski, J.; Okamoto, K.-I.; Hayashi, Y.; Sheng, M.; Lippard, S. J., *J. Am. Chem. Soc.* **2005**, *127*, 16812-16823.
- (32) Nolan, E. M.; Burdette, S. C.; Harvey, J. H.; Hilderbrand, S. A.; Lippard, S. J., *Inorg. Chem.* **2004**, *43*, 2624-2635.
- (33) Sjöback, R.; Nygren, J.; Kubista, M., *Spectrochim. Acta Part A* **1995**, *51*, L7-L21.
- (34) Sono, M., *J. Biol. Chem.* **1989**, *264*, 1616-1622.

- (35) Yang, D.; Wang, H.-L.; Sun, Z.-N.; Chung, N.-W.; Shen, J.-G., *J. Am. Chem. Soc.* **2006**, *128*, 6004-6005.
- (36) Lee, J.; Chen, L.; West, A. H.; Richter-Addo, G. B., *Chem. Rev.* **2002**, *102*, 1019-1065 and references cited therein.
- (37) Bonnett, R.; Holleyhead, R.; Johnson, B. L.; Randall, E. W., *J. C. S. Perkin I* **1975**, *22*, 2261-2264.
- (38) Karaghiosoff, K.; Klapoetke, T. M.; Mayer, P.; Piotrowski, H.; Polborn, K.; Willer, R. L.; Weigand, J. J., *J. Org. Chem.* **2006**, *71*, 1295-1305.
- (39) Brannon, J. H.; Madge, D., *J. Phys. Chem.* **1978**, *82*, 705-709.
- (40) Chanon, M.; Hawley, M. D.; Fox, M. A., *In Photoinduced Electron Transfer*, Fox, M. A.; Chanon, M., Eds. Elsevier: Amsterdam, 1988; pp 1-60.
- (41) Callan, J. F.; de Silva, A. P.; Magri, D. C., *Tetrahedron* **2005**, *61*, 8551-8588.
- (42) Chang, J. H.; Choi, Y. M.; Shin, Y.-K., *Bull. Kor. Chem. Soc.* **2001**, *22*, 527-530.

Table 5.1. Spectroscopic Results^a

	Absorption		Emission		Ref.
	λ_{\max} (nm), ϵ ($\times 10^4$ M ⁻¹ cm ⁻¹)		λ_{\max} (nm), Φ^b or %		
	Unbound	Cu(II) ^c	Unbound (Φ)	Cu(II) ^d	
FL ₁	504, 4.3 ± 0.1	499, 4.0 ± 0.1	520, 0.083 ± 0.004	520, 32% ± 2	this work
FL ₂	503, 3.8 ± 0.5	496, 3.8 ± 0.3	520, 0.084 ± 0.002	520, 26% ± 3	this work
FL ₃	503, 3.9 ± 0.1	497, 3.9 ± 0.5	520, 0.31 ± 0.01	520, 19% ± 2	this work
FL ₄	505, 6.9 ± 0.1	496, 5.7 ± 0.1	520, 0.024 ± 0.001	520, 30% ± 3	31 & this work
FL ₅	504, 4.2 ± 0.1	499, 4.0 ± 0.1	520, 0.077 ± 0.002	520, 18% ± 3	31 & this work

^a All spectroscopic measurements were performed at pH 7.0 by using 50 mM PIPES, 100 mM KCl buffer. ^b Reported quantum yields are based on fluorescein, $\Phi = 0.95$ in 0.1 N NaOH.³⁹ ^c One equivalent of CuCl₂ is added. ^d % of fluorescence decrease upon addition of 1 equiv of Cu(II) to the pH 7.0 buffered solution of FL_n (1 μ M), relative to that of free FL_n (50 mM PIPES, 100 mM KCl).

Table 5.2. Summary of X-ray Crystallographic Data

	[Cu(modL) ₂](BF ₄) ₂ ·2CH ₃ OH	[Cu ₂ (modL') ₂ (CH ₃ OH)](BF ₄) ₂ ·CH ₃ OH
formula	C ₃₄ H ₃₂ B ₂ CuF ₈ N ₄ O ₄	C ₃₄ H ₃₄ B ₂ Cu ₂ F ₈ N ₄ O ₄
formula weight	797.80	863.35
space group	P2 ₁ /n	P2 ₁ /n
a, Å	8.1902(8)	18.9017(9)
b, Å	11.6112(11)	11.5733(5)
c, Å	18.2776(18)	33.3820(15)
β, deg	95.235(2)	103.5840(10)
V, Å ³	1730.9(3)	7098.2(6)
Z	2	8
ρ _{calc} , g/cm ³	1.531	1.616
crystal size (mm ³)	0.10 x 0.08 x 0.03	0.15 x 0.10 x 0.08
T, °C	-100	-100
μ(Mo Kα), mm ⁻¹	0.719	1.285
θ limits, deg	2.08 – 26.49	1.87 – 26.50
total no. of data	14096	57985
no. of unique data	3585	14691
no. of params	258	1113
GOF ^a	1.046	1.057
R ^b	0.0482	0.0575
wR ^{2 c}	0.1210	0.1079
max, min peaks, e/Å ³	0.731, -0.407	0.623, -0.340

^a GOF (Goodness of fit on F²) = {Σ[w(F_o²-F_c²)²]/(m-n)}^{1/2} (m = number of reflections, n = number of parameters refined)

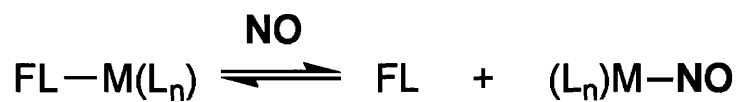
^b R = Σ||F_o|-|F_c||/Σ|F_o|

^c wR² = {Σ[w(F_o²-F_c²)²]/Σ[w(F_o²)²]}^{1/2}

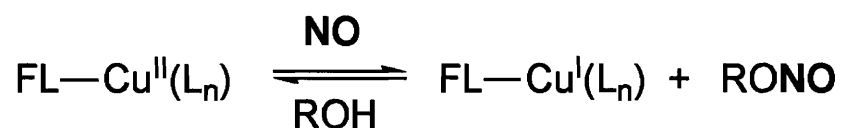
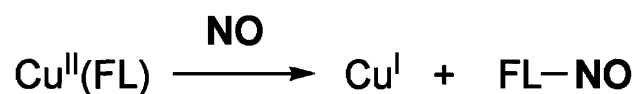
Table 5.3. Selected Bond Distances (Å) and Angles (deg)^a

[Cu(L)₂](BF₄)₂·2CH₃OH			
Cu1-N1	1.996(2)		
Cu1-N2	2.033(2)		
N1-Cu1-N2	82.66(16)		
N1-Cu1-N1A	180.000(1)		
N1-Cu1-N2A	82.74(9)		
[Cu₂(L)₂(CH₃OH)](BF₄)₂·CH₃OH			
Cu1-N1	1.956(3)	O1-Cu1-O2	77.46(11)
Cu1-N2	2.005(4)	Cu1-O1-Cu2	100.87(12)
Cu1-O1	1.927(3)	Cu1-O2-Cu2	99.97(12)
Cu1-O2	1.947(3)	N3-Cu2-N4	85.36(15)
N1-Cu1-N2	85.25(14)	O1-Cu2-O2	76.65(11)

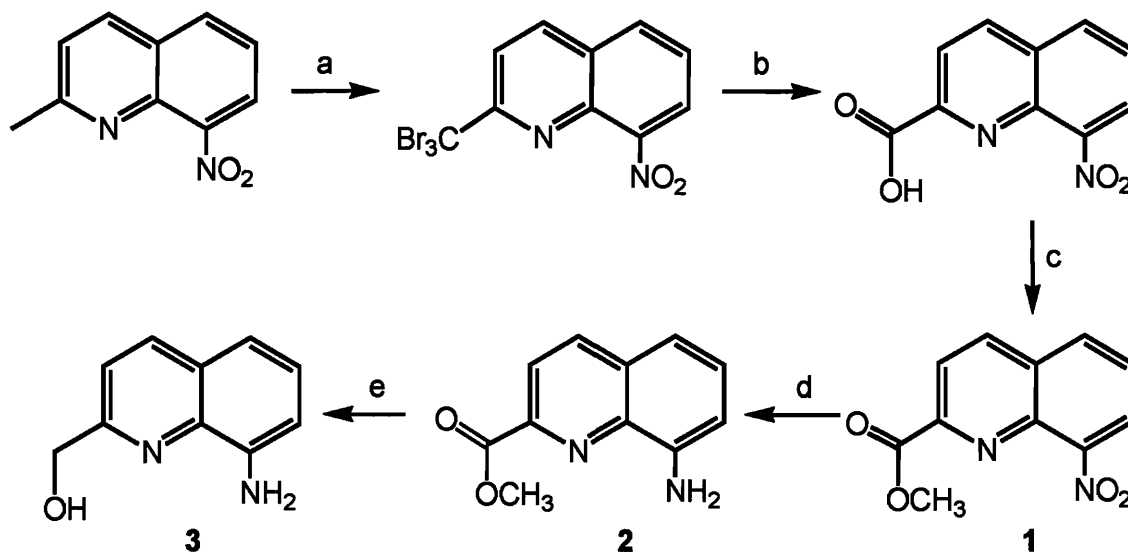
^a Numbers in parentheses are estimated standard deviations of the last significant figures. Atoms are labeled as indicated in Figure 5.3.

(a) Fluorophore Displacement by NO

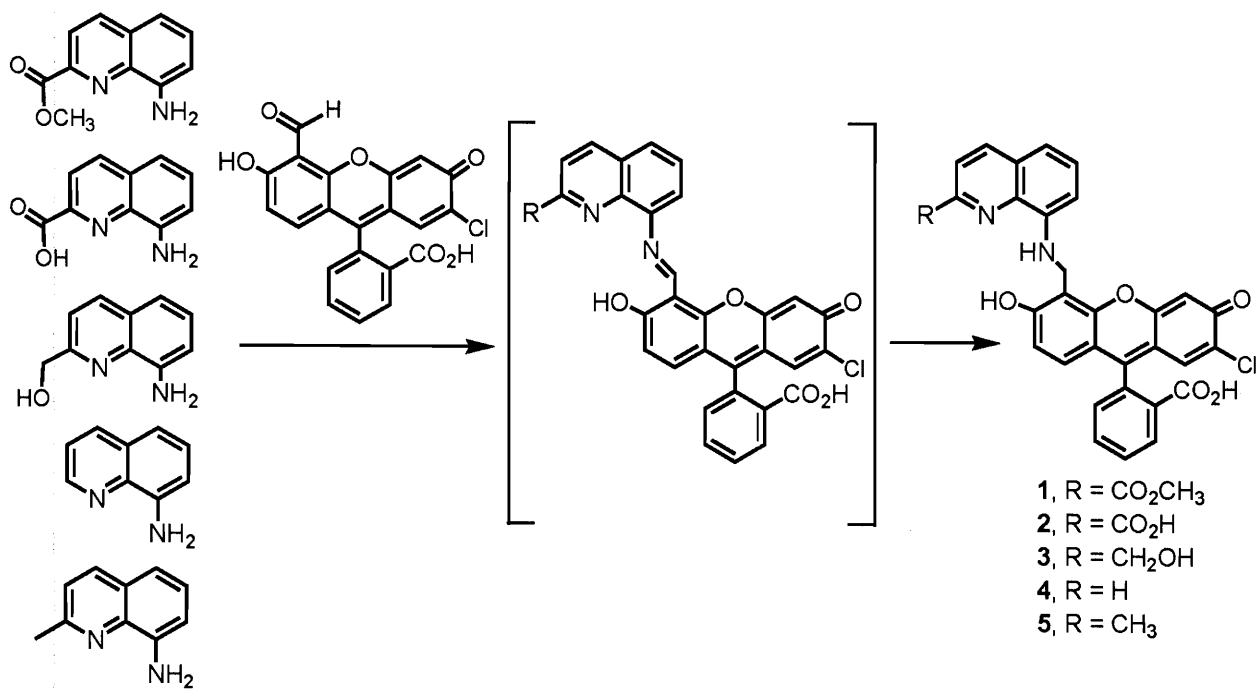
FL = Fluorophore ligand, M = Metal, L = Ligand

(b) Copper(II) Reduction by NO**(c) Ligand Nitrosation via Cu(II) reduction by NO**

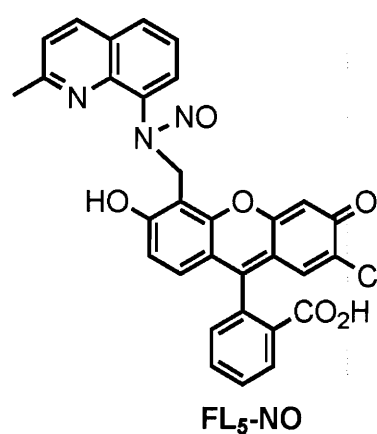
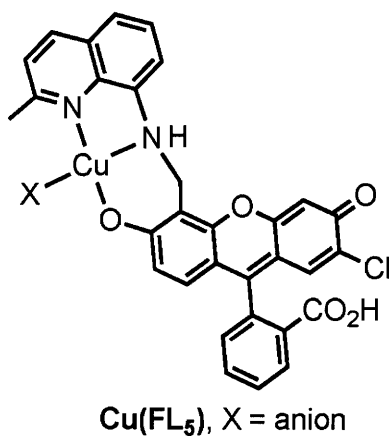
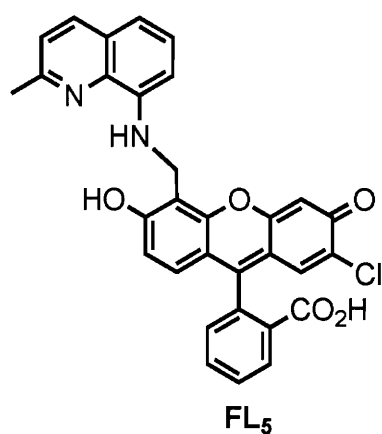
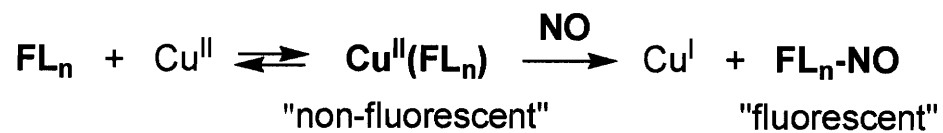
Scheme 5.1. Strategies for Nitric Oxide Detection.



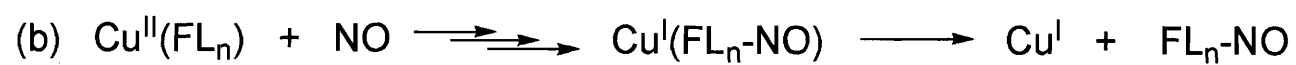
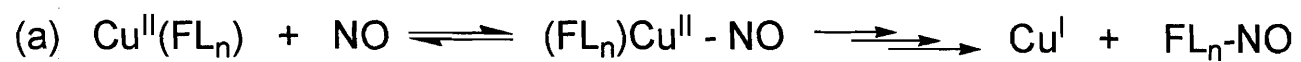
Scheme 5.2. Syntheses of Compounds 1, 2, and 3. (a) Br_2 , AcONa , and AcOH (ref. 30), (b) 20% H_2SO_4 (aq) (ref. 30), (c) $\text{Me}_3\text{SiCHN}_2$, (d) Pd/C , H_2 , and (e) NaBH_4 .



Scheme 5.3. Syntheses of FL_n Ligands (n = 1 – 5, FL_4^{31}).



Scheme 5.4. NO Reactivity of Cu(FL_n).



Scheme 5.5. Plausible Pathways of the Reaction of $\text{Cu}(\text{FL}_n)$ with NO.

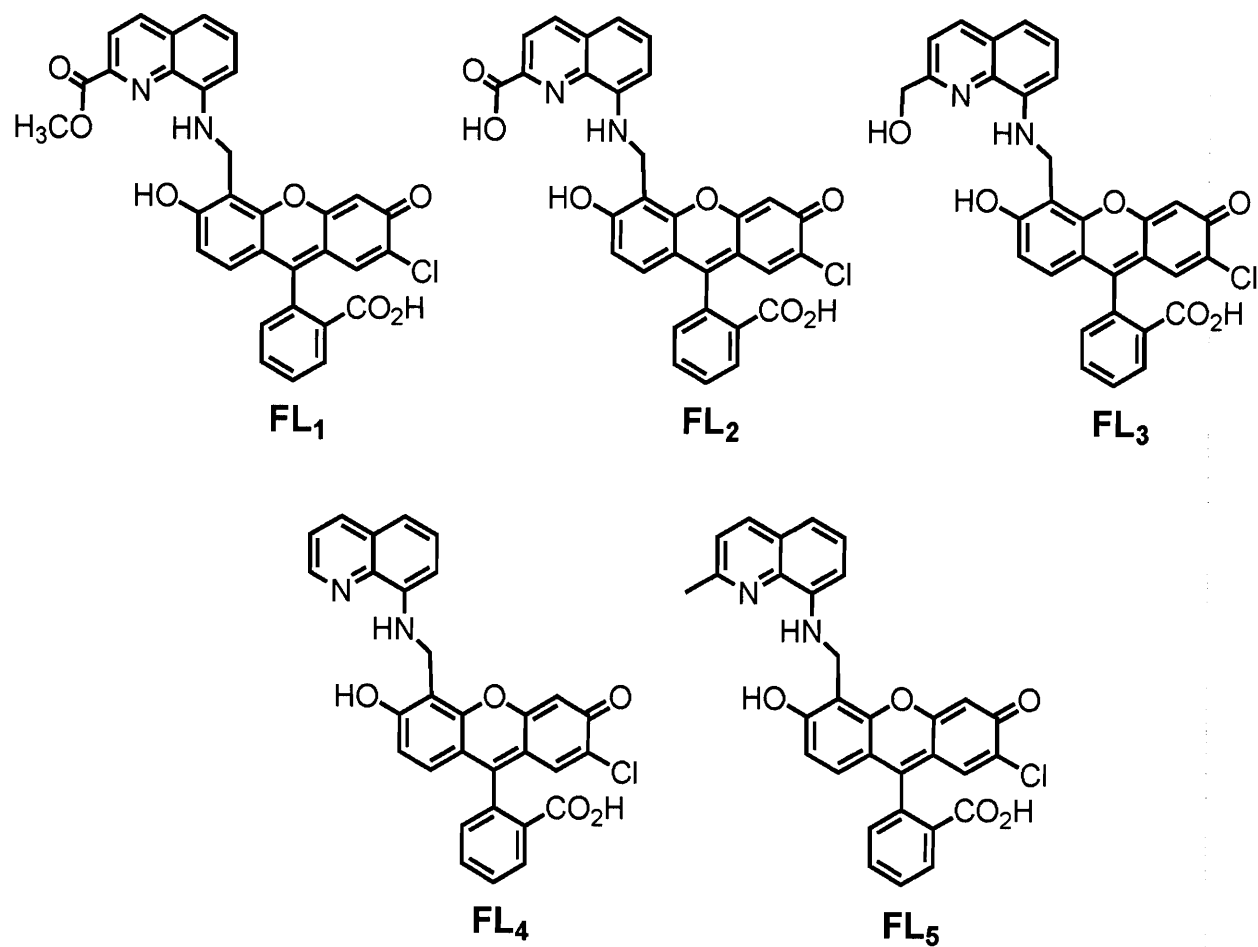


Figure 5.1. Schematic drawings of FL_n (n = 1 - 5).

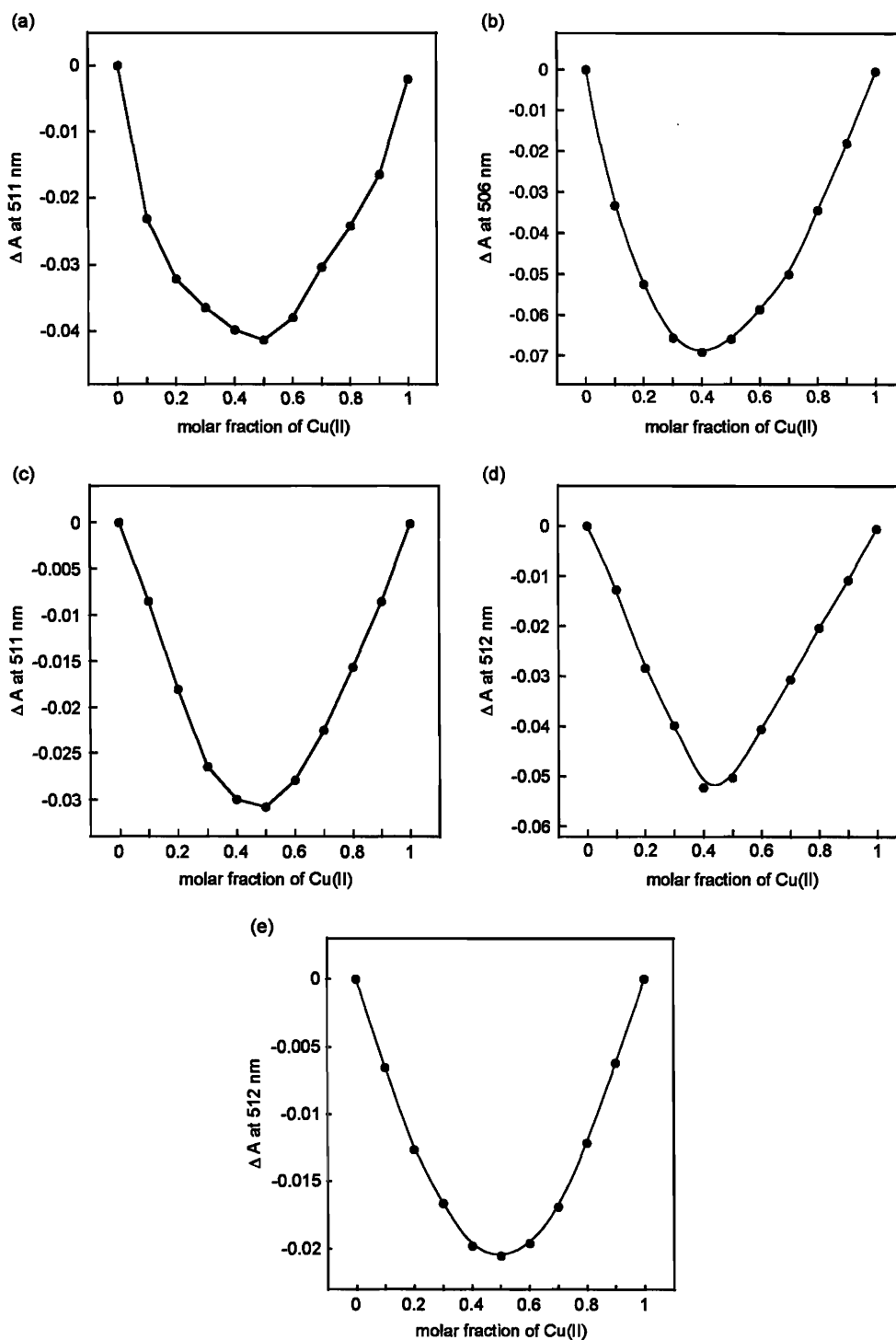


Figure 5.2. Job's plot for the formation of the $FL_n:Cu(II)$ complex ($n = 1$ (a), 2 (b), 3 (c), 4 (d), and 5 (e)) determined by using UV-vis spectroscopy in a pH 7.0 buffered solution (50 mM PIPES, 100 mM KCl). The concentrations of the initial FL_n ($n = 1 - 5$) and Cu(II) solutions were 10, 10, 5, 5, and 5 μM , respectively.

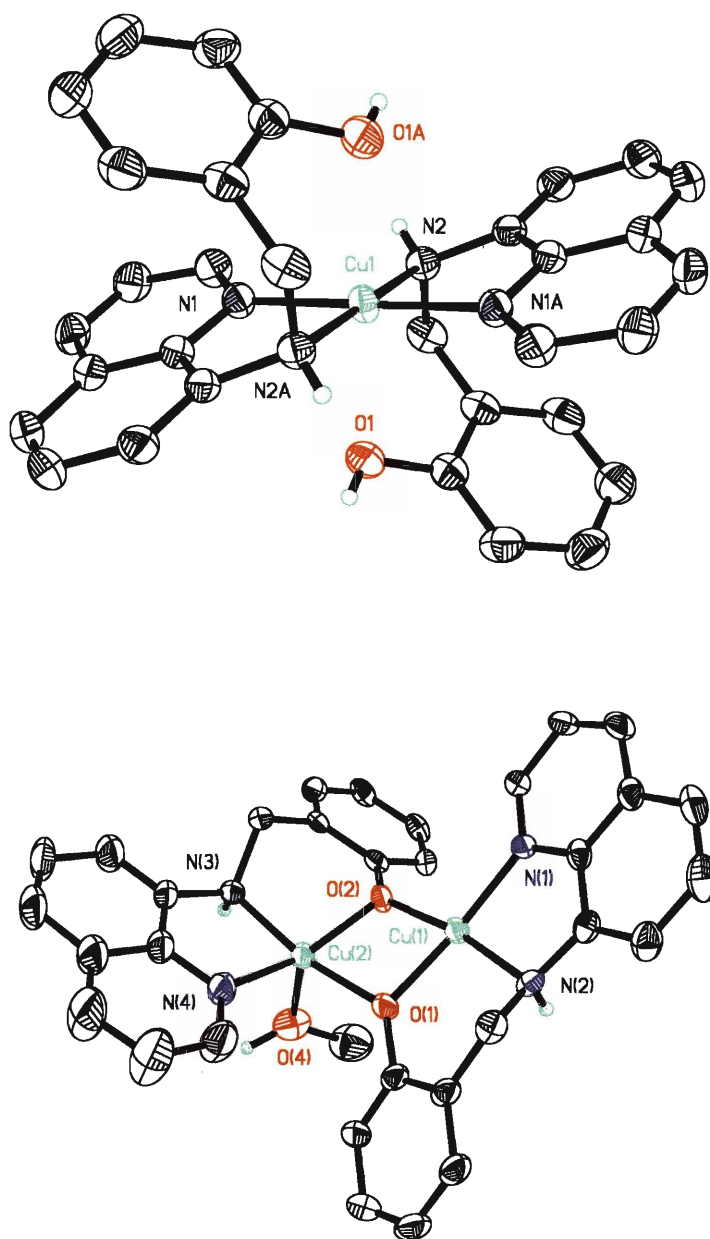


Figure 5.3. ORTEP diagrams of $[\text{Cu}(\text{modL})](\text{BF}_4)_2$ (top) and $[\text{Cu}_2(\text{modL}')_2(\text{CH}_3\text{OH})](\text{BF}_4)_2$ (bottom) showing 50% probability thermal ellipsoids. The Cu1–O1 distance is 2.494 Å in the structure of $[\text{Cu}(\text{modL})](\text{BF}_4)_2$. The BF_4^- anions were omitted in the figure.

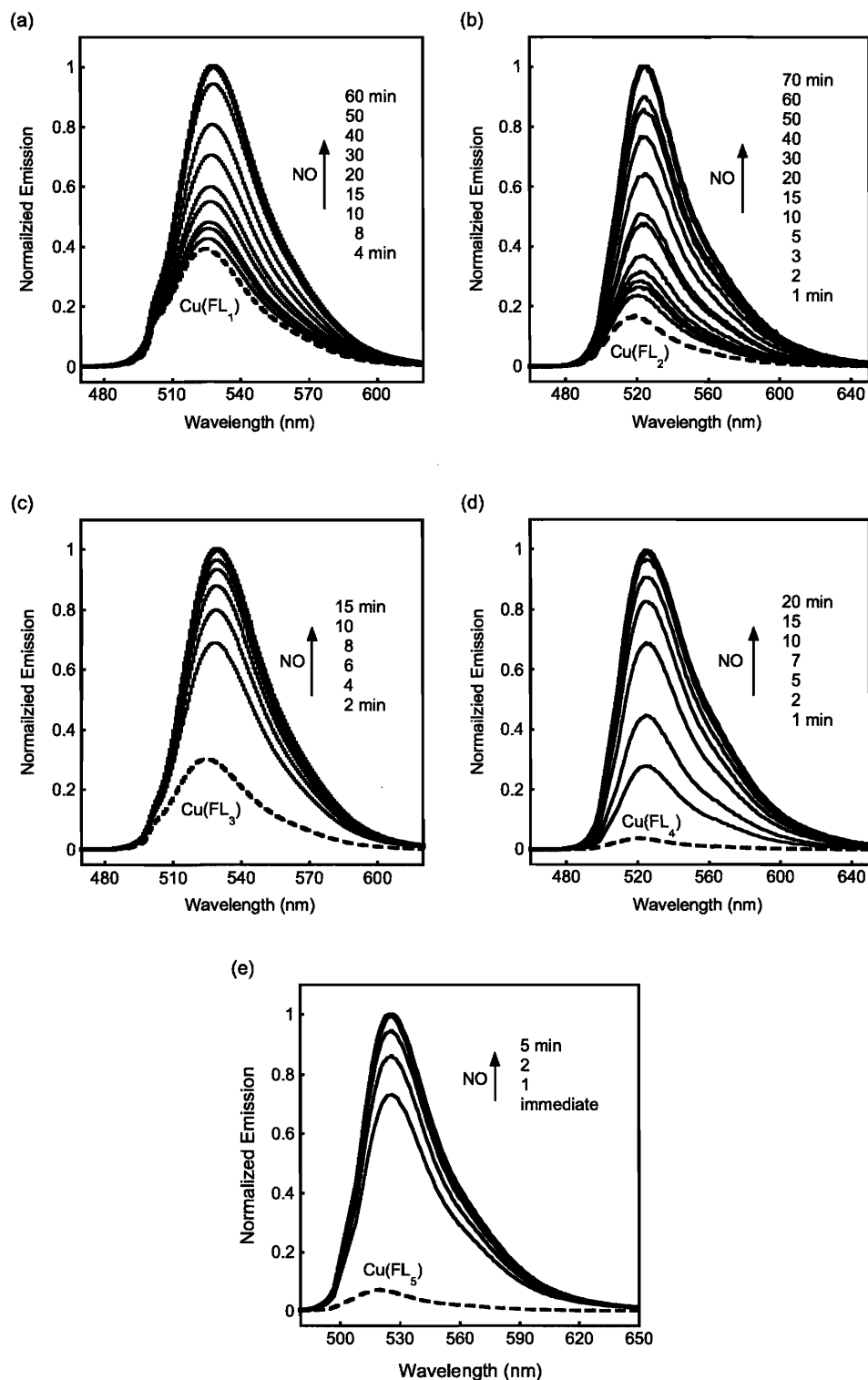


Figure 5.4. Fluorescence emission spectra of a solution of $\text{Cu}(\text{FL}_n)$ ($1 \mu\text{M FL}_n$ and $1 \mu\text{M CuCl}_2$) in deoxygenated buffered solution (50 mM PIPES, pH 7.0, 100 mM KCl) before (dashed line) and after (solid lines) admission of 1300 equiv of NO (g) at 37 °C.

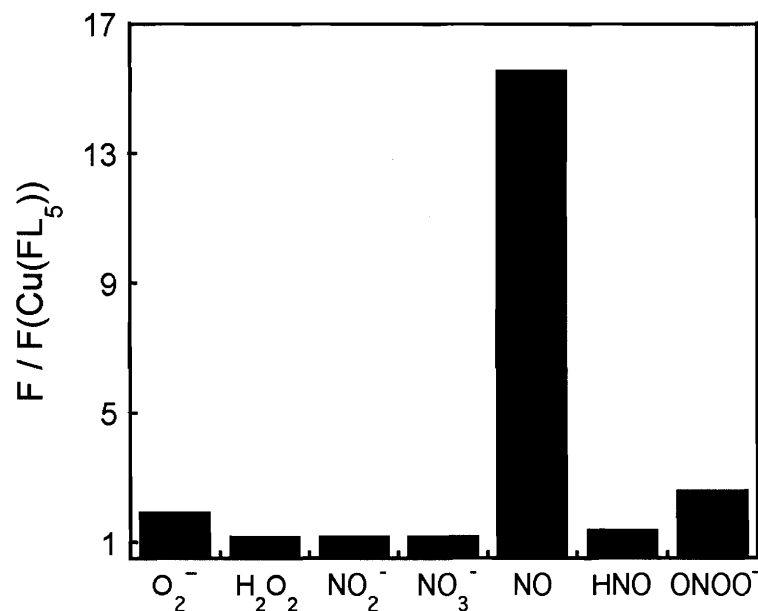


Figure 5.5. Specificity of Cu(FL₅) for NO in buffered aqueous solution (50 mM PIPES, pH 7.0, 100 mM KCl), determined as the fluorescence response of Cu(FL₅) after addition of 100 equivalents of O₂⁻ (0.1 U xanthine oxidase and 100 μM xanthine), H₂O₂, NO₂⁻, NO₃⁻, HNO (Angeli's salt Na₂N₂O₃), NO (1.9 mM NO-saturated aqueous solution) and ONOO⁻ (sodium peroxyxynitrite) for 2 h. The excitation wavelength was 503 nm. All data (F) are normalized with respect to the emission of Cu(FL₅) (F(Cu(FL₅))). The Cu(II) species Cu(FL₅) was prepared *in situ* by reacting FL₅ (1 μM) with CuCl₂ (1 μM).

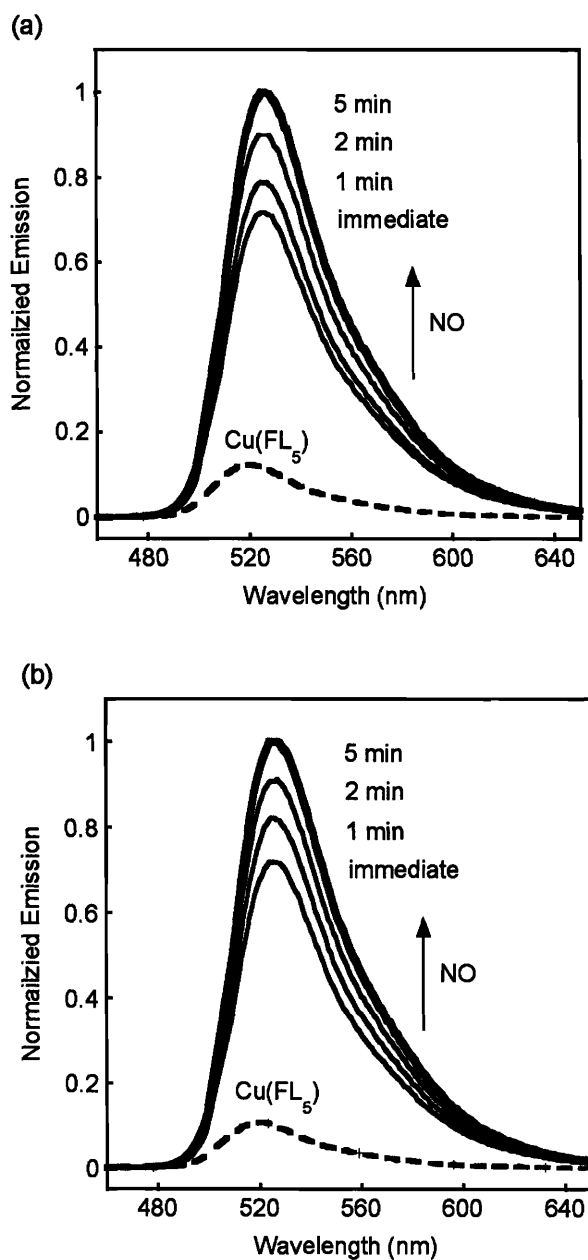


Figure 5.6. Fluorescence emission spectra of a solution of $\text{Cu}(\text{FL}_5)$ upon addition of excess NO. (a) Fluorescence response of $\text{Cu}(\text{FL}_5)$ ($1 \mu\text{M}$ FL_5 and $1 \mu\text{M}$ CuCl_2) in a deoxygenated pH 7.0 buffered solution (20 mM phosphate) before (dashed line) and after (solid lines) addition of 1300 equiv of NO (g) at 37°C . (b) Fluorescence emission spectra of an aerobic solution of $\text{Cu}(\text{FL}_5)$ ($1 \mu\text{M}$ FL_5 and $1 \mu\text{M}$ $\text{Cu}(\text{NO}_3)_2$) upon admission of 1300 equiv of NO at 37°C (50 mM PIPES, pH 7.0, 100 mM KNO_3).

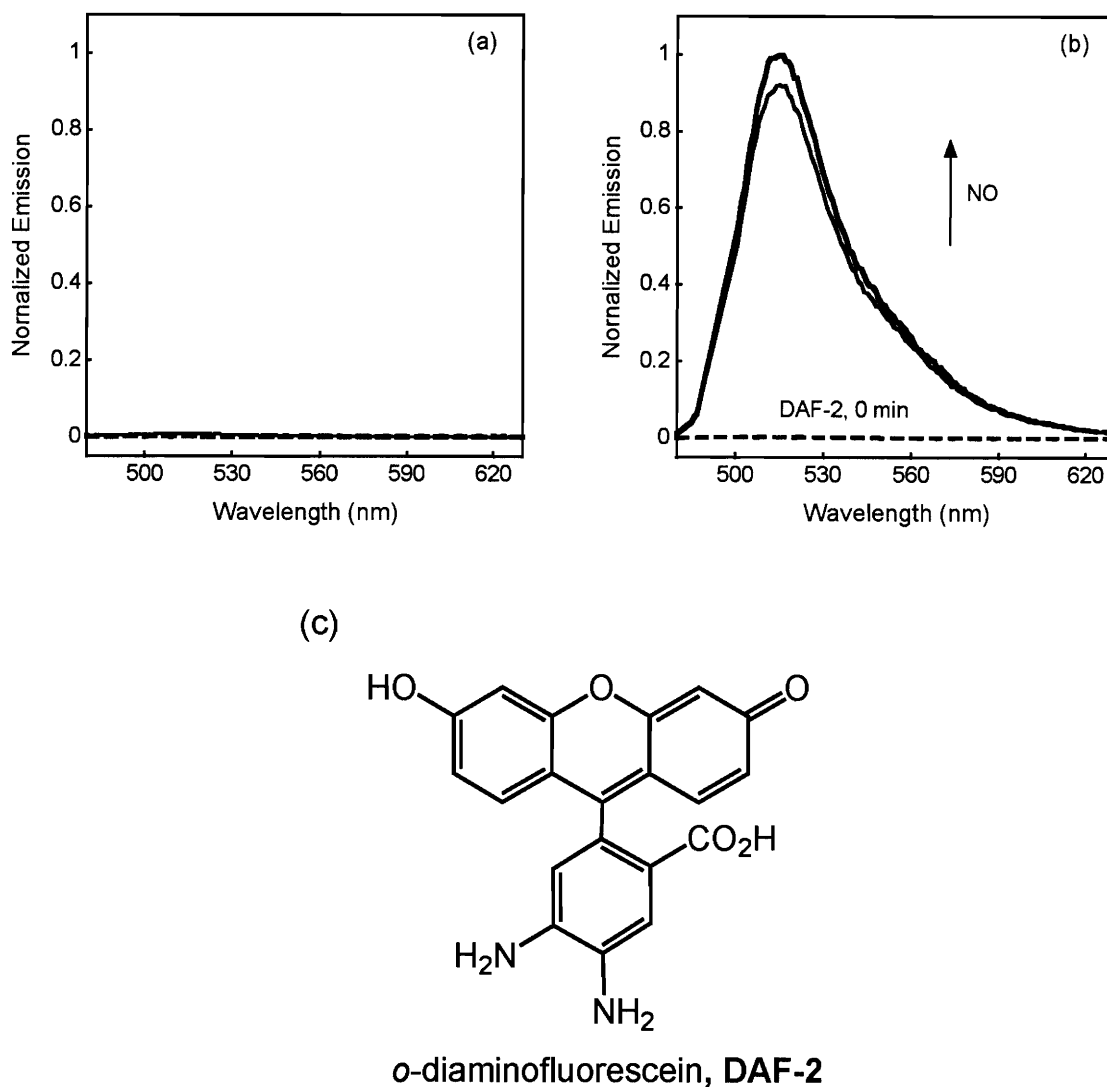


Figure 5.7. Fluorescence response of DAF-2 to NO. (a) Fluorescence emission spectra ($\lambda_{\text{ex}} = 495 \text{ nm}$) of DAF-2 (1 μM) before (dashed line) and 60 min after (solid line) treatment with 1300 equiv of NO in an anaerobic buffered solution (50 mM PIPES, pH 7.0, 100 mM KCl). (b) Fluorescence emission spectra ($\lambda_{\text{ex}} = 495 \text{ nm}$) of DAF-2 (1 μM) before (dashed black line) and 1 and 6 min after addition of 1300 equiv of NO (solid lines) in an aerobic buffered solution (50 mM PIPES, pH 7.0, 100 mM KCl). (c) Schematic drawing of DAF-2.

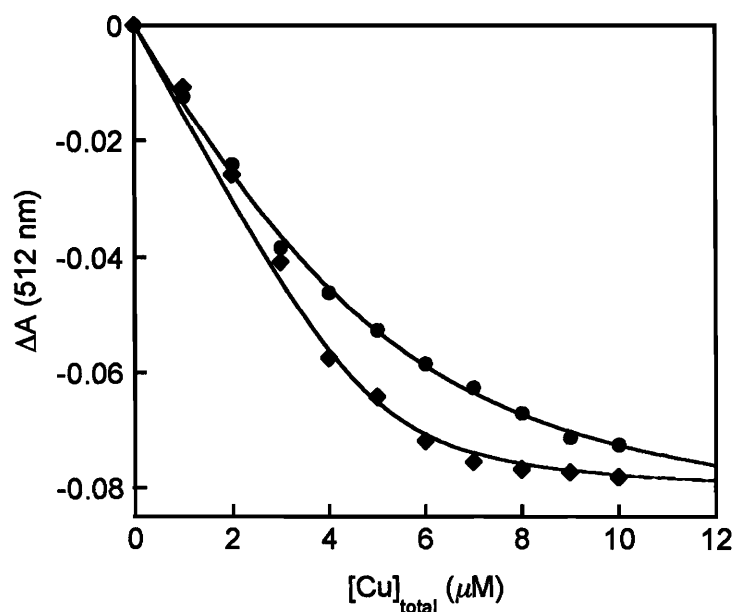
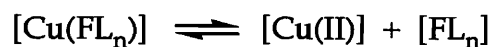


Figure 5.8. Measurement of the dissociation constant (K_d) of $\text{Cu}(\text{FL}_1)$ (\blacklozenge) or $\text{Cu}(\text{FL}_5)$ (\bullet). CuCl_2 was titrated into a $5 \mu\text{M}$ FL_1 or FL_5 solution (50 mM PIPES, pH 7.0, 100 mM KCl). The formation of $\text{Cu}(\text{FL}_1)$ or $\text{Cu}(\text{FL}_5)$ was followed by the absorbance change (ΔA) at 512 nm. The titration trace was fit to the equation

$$\Delta A = \frac{\Delta A_{\infty} \times \left([\text{Cu}]_{\text{total}} + [\text{FL}^n]_{\text{total}} + K_d - \sqrt{([\text{Cu}]_{\text{total}} + [\text{FL}^n]_{\text{total}} + K_d)^2 - 4 \times [\text{FL}^n]_{\text{total}} \times [\text{Cu}]_{\text{total}}} \right)}{2 \times [\text{FL}^n]_{\text{total}}}$$

which is deduced from the equilibrium for one-step binding of $\text{Cu}(\text{II})$ to FL_n with a dissociation constant of K_d :



In the fitting equation and the figure, $[\text{Cu}]_{\text{total}}$ is the sum of $[\text{Cu}(\text{II})]$ and $[\text{Cu}(\text{FL}_n)]$. It equals the total amount of CuCl_2 titrated into the solution divided by volume. $[\text{FL}_n]_{\text{total}}$ is the sum of $[\text{FL}_n]$ and $[\text{Cu}(\text{FL}_n)]$ ($n = 1, 5$) and equals $5 \mu\text{M}$.

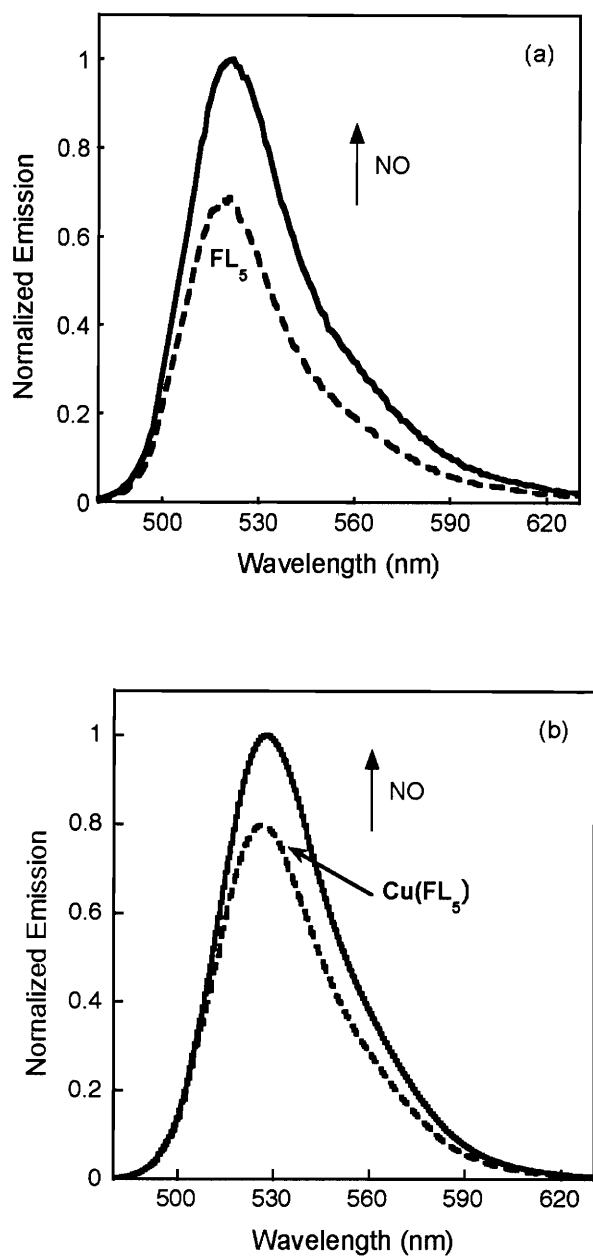


Figure 5.9. Fluorescence response of FL₅ and Cu(FL₅) to NO. (a) Fluorescence emission spectra ($\lambda_{\text{ex}} = 503$ nm) of FL₅ (1 μM , dashed line) and 30 min after the addition of 1300 equiv of NO (g) (50 mM PIPES, pH 7.0, 100 mM KCl) (solid line) at 37 °C. (b) Emission spectra ($\lambda_{\text{ex}} = 503$ nm) of Cu(FL₅) (1 μM CuCl₂ and 1 μM FL₅) in the presence of 100 equiv of EDTA (dashed line) and the spectrum 30 min after the addition of 1300 equiv of NO (g) (solid line) at 37 °C (50 mM PIPES, pH 7.0, 100 mM KCl).

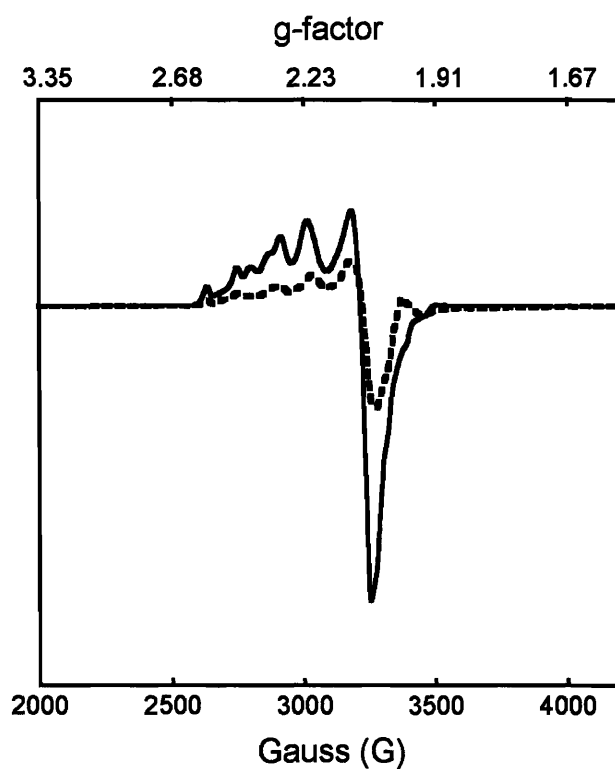


Figure 5.10. EPR spectra of Cu(FL₅) (2.5 mM, solid line) and Cu(FL₅) with 5 equiv of NO (dashed line) in DMF solution, subsequently frozen liquid N₂ temperature and measured at 5 K. The very small signal at $g = 1.96$ is indicative of free NO. Both the FL₅-bound and free Cu(II) species exist in solution at this concentration, based on the K_d value for Cu(FL₅), which may account for the two overlapping copper(II) EPR signals.

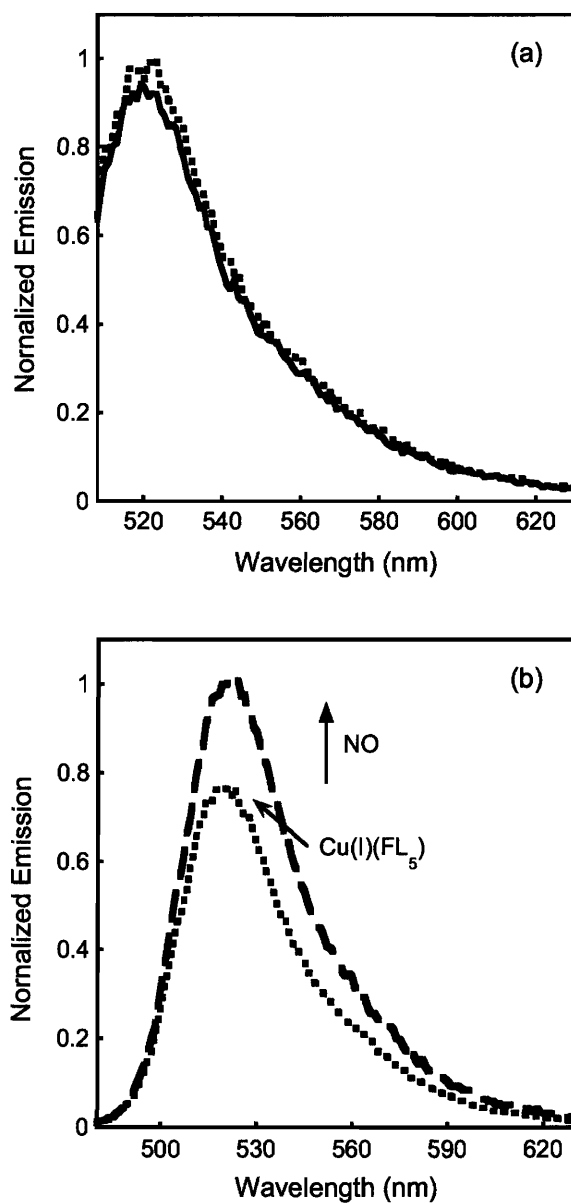


Figure 5.11. Fluorescence spectra of a mixture of FL_5 and Cu(I) in the absence and presence of NO . (a) Fluorescence emission spectra ($\lambda_{\text{ex}} = 503 \text{ nm}$) of $1 \mu\text{M}$ FL_5 (solid line) and FL_5 with the addition of 1 equiv of $[\text{Cu}(\text{CH}_3\text{CN}_4)](\text{BF}_4)$ (dotted line). (b) Fluorescence spectra of a mixture of FL_5 and Cu(I) before (dotted line) and after addition of 1300 equiv of NO (dashed line). The spectra were recorded at 37°C in 50 mM PIPES, pH 7.0, 100 mM KCl .

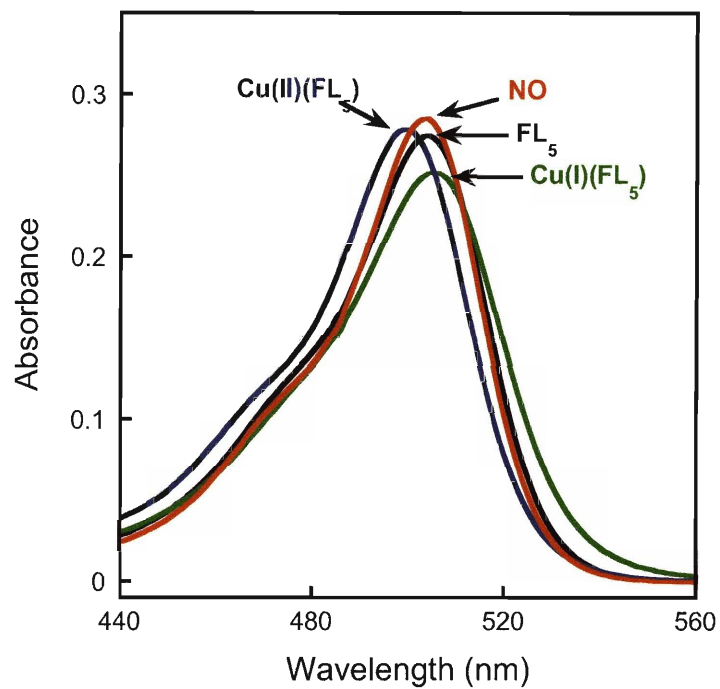


Figure 5.12. UV-vis spectra of FL₅ (5 μM, black line), Cu(FL₅) (5 μM CuCl₂ and 5 μM FL₅, blue line) and Cu(FL₅) treated with 1300 equiv of NO (g) (red line) in aqueous solution (50 mM PIPES, pH 7.0, 100 mM KCl). The green line is the spectrum of FL₅ (5 μM) with the addition of 1 equiv [Cu(CH₃CN₄)](BF₄).

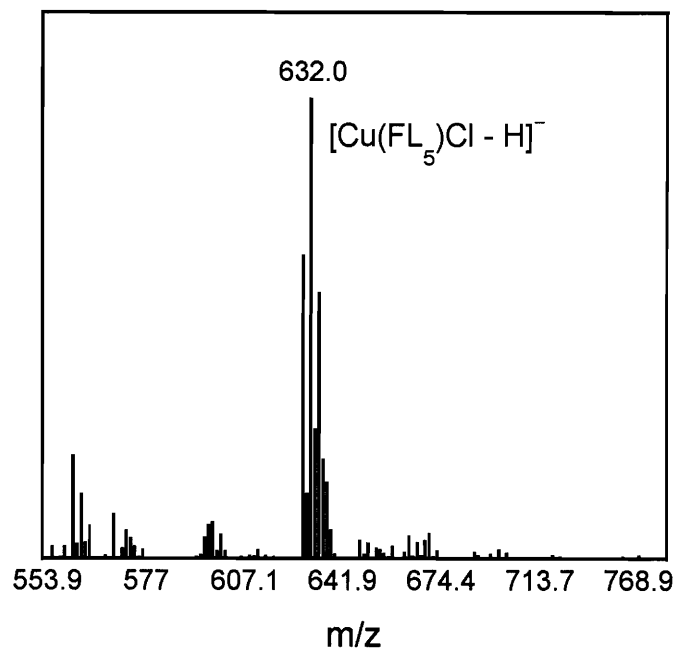


Figure 5.13. ESI(-)MS spectrum of the $\text{Cu}(\text{FL}_5)$ species. A peak at m/z 632.0 corresponds to $[\text{Cu}(\text{FL}_5)\text{Cl} - \text{H}]^-$ (Calcd. m/z 632.0).

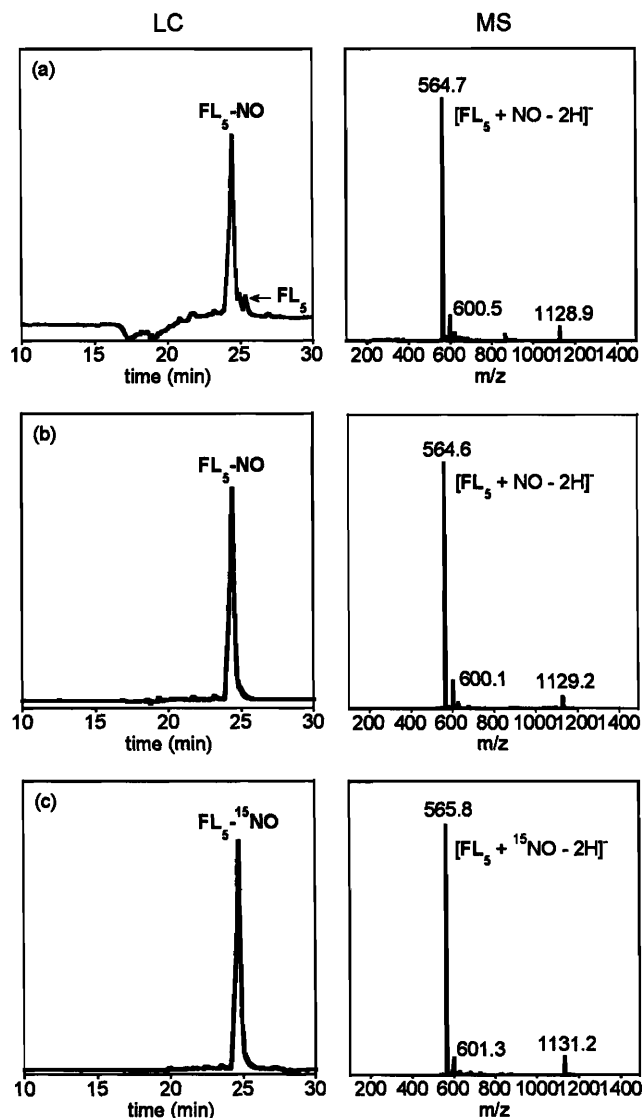


Figure 5.14. LC-MS analyses of $\text{FL}_5\text{-NO}$ (left, LC; right, ESI-MS). (a) A solution obtained by reacting $\text{Cu}(\text{FL}_5)$ ($7 \mu\text{M}$) with 670 equiv of NO (50 mM PIPES, pH 7.0, 100 mM KCl). Chelex was added to the NO reaction solution followed by filtration to remove copper residues for LC-MS analysis. The peaks with m/z of 564.7, 600.5, and 1128.9 correspond to $[\text{FL}_5 + \text{NO} - 2\text{H}]^-$ (Calcd. m/z 564.1), $[\text{FL}_5 + \text{NO} - \text{H} + \text{Cl}]^-$ (Calcd. m/z 600.1), and $[2(\text{FL}_5 + \text{NO}) - 3\text{H}]^-$, (Calcd. m/z 1129.2). (b) $\text{FL}_5\text{-NO}$ after dialyzing (H_2O) the reaction solution of FL_5 with $\text{Na}^{14}\text{NO}_2$ to remove residual sodium nitrite. (c) $\text{FL}_5\text{-}^{15}\text{NO}$ obtained by the reaction of FL_5 with H^{15}NO_2 , followed by dialysis against H_2O . The peaks with m/z of 565.8, 601.3, and 1131.2 correspond to $[\text{FL}_5 + ^{15}\text{NO} - 2\text{H}]^-$ (Calcd. m/z 565.1), $[\text{FL}_5 + ^{15}\text{NO} - \text{H} + \text{Cl}]^-$ (Calcd. m/z 601.1), and $[2(\text{FL}_5 + ^{15}\text{NO}) - 3\text{H}]^-$, (Calcd. m/z 1131.2).

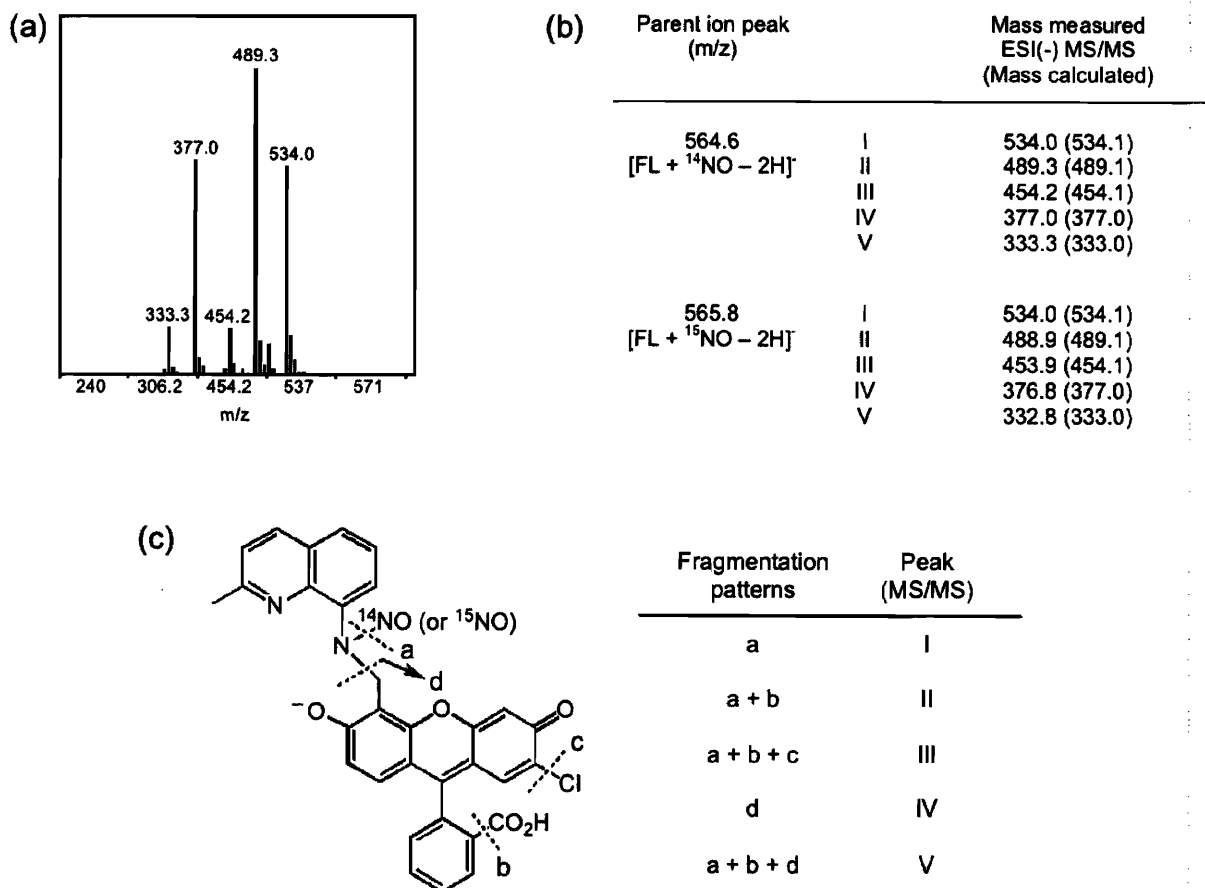


Figure 5.15. MS/MS analyses of FL₅-NO. (a) MS/MS analysis for 564.7 or 546.6 MS peaks in Figures 14a & 14b. (b) Summarized MS/MS analyses of the 564.6 peak for FL₅-¹⁴NO and 565.8 peak for FL₅-¹⁵NO MS peaks. (c) Proposed fragmentation patterns of FL₅-NO based on MS/MS analyses of (b).

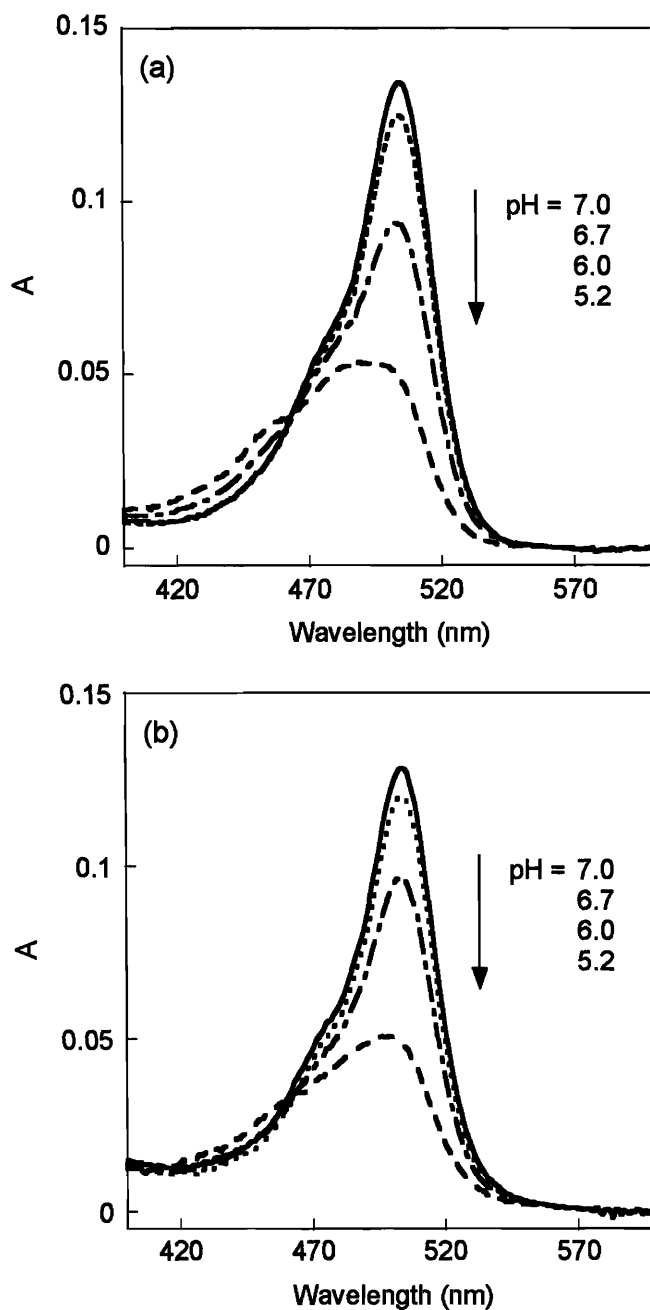


Figure 5.16. UV-vis spectra of FL₅ and NO reaction solutions. (a) Spectra of FL₅ (3 μ M) at pH 5.2, 6.0, 6.7, and 7.0 (dashed, dot-dashed, dotted, and solid lines) in aqueous solution (100 mM KCl) with pH adjusted by KOH or HCl. (b) Spectra of Cu(FL₅) (3 μ M CuCl₂ & 3 μ M FL₅) solution after NO reaction taken at pH 5.0, 5.8, 6.7, and 7.0 (dashed, dot-dashed, dotted, and solid lines).

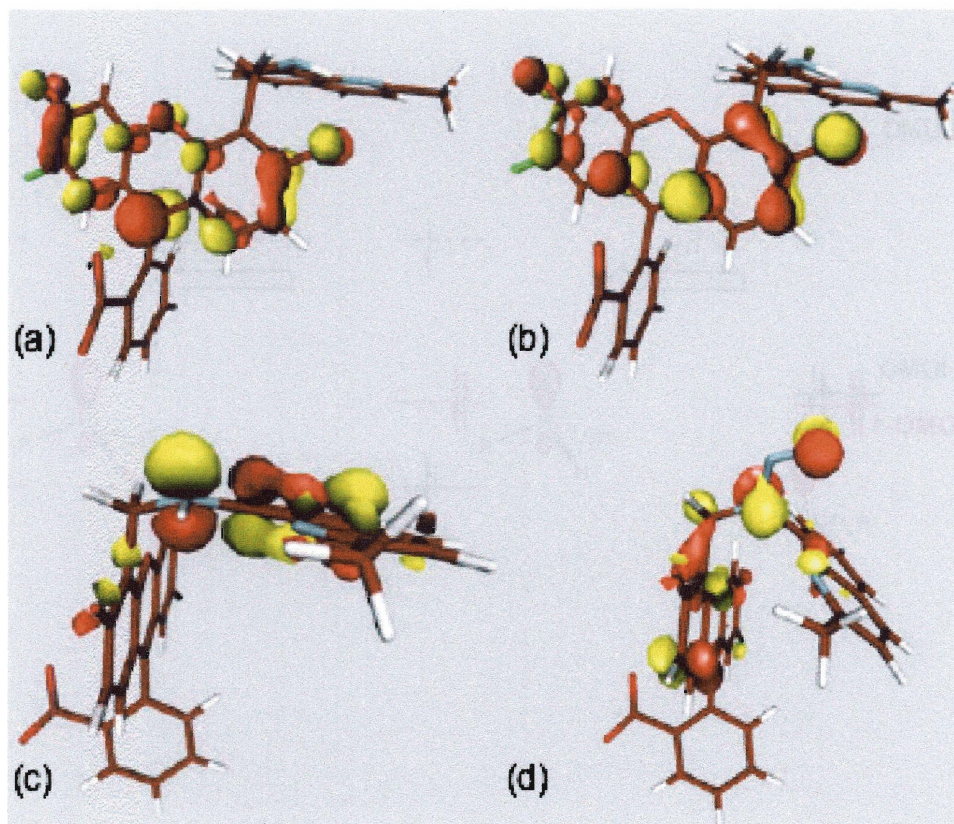


Figure 5.17. Isosurface plots (isodensity value = 0.5 a.u.) of the key molecular orbitals in the FL₅/FL₅-NO system. The LUMO (a), HOMO (b), and HOMO-1 (c) of FL₅ and HOMO-15 (d) of FL₅-NO are shown.

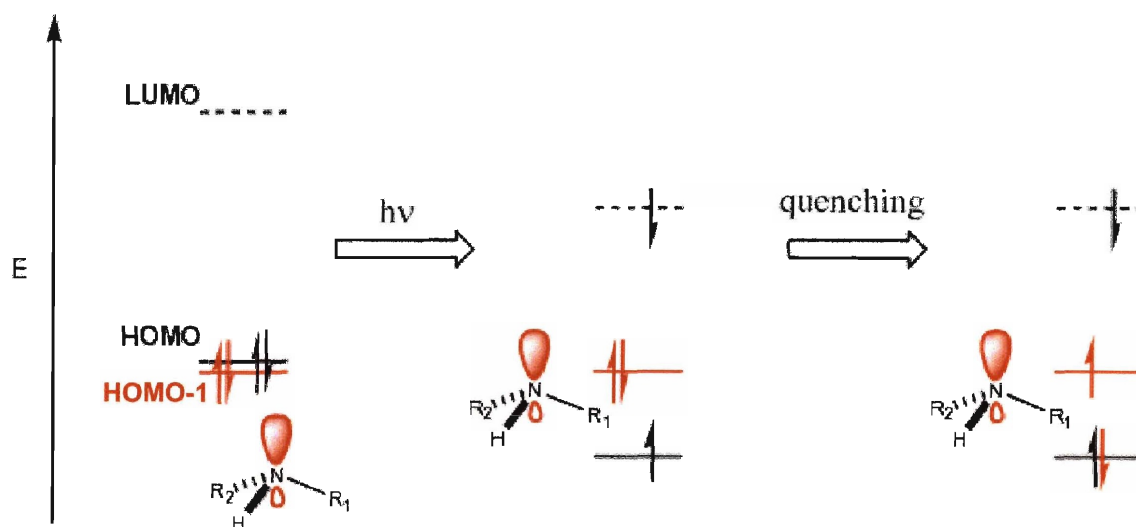


Figure 5.18. Molecular orbital diagram for the ground (left), excited (middle), and charge-transfer (right) states of FL₅. The lowering of the HOMO and LUMO associated with the fluorophore in the excited state is due to electronic relaxation which would not be expected to significantly alter the energy of the nitrogen-based MO. Non-radiative relaxation of the charge-transfer state returns the molecule to the ground state. R₁ = 2-methylquinoline and R₂ = fluorophore.

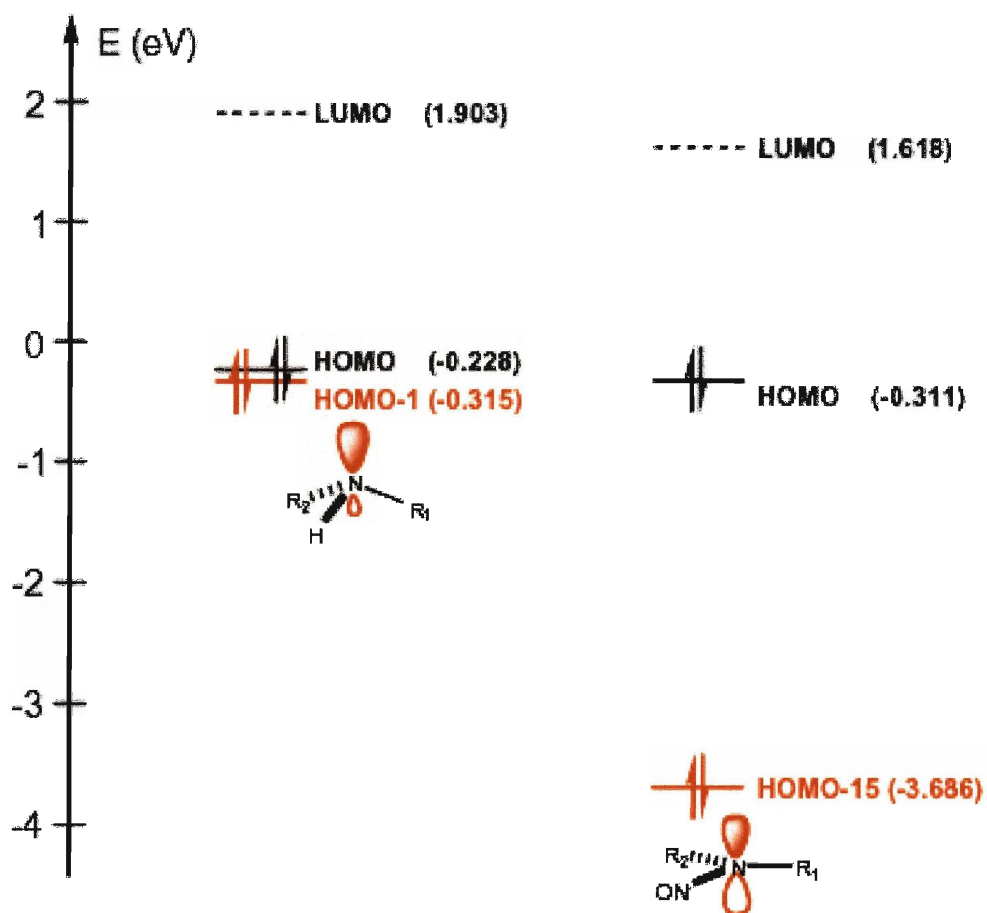


Figure 5.19. Relative energy spacings of the molecular orbitals for the ground states of FL_5 (left) and FL_5-NO (right). The NNO-based orbital, HOMO-15, of FL_5-NO is expected to be too low in energy to act as a donor for fluorescence quenching.

Chapter 6

Visualization of Nitric Oxide in Living Cells by a Copper-Based Fluorescent Probe

This chapter is based on previously published work (Lim, M. H.; Xu, D.; Lippard, S. J., *Nat. Chem. Biol.* **2006**, in press). This work was supported by grant CHE-0234951 from the National Science Foundation. I thank the Martin Family Society at MIT for fellowship. We thank Dr. Dong Xu for RNAi experiments. We also thank Professor Alice Y. Ting and Mr. Chi-Wang. Lin for assistance with epifluorescence microscopy. We are grateful to Drs. Carl D. Novina and Derek M. Dykxhoorn for a gift of plasmid pcDNA3.1-Zeo(-)-U6 used in the RNA interference experiments.

Introduction

In biological systems nitric oxide (NO) is a ubiquitous species. It mediates both physiological and pathological processes in living organisms.¹⁻⁷ In mammalian cells, NO is produced by three isoforms of NO synthase (NOS): neuronal NOS (nNOS), endothelial NOS (eNOS) and inducible NOS (iNOS), the catalytic activities of which are well-characterized.^{1,5-8} Functionally, NOSs can be categorized as cNOS or iNOS. cNOS, including nNOS and eNOS, is regulated by the cytosolic calcium concentration and produces physiological quantities of NO. The Ca(II)-independent iNOS that provides the pathophysiological concentrations of NO is controlled by gene transcription. Direct *in vivo* detection of NO in real time is difficult, since it rapidly diffuses and reacts with cellular components. Although methods like chemiluminescence,⁹ EPR spectroscopy,¹⁰ and amperometry¹¹ have been applied for NO bio-imaging, they suffer from low spatial resolution and, in some cases, require complicated instrumentation. An alternative means to image intracellular and extracellular NO is by light emission from fluorescent sensors in combination with microscopy.^{10,12} A protein-based intracellular NO sensor incorporating soluble guanylate cyclase was recently reported, but the probe requires genetic encoding for its preparation and generates another biologically active molecule, cyclic guanosine monophosphate (cGMP), which can induce further cellular responses.¹⁻⁷ The cGMP molecules bind both NO-associated and NO-free protein probes, resulting in fluorescence increase. The signal thus generated reflects the intracellular level of cGMP rather than NO.¹³ Other small-molecule-based fluorescent probes for NO, including *o*-diaminonaphthalene (DAN), *o*-diaminofluoresceins (DAFs), and *o*-diaminocyanines (DACs), have been documented,^{10,14,15} but their fluorescence changes upon reacting with oxidized NO products, not with NO itself. Since NO has a lifetime

up to several minutes under certain conditions,¹⁶ alteration of the fluorescence of organic molecules containing an *o*-diamine functionality does not monitor real-time production of NO. A previously described pyrene-nitronyl probe detects NO directly, but requires high excitation energy,¹⁷ which produces cellular autofluorescence, and it cannot provide spatiotemporal information.

In previous work (chapter 5), we devised imaging agents to detect NO directly *in vitro* at neutral pH. These probes are Cu(II) complexes containing a fluorescein-based ligand that provides suitable excitation and emission wavelengths as well as brightness for NO bioimaging. This chapter describes application of a copper(II) fluorescein-based compound, CuFL (FL = FL₅ in chapter 5, Figure 6.1), to cellular imaging of NO. This probe reacts rapidly and specifically with NO over other potentially interfering reactive nitrogen species (RNS) to afford bright light emission with nM sensitivity, as reported in chapter 5. This cell-permeable reagent images NO produced by cNOS and iNOS in live cells. The present study demonstrates that CuFL can directly image nitric oxide production in living cells by turn-on fluorescence, a significant advance over all prior agents. Furthermore, our work proves the utility of metal coordination chemistry for biological imaging in the complex milieu of the cell.

Experimental

Cell Culture and Materials. Raw 264.7, SK-N-SH, and HeLa cells were purchased from the American Type Culture Collection (ATCC). All three cell lines were maintained in Dulbecco's modified Eagles' media (DMEM) (GibcoBRL) containing 10% (v/v) heat-inactivated fetal bovine serum (FBS) (HyClone), 1 mM sodium pyruvate (Sigma), 100 units/ml penicillin, 100 μ g/ml streptomycin (Invitrogen), and 0.1 mM nonessential amino acid solution for minimal essential

medium (Sigma). All cells were grown at 37 °C in a humidified atmosphere of 10% CO₂. A nitrite assay was performed with Griess reagents (Promega) on Raw 264.7 cells grown in DMEM free of phenol red. Calcium sensor fluo-4 AM was purchased from Invitrogen. MTT [3-(4,5-dimethylthiazol-2-yl)-2,5-diphenyltetrazolium bromide] was obtained from Sigma-Aldrich.

MTT Cytotoxicity Assay. SK-N-SH cells were seeded in 96 well plates (1000 cells in 100 μ L per well) for 24 h, after which CuFL (FL = FL₅ in chapter 5) or the *N*-nitrosofluorescein derivative (FL-NO = FL₅-NO in chapter 5) (1 μ M) in DMEM (100 μ L) was introduced (stock solution of CuFL or FL-NO: 5 mM in 1:1 DMSO:H₂O). Cells treated with or without (control) CuFL were incubated for 5 days followed by the addition of 20 μ L MTT (5 mg/ mL in PBS) for 2 or 4 h. The media were removed and DMSO (200 μ L) was added into each well to dissolve the residue. The absorbance at 550 nm was measured by using a microplate reader. An MTT assay for Raw 264.7 cells was performed by essentially the same method, except that fewer cells (500 per well) were seeded and a lower concentration of MTT (20 μ L of 1 mg/ mL) was employed.

Silencing of iNOS in Raw 264.7 Cells by Short Hairpin RNA-Induced RNA Interference. In order to establish that NO is responsible for the fluorescence response detected in stimulated Raw 264.7 cells, we generated a cell line in which the expression of iNOS was constitutively silenced by RNA interference. The RNAi experiment was performed by Dr. Dong Xu. The plasmid vector used for short hairpin RNA-induced RNAi on iNOS was pcDNA3.1-Zeo(-)-U6, a derivative of pcDNA3.1-Zeo(-) (Invitrogen) with a U6 promoter at the 5' end of its multiple cloning site.¹⁸ The pair of DNA strands designed for hairpin RNA-induced silencing of iNOS in Raw 264.7 cells (Scheme 6.1) was synthesized by Invitrogen. Experimental details

are described elsewhere.¹⁹

Western Blot Analysis on iNOS Expression in Raw 264.7 Cells. Cytosolic and nuclear extracts of Raw264.7 cells were prepared as previously published.²⁰ The procedure is slightly revised from that described in the TransFactor extraction kit manual (Clontech). The protein components of the extracts were resolved by SDS-PAGE on 4 – 20% Tris-HCl ready gels (Bio-Rad) with a BenchMark Prestained Protein Ladder (Invitrogen) as the molecular weight indicator. The proteins separated on the gel were then electroblotted to a polyvinylidene difluoride membrane (Bio-Rad). The membrane was subsequently cut horizontally into two parts along the 60.4 kDa band made by the protein ladder. The bottom part, where proteins of lower molecular weights were blotted, was incubated with a 1:5,000 dilution of mouse anti-actin antibody (Upstate). The top part of the membrane, to which proteins of higher molecular weights were transferred, was incubated with 1:1,000 dilution of rabbit anti-iNOS antibody (QED Bioscience). The two pieces of membrane were then incubated respectively with horseradish peroxidase conjugated anti-mouse (Pierce) (1:4,000 dilution) and anti-rabbit (Promega) antibodies (1:5,000 dilution). Both pieces were subsequently soaked with the ECL plus reagents (Amersham) for 1 min to develop chemiluminescent signals through a peroxidase-catalyzed reaction. The signals were later detected by exposing the membrane pieces to BioMax MR film (Eastman Kodak Co.). Alternatively, the PVDF membrane pieces were soaked in AEC solution (Calbiochem) to develop colorimetric signals.

Results

CuFL Detection of NO Produced by cNOS.

We investigated the ability of CuFL to detect NO produced in SK-N-SH human

neuroblastoma cells under physiological conditions, since cNOS in this cell line can be activated by estrogen to produce NO.²¹ Estrogen administration leads to an increase in the cytosolic Ca(II) concentration that alters the structure of calmodulin, which in turn activates cNOS. The NO-dependent fluorescence response, monitored after simultaneous administration of 17 β -estradiol (100 nM) and CuFL (1 μ M) to the cells, was complete within 5 min with a 4.0 ± 0.6 -fold increase in fluorescence (Figure 6.2). We also demonstrated an increase in cytosolic Ca(II) levels following addition of 17 β -estradiol to SK-N-SH cells using the calcium dye fluo-4 AM, which is consistent with estrogen induction of Ca(II)-dependent NO production (Figure 6.3). A notably weaker intense fluorescence response was observed in the presence of the cNOS inhibitor *N*^G-nitro-*L*-arginine (*L*-NNA), pinpointing nitric oxide to be responsible for the fluorescence change (Figure 6.4). In a control experiment, stimulated SK-N-SH cells incubated with FL in the absence of Cu(II) ion exhibited no fluorescence increase over a period of 25 min (Figure 6.5). This result demonstrates that CuFL, but not FL, is responsible for the fluorescence change. As another control, HeLa cells (a human cervical cancer cell line lacking the estrogen receptor) were co-treated with 17 β -estradiol (100 nM) and CuFL (1 μ M) (Figure 6.6). The absence of turn-on emission in these cells, which do not produce nitric oxide, indicates that the fluorescence response of CuFL is not a consequence of its interaction with 17 β -estradiol.

To evaluate the toxicity of CuFL, an MTT [3-(4,5-dimethylthiazol-2-yl)-2,5-diphenyltetrazolium bromide] assay was performed on SK-N-SH cells after 5 days of incubation with CuFL (1 μ M). The result [$80 \pm 9\%$ survival of cells] (Figure 6.7) indicates that the Cu(II)-containing probe is not toxic to SK-N-SH cells under the conditions of NO imaging employed herein.

CuFL Detection of NO Produced by iNOS.

In macrophages, nitric oxide is produced by iNOS.^{1,6-8} Time-dependent NO production by Raw 264.7 murine macrophage cells pretreated with bacterial lipopolysaccharide (LPS) and interferon- γ (IFN- γ) has been previously demonstrated by using the Griess assay.²² This method colorimetrically determines the concentration of NO₂⁻ resulting from NO oxidation in the extracellular space. Fluorescence detection of NO production by stimulated macrophage cells was also achieved by incubation of the extracellular fluid with DAN and DAFs.²³⁻²⁵ These dyes improved upon the sensitivity of Griess assay, but were unable to reveal NO production inside cells with spatial and temporal fidelity.²⁵ The present CuFL construct, however, readily detects NO produced in activated Raw 264.7 cells by fluorescence turn-on. Macrophage cells were incubated with LPS (500 ng/mL) and IFN- γ (250 U/mL) for 4 h, after which 1 μ M CuFL was applied. The fluorescence response was monitored at 2 h intervals by microscopy (Figure 6.8). The fluorescence slowly increased over 12 h in almost every region of the treated cells.

The production of nitric oxide in LPS- and IFN- γ treated macrophages was independently confirmed by the Griess assay (Figure 6.9), which revealed identical kinetics of NO formation inside and outside the cells over the 12 h period of the experiment. To investigate further the origin of fluorescence detected by CuFL, iNOS was silenced in Raw 264.7 cells by short hairpin RNA (shRNA)-induced RNA interference (RNAi) (Figure 6.10). Upon stimulation by LPS and IFN- γ , the cells with iNOS attenuated displayed a much weaker fluorescence response than those harboring only the plasmid vector (Figure 6.10), clearly demonstrating that the fluorescence enhancement is caused by nitric oxide production in Raw 264.7 cells. In

addition, a notably weaker fluorescence response was observed for stimulated Raw 264.7 cells in the presence of N^G -methyl-*L*-arginine (*L*-NMA), a known inhibitor of iNOS that attenuates NO production, than in its absence (Figure 6.11). In control experiments, we did not observe turn-on fluorescence emission either for Raw 264.7 cells stimulated by LPS and IFN- γ followed by FL treatment without Cu(II) ion over the 12 h incubation period or for HeLa cells treated with LPS and IFN- γ prior to CuFL incubation (Figures 6.12 & 6.13).

The MTT assay indicated $90 \pm 3\%$ survival of Raw 264.7 cells after incubation with CuFL (1 μ M) for 5 days (Figure 6.14), indicating that CuFL is not toxic to this cell line. CuFL does not affect the expression of iNOS in Raw 264.7 cells upon introduction of LPS and IFN- γ (Figure 6.15, Western blot analysis), which reveals that the concentration of CuFL used for imaging does not interrupt the biological pathways required for NO production via gene expression.

NO Imaging in a Raw 264.7 and SK-N-SH Co-culture.

The fluorescence response was also monitored in a mixture of Raw 264.7 and SK-N-SH cells grown on the same plate and co-treated with 17β -estradiol (500 nM) and CuFL (1 μ M) for 10 min. As shown in Figure 6.16, a fluorescence increase was observed exclusively in the SK-N-SH cells following cNOS activation by 17β -estradiol-triggered Ca(II) release into cytosol. This result demonstrates that CuFL might be used to provide information about which types of cells are producing NO in a heterogeneous tissue, and possibly be useful for identifying the time and location of intercellular signaling events.

Discussion

As described in chapter 5, copper(II)-based probes were synthesized for direct NO detection. Among them, CuFL rapidly and directly detects NO at a physiologically relevant pH. The ability of CuFL to image NO specifically over other reactive nitrogen or oxygen species in living organisms, such as HNO, NO_2^- , NO_3^- , ONOO^- , H_2O_2 and O_2^- , increases its value for a wide range of biological studies. To our knowledge, CuFL is the first probe capable of direct, fast and specific NO detection in aqueous buffered solution.

We applied CuFL to image NO production in Raw 264.7 murine macrophage and SK-N-SH human neuroblastoma cells (Figures 6.2 and 6.8). Our studies in both cell lines demonstrate that CuFL affords direct visual detection of NO production in a time- and concentration-dependent manner in both cNOS and iNOS living cells with > 4-fold fluorescence enhancement and spatial resolution at the cellular level. Cell-type specific fluorescent NO imaging in a co-culture of the two cell lines demonstrates that CuFL is capable of detecting a source of nitric oxide production in a complex and heterogeneous biological system (Figure 6.16).

The present study reveals the value of CuFL as a very useful probe through comparison of its NO imaging ability versus that of a commercially available sensor DAF-2 DA (*o*-diaminofluorescein diacetate). First of all, CuFL visualizes NO in estrogen-stimulated neuroblastoma cells with brighter fluorescence than DAF-2 DA (*o*-diaminofluorescein diacetate) (Figure 6.17). Secondly, the slight fluorescence increase of DAF-2 DA occurs 30 min after activation of cNOS, but CuFL provides the complete fluorescence enhancement within 5 min (Figure 6.2), the time required to transfer the cells to the microscope stage and image them. These results indicate that CuFL allows superior visualization of NO in live cells. Certain questions remain, however. The *N*-

nitrosamine FL-NO generated by the chemistry is a member of a class of reactive molecules,²⁶ however, an MTT assay indicates that it is not toxic at the concentration required for NO imaging herein with $97 \pm 2\%$ survival of SK-N-SH cells treated with FL-NO for 5 days (Figure 6.18). Another potential problem is that the copper ion in this metal-based sensor might damage cells before or following its reaction with NO. In order to address this issue, we performed an MTT assay for cytotoxicity, which indicated that cells treated with $1 \mu\text{M}$ CuFL for 5 days were largely viable ($> 80\%$) (Figure 6.7 and 6.14). Thus, under the conditions used for the present NO bioimaging experiments, the toxicity of CuFL is negligible.

The cytosol contains thiols that bind Cu(II) and might possibly convert it to Cu(I), a species which itself might react with oxidized NO products such as NO^+ or N_2O_3 . Since NO^+ is rapidly hydrolyzed to NO_2^- in water,^{16,27,28} it will not interfere with NO imaging by CuFL. S-nitrosothiols, formed by reactions of thiols with NO in the presence of O_2 , react with both Cu(II)FL and Cu(I)FL to display turn-on fluorescence, as demonstrated in experiments with S-nitroso-N-acetylpenicillamine (SNAP), (Figure 6.19).²⁹ We, thus, cannot completely rule out the possibility that the fluorescence increase results from reaction of CuFL with S-nitrosothiols produced by NO in the stimulated cells. Since the formation of S-nitrosothiol species in Raw 264.7 cells is very slow, in the range of 3 – 4 pmol/mg of protein/h ($t_{1/2} > 1000 \text{ h}$),³⁰ however, CuFL may not react with S-nitrosothiols as fast as it does with NO in cells. Finally, reduction of Cu(II) by thiols may not alter the integrity or otherwise disrupt the NO-imaging ability of CuFL in cells. As shown in chapter 5, Cu(II) binding to FL is necessary for fluorescence turn-on by NO. Moreover, a mixture of FL and Cu(I) does not lead to fluorescence increase with and without the presence of NO, compared to FL. These

experiments strongly support the conclusion that the turn-on fluorescence in the stimulated cells results from the direct reaction of CuFL with NO and that intracellular thiols do not interfere with this reaction.

Summary

This research has produced a Cu(II)-based fluorescein compound CuFL for imaging NO in biology, a long sought obligation of many laboratories. The probe readily passes through cell membranes and can detect NO under physiological conditions. CuFL on cultures of macrophage and neuroblastoma cells reveals the time-dependent production of NO measurable by fluorescence enhancement, demonstrating the ability of the reagent to image NO over a wide range of concentrations. The power of CuFL is also manifest in its ability to select out cells that emit NO in a background of those that do not with spatiotemporal resolution at the cellular level. These results will encourage the use of CuFL as a direct nitric oxide probe for investigating NO biology in a variety of contexts.

References

- (1) Murad, F., *Angew. Chem. Int. Ed.* **1999**, *38*, 1856-1868.
- (2) Furchgott, R. F., *Angew. Chem. Int. Ed.* **1999**, *38*, 1870-1880.
- (3) Ignarro, L. J., *Angew. Chem. Int. Ed.* **1999**, *38*, 1882-1892.
- (4) Packer, L., *Methods in Enzymology, Nitric Oxide. Part B, Physiological and Pathological Processes*. Academic Press: San Diego, CA, 1996; Vol. 269.
- (5) Moncada, S.; Palmer, R. M. J.; Higgs, E. A., *Pharmacol. Rev.* **1991**, *43*, 109-142.
- (6) Ricciardolo, F. L. M.; Sterk, P. J.; Gaston, B.; Folkerts, G., *Physiol. Rev.* **2004**, *84*, 731-765.
- (7) Conner, E. M.; Grisham, M. B., *Methods Enzymol.* **1995**, *7*, 3-13.

- (8) Marletta, M. A.; Hurshman, A. R.; Rusche, K. M., *Curr. Opin. Chem. Biol.* **1998**, *2*, 656-663.
- (9) Hampl, V.; Walters, C. L.; Archer, S. L., *In Methods in Nitric Oxide Research*, Feelisch, M.; Stamler, J. S., Eds. John Wiley & Sons: New York, 1996; pp 309-318.
- (10) Nagano, T.; Yoshimura, T., *Chem. Rev.* **2002**, *102*, 1235-1269.
- (11) Malinski, T.; Mesaros, S.; Tombouliau, P., *Methods Enzymol.* **1996**, *268*, 58-69.
- (12) Hilderbrand, S. A.; Lim, M. H.; Lippard, S. J., *In Topics in Fluorescence Spectroscopy*, Geddes, C. D.; Lakowicz, J. R., Eds. Springer: 2005; pp 163-188.
- (13) Sato, M.; Hida, N.; Umezawa, Y., *Proc. Natl. Acad. Sci. USA* **2005**, *102*, 14515-14520.
- (14) Miles, A. M.; Chen, Y.; Owens, M. W.; Grisham, M. B., *Methods Enzymol.* **1995**, *7*, 40-47.
- (15) Sasaki, E.; Kojima, H.; Nishimatsu, H.; Urano, Y.; Kikuchi, K.; Hirata, Y.; Nagano, T., *J. Am. Chem. Soc.* **2005**, *127*, 3684-3685.
- (16) Wink, D. A.; Grisham, M. B.; Mitchell, J. B.; Ford, P. C., *Methods Enzymol.* **1996**, *268*, 12-31.
- (17) Lozinsky, E. M.; Martina, L. V.; Shames, A. I.; Uzlaner, N.; Masarwa, A.; Likhtenshtein, G. I.; Meyerstein, D.; Martin, V. V.; Priel, Z., *Anal. Biochem.* **2004**, *326*, 139-145.
- (18) Stewart, S. A.; Dykxhoorn, D. M.; Palliser, D.; Mizuno, H.; Yu, E. Y.; An, D. S.; Sabatini, D. M.; Chen, I. S. Y.; Hahn, W. C.; Sharp, P. A.; Weinberg, R. A.; Novina, C. D., *RNA* **2003**, *9*, 493-501.
- (19) Lim, M. H.; Xu, D.; Lippard, S. J., *Nat. Chem. Biol.* **2006**, in press.
- (20) Wang, D.; Lippard, S. J., *J. Biol. Chem.* **2004**, *279*, 20622-20625.
- (21) Xia, Y.; Krukoff, T. L., *Endocrinology* **2004**, *145*, 4550-4557.

- (22) Miwa, M.; Stuehr, D. J.; Marletta, M. A.; Wishnok, J. S.; Tannenbaum, S. R., *Carcinogenesis* **1987**, *8*, 955-958.
- (23) Ralt, D.; Wishnok, J. S.; Fitts, R.; Tannenbaum, S. R., *J. Bacteriol.* **1988**, *170*, 359-364.
- (24) Ji, X.-B.; Hollocher, T. C., *Appl. Environ. Microbiol.* **1988**, *54*, 1791-1794.
- (25) Nakatsubo, N.; Kojima, H.; Kikuchi, K.; Nagoshi, H.; Hirata, Y.; Maeda, D.; Imai, Y.; Irimura, T.; Nagano, T., *FEBS Lett.* **1998**, *427*, 263-266.
- (26) Lijinsky, W., *Chemistry and biology of N-nitroso compounds*. Cambridge University Press: Cambridge, 1992.
- (27) Koppenol, W. H., *Methods Enzymol.* **1996**, *268*, 7-12.
- (28) Ford, P. C.; Lorkovic, I. M., *Chem. Rev.* **2002**, *2002*, 993-1017.
- (29) Lim, M. H.; Lippard, S. J., 2005, unpublished results.
- (30) Zhang, Y.; Hogg, N., *Am. J. Physiol. Lung Cell Mol. Physiol.* **2003**, *287*, L467-L474.

5'p-ACATCGGATTTCACTTGCACTCGAGTGCAAGTGAAATCCGATGTTTTTTG
TGTAGCCTAAAGTGAACGTGAGCTCACGTTCACTTTAGGCTACAAAAACCTAG-p5'

Scheme 6.1. DNA Inserts for Silencing Inducible Nitric Oxide Synthase (iNOS) in Mouse Raw 264.7 Cells in Figure 6.10.

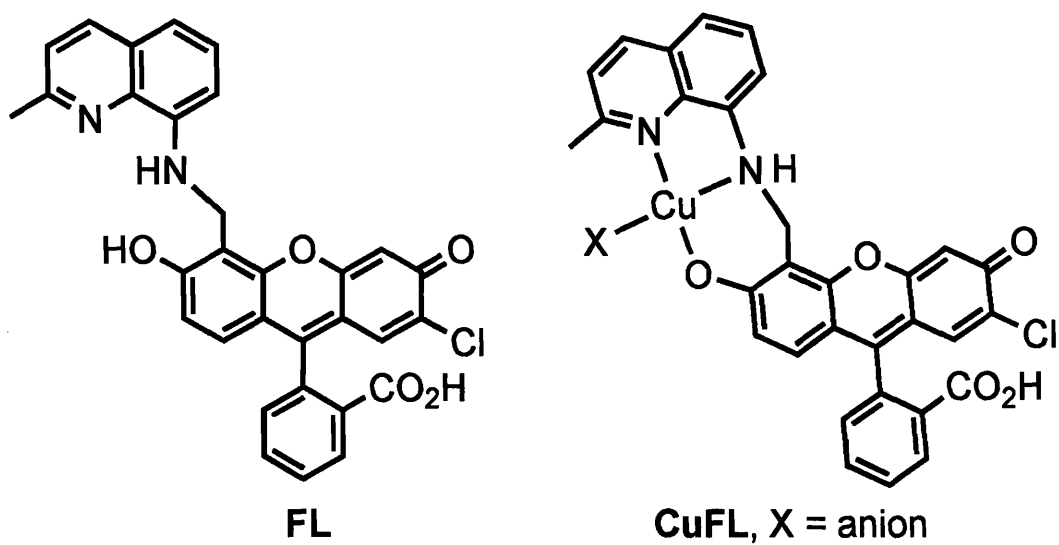


Figure 6.1. Schematic drawings of FL and CuFL (FL = FL₅ and CuFL = Cu(FL₅) in chapter 5).

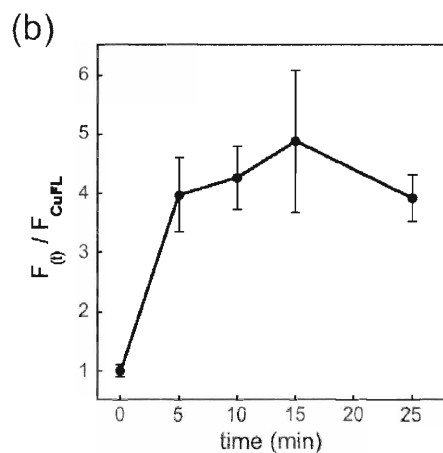
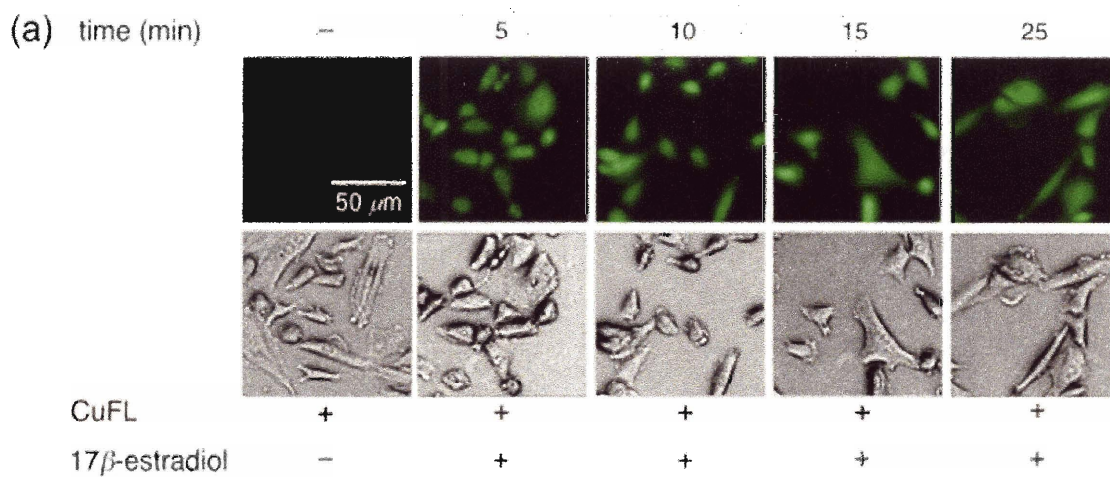
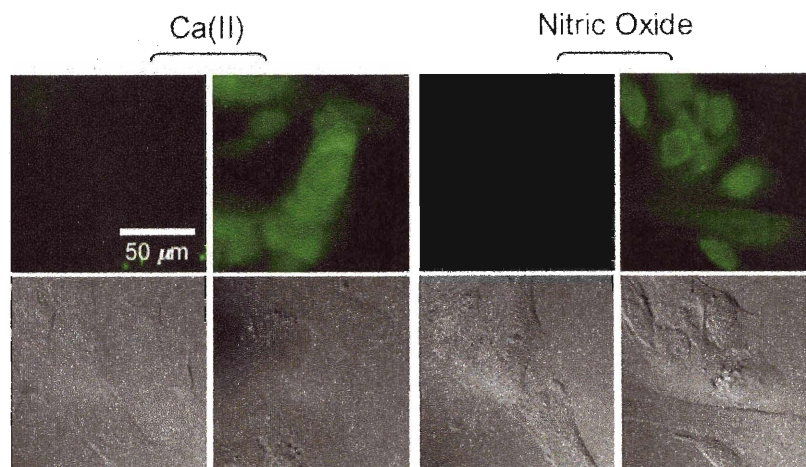


Figure 6.2. (a) NO detection in SK-N-SH cells by **CuFL**. Left to right: 25 min incubation of **CuFL** (1 μM) and 5, 10, 15, 25 min after co-treatment of **CuFL** (1 μM) and 17 β -estradiol (100 nM). Images were taken with a Nikon Eclipse TS100 microscope after removing the DMEM media and washing the cells with PBS. Top: fluorescence images; bottom: phase contrast images. (b) Fluorescence intensity ($F(t)/F_{\text{CuFL}}$) from (a) was plotted against incubation time.

(a)



(b)

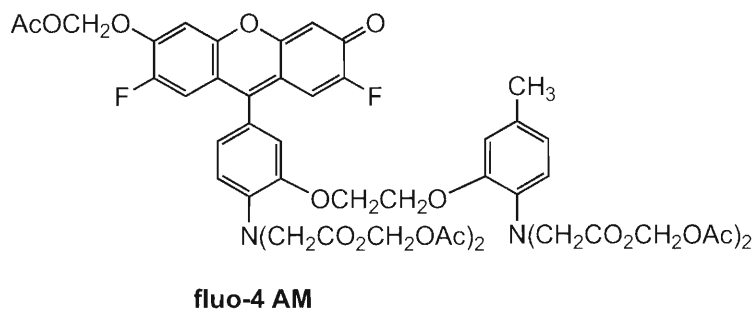


Figure 6.3. Fluorescence response of fluo-4 AM and **CuFL** in SK-N-SH cells. (a) Left to right: cells incubated with fluo-4 AM (2 μ M) for 40 min, with fluo-4 AM (2 μ M) for 40 min followed by 17 β -estradiol (100 nM) for 10 min, with **CuFL** (1 μ M) for 10 min, and co-treated with **CuFL** and 17 β -estradiol for 10 min. Images were taken with a Zeiss Axiovert 200M inverted epifluorescence microscope after removing DMEM and washing the cells three times with PBS. The top panels are the fluorescent images and the bottom panels display DIC images. (b) Schematic drawing of fluo-4 AM.

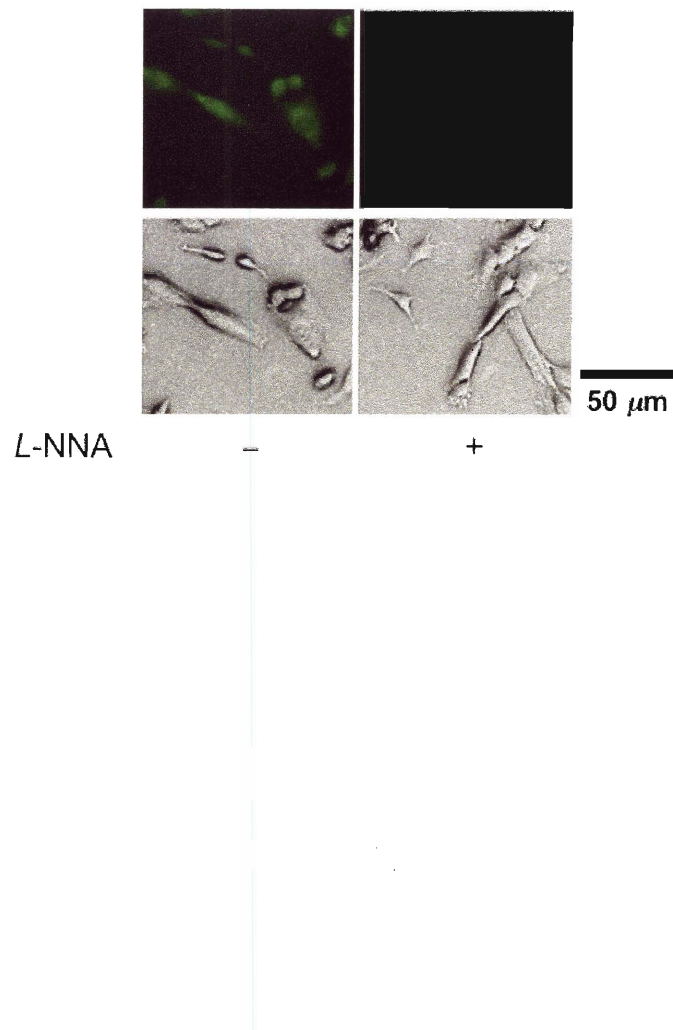


Figure 6.4. NO production with or without *L*-NNA. Right: NO detection in cells after 10min co-incubation of **CuFL** (1 μ M) and 17β -estradiol (100 nM). Left: NO detection in cells pre-treated with *L*-NNA for 1 h before addition of **CuFL** and 17β -estradiol.

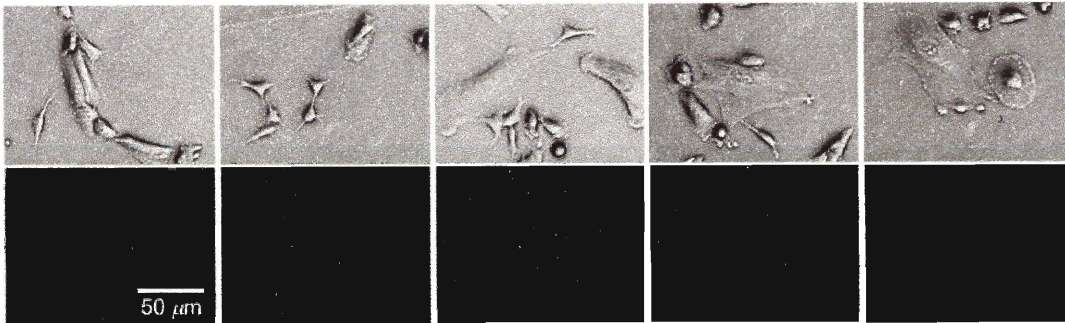


Figure 6.5. Fluorescence response of FL in SK-N-SH cells. Left to right: 25 min incubation of FL ($1 \mu\text{M}$), and 5, 10, 15, 25 min co-treatment of FL and 17β -estradiol (100 nM). Images were taken with a Nikon Eclipse TS100 microscope after removing DMEM and washing the cells three times with PBS (top: phase contrast images, bottom: fluorescence images).

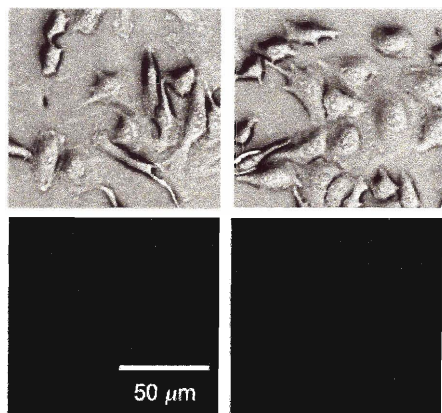


Figure 6.6. HeLa cells were cultured with DMEM. The fluorescence response was monitored after 30 min of incubation with **CuFL** (1 μM) (left) and for the cells co-treated with 17β -estradiol (100 nM) and **CuFL** (1 μM) for 30 min (top: phase contrast images, bottom: fluorescence images). Images were taken with a Nikon Eclipse TS100 microscope after removing DMEM and washing the cells three times with PBS.

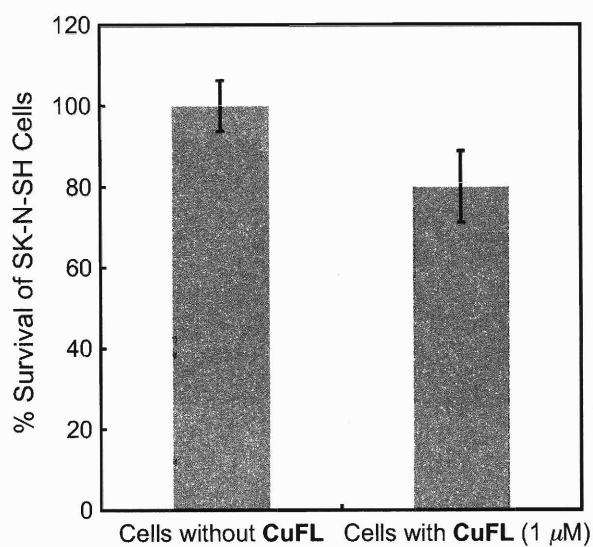


Figure 6.7. MTT assay of SK-N-SH cells treated with **CuFL**. Cells (1000 cells/well) were grown in 96 well plate for 1 day and then treated with **CuFL** (1 μ M). After 5 days, MTT (20 μ L of 5 mg/mL) was added to each well for 4 h. DMSO (200 μ L) was added to each well after removing media. The absorbance was measured by a microplate reader.

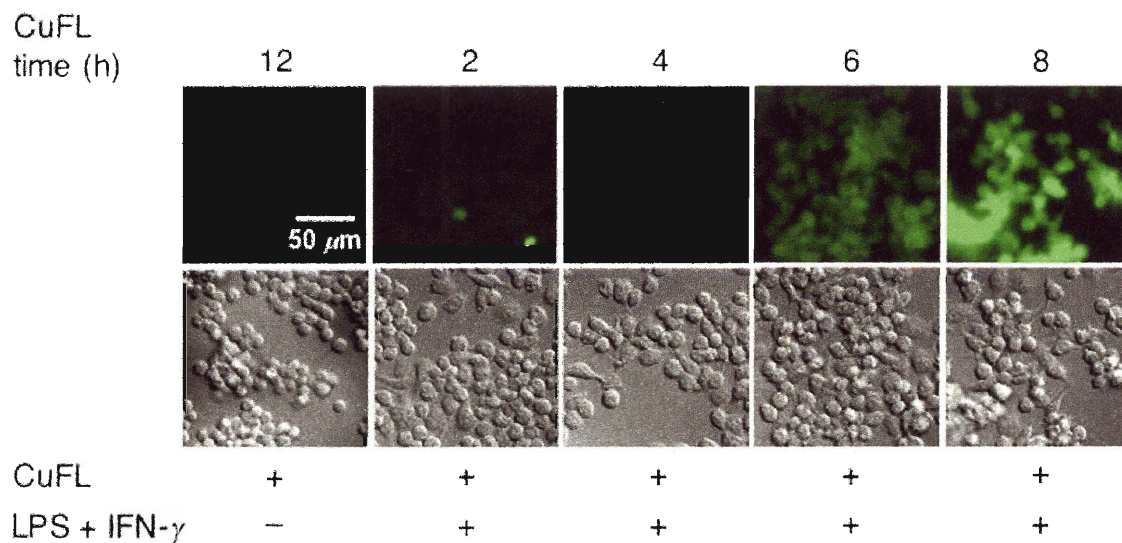


Figure 6.8. NO detection in Raw 264.7 macrophage cells by **CuFL**. Left to right: **CuFL** (1 μ M) incubation with cells for 12 h, and 2, 4, 6, 8 h after addition of **CuFL** into Raw 264.7 cells that were pre-stimulated for 4 h with LPS (500 ng/mL) and IFN- γ (250 U/mL). The times depicted in the figure are the total incubation times with **CuFL**. Images were taken immediately after removing the media and washing the cells three times with phosphate-buffered saline (PBS). The instrument used was a Zeiss Axiovert 200M inverted epifluorescence microscope with differential interference contrast (DIC). Top: fluorescence images; bottom: DIC images.

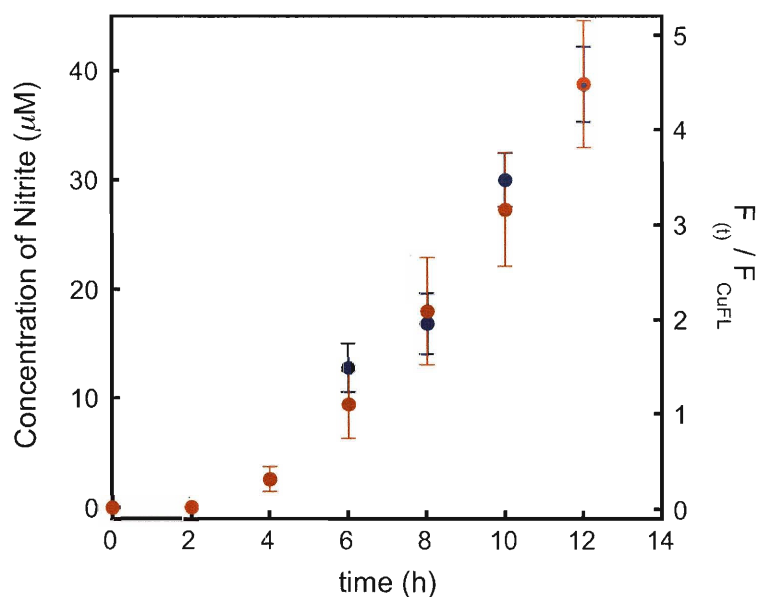


Figure 6.9. A comparison of the time dependence of NO detection by **CuFL** and with the Griess assay. The fluorescence intensity ($F_{(t)}/F_{\text{CuFL}}$ (●)) from Figure 6.8 (right axis) was plotted against incubation time. For the Griess assay, Raw 264.7 cells were grown in 6-well plates with DMEM free of phenol red. The plates were treated with LPS (500 ng/mL) and IFN- γ (250 U/mL) for various time periods before aliquots of media were taken into the 96-well plates. Griess assay reagents were then added to 96-well plates. The kinetics of nitrite ion formation were followed by the absorbance change at 550 nm with a microplate reader (left axis, (●)).

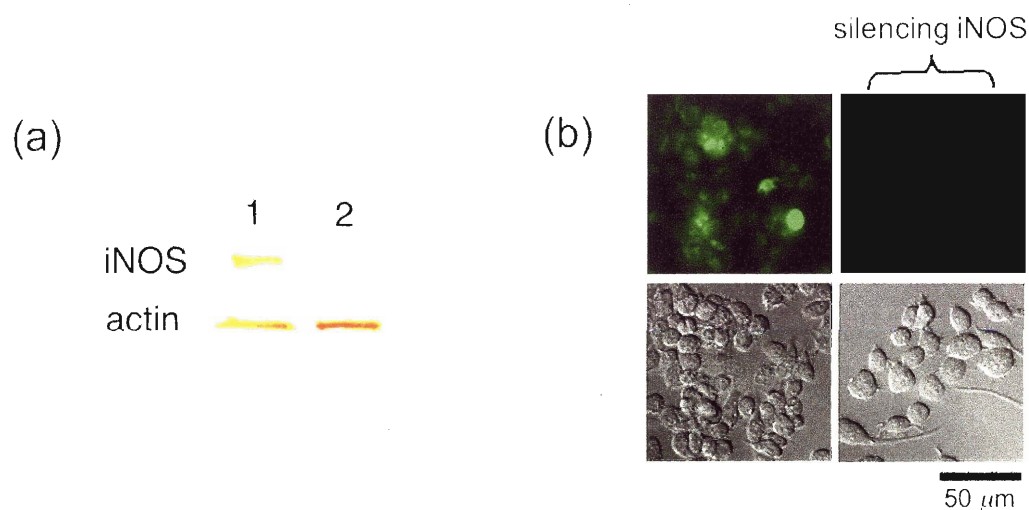


Figure 6.10. Silencing of iNOS by RNAi in Raw264.7 cells. A plasmid expressing shRNA was constructed to target the mRNA of iNOS (Scheme 6.1) and transfected into Raw 264.7 cells. The plasmid vector without insert for RNAi was transfected to establish a control cell line. (a) The expression of iNOS in these two cell lines after stimulation by LPS and IFN- γ for 12 h was investigated by Western blot analysis of whole cell extracts with antibodies against the protein and actin, which served as loading control (lane 1: cells with control plasmid vector, lane 2: cells with plasmid expressing shRNA for iNOS). (b) NO detection in Raw 264.7 cells with iNOS silenced by RNAi. The two lines in (a) were treated with LPS and IFN- γ for 4 h before 8 h of incubation with **CuFL**.

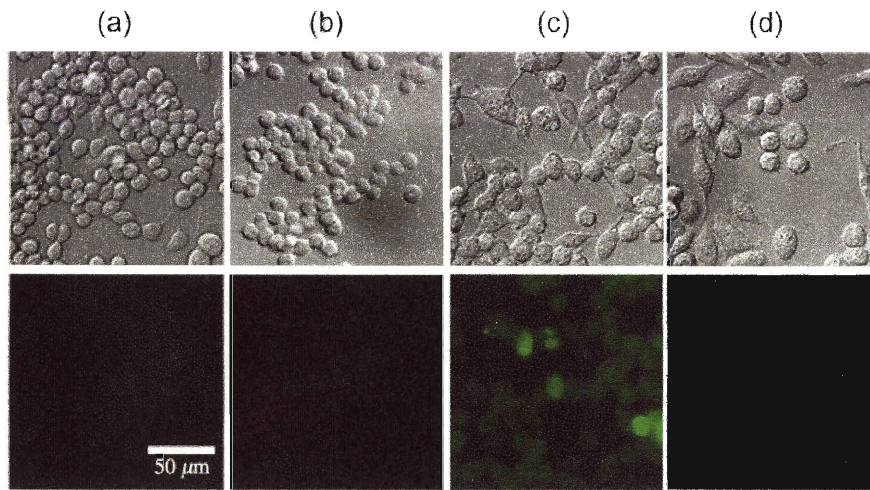


Figure 6.11. Fluorescence response of **CuFL** in Raw 264.7 cells. From left to right: Raw 264.7 cells after 12 h of incubation with **CuFL** ($1 \mu\text{M}$) in the absence (a) and presence (b) of *L*-NMA (2 mM), and for cells pretreated by stimulation with LPS (500 ng/mL) and IFN- γ (250 U/mL) for 4 h followed by 8 h **CuFL** incubation (c). Raw 264.7 cells sequentially treated with *L*-NMA for 1 h, LPS and IFN- γ for 4 h, and **CuFL** for 8 h are shown in (d). Images were taken with a Zeiss Axiovert 200M inverted epifluorescence microscope after removing DMEM and washing the cells three times with PBS. Top: DIC images, bottom: fluorescence images.

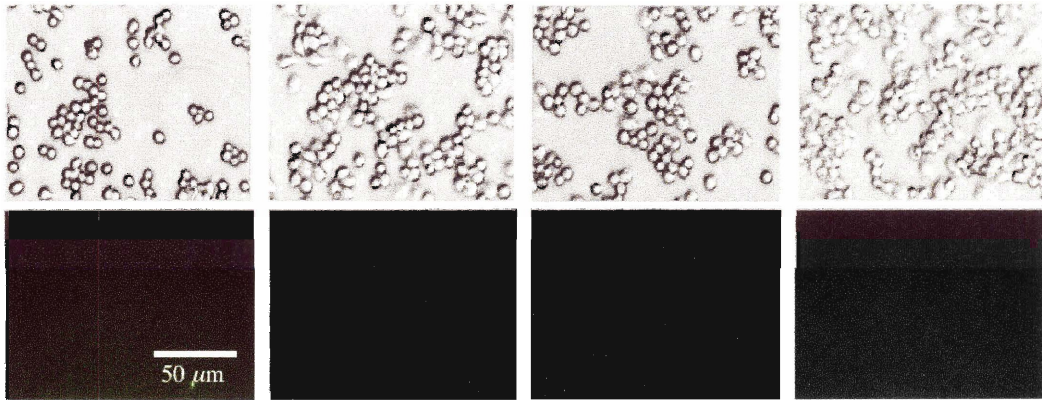


Figure 6.12. Fluorescence response of FL in Raw 264.7 cells. Left to right: 0, 2, 4, 8 h after addition of FL ($1 \mu\text{M}$) into Raw 264.7 cells pre-stimulated for 4 h by LPS (500 ng/mL) and IFN- γ (250 U/mL). Images were taken on a Nikon Eclipse TS100 microscope after removing DMEM and washing the cells three times with phosphate-buffered saline (PBS) (top: phase contrast images, bottom: fluorescence images).

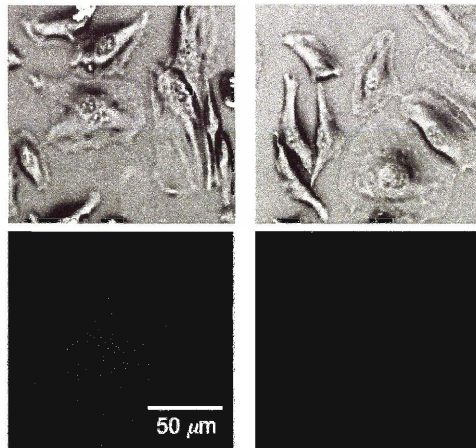


Figure 6.13. HeLa cells co-treated with **CuFL**, LPS and IFN- γ . HeLa cells were cultured in DMEM. The fluorescence responses were monitored for cells after 12 h of incubation with **CuFL** (1 μ M) (left) and for cells incubated with **CuFL** for 8 h following 4 h of stimulation by LPS (500 ng/mL) and IFN- γ (250 U/mL) (top: phase contrast images, bottom: fluorescence images). Images were taken by Nikon Eclipse TS100 microscope after removing DMEM and washing the cells three times with PBS.

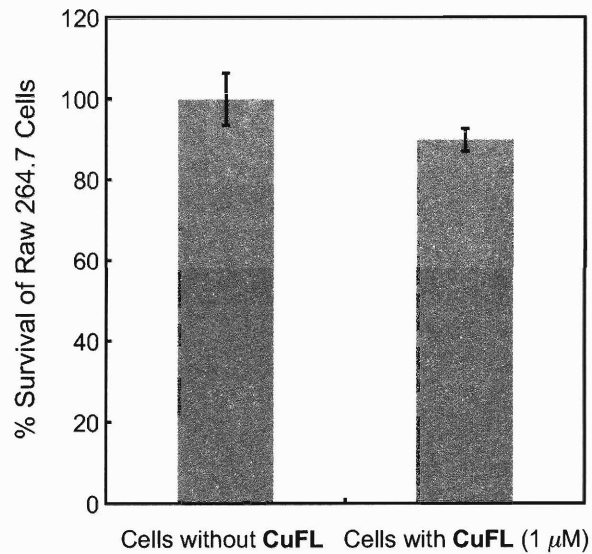


Figure 6.14. MTT assay on Raw 264.7 cells treated with CuFL. Cells (500 cells/well) were grown in a 96 well plate for 1 day and then treated with CuFL (1 μ M). After 5 days, MTT (20 μ L of 5 mg/mL) was added to each well for 2 h. DMSO (200 μ L) was added to each well after removing the media. The absorbance was measured by a microplate reader.

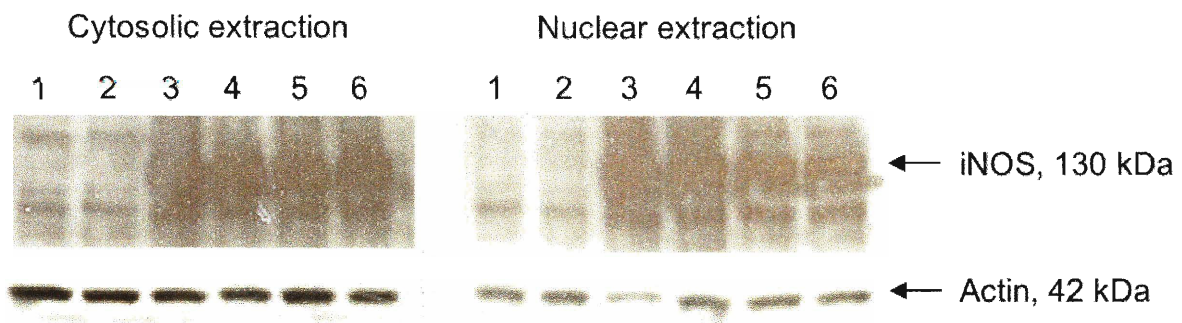


Figure 6.15. Western blot analysis of cytosolic and nuclear extracts of Raw 264.7 cells. Lanes 1) cells without any treatment, 2) treated with **CuFL** ($1 \mu\text{M}$), 3) co-incubated with **FL** ($1 \mu\text{M}$), LPS (500 ng/mL) and IFN- γ (250 U/mL), 4) pretreated with LPS and IFN- γ for 2 h followed by addition of **CuFL**, 5) co-treated with **CuFL**, LPS and IFN- γ , and 6) incubated with LPS and IFN- γ .

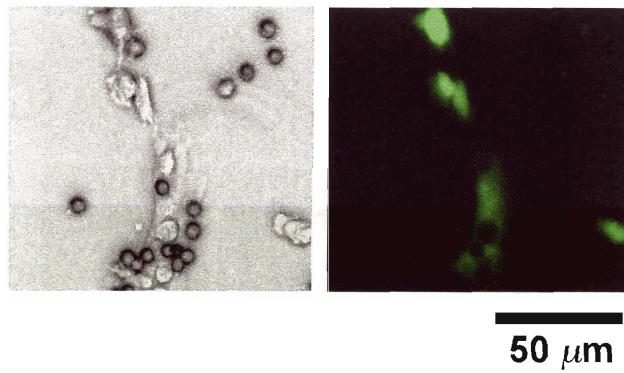


Figure 6.16. NO detection in SK-N-SH and Raw 264.7 cells by **CuFL**. Cells were treated with **CuFL** ($1 \mu\text{M}$) and 17β -estradiol (500 nM) for 10 min. The media were subsequently removed and the cells washed with PBS. Images were taken with a Nikon Eclipse TS100 microscope.

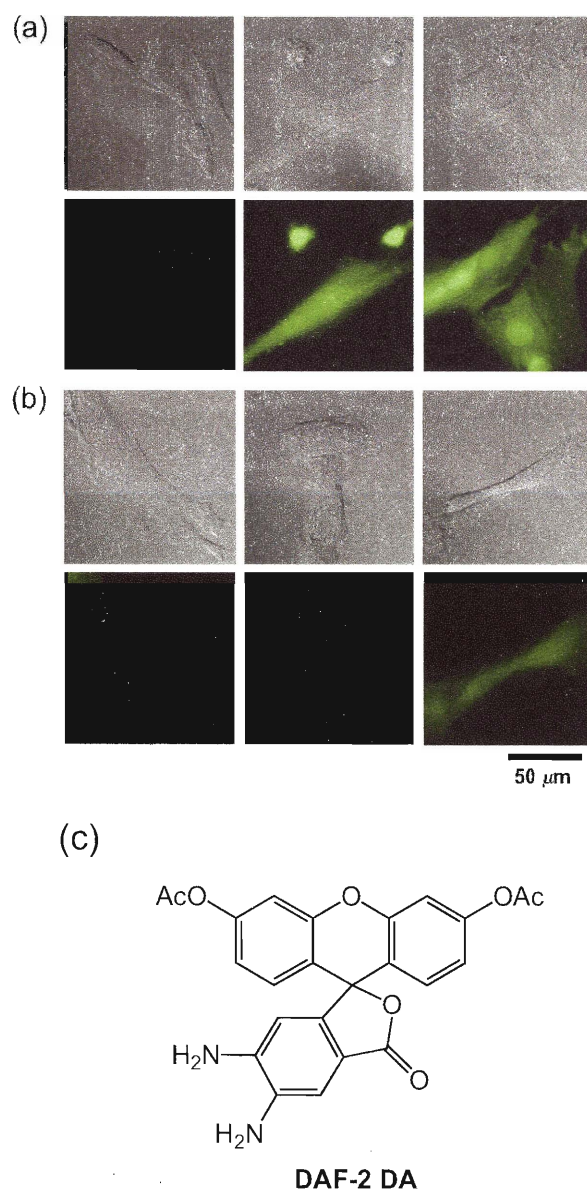


Figure 6.17. Fluorescence response of **CuFL** and DAF-2 DA to nitric oxide generation in SK-N-SH cells. (a) Cells incubated with **CuFL** ($1 \mu\text{M}$ CuCl_2 & $1 \mu\text{M}$ **FL**) for 20 min (left), co-treated with **CuFL** and 17β -estradiol (100 nM) for 5 min (middle) and 30 min (right). (b) Cells treated with DAF-2 DA ($2 \mu\text{M}$) for 30 min (left), with DAF-2 DA ($2 \mu\text{M}$) for 30 min followed by 17β -estradiol (100 nM) for 5 min (middle) and 30 min (right). Images were taken with a Zeiss Axiovert 200M inverted epifluorescence microscope after removing DMEM and washing the cells with PBS. The top panels are DIC images and the bottom panels display the fluorescent images. (c) Schematic drawing of DAF-2 DA.

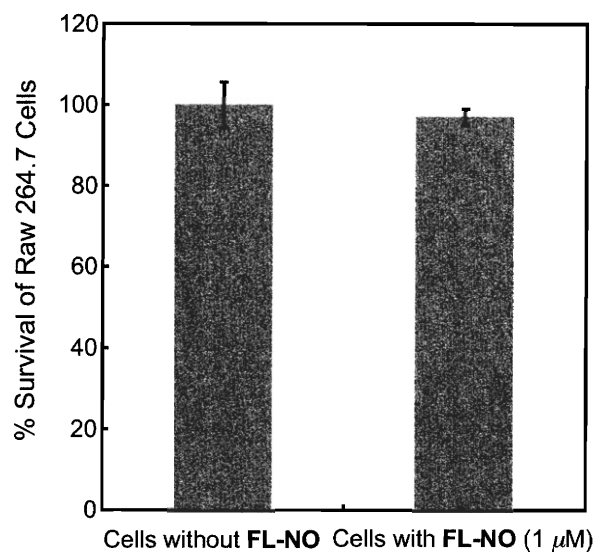


Figure 6.18. MTT assay of SK-N-SH cells treated with FL-NO. Cells (1000 cells/well) were grown in 96 well plate for 1 day and then treated with FL-NO (1 μ M). After 5 days, MTT (20 μ L of 5 mg/mL) was added to each well for 2 h. DMSO (200 μ L) was added to each well after removing media. The absorbance was measured by a microplate reader.

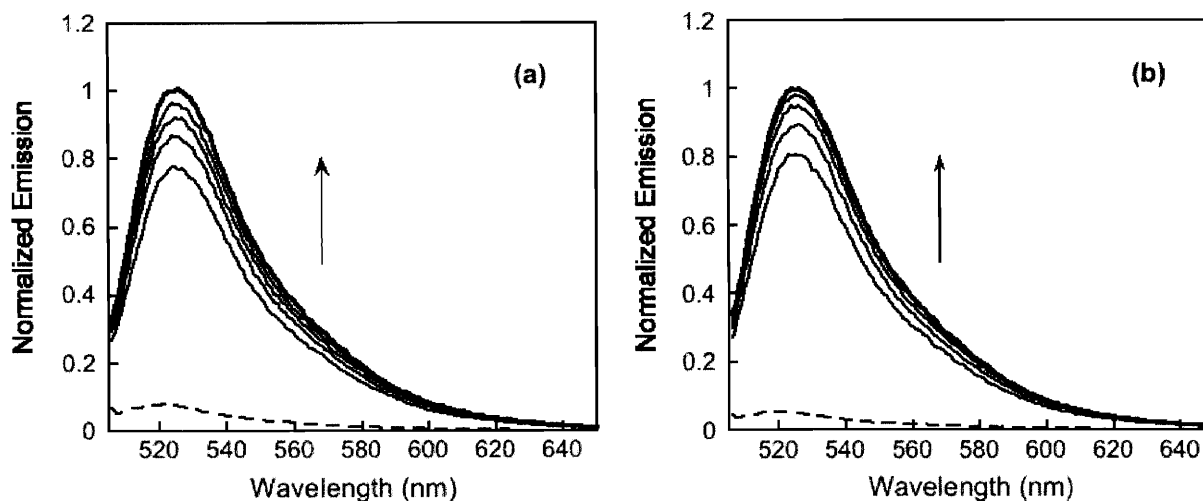


Figure 6.19. Fluorescence response of Cu(I)FL and Cu(II)FL to SNAP. (a) emission spectra ($\lambda_{\text{ex}} = 503$ nm) obtained upon addition of 100 equiv of SNAP to a solution of FL with 1 equiv of $[\text{Cu}(\text{CH}_3\text{CN})_4](\text{BF}_4)$ before (dashed black line) and after 5, 10, 15, 20, and 30 min of incubation (black and blue solid lines). (b) emission spectra of **CuFL** before (dashed black line) and 5, 10, 15, 20, and 30 min after addition of 100 equiv of SNAP (black solid lines). Spectra were taken in 50 mM PIPES, pH 7.0, 100 mM KCl.

Appendix

Fluorescent Detection of Nitric Oxide in a Rhodium Fluorophore Embedded in a Silastic Polymer Using Two-Photon Microscopy

This work was supported by NSF grant CHE-0234951. We thank Professor Peter T. C. So and Dr. Siavash Yazdanfar for collaboration with two-photon microscopy.

Introduction

Nitric oxide (NO) has generated remarkable interest among biologists, chemists, and physicians since it was discovered as a cellular signaling molecule.¹⁻³ NO regulates several biological events as a messenger in the cardiovascular, immune, and nervous systems.^{4,13} The involvement of NO in biology has been extensively investigated; however, studies to date have relied upon indirect methods for determining the presence and concentration of NO. Thus, a sensor for the direct detection of NO is highly desired. Over the past two decades, several NO sensors have been developed employing methods such as chemiluminescence,¹⁴ amperometry,¹⁵ and EPR spectroscopy,¹⁶⁻¹⁸ in addition to fluorescence-based technologies.¹⁹⁻³¹ Fluorescence is ideally suited for monitoring NO in biological systems, since it can provide both temporal and spatial information with minimal invasiveness. Research in our laboratory focuses on developing turn-on fluorescence-based NO sensors, in which a transition metal center serves as a binding site for the analyte. Initially, the fluorophore is bound to a metal center with partially filled d-shells, resulting in a quenching of fluorescence. Upon NO binding to the metal center, the fluorophore is displaced, restoring the fluorescence. Reversible, fast responding fluorescence-based NO sensors containing dirhodium tetracarboxylates that operate under these parameters were previously reported by our laboratory.²⁵ In that work, NO replaces a bound fluorophore such as dansyl-piperazine from the dirhodium core, a quenching environment, leading to turn-on emission (Scheme A.1). To utilize this dirhodium-based NO sensor in biological systems, we have extended this work to facilitate its application in aqueous media. Here we report that aqueous NO can be monitored with a dirhodium-containing polymer and two-photon microscopy (TPM), which is the first step toward fiber-optic-based TPM NO sensing based on small molecule inorganic compounds.

Experimental

Materials and Procedures

All reagents were purchased from commercial suppliers and used without further purification. 1,2-Dichloroethane (DCE) was used as received. Dansyl-piperazine (Ds-pip)³² and the dirhodium complex $[\text{Rh}_2(\mu\text{-O}_2\text{CPr})_4]$ ³³ were prepared according to published procedures. A Silastic® Q7-4656 Biomedical Grade ETR Elastomer was purchased from Dow Corning; it is composed of a dimethyl and methylvinyl siloxane copolymer. Silastic (polydimethylsiloxane) tubing is permeable to NO and O₂ gases.³⁰ Nitric oxide (NO) (Matheson 99%) was purified by a method adapted from the literature.^{25,34} UV light was applied by a hand-held lamp (UVGL-25, VWR International).

Preparation of a Silastic Membrane with the Dirhodium Complex and Ds-pip.

The silastic membrane was sliced into 1 mm thick pieces and dried *in vacuo* for 1 d. The membrane pieces were soaked in a DCE solution of $[\text{Rh}_2(\mu\text{-O}_2\text{CPr})_4]$ (100 μM) and Ds-pip (50 μM) for 1 d and dried in air. The membrane embedded dirhodium complex was dried *in vacuo* for 1 d and stored in a glove box. The fluorescence response was monitored by taking a photograph with a digital camera in light of long wave (350 nm) UV from the hand-held lamp.

Study of a Dirhodium-Containing Silastic Membrane with NO.

An aqueous solution saturated with NO was prepared by bubbling a stream of NO gas into deionized water for 30 min at 25 °C. A saturated aqueous NO solution (1.5 mL) was transferred by a gastight syringe into an anaerobic fluorescence cuvette containing a slice of dirhodium-containing Silastic membrane. All procedures were performed under an anaerobic atmosphere. After 20 min, the piece was removed from the aqueous

solution and transferred to a storage vessel at $-80\text{ }^{\circ}\text{C}$.

Two-Photon Measurements. A schematic diagram of the microscopic system is shown in Figure A.1. Sub-100 fs pulses from a tunable, mode-locked Ti:sapphire laser (Tsunami, Spectra-Physics, Inc.) were directed into an inverted microscope (Axiovert S100 TV, Carl Zeiss, Inc.). The center wavelength was varied from 740 – 780 nm while the bandwidth was kept constant at approximately 10 nm. The average power from the laser was adjusted by using a variable attenuator constructed with a half-wave plate and Glan-Thomson polarizer. Typically, 20 mW of average power was incident on the microscope. Lateral scanning of the beam was achieved outside the microscope by using a galvanometric XY-scanning mirror pair (Model 6350, Cambridge Technologies, Inc.). The excitation light was directed towards the sample and focused using a 20X, 0.75NA objective (Fluar, Carl Zeiss, Inc.).

Two-photon-excited fluorescence emission was collected in the epi-direction through the same objective and separated from the excitation beam by using a dichroic mirror (Chroma Technologies, Inc.). Residual excitation power was removed with an additional barrier filter (Schott BG39, Chroma Technologies, Inc.). The remaining fluorescence was collected with a photomultiplier tube (Model 7400P, Hamamatsu Photonics K.K.). Individual current pulses resulting from photon incidences were counted at the repetition rate of the laser (80 MHz) using a custom single-photon-counting data acquisition card. In order to construct an image, the image intensity at each pixel corresponded to the total photon flux collected during the pixel acquisition time, variable from 0.04 – 1 msec, was used. Each image consisted of 256×256 pixels spanning approximately $200 \times 200\text{ }\mu\text{m}^2$.

Results and Discussion

Preparation and Nitric Oxide Reactivity of the Dirhodium-Containing Silastic Membrane.

A slice of Silastic membrane was soaked in a DCE solution of dirhodium tetracarboxylate complex $[\text{Rh}_2(\mu\text{-O}_2\text{CPr})_4]$ (100 μM) and Ds-pip (50 μM) for one day. After $[\text{Rh}_2(\mu\text{-O}_2\text{CPr})_4(\text{Ds-pip})]$ was loaded onto the Silastic membrane, the fluorescence response was monitored by a hand-held UV lamp. The Silastic membrane containing $[\text{Rh}_2(\mu\text{-O}_2\text{CPr})_4(\text{Ds-pip})]$ showed a significant fluorescence quenching relative to that of free Ds-pip (Figure A.2). When a saturated aqueous NO solution (1.9 mM) was introduced into an anaerobic fluorescence cuvette containing the silastic membrane embedding $[\text{Rh}_2(\mu\text{-O}_2\text{CPr})_4(\text{Ds-pip})]$, a fluorescence increase was immediately observed (Figure A.3). Treatment at different concentrations (1.9 mM, 0.63 mM, and 0.38 mM) immediately displayed enhanced fluorescence as well (Figure A.4).

Two-Photon Experiment.

Initial images of the Silastic membranes of Ds-pip and $[\text{Rh}_2(\mu\text{-O}_2\text{CPr})_4(\text{Ds-pip})]$ were obtained by two-photon microscopy (Figure A.5). The average number of photons emitted from the membrane of $[\text{Rh}_2(\mu\text{-O}_2\text{CPr})_4(\text{Ds-pip})]$ is 3.38, which is decreased compared to that of free Ds-pip (# of photons = 6.02), when excited at 740 nm. Treatment of the membrane of $[\text{Rh}_2(\mu\text{-O}_2\text{CPr})_4(\text{Ds-pip})]$ with NO (1.9 mM, aq) restored the number of photons to a value similar to that of Ds-pip (Figure A.5), indicating that NO binds and Ds-pip is dissociated from the dirhodium core. Images of Silastic membranes of $[\text{Rh}_2(\mu\text{-O}_2\text{CPr})_4(\text{Ds-pip})]$ at different concentrations of NO (0.38 mM, 0.63 mM, and 1.9 mM) were acquired by two-photon microscopy. More photons were emitted from the membrane treated with 1.9 mM NO (aq) than with 0.38 and 0.68 mM

NO (aq) (Figure A.6). These observations confirm that the NO reactivity of the dirhodium tetracarboxylate complex in solid state is consistent with that previously studied in solution.²⁵

The stability of the signal of the membrane of $[\text{Rh}_2(\mu\text{-O}_2\text{CPr})_4(\text{Ds-pip})]$ with 1.9 mM NO (aq) was examined at a single location over 1 h, when excited at 780 nm (Figure A.7). No noticeable effects of photobleaching or membrane decomposition were observed during the collection of signals.

The increased number of photons emitted in the reaction of the membrane of $[\text{Rh}_2(\mu\text{-O}_2\text{CPr})_4(\text{Ds-pip})]$ with NO indicates that NO can be monitored by using this inorganic material Silastic membrane having a dirhodium tetracarboxylate fluorophore complex combined with two-photon microscopy. Moreover, these results hold promise for the development of fiber-optics, using dirhodium-containing polymer capable of detecting NO in living systems.

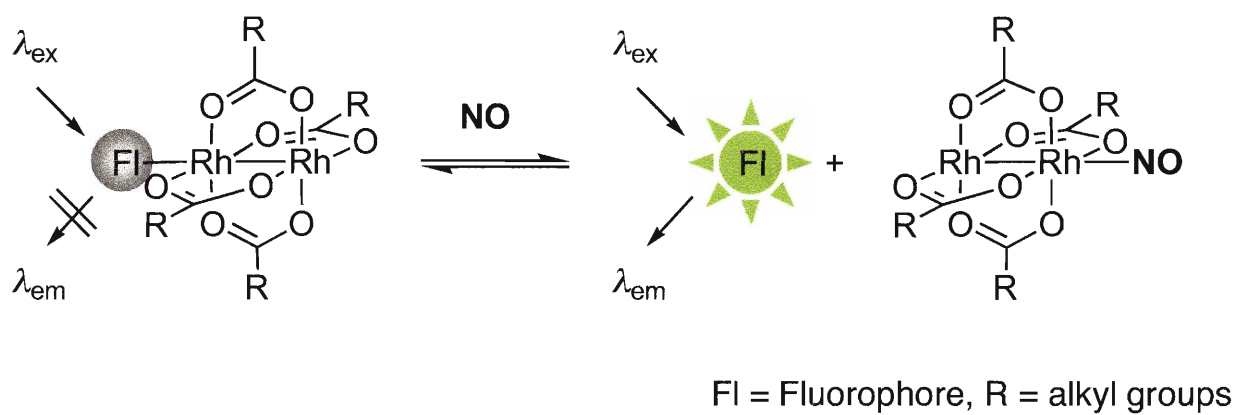
Summary

A Silastic membrane containing embedded $[\text{Rh}_2(\mu\text{-O}_2\text{CPr})_4(\text{Ds-pip})]$ showed a decreased number of photons emitted relative to that of Ds-pip. When the membrane-encapsulated $[\text{Rh}_2(\mu\text{-O}_2\text{CPr})_4(\text{Ds-pip})]$ was treated with an aqueous solution of NO, an immediate increase in fluorescence was observed by two-photon spectroscopy. These observations represent the first example of NO detection by the combination of two-photon microscopy and an inorganic complex. These membrane studies are a first step toward fiber-optic-based NO sensing in aqueous media using a dirhodium-containing polymer and two-photon microscopy.

References

- (1) Furchgott, R. F., *Angew. Chem. Int. Ed.* **1999**, *38*, 1870-1880.
- (2) Ignarro, L. J.; Buga, G. M.; Wood, K. S.; Byrns, R. E.; Chaudhuri, G., *Proc. Natl. Acad. Sci. USA* **1987**, *84*, 9265-9269.
- (3) Palmer, R. M. J.; Ferrige, A. G.; Moncada, S., *Nature* **1987**, *327*, 524-526.
- (4) Furchgott, R. F., *Angew. Chem. Int. Ed.* **1999**, *38*, 1870-1880.
- (5) Wink, D. A.; Vodovotz, Y.; Laval, J.; Laval, F.; Dewhirst, M. W.; Mitchell, J. B., *Carcinogenesis* **1998**, *19*, 711-721.
- (6) Moncada, S.; Palmer, R. M. J.; Higgs, E. A., *Pharmacol. Rev.* **1991**, *43*, 109-142.
- (7) Kerwin, J. F., Jr.; Lancaster, J. R., Jr.; Feldman, P. L., *J. Med. Chem.* **1995**, *38*, 4343-4362.
- (8) Feldman, P. L.; Griffith, O. W.; Stuehr, D. J., *J. Chem. Eng. News* **1993**, *71*, 26-38.
- (9) Brecht, D. S.; Snyder, S. H., *Annu. Rev. Biochem.* **1994**, *63*, 175-195.
- (10) Murad, F., *Angew. Chem. Int. Ed.* **1999**, *38*, 1856-1868.
- (11) Ignarro, L. J., *Angew. Chem. Int. Ed.* **1999**, *38*, 1882-1892.
- (12) Butler, A. R.; Williams, D. L. H., *Chem. Soc. Rev.* **1993**, 233-241.
- (13) Rubbo, H.; Darley-Usmar, V.; Freeman, B. A., *Chem. Res. Toxicol.* **1996**, *9*, 809-820.
- (14) Hampl, V.; Walters, C.; Archer, S. L., *In Methods in Nitric Oxide Research*, Feelisch, M.; Stamler, J. S., Eds. John Wiley & Sons: New York, 1996; pp 309-318.
- (15) Mao, L.; Tian, Y.; Shi, G.; Liu, H.; Jin, L., *Anal. Lett.* **1998**, *31*, 1991-2007.
- (16) Kotake, Y.; Tanigawa, T.; Tanigawa, m.; Ueno, I.; Allen, D. R.; Lai, C.-S., *Biochim. Biophys. Acta* **1996**, *1289*, 362-368.
- (17) Komarov, A. M.; Lai, C.-S., *Biochim. Biophys. Acta* **1995**, *1272*, 29-36.
- (18) Yoshimura, T.; Fujii, S.; Yokoyama, H.; Kamada, H., *Chem. Lett.* **1995**, 309-310.
- (19) Kojima, H.; Nakatsubo, N.; Kikuchi, K.; Kawahara, S.; Kirno, Y.; Nagoshi, H.; Hirata, Y.; Nagano, T., *Anal. Chem.* **1998**, *70*, 2446-2453.

- (20) Kojima, H.; Urano, Y.; Kikuchi, K.; Higuchi, T.; Hirata, Y.; Nagano, T., *Angew. Chem. Int. Ed.* **1999**, *38*, 3209-3212.
- (21) Miles, A. M.; Chen, Y.; Owens, M. W.; Grisham, M. B., *Methods* **1995**, *7*, 40-47.
- (22) Bätz, M.; Korth, H.-G.; Sustmann, R., *Angew. Chem. Int. Ed.* **1997**, *36*, 1501-1503.
- (23) Meineke, P.; Rauen, U.; de Groot, H.; Korth, H.-G.; Sustmann, R., *Chem. Eur. J.* **1999**, *5*, 1738-1747.
- (24) Franz, K. J.; Singh, N.; Spingler, B.; Lippard, S. J., *Inorg. Chem.* **2000**, *39*, 4081-4092.
- (25) Hilderbrand, S. A.; Lim, M. H.; Lippard, S. J., *J. Am. Chem. Soc.* **2004**, *126*, 4972-4978.
- (26) Hilderbrand, S. A.; Lippard, S. J., *Inorg. Chem.* **2004**, *43*, 4674-4682.
- (27) Hilderbrand, S. A.; Lippard, S. J., *Inorg. Chem.* **2004**, *43*, 5294-5301.
- (28) Nagano, T.; Yoshimura, T., *Chem. Rev.* **2002**, *102*, 1235-1269
- (29) Hilderbrand, S. A.; Lim, M. H.; Lippard, S. J., *In Topics in Fluorescence Spectroscopy*, Geddes, C. D.; Lakowicz, J. R., Eds. Springer: 2005; pp 163-188.
- (30) Lim, M. H.; Lippard, S. J., *J. Am. Chem. Soc.* **2005**, *127*, 12170-12171.
- (31) Smith, R. C.; Tennyson, A. G.; Lim, M. H.; Lippard, S. J., *Org. Lett.* **2005**, *7*, 3573-3575.
- (32) Saavedra, J. E.; Booth, M. N.; Hrabie, J. A.; Davies, K. M.; Keefer, L. K., *J. Org. Chem.* **1999**, *64*, 5124-5131.
- (33) Drago, R. S.; Long, J. R.; Cosmano, R., *Inorg. Chem.* **1981**, *20*, 2920-2927.
- (34) Lorkovic, I. M.; Ford, P. C., *Inorg. Chem.* **2000**, *39*, 632-633.



Scheme A.1. Nitric Oxide Detection of Dirhodium Dansyl Complexes.

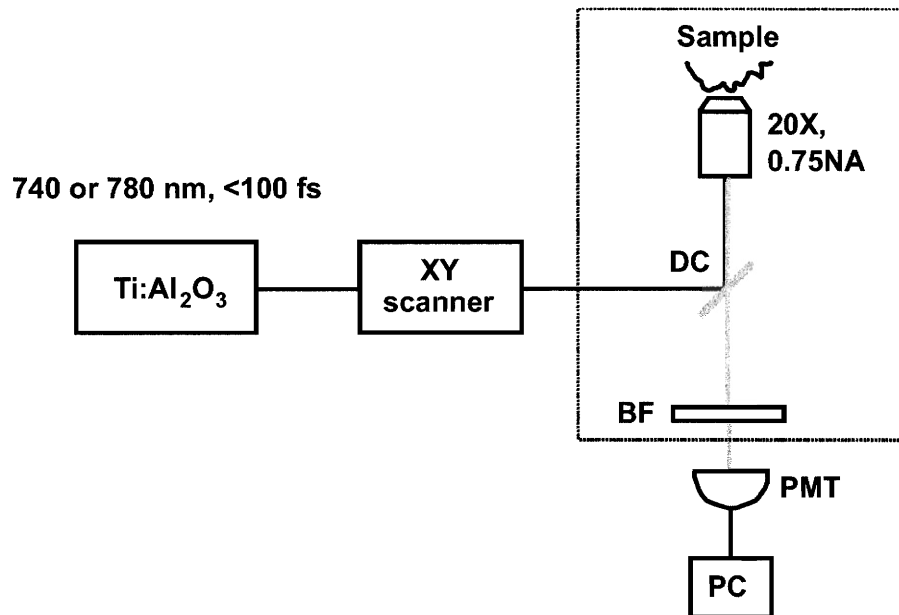


Figure A.1. Schematic diagram of two-photon microscope. The commercial inverted microscope is indicated by the dotted line. DC, dichroic mirror; BF, barrier filter; PMT, photomultiplier tube; PC, personal computer.

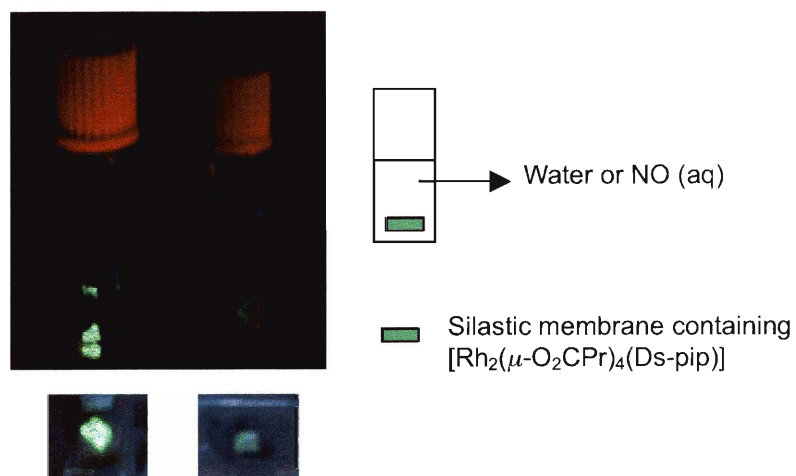


Figure A.2. Left: a photo monitoring the fluorescence response of Silastic membranes of Ds-pip (left) and $[\text{Rh}_2(\mu\text{-O}_2\text{CPr})_4(\text{Ds-pip})]$ (right) with a hand-held UV lamp. Right: description of experimental apparatus.



Figure A.3. A photo monitoring the fluorescence response in the reaction of the Silastic membrane containing $[\text{Rh}_2(\mu\text{-O}_2\text{CPr})_4(\text{Ds-pip})]$ (right) with NO (1.9 mM, aq) (left).

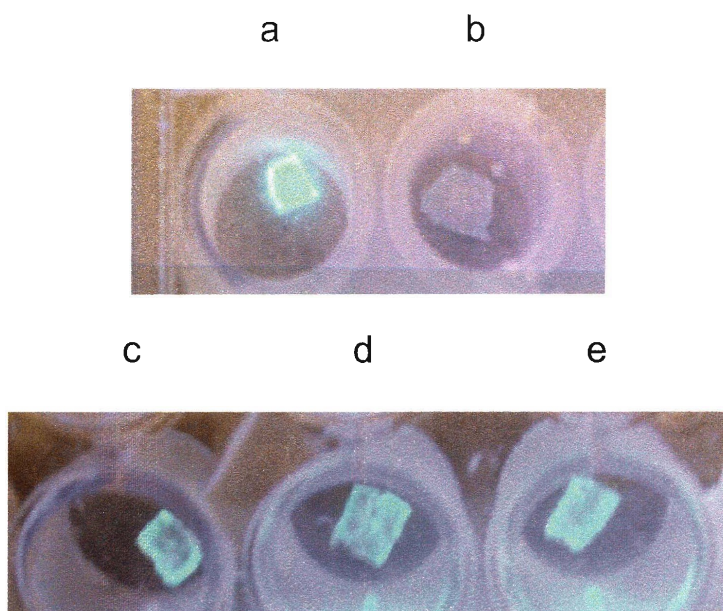


Figure A.4. A photo monitoring the fluorescence response in the reaction of the Silastic membrane containing $[\text{Rh}_2(\mu\text{-O}_2\text{CPr})_4(\text{Ds-pip})]$ with NO (c: 1.9 mM; d: 0.63 mM; e: 0.38 mM) (bottom). Top: a: Ds-pip; b: $[\text{Rh}_2(\mu\text{-O}_2\text{CPr})_4]$ and Ds-pip.



Figure A.5. Images of the membrane of Ds-pip (left, # of photons = 6.02), $[\text{Rh}_2(\mu\text{-O}_2\text{CPr})_4(\text{Ds-pip})]$ (center, # of photons = 3.38), and $[\text{Rh}_2(\mu\text{-O}_2\text{CPr})_4(\text{Ds-pip})]$ with NO (1.9 mM, aq) (right, # of photons = 8.41) by two photon microscopy. Excitation is at 740 nm (20 mW, 25 kHz).

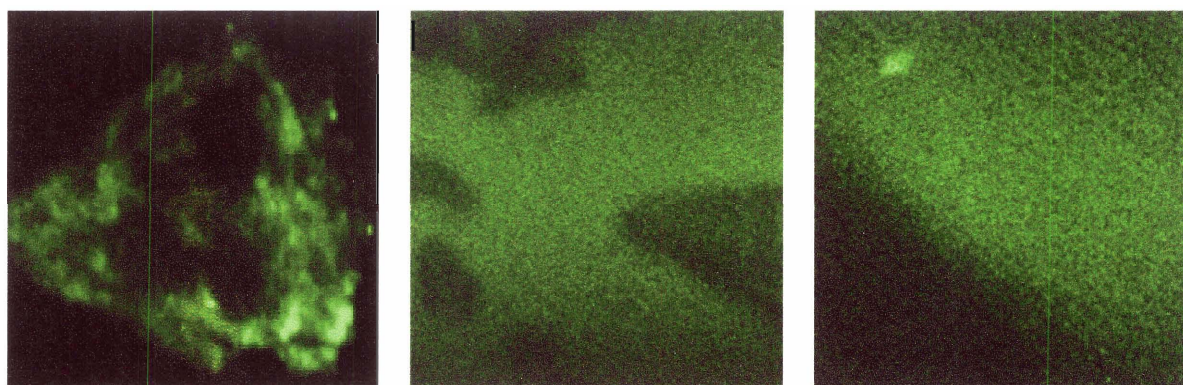


Figure A.6. Images of the membrane of $[\text{Rh}_2(\mu\text{-O}_2\text{CPr})_4(\text{Ds-pip})]$ with 1.9 mM NO (aq) (right, # of photons = 8.5 at 10 kHz), 0.63 mM NO (aq) (center, # of photons = 49 at 1 kHz), and 0.38 mM NO (aq) (right, # of photons = 35) by two photon microscopy. Excitation is at 780 nm (20 mW).

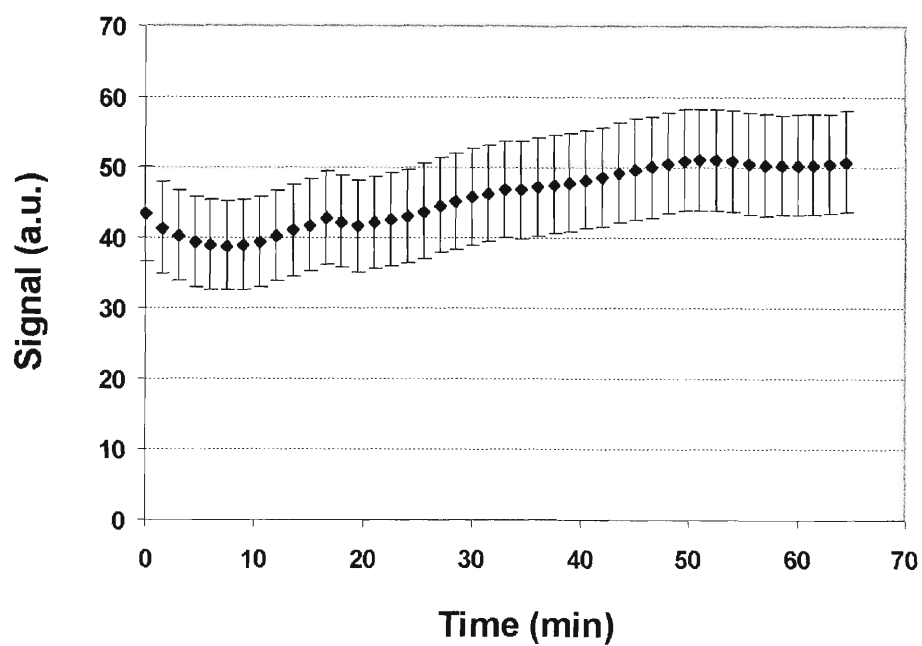


Figure A.7. Stability of the signal of the membrane of $[\text{Rh}_2(\mu\text{-O}_2\text{CPr})_4(\text{Ds-pip})]$ with 1.9 mM NO (aq) over 1 h. Excitation is at 780 nm (20 mW).

Biographical Note

The author was born on January 21, 1977 in Kwang Myung-City, KyungKi-Do, Korea. She received a 1999 B.S. degree in Chemistry and a 2001 M.Sc. in Molecular Life Science (Inorganic Chemistry) under the direction of Professor Wonwoo Nam from Ewha Womans University, Seoul, Korea. In September 2002, the author began a doctoral course in inorganic chemistry under the supervision of Professor Stephen J. Lippard at Massachusetts Institute of Technology. Following her graduation, she will pursue postdoctoral research in the laboratory of Professor Jacqueline K. Barton at California Institute of Technology.

Mi Hee Lim

Education

- 2002 – 2006 **Massachusetts Institute of Technology**, Cambridge, MA
Ph.D. in Chemistry
Thesis Advisor: Professor Stephen J. Lippard
- 1999 – 2001 **Ewha Womans University**, Seoul, Korea
M.Sc. in Molecular Life Science (Inorganic Chemistry)
- 1995 – 1999 **B.Sc. in Chemistry**, *Graduated Summa Cum Laude*
Thesis Advisor: Professor Wonwoo Nam

Selected Publications

1. **Mi Hee Lim**, Dong Xu, Stephen J. Lippard, **2006**, *Nat. Chem. Biol.* in press. "Visualization of Nitric Oxide in Living Cells by a Copper-Based Fluorescent Probe".
2. **Mi Hee Lim**, Chaoyuan Kuang, Stephen J. Lippard, *ChemBioChem*, **2006**, in press. "Nitric Oxide-Induced Fluorescence Enhancement by Displacement of Dansylated Ligands from Cobalt".
3. **Mi Hee Lim**, Stephen J. Lippard, *J. Am. Chem. Soc.* **2005**, *127*, 12170-12171. "Copper Complexes for Fluorescence-Based NO Detection in Aqueous Solution".
4. Rhett C. Smith, Andrew G. Tennyson, **Mi Hee Lim**, Stephen J. Lippard, *Org. Lett.* **2005**, *7*, 3573-3575. "Conjugated Polymer-Based Fluorescence Turn-On Sensor for Nitric Oxide".
5. Scott A. Hilderbrand, **Mi Hee Lim**, Stephen J. Lippard, In *Topics in Fluorescence Spectroscopy*; C. D. Geddes, J. R. Lakowicz, Eds; Springer, **2005**, Vol. 9, pp. 163-188. "Fluorescence-Based Nitric Oxide Detection".
6. **Mi Hee Lim**, Stephen J. Lippard, *Inorg. Chem.* **2004**, *43*, 6366-6370. "Fluorescence-Based Nitric Oxide Detection by Ruthenium Porphyrin Fluorophore Complexes".
7. Scott A. Hilderbrand, **Mi Hee Lim**, Stephen J. Lippard, *J. Am. Chem. Soc.* **2004**, *126*, 4972-4978. "Dirhodium Tetracarboxylate Scaffolds as Reversible Fluorescence-Based Nitric Oxide Sensors".
8. **Mi Hee Lim**, Jan-Uwe Rohde, Audria Stubna, Michael R. Bukowski, Miquel Costas, Raymond Y. N. Ho, Eckard Munck, Wonwoo Nam, Lawrence Que, Jr., *Proc. Natl. Acad. Sci. U.S.A.*, **2003**, *100*, 3665-3670. "An Fe^{IV}=O Complex of a Tetradentate Tripodal Nonheme Ligand".
9. Jan-Uwe Rohde, Jun-Hee In, **Mi Hee Lim**, William W. Brennessel, Michael R. Bukowski, Audria Stubna, Eckard Munck, Wonwoo Nam, Lawrence Que, Jr., *Science*, **2003**, *299*, 1037-1039. "Crystallographic and Spectroscopic Characterization of a Nonheme Fe(IV)=O Complex".
10. Wonwoo Nam, **Mi Hee Lim**, Sun Kyung Moon, Cheal Kim, *J. Am. Chem. Soc.* **2000**, *122*, 10805-10809. "Participation of Two Distinct Hydroxylating Intermediates in Iron(III) Porphyrin Complex-Catalyzed Hydroxylation of Alkanes".

Selected Presentations

1. **Mi Hee Lim** and S. J. Lippard. "Metal-Based Fluorescent Nitric Oxide Detection" at the 232nd ACS National Meeting (San Francisco, CA, September 10-14, 2006).
2. **Mi Hee Lim** and S. J. Lippard. "Metal-Based Turn-On Fluorescent Probes for Sensing Nitric Oxide" at Gordon-Kenan Graduate Research Seminar (Gordon Conference): Bioinorganic (Ventura, CA: February 2-5, 2006).